5-15-2018

Pyrolysis of Jet Propellants and Oxidation of Polycyclic Aromatic Radicals with Molecular Oxygen: Theoretical Study of Potential Energy Surfaces, Mechanisms, and Kinetics

Daniel E. Belisario-Lara
dbeli001@fiu.edu

FLORIDA INTERNATIONAL UNIVERSITY

Miami, Florida

PYROLYSIS OF JET PROPELLANTS AND OXIDATION OF POLYCYCLIC AROMATIC

RADICALS WITH MOLECULAR OXYGEN: THEORETICAL STUDY OF POTENTIAL

ENERGY SURFACES, MECHANISMS, AND KINETICS

A dissertation submitted in partial fulfillment of the

requirements for the degree of

DOCTOR OF PHILOSOPHY

in

CHEMISTRY

by

Daniel Belisario-Lara

2018

To: Dean Michael R. Heithaus
     College of Arts, Sciences and Education

This dissertation, written by Daniel Belisario-Lara, and entitled Pyrolysis of Jet Propellants and Oxidation of Polycyclic Aromatic Radicals with Molecular Oxygen: Theoretical Study of Potential Energy Surfaces, Mechanisms, and Kinetics, having been approved in respect to style and intellectual content, is referred to you for judgment.

We have read this dissertation and recommend that it be approved.

_____
Joong Ho Moon

_____
Wenzhi Li

_____
Jeffrey Joens

_____
David C. Chatfield

_____
Alexander M. Mebel, Major Professor

Date of Defense: May 15, 2018

The dissertation of Daniel Belisario-Lara is approved.

_____
Dean Michael R. Heithaus
College of Arts, Sciences and Education

_____
Andrés G. Gil
Vice President for Research and Economic Development
and Dean of the University Graduate School

Florida International University, 2018

ACKNOWLEDGMENTS

ABSTRACT OF THE DISSERTATION

PYROLYSIS OF JET PROPELLANTS AND OXIDATION OF POLYCYLIC AROMATIC

RADICALS WITH MOLECULAR OXYGEN: THEORETICAL STUDY OF POTENIAL

ENERGY SURFACES, MECHANISMS, AND KINETICS

by

Daniel Belisario-Lara

Florida International University, 2018

Miami, Florida

Professor Alexander M. Mebel, Major Professor

Two reaction classes have been studied computationally including the pyrolysis of various components of airplane fuels, such as decane, dodecane, butylbenzene isomers, and JP-10 (*exo*-tetrahydrodicyclopentadiene), and oxidation of a group of molecules belonging to the class of Polycyclic Aromatic Hydrocarbons (PAHs). Investigation of both reaction classes has been performed using ab initio quantum chemistry methods with the Gaussian 09 and MOLPRO programs at various levels of theory. Initially, Potential Energy Surfaces (PES) were generated at the G3(MP2,CC)/B3LYP/6-311G** level of theory for various radicals involved in the reactions as reactants, intermediates, transition states, and products. The next step was to perform Rice-Ramsperger-Kassel-Marcus (RRKM) / Master Equation calculations in order to calculate rate constants and branching ratios of different products at various temperatures and pressures characteristic for combustion flames. All calculations were then compared with previous works on similar systems available in the literature. The results of these simulations along with previous data were then used to formulate

guidelines for the pyrolysis and oxidation patterns of larger and more complex systems, in order to achieve a better understanding of the pathways to the end products in airplane jet engines.

TABLE OF CONTENTS

LIST OF TABLES

LIST OF FIGURES

CHAPTER I

Introduction

Scientific Rationale

<u>The Complete Combustion Process</u>

Combustion is an intricate multi-step process that is not fully understood. The complexity is provided by a large range of combustible systems, which inhibits any trivial mechanism for the process. However, by studying different classes of compounds and chemical reactions involved in combustion, information and scientific knowledge can be gained. In order to begin there are certain classifications that can simplify the process.[1] A flame is a self-sustaining propagation of a localized combustion zone at subsonic velocities. There are many physical parameters/components that contribute to the process of flame such as flame speed, temperature, pressure, fuel/oxygen ratio, and the presence of additives or catalysts.[2] These conditions can all be shifted toward the formation of desirable products if the underlying mechanism can be well understood. Theoretical and experimental investigations into major reaction pathways, rate coefficients, and major products give insight into the mechanism and maximize our understanding of the combustion processes and the efficiency of predictive models.

To effectively contribute to the scientific literature, modelers need to be able to point to species of interest either from prior knowledge or from the foundations of a study using species difficult to measure experimentally. Predicting relevant chemical species is the most efficient way to assist experimentalists and theoreticians in their pursuit of choosing reactions of significance to study. Depending on the model being probed, there are aspects that will take precedence on importance. A standard way of deciding which reactions should be considered significant is to identify those that influence the total concentration of the key species present in the reaction system. The overall mixture after all is mainly dependent on the concentration of species over time and their individual

contributions. Which is often presented in the form of product branching ratios which are made up of total and individual rate coefficients.[3] Another standard of determining which reactions should be probed are any that effect the final model's uncertainties. By removing sources of uncertainty, the predictions of the model will be improved. Comparison to direct observations requires a certain level of trust in the predictive capabilities of the model in question.

In the most basic distinction between phases of overall combustion we can define two large categories or stages, pyrolysis and oxidation. Pyrolysis is the thermal decomposition of compounds in an inert atmosphere or lack of atmosphere. Oxidation is the more commonly known version involving a high temperature exothermic chemical reaction of an oxidant and reductant to form oxidized products, typically in gas phase, and energy in the form of heat and/or light. To truly understand the complete combustion process it is necessary to define the class of compounds being burned. To cover all species is out of the scope of this research so the main focus will be on various forms of hydrocarbons including their contribution to a class of compounds named Polycyclic Aromatic Hydrocarbons (PAH). These molecules are composed of hydrocarbons with multiple aromatic rings fused together. The complete process when there is no loss of energy to side reactions proceeds thusly.

$$C_xH_x + O_2 \rightarrow CO_2 + H_2O,$$
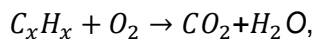
with C_xH_x being the generic form that the polycyclic aromatic hydrocarbons take.[4] Other molecules also being studied are aliphatic paraffins and alkyl substituted benzenes. However, rarely is this combustion process taken to completion. Understanding the mechanisms of pyrolysis and oxidation becomes necessary.

Pyrolysis proceeds upon the addition of heat to the chemical system. Typically, this occurs in the temperature range of 800-1500 K and without the presence of any reactive species gas. When the available temperature becomes enough to overcome the stability of chemical bonds, those bonds break resulting in a separation of radical species to be formed. These radicals can then be stabilized through two different processes: they can become resonantly stabilized free radicals (RSFRs) which maintain their form as a result of conjugation of the electrostatic system or they can become stabilized by collisions with the inert bath gas.[5] These RSFRs are important to the growth of larger PAH systems. They also are believed to contribute to soot production, the chemistry of the interstellar medium, and planetary atmospheres. The pathway to the first aromatic ring has been found to heavily depend on the propargyl radicals, C_3H_3, and other pathways involving RSFRs such as reactions with methyl and ethyl radicals. These molecules can also be formed by photolytic decomposition when pyrolysis is not feasible. Atomic carbon, dicarbon, and tricarbon can also react with unsaturated hydrocarbons to form RSFRs.

Oxidation is one of the most common reactions in nature, but the focus in this study is specifically the reaction of molecular oxygen as the oxidant and a relevant chemical species as the reductant. The oxidation reaction typically takes place as a complicated sequence of elementary radical reactions. The release of energy in the form of heat and/or light is observed in this process because the bond energies of the O_2 molecule are much lower than the bond energies of the products that form. The typical combustion temperatures used for engines range from 1000 K to 2000 K although oxidation can occur at any range. Oxidation as a process has many avenues that lead to incomplete combustion which causes side reactions which are of interest for environmental reasons as discussed further below. The main cause of incomplete

combustion is the leaving of the offgas. The loss of carbon dioxide gas and water vapor reduces the overall heat and slows down the process. Another contributor to incomplete combustion is the insufficient concentration of oxygen. Depending on the method of heating control of air flow will determine the efficiency of combustion.

Theoretical modeling of pyrolysis and oxidation provide useful information for future studies in these reaction systems and for overall improvement of models. Combined with experimental data, they are a useful tool to elucidate and understand complicated experimental results. Perhaps the greatest benefit comes from the capability to investigate conditions that are too hazardous or costly to recreate in a laboratory setting, such as exotic temperature and pressure conditions that are present in the interstellar medium (low temperature - low pressure) or in high-performance combustion engines (high temperature - high pressure). With the prevalence of super computers and the enhancement of theoretical methods it is sometimes preferable to begin with theoretical calculations which can provide accurate results in a fast and low-cost way. In some cases, the accuracy of these theoretical calculations can rival that of experiments, especially in terms of chemical kinetic results which are difficult to measure precisely. With the proliferation of advanced computers and improvements in theoretical methods the modeling of these reactions will take place increasingly often computationally.

<u>Pyrolysis of Jet Propellant 8, Jet Propellant 10, and aliphatic/non-aliphatic alkyl rings</u>

The initial reaction step began with the analysis of the components of a kerosene fuel named JP-8 by the United States Air Force. The JP-8 fuel was introduced in 1978 and fully replaced its precursor fuel JP-4 by 1995. A three-year grant has been obtained to determine the major products and rate constants of the main components that JP-8

forms after pyrolysis. Kerosene fuels are defined as fuels that consist mainly of hydrocarbons ranging from six to sixteen carbons in length. There is no set formula for JP-8 as it is created by the process of cracking where larger alkanes are broken down into smaller alkanes and alkenes. By percent weight some of the major components are dodecane (22.54%), decane (16.08%) and butylbenzene (4.72%). Alternatively, JP-10 is a synthetic fuel that is composed of a single tricyclic molecule. The main interest in the present study would be to enhance the efficiency of these fuels to reduce total operating costs by better understanding the products of the pyrolysis reactions these molecules undergo. There are four possible reactions that occur with these molecules upon pyrolysis which include carbon-carbon bond cleavage, H atom loss, beta scission, and direct hydrogen atom abstraction. The carbon-carbon bond cleavage and H atom loss processes are both barrierless reactions that occur because of the high temperatures found in the jet propulsion engines, whereas hydrogen atom abstraction requires a barrier to be overcome. The carbon-carbon bond cleavage results in unique sets of two hydrocarbon radicals while both the H loss and abstraction reactions result in unique hydrocarbon radicals at different locations. Afterwards, each separate radical can undergo a process known as beta scission. During beta scission the free radical that is formed reacts with itself to form an alkene and another smaller hydrocarbon radical.
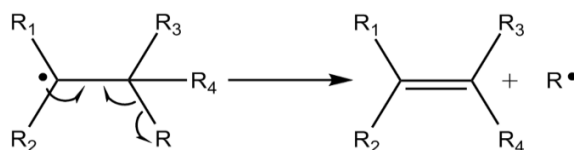
Mechanism of Beta Scission

 Any hydrocarbon radical larger than propyl can go through the beta scission reaction and accounts for experimental results indicating that the major end product is an alkene.

Analysis of these molecules will allow for the design of choosing more efficient molecules for use in future versions of jet propellants.

Oxidation of Polycyclic Aromatic Radicals

Incomplete combustion reactions lead to the formation of soot particles that can aggregate and contaminate the environment. The major anthropogenic source of these soot particles involves transportation that depends on the burning of fossil fuels and any use of combustion engines. Naturogenic sources of soot include volcanoes, forest fires, industrial plants and leakage from storage facilities. Soot is a mixture of impure carbon particles that when created from gas phase combustion reactions contain many PAHs. Polycyclic aromatic hydrocarbons negatively affect air quality and have been linked to increasing chances of heart disease and cancer.[6] Soot also contributes to global warming by acting as a short-term climate forcer in that it absorbs sunlight and directly heats the surrounding air and also changing reflecting surfaces to absorbing ones reducing the albedo.[7] Therefore, a deeper understanding of soot formation is necessary in order to combat its negative effects. The efficiency of removal methods can be increased by knowing the products of the reaction pathways to soot formation. Of particular interest is oxidation of PAH radicals as these species are highly reactive and can lead to larger more complex systems. When PAH or soot particles are oxidized they first undergo H-atom abstraction by another radical and then the PAH radicals can react with O_2.[8] By studying unique features of small systems it is hoped that patterns will emerge that can predict the behavior of large systems. Specific radicals that will be examined include phenanthrenyl, anthracyl, cyclopentadienyl, indenyl, and acenapthyl.
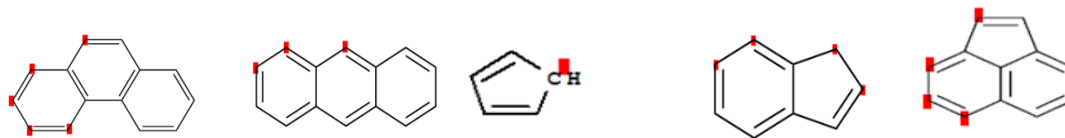
Phenanthrenyl, anthracyl, cyclopentadienyl, indenyl and acenapthyl
with varying radical positions

To achieve a characterization of the system that is within chemical accuracy computationally but can be extrapolated to larger systems radicals with different edge-like features were chosen. The oxidation of these species provides clear examples of large system motifs that can be categorized as armchair, zigzag, and 5-member ring configurations. From previous work it is hypothesized that oxidation of six member rings is dominated by elimination of an oxygen atom followed by elimination of CO which turns 6-member rings into 5-member rings. However there are other minor products that will form. Looking for aliphatic changes from 5-member rings to 6-member rings or ring openings is essential in determining the most common reaction pathways. Oxidation mechanisms, rate constants, and branching ratios calculated for these relatively small systems will allow for extrapolation of oxidation to larger systems.

<u>Formation of Large Hydrocarbons</u>

An important process to the many chemical environments is the growth of complex organic molecules. Complexity is introduced from the proliferation of larger and larger species providing access to larger ranges of products. However, the mechanisms of this growth are poorly understood even after decades of study. One of the many reasons contributing to the lack of data is that multiple environments need to be studied. For example, this work contains research done on the growth of PAHs in both low

temperature low pressure environments and in high temperature high pressure environments. Depending on the system of interest, the conditions can greatly alter the result. Polycyclic aromatic hydrocarbons in particular are of great interest because they are known to have a large impact on the environment and health, along with the fact that the decomposition of these compounds typically occurs on a slow timescale. These compounds are ubiquitous through industrialized areas and have been proven to cause tumors, birth defects, and many pulmonary diseases. Along with these complications PAHs also have been shown to be mutagenic and carcinogenic.[7] Numerous studies showed that emissions from coke and aluminum production, coal gasification, iron and steel founding, coal tars, coal tar pitches, and soot have produced lung cancer in humans. [8] The major formation path to these multicyclic PAHs in combustion occurs through the HACA (hydrogen abstraction/ C_2H_2 addition) mechanism.[9-18] The HACA mechanism is notable for having low reaction barriers, high exothermicities, and the typical abundance of acetylene, phenyl, and benzene in flame. [9]
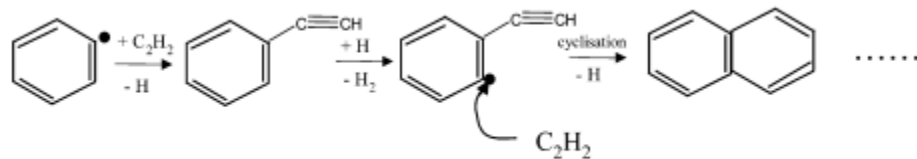
Schematic of the HACA mechanism.

The HACA mechanism provides a pathway that is commonly available in combustion systems that allows for the presence of many larger PAH species.

For low temperature growth PAHs the HACA is still viable however there are other pathways available. Conventional wisdom has dictated that PAH growth is a high temperature process involving multiple acetylene additions. However, investigation has shown a facile barrier-less synthesis from aryl-type radical additions.[19-24] The aryl-type

9

radical addition happens to conjugated hydrocarbons via RSFR intermediates and takes place primarily in the interstellar medium. The mechanism behind the aryl-type radical addition takes place via a weakly bound van-der-Waals complex which can isomerize and then form an RSFR that after hydrogen loss aromatizes. The van-der-Waals complex mechanism presents a novel pathway that changes the way that molecular growth processes of PAHs are understood and leaves open possibilities of finding more low temperature pathways.[24-30] Multiple pathways have been studied for all the above processes and new mechanisms continued to be discovered.

Objectives and Hypotheses:

1. Relevant decomposition reactions for alkyl chains of a varying length are expected to provide similar results and therefore decane and dodecane initial pyrolysis and secondary decomposition reactions will be studied.
2. Alkyl-substituted benzenes are expected to behave similar to alkyl chains in that the stability of the aromaticity of the species prevents reactions directly to the ring.
    a. It is expected that growth of larger aromatic systems can be supported by this and will explain the presence of PAHs in combustion systems
3. The tricyclic compound JP-10 (*exo*-tetrahydrodicyclopentadiene) is expected to behave similarly to alkyl chains in some aspects while providing unique features typical for highly strained cyclic alkane compounds.
4. The formation of larger more complex PAH systems is observed through the reaction of small hydrocarbons and expected to contribute to the formation of C_7H_7 isomers, a suspected pathway to PAH growth.

5. Growth of PAHs is expected to primarily be a high temperature phenomenon. However, a low temperature mechanism is shown to be feasible.

6. Pyrolysis modeling of fundamental classes of molecules creates a systematic understanding of combustion at the highest level.

7. Growth of aromatic systems in the interstellar medium if understood can give insight not only to the evolution of carbon-containing molecules in the Universe but also to the formation of prebiotic molecules.

8. High level ab initio calculations on unique surfaces of aromatic systems will lead to improvements of combustion engines and reduction of environmental pollution.

Enhancement of combustion models leads to a deeper fundamental understanding of a major chemical reaction.

References:

1. Turns, S. R. (1996). *An introduction to combustion* (Vol. 499). New York: McGraw-Hill.

2. Russell, Glen A. "Oxidation of Unsaturated Compunds. III. Products of the Reaction of Indene and Oxygen; Stereochemistry of the Addition of a Peroxy Radical and Oxygen to a Double Bond1." *Journal of the American Chemical Society* 78.5 (1956): 1035-1040.

3. Raj, Abhijeet, et al. "Structural effects on the oxidation of soot particles by O 2: Experimental and theoretical study." *Combustion and Flame* 160.9 (2013): 1812-1826.

4. Truhlar, Donald G., William L. Hase, and James T. Hynes. "Current status of transition-state theory." *The Journal of Physical Chemistry* 87.15 (1983): 2664-2682.

5. Kislov, V. V., A. I. Sadovnikov, and A. M. Mebel. "Formation mechanism of polycyclic aromatic hydrocarbons beyond the second aromatic ring." *The Journal of Physical Chemistry A*117.23 (2013): 4794-4816.)

6. Mulas, G., et al. "Estimated IR and phosphorescence emission fluxes for specific polycyclic aromatic hydrocarbons in the Red Rectangle." *Astronomy & Astrophysics* 446.2 (2006): 537-549.

7. Walsh, Michael. "Global trends in motor vehicle pollution control: a 2011 update. Part 1." *Silniki Spalinowe* 50 (2011): 106-117.

8. Kislov, V. V., A. I. Sadovnikov, and A. M. Mebel. "Formation mechanism of polycyclic aromatic hydrocarbons beyond the second aromatic ring." *The Journal of Physical Chemistry A*117.23 (2013): 4794-4816.

9. Hassouni, K., F. Mohasseb, F. Bénédic, G. Lombardi, and A. Gicquel. "Formation of soot particles in $Ar/H_2/CH_4$ microwave discharges during nanocrystalline diamond deposition: A modeling approach." *Pure and Applied Chemistry* 78, no. 6 (2006): 1127-1145.

10. Yan, Jian, et al. "Photomutagenicity of 16 polycyclic aromatic hydrocarbons from the US EPA priority pollutant list." *Mutation Research/Genetic Toxicology and Environmental Mutagenesis* 557.1 (2004): 99-108.

11. Bond, Tami C., et al. "Bounding the role of black carbon in the climate system: A scientific assessment." *Journal of Geophysical Research: Atmospheres* 118.11 (2013): 5380-5552.

12. Lewars, Errol G. *Computational chemistry: introduction to the theory and applications of molecular and quantum mechanics*. Springer Science & Business Media, 2010.

13. Lewars, Errol. "The concept of the potential energy surface." *Computational Chemistry: Introduction to the Theory and Applications of Molecular and Quantum Mechanics* (2003): 9-41.

14. Dreizler, Reiner M., and Eberhard KU Gross. *Density functional theory: an approach to the quantum many-body problem*. Springer Science & Business Media, 2012.

15. DeYonker, Nathan J., et al. "The correlation-consistent composite approach: Application to the G3/99 test set." *The Journal of Chemical Physics* 125.10 (2006): 104111.

16. Davidson, Ernest R., and David Feller. "Basis set selection for molecular calculations." *Chemical Reviews* 86.4 (1986): 681-696.

17. Pechukas, Philip. "Transition state theory." *Annual Review of Physical Chemistry* 32.1 (1981): 159-177.

18. Tokmakov, Igor V., et al. "The reaction of phenyl radical with molecular oxygen: a G2M study of the potential energy surface." *The Journal of Physical Chemistry A* 109.27 (2005): 6114-6127.

19. Lin, Chin-Yu, and M. C. Lin. "Unimolecular decomposition of the phenoxy radical in shock waves." *International Journal of Chemical Kinetics* 17.10 (1985): 1025-1028.

20. Colussi, A. J., F. Zabel, and S. W. Benson. "The very low-pressure pyrolysis of phenyl ethyl ether, phenyl allyl ether, and benzyl methyl ether and the enthalpy of formation of the phenoxy radical." *International Journal of Chemical Kinetics* 9.2 (1977): 161-178.

21. Harrison, A. G., et al. "Free radicals by mass spectrometry. XX. Ionization potentials of cyclopentadienyl and cycloheptatrienyl radicals." *Journal of the American Chemical Society* 82.21 (1960): 5593-5598.

22. Schmoltner, Anne Marie, Deon S. Anex, and Yuan T. Lee. "Infrared multiphoton dissociation of anisole: production and dissociation of phenoxy radical." *The Journal of Physical Chemistry* 96.3 (1992): 1236-1240.

23. Olivella, Santiago, Albert Sole, and Angel Garcia-Raso. "Ab initio calculations of the potential surface for the thermal decomposition of the phenoxyl radical." *The Journal of Physical Chemistry* 99.26 (1995): 10549-10556.

24. Zhou, Chong-Wen, Vadim V. Kislov, and Alexander M. Mebel. "Reaction Mechanism of Naphthyl Radicals with Molecular Oxygen. 1. Theoretical Study of the Potential Energy Surface." *The Journal of Physical Chemistry A* 116.6 (2012): 1571-1585.

25. Altarawneh, Mohammednoor, et al. "Theoretical study of reactions of HO_2 in low-temperature oxidation of benzene." *Combustion and Flame* 157.7 (2010): 1325-1330.

26. Klippenstein, Stephen J., Vijay S. Pande, and Donald G. Truhlar. "Chemical kinetics and mechanisms of complex systems: A perspective on recent theoretical advances." *Journal of the American Chemical Society* 136.2 (2014): 528-546.

27. Fernández-Ramos, Antonio, et al. "Modeling the kinetics of bimolecular reactions." *Chemical Reviews* 106.11 (2006): 4518-4584.

28. Parker, Dorian SN, et al. "Toward the Oxidation of the Phenyl Radical and Prevention of PAH Formation in Combustion Systems." *The Journal of Physical Chemistry A* 119.28 (2014): 7145-7154.

29. Kislov, V. V., et al. "Rate coefficients and product branching ratios for the oxidation of phenyl and naphthyl radicals: A theoretical RRKM-ME study." *Proceedings of the Combustion Institute* 35.2 (2015): 1861-1869.

30. Carpenter, Barry K. "Computational prediction of new mechanisms for the reactions of vinyl and phenyl radicals with molecular oxygen." *Journal of the American Chemical Society* 115.21 (1993): 9806-9807.

CHAPTER II

Theoretical Approach and Methodology:

Potential Energy Surface

To utilize computational models efficiently, the concept of a potential energy surface is necessary. Understanding of chemical reactions can be greatly enhanced by considering a landscape of all possible geometry configurations available to a system. Solutions to the Schrodinger equation are greatly simplified by making the Born-Oppenheimer approximation which allows for the separation of the electronic and nuclear terms in its formulation. A powerful benefit from making the Born-Oppenheimer approximation is that by treating nuclei as having fixed positions in comparison to electrons, potential energy functions can be written that describe the geometry of the molecule of interest. A surface can then be generated that describes all possible conformations and chemical reactions available to a system on the basis of favorable or unfavorable nuclear arrangements. The Born-Oppenheimer approximation cannot be applied to all systems. However, it is relevant to all systems under study here.

The approach to all systems treated here will be mostly equivalent. Systems will be studied by mapping out their respective Potential Energy Surfaces (PES). A PES is a mathematical function describing the geometry of a species and its relation to the species energy. Contained on the PES are all configurations possible for the nuclei to take and thusly contains 3N-6 coordinate dimensions once redundant degrees of freedom are removed, those that relate to translation and rotation.[1] For a linear molecule, rotation about the axis of the molecule is also redundant reducing the coordinate dimensions to 3N-5. The chemical application of the surface requires the identification of stable species that directly determine what the reaction products will be. In a mathematical sense the stable species can be defined as minima along the surface

where the second derivatives of potential energy with respect to the coordinate systems are positive while the gradient change itself is zero. In between these minima lie transition states that while the energy gradient is still zero the second derivative with respect to the reaction coordinate is now negative describing a structure where energy will decrease in with any conformation change. Therefore, the structure acts as a barrier to the overall reaction between the minima they connect.

Calculations are done using Density Functional Theory and the specific functional used for this work is the hybrid density functional Becke's 3-parameter Lee Yang Parr (B3LYP). With this method, zero-point energies and harmonic frequencies are calculated to use for the calculation of relative energies and rate constants for use in tandem with the potential energy surfaces to describe a chemical system.[2] The harmonic frequencies are especially useful to identify optimized structures such as minima or transition states. The errors associated with the B3LYP functional are around 0.004 Å for bond lengths and 30 cm^{-1} for vibrational frequencies along with 9.6 kcal/mol for energetics. The composite G3 technique will be used to improve upon energetics which have typical errors in the range of 0.9 kcal/mol. The G3 composite method incorporates a basis set correction calculated thusly

E (total) = E(CCSD(T)/6-311G**)+E(MP2/G3)-E(MP2/6-311G**)+E(ZPE/B3LYP)

and includes using other theories such as Moller-Plesset (MP) and Couple Cluster (CCSD(T)) methods.[3] These energy refinements mainly rely on the robustness of coupled-cluster methods with single and double excitations with perturbative approximation to triple excitation,which while highly accurate, scale very rapidly in terms of computation time and are prohibitively expensive for large systems.

TRANSITION STATE THEORY

In regard to confirming the paths elucidated from potential energy surfaces, an important comment must be made. There are paths between reactants and products that define the surface and potential wells. These paths need to be specified as being the boundary points or barriers that will determine the overall reaction. These barriers are the point of no return that cause energetic species to fall into wells where they are thermalized and remain as irreversible stable products. Formally this involves treating the potential energy surface so that instead of considering all possible reactions, only relevant, meaning competing energetically with each other, portions of the surface need be considered. A large assumption made here is that a surface exists such that there is a region pertaining to reactants and a region pertaining to products where transition states paths do not flow back into the reactant region. If this holds true than the kinetics of the entire system is controlled by the flux of these paths into the reactant surface. Thusly the rate constant can be defined as the limiting step to the local reaction potential energy surface through the reactant region surface to the product region surface in the forward direction.[4] In terms of energetic barriers, the reactant molecule that crosses a barrier is then placed onto a minimum on the product region where it can be thermalized. From the thermalized minimum the molecules future behavior is then changed to be considered a reactant molecule again. Rate constants can then be calculated through statistical mechanics that depends on various molecule specific features such as partition functions, vibrational frequencies, and barrier heights of the potential energy surface.

MASTER EQUATION

Modeling kinetics is one of the most chemically complex tasks currently being studied. Most reactions of interest are rarely straightforward or involve only a single set of products. Therefore, the formalism created to study them must involve multiple possibilities or wells that can be inhabited by all the interconnected channels that are possible. The most basic method of expressing the modeling that is used here is as such

$$\frac{dn_i(t)}{dt} = \sum_j (p_{ij} n_j(t) - p_{ji} n_i(t))$$

where $n_i(t)$ is a measure of probability of a particular molecule being in a state i at a time t and p_{ij} is the probability per time of a transition from state j to state i. Therefore $n_i(t)$ is regarded as the population of molecules in a sufficiently large group.[5] The equation describes the time evolution of the populations of the species of interest. The equation is known as the Pauli master equation and can be derived from Schrodinger equation describing the evolution over time of a many body system. It is important to note that the Pauli master equation only applies in chaotic systems as it relies on properties of microscopic systems. The master equation is effective in describing a change in systems of limited quantum states, such as diatomics. As degrees of freedom increase the usefulness of the Pauli equation becomes limited as there are simply too many states of interest available. For combustion modeling typically multi atom systems are being collided against each other at high energies meaning the density of quantum states is quite large, causing modeling to be problematic. Consequently, a different formalism that followed the master equation concept was developed. To discuss the types of systems modeled kinetically in this work it is useful to describe a general form the reactions adhere to.

A basic kinetic system can be modeled as follows

$$A + B \leftrightarrow products$$
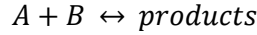
where A is in this case a radical or reactive species and B is a reactant. It is also assumed here that the model reaction takes place in conditions where a third component, C, is present. The component labeld C is an inert bath gas that is in excess concentration to both A and B while also allowing the reactive species enough to time to stabilize in order to react with B.

The full master equation for conditions as described above can be given as follows

$$\frac{dn_i(E,J)}{dt} = Z_i \sum_{\cap} \int_{E_{0_i}}^{\infty} P_i(E,J;E',J')n_i(E',J')dE' - Z_i n_i(E,J) - \sum_{j \neq i}^{M} k_{ji}(E,J)n_i(E,J)$$

$$+ \sum_{j \neq 1}^{M} k_{ij}(E,J)n_j(E,J) - k_{d_i}(E,J)n_i(E,J) + k_{a_i}(E,J)n_A n_B \rho_{AB}(E,J)e^{\frac{-\beta E}{Q_{AB}}}$$

$$- \sum_{p=1}^{N_p} k_{p_i}(E,J)n_i(E,J)$$

$$i = I, \dots, M$$

The equation the concentration of isomer *i* in the reaction schema of interest, which corresponds to an *i*th minima of the surface with energy between *E* and *E*+d*E*, is given with $n_i(E,J)dE$. The collision rate of the complex is given by Z, the ground state energy by E_0, collision transfer probability by $P_i(E,J;E',J')$, unimolecular rate coefficient from minima *j* to minima *i* for isomerization by $k_{ij}(E,J)$, dissociation coefficient by k_{d_i}, the rate coefficient for dissociation to bimolecular products by k_{p_i}, number of products by N_p,

number of wells by A and the reactant partition function is given by Q_{AB}.[5] The formulation

is extremely powerful in describing chemical systems however it also demands a large

amount of information. Particularly the inclusion of the angular quantum number J and

partition functions of all reactant species. Finding this involves solving a complicated

convolution of state densities of fragments A and B. To sidestep this issue we take this

two-dimensional master equation into the form below, the one-dimensional master

equation.

$$\frac{dn_i(E)}{dt} = Z_i \sum \int_{E_{0_i}}^{\infty} P_i(E,E')n_i(E')dE' - Z_i n_i(E) - \sum_{j \neq i}^{M} k_{ji}(E)n_i(E) + \sum_{j \neq 1}^{M} k_{ij}(E)n_j(E)$$

$$- k_{d_i}(E,J)n_i(E,J) + K_{eqi}k_{d_i}(E)F_i(E)n_A n_B - \sum_{p=1}^{N_p} k_{p_i}(E,J)n_i(E,J)$$

$$i = I, \dots, M$$

Rather than considering contributions from J only E is considered an independent

variable. Only taking contributions from the E terms vastly simplifies the amount of

information required to properly solve for rate coefficients.[6-10] Added to the master

equation is an equilibrium constant, K_{eqi}, and equilibrium population distribution, $F_i(E)$,

which is how the need for the partition function is excluded. Thermal equilibrium is

assumed here as long as the reactants are in equilibrium with the bath gas and this

assumption has been shown to be experimentally accurate. This is accurate for all

combustion, atmospheric, and chemical-vapor-deposition modeling.

There are some assumptions worth mentioning that are made in this equation.

This involves the collisional energy transfer term Z. The assumptions are that any rate

coefficient involving energy transfer can be split into two terms: collision rate and a

probability density function. It is also assumed that the collision rate is a constant

independent of energy. The collisional energy transfer term Z is commonly chosen to be

the Lennard-Jones collision rate which is accurate for weak collisions but quickly

becomes insufficient for large molecules. When appropriate this collisional energy

transfer term can be adjusted empirically.[10] Another important distinction about transition

probabilities that appear in these master equations is they involve the flux from one state

to another, or from one set of states to another. An exponential down model was also

used to treat the probabilities of inducing a given transition.[10]

The Rice-Ramsperger-Kassel-Marcus (RRKM) theory Master equation method

will be used to calculate pressure and temperature dependent rate constants and

branching ratios of the various oxidation reactions occurring.[11-13] The RRKM-ME method

is completely *a priori* and uses a solution of the one-dimensional master equation

(1DME) for the simple dissociation reaction A->B+C. The reverse rate constant is related

by the equilibrium constant. The 1DME represents the time variation of energy

dependent species populations in terms of the energy transfer rates and dissociation

rate constants. All kinetics calculations are done without experimental parameters and

these dissociation rate constants are calculated using variable reaction coordinate

transition state theory. Analytical representations are used for the characterization of the

energy transfer rate constants. This modeling requires precise information of the

potential energy surface as discussed earlier and require the use of transition state

theory.

References

1. Lewars, Errol. "The concept of the potential energy surface." *Computational Chemistry: Introduction to the Theory and Applications of Molecular and Quantum Mechanics* (2003): 9-41.

2. Lewars, Errol G. *Computational chemistry: introduction to the theory and applications of molecular and quantum mechanics.* Springer Science & Business Media, 2010.

3. DeYonker, Nathan J., et al. "The correlation-consistent composite approach: Application to the G3/99 test set." *The Journal of Chemical Physics* 125.10 (2006): 104111.

4. Pechukas, Philip. "Transition state theory." *Annual Review of Physical Chemistry* 32.1 (1981): 159-177.

5. James A. Miller* and Stephen J. Klippenstein *The Journal of Physical Chemistry A* (2006) *110* (36), 10528-10544

6. Dreizler, Reiner M., and Eberhard KU Gross. *Density functional theory: an approach to the quantum many-body problem.* Springer Science & Business Media, 2012.

7. Davidson, Ernest R., and David Feller. "Basis set selection for molecular calculations." *Chemical Reviews* 86.4 (1986): 681-696.

8. Klippenstein, S. J.; Miller, J. A. From the Time-Dependent, Multiple-Well Master Equation to Phenomenological Rate Coefficients. *The Journal of Physical Chemistry* A 2002, 106, 9267-9277.

9. Georgievskii, Y.; Miller, J. A.; Burke, M. P.; Klippenstein S. J. Reformulation and Solution of the Master Equation for Multiple-Well Chemical Reactions. *The Journal of Physical Chemistry* A 2013, 117, 12146−12154.

10. Truhlar, D. G.; Garrett, B. C.; Klippenstein, S. J. Current Status of Transition-State Theory. *The Journal of Physical Chemistry* 1996, 100, 12771-12800.

11. Georgievskii, Y.; Klippenstein, S. J. Variable Reaction Coordinate Transition State Theory: Analytic Results and Application to the C2H3 + H → C2H4 Reaction. J. Chem. Phys. 2003, 118, 5442-5455.

12. Truhlar, D. G.; Garrett, B. C. Variational Transition State Theory. *Annual Review of Physical Chemistry* 1984, 35,159-189.

13. Steinfeld, J.I.; Francisco, J.S.; Hase, W.L. Chemical Kinetics and Dynamics; PrenticeHall: Upper Saddle River, NJ, 1999.

CHAPTER III

Combined Experimental and Computational Study on the Unimolecular Decomposition
of JP-8 Jet Fuel Surrogates. I. n-Decane (n-$C_{10}H_{22}$)

Introduction

Kerosene-based jet fuel JP-8 presents the single battlefield fuel for the US Air Force and Army equipment. It consists of several hundred hydrocarbons, which can be grouped into four main classes: (i) aliphatic "paraffins" (33−61% n-alkanes and isoalkanes; 1−5% olefins), (ii) monocyclic "paraffins" (10− 20%), (iii) alkyl-substituted benzenes (12−22%), and (iv) polycyclic aromatic hydrocarbons (PAHs) (10−20%); additives acting as fuel system icing inhibitors, corrosion inhibitors, and static dissipaters at the subpercent level complement the mixture.[1−11] Because of the chemical complexity of JP-8, engineering and combustion scientists have been searching for surrogate fuels that can reasonably represent the performance and emissions behavior of JP-8 jet fuel engines thus providing a baseline for performance and emissions.[12−23] The scientific community concluded that accurate modeling of the combustion of JP-8 jet fuel is currently not feasible because of the chemical complexity. Therefore, surrogate fuel and their mixtures are considered as a key step toward modeling and understanding the combustion of practical aviation fuel.[3,24−26] Single-component fuels are adequate for simple applications like combustion efficiency, while multicomponent surrogates are required for chemistry-dependent applications such as soot formation and emissions, combustion staging, and numerical modeling of flames.[27] The development of these chemical kinetic models requires accurate input parameters and an intimate understanding of the very first processes, which initiate bond rupture processes in JP8 surrogates, provide a pool of radicals, and control the autoignition, under realistic, combustion relevant physical conditions.[10,26,28−30] These are typically temperatures up to 1600 K and pressures up to a few atmospheres. In principle, the unimolecular decomposition and "pyrolysis" of these surrogates leads to smaller hydrocarbon molecules and reactive transient species, among them aliphatic radicals, resonantly

stabilized free radicals (RSFRs), and aromatic radicals (ARs), which initiate and drive the complex chemistry in the combustion of JP-8 based jet fuel. Here, the initial decomposition chemistry is often dubbed as "delivering the building blocks" for the oxidation of JP-8 based jet fuel. Nevertheless, despite decades of research, the fundamental question "What are the basic, most fundamental processes, which initiate the combustion of JP-8 based jet fuel?" has not been resolved to date, predominantly because well-defined experimentally derived mechanistic information and identification of the nascent pyrolysis products are lacking with about 95% of the reaction pathways in models being "assumed"; which even holds for sophisticated chemical kinetic models of n-alkane surrogates such as n-decane and n-dodecane.[31–37] However, detailed data on the mechanism and products formed in the initial decomposition steps of JP-8 based fuel components are crucial to elucidate the underlying reaction mechanisms how JP-8 based engines are operating. Therefore, an innovative approach is carried out here to investigate the decomposition ("pyrolysis") of prototype JP-8 jet fuel surrogates and to probe the nascent product(s) together with the underlying mechanisms comprehensively thus advancing the current understanding of these fundamental, elementary processes, which initiate and drive the complex chemistry in the combustion of JP-8 based jet fuel

The current study revealed that n-decane was mainly consumed via hydrogen abstraction reactions followed by β-scission to form small C1 to C6 products. High-level theoretical data on the structure and energetics of the surrogate molecules and their decomposition products are sparse owing to their relatively large molecular size. Multiple combined experimental and theoretical studies devoted to the conformational stability and the molecular shape, rotational constants, and ionization energies of n-decane and n-dodecane were conducted.[34] Considering the thermochemical properties, density functional theory (DFT) calculations were performed to evaluate the enthalpy of

formation of n-decane and n-dodecane together with their C−C bond dissociation energies.[35] Finally, we would like to address briefly modeling studies on the JP-8 surrogate n-decane. Ranzi et al.[47] generated a wide range kinetic modeling study of the pyrolysis, partial oxidation, and combustion of n-alkanes including n-decane, n-dodecane, and n-hexadecane. A work that is a comprehensive experimental and modeling investigation on n-decane, unravelling its pyrolysis and oxidation properties at both low and high pressures. Whereas these investigations yielded valuable information on the formation of closed-shell hydrocarbon intermediates and products, these species were mainly analyzed off-line and *ex situ* (HPLC, GC MS); neither HPLC nor GCMS can sample radical transient species nor thermally labile closed-shell molecules. Therefore, the "molecular inventory" might have been altered since its formation, crucial reaction intermediates cannot be sampled, and detailed information on the reaction mechanisms the role of radicals and intermediates cannot always be obtained but are at best inferred indirectly and qualitatively. On the basis of these considerations, a novel methodology to investigate the unimolecular decomposition of JP-8 fuel surrogates is necessary. An approach which requires probing the open- and closed-shell products online and in situ without changing the initial "molecular inventory" and exploiting versatile, nonspectroscopic detection systems so that the complete product spectrum can be sampled quantitatively. These studies will be combined with electronic structure calculations to yield a unified picture on the temperature and pressure dependent decomposition mechanisms of JP-8 jet fuel surrogates. The present investigation represents the first in a series of combined experimental and theoretical studies to probe the pyrolysis and decomposition of prototype JP-8 jet fuel surrogates: n-decane ($C_{10}H_{22}$). Finally, by carrying out molecular beam experiments and combining these studies with electronic structure calculations, we elucidate data on the products, their branching

ratios, and reaction mechanisms involved in the decomposition of JP-8 surrogates over a broad range of combustion-relevant temperatures and pressures.

Methods:

Geometries of n-decane and its primary and secondary decomposition products as well as transition states for secondary decomposition reactions (isomerizations and C−C and C−H bond β-scissions) and for direct hydrogen atom abstractions by hydrogen atoms have been optimized using the density functional B3LYP method with the 6-311G(d,p) basis set. Vibrational frequencies of various local minima and transition states have been computed at the same level of theory. Relative energies for all species have been refined by single-point calculations at the G3(CCSD,MP2) level of theory,[38-40] which included the empirical higher level correction (HLC),[41] using B3LYP/6-311G(d,p) optimized geometries and including zero-point vibrational energy corrections (ZPE) also obtained at B3LYP/6-311G(d,p). The inclusion of the HLC increases the calculated strengths of C−H bonds by 7 kJ mol^{-1}, decreases relative energies of transition states and products for the $C_{10}H_{22} + H \rightarrow C_{10}H_{21} + H_2$ hydrogen atom abstraction reactions also by 7 kJ mol^{-1}, is insignificant for C−C bond cleavages, and zero by definition for C−C bond β-scissions. The G3(CCSD,MP2)//B3LYP theoretical level is expected to provide the energetic parameters with "chemical accuracy" within 3−6 kJ mol^{-1} in terms of average absolute deviations.[41] The ab initio calculations were performed using the GAUSSIAN 09[41] and MOLPRO 2010[39] program packages. Rate constants for various primary and secondary reactions involved in the pyrolysis of n-decane have been computed by solving the one-dimensional master equation[39] using the MESS package.[40] Here, rate constants k(T) for individual reaction steps were calculated within RRKM (unimolecular reactions) or transition state theory (TST, bimolecular reactions) generally

utilizing the rigid-rotor, harmonic-oscillator (RRHO) model for the calculations of partition functions for molecular complexes and transition states. Collisional energy transfer rates in the master equation were expressed using the "exponential down" model,[40] with the temperature dependence of the range parameter α for the deactivating wing of the energy transfer function expressed as $\alpha(T) = \alpha_{300}(T/300 \text{ K})^n$, with $n = 0.86$ and $\alpha_{300} = 228 \text{ cm}^{-1}$ obtained earlier from classical trajectories calculations as "universal" parameters for hydrocarbons in the nitrogen bath gas.[40] We used the Lennard-Jones parameters $(\varepsilon/\text{cm}^{-1}, \sigma/\text{Å}) = (237, 5.02)$ for the n-decane/ nitrogen system derived by Jasper et al.[41] using the fit of results using the "one-dimensional optimization" method.[39] For β-scission reactions of smaller 1-alkyls we employed Lennard-Jones parameters for the corresponding n-alkane/N_2 combinations also derived by Jasper et al.[39] Two issues are challenging in rate constant calculations, the treatment of barrierless reactions, such as the C−C and C−H single bond cleavages in the original n-decane molecule, and the description of multiple (and often coupled) hindered rotors in the molecule and radical products, which possess a large number of single bonds. Since our goal here is not quantitative prediction of reaction rate constants but rather qualitative evaluation of relative yields of various products at different stages of the pyrolysis in order to account for the observed experimental results, we utilized a number of approximations to address these issues. First, the barrierless single-bond cleavage reactions were treated using phase space theory with the empirical potential energy parameters selected in such a way that the calculated rate constants for the reverse $C_xH_y + C_{10-x}H_{22-y}$ and $C_{10}H_{21} + H$ radical recombination reactions reproduce the rate constants for the prototype $C_2H_5 + C_2H_5$ and $C_2H_5 + H$ reactions in the experimental 1100−1600 K temperature interval studied earlier by Klippenstein and coworkers[40,41] using the most accurate up-to-date theoretical approach, variable reaction coordinated transition state

theory (VRC-TST). Second, the hindered rotor treatment was applied only to smaller C_3H_7 and C_4H_9 radicals while dealing with their β-scission reactions. For these species, soft normal modes were visually examined and those representing internal rotations were considered as one-dimensional hindered rotors in partition function calculations. For larger alkyl radicals, C_5H_{11}, C_6H_{13}, C_7H_{15}, C_8H_{17}, and C_9H_{19}, only terminal CH_2, CH_3, and C_2H_4 rotations were treated as hindered rotors, whereas all other convoluted rotations were treated as harmonic oscillators. One-dimensional torsional potentials were calculated by scanning PESs at the B3LYP/6-311G(d,p) level of theory. For comparison, we also performed calculations of the same rate constants in pure RRHO approximation and found that the replacement of harmonic oscillators with hindered rotors increases the β-scission rate constants by 8− 41% at 1000 K, but the difference drops to only 2−25% at 1600 K. For n-decane and decyl radicals, visual identification of internal rotations is not practically possible because those are coupled with one another and with other types of motions. Therefore, these species were treated within RRHO keeping in mind the above-mentioned error bars in rate constants. At the same time, the expected errors in ratios of rate constants are expected to be smaller than the errors in their absolute values as a consequence of the cancelations of similar inaccuracies. Hence we anticipate that the relative product yields are predicted by our calculations with significant accuracy.

Results and Discussion:

In order to understand the mechanism of n-decane pyrolysis and to account for the products observed experimentally, we computed the potential energy diagrams for the unimolecular decomposition of n-decane ($C_{10}H_{22}$) along with the primary products as a first step. The n-decane molecule can break apart by initial cleavage of various C−C

reaction R1) and C−H bonds (reaction R2 producing pairs of 1-alkyl radicals and n-decyl radicals plus a hydrogen atom, respectively.

$$C_{10}H_{22} \rightarrow + C_xH_y + Cx'H_{y'} \text{ (R1)}$$

$$C_{10}H_{22} \rightarrow C_{10}H_{21} + H \qquad \text{(R2)}$$
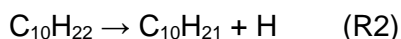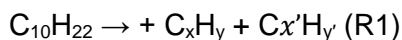
Homolytic C−C and C−H Bond Cleavages and Consecutive β-Scissions (C−C; C−H). Let us consider first the C−C bond cleavages as illustrated in Figure 3.1. The strengths of the C−C bonds are computed to be in the range of 360−368 kJ mol^{-1}, with the C2−C3 bond being the weakest and the C4−C5 bond being the strongest. However, the differences in the C−C bond strengths are rather small and hence it is reasonable to expect that all product pairs, CH_3 + C_9H_{19}, C_2H_5 + C_8H_{17}, C_3H_7 + C_7H_{15}, C_4H_9 + C_6H_{13}, and C_5H_{11} + C_5H_{11}, can be in principle formed. Alternatively, the strengths of C−H bonds appeared to be significantly higher than C-C bonds, in the 406−418 kJ mol^{-1} range. Here, primary C1−H bonds in terminal CH_3 groups are the strongest and secondary C−H bonds in CH_2 groups vary in a very narrow interval of 406−408 kJ mol^{-1}. These results are consistent with the corresponding experimental C−C and C−H bond strengths in n-butane, propane, and ethane evaluated taken from the enthalpies of formation at 0 K from the Active Thermochemical Tables.[91] The difference in the bond strengths makes rate constants for the C−H cleavages 4−5 orders of magnitude slower than those for the C−C cleavages and, hence, the cleavage of the C−C bonds is anticipated to be the dominant process in $C_{10}H_{22}$ unimolecular decomposition. In the temperature range of 1000−1600 K and 1 atm, the rate constants for the C−C cleavages exhibit well-defined Arrhenius behavior and grow from few s^{-1} to 1−2 × 10^6 s^{-1}. These values are in accord with the experimental observations that only a small fraction of n-decane is consumed at 1100 K, but no parent molecules survive above 1500 K during the residence time, which

is tens of microseconds. The computed rates to cleave different C−C bonds are close to each other, and grow to $3-6 \times 10^7 \, \text{s}^{-1}$ at 2500 K, except for the one to produce CH_3 + C_9H_{19}, which remains more than an order of magnitude lower. The calculated relative product yields 1.6−1.7% for CH_3 + C_9H_{19}, 37.7−34.1% for C_2H_5 + C_8H_{17}, 19.1−19.2% for C_3H_7 + C_7H_{15}, 16.6−18.3% for C_4H_9 + C_6H_{13}, and 25.0−26.7 for C_5H_{11} + C_5H_{11} in the 1000−1600 K interval, exhibiting only slight temperature dependence up to 2500 K. Calculations at different pressures from 600 Torr to 100 atm show that the product branching ratios are practically independent of pressure. Summarizing, the pyrolysis of n-decane at 1500 K and above is predicted to predominantly produce a mixture of 1-alkyl radicals, from ethyl to 1-octyl, on the time scale of 1 µs or less. The 1-alkyl radicals appeared to be unstable at the experimental conditions and are subjected to a rapid C−C bond β-scission producing ethylene C_2H_4 in conjunction with a two carbon shorter 1-alkyl. As seen in Figure 3.1 and Table 3.2, the calculated barrier heights and reaction energies for the C−C bond β-scissions are 123−126 and 86−90 kJ mol^{-1}, respectively. The computed rate constants for C−C bond β-scissions are approximately in the range of $10^7-10^8 \, \text{s}^{-1}$ in the experimental temperature interval. Thus, the lifetimes of the primary dissociation products, 1-alkyl radicals, is shorter than 1 µs under the experimental conditions and they are predicted to rapidly decompose forming the ultimate products C_2H_4, CH_3, and C_2H_5 as detected experimentally via the stepwise mechanism shown below. The ethyl radical would further lose an H atom via a C−H bond β-scission producing ethylene.

$$C_8H_{17} \rightarrow C_6H_{13} + C_2H_4$$

$$C_7H_{15} \rightarrow C_5H_{11} + C_2H_4$$

$$C_6H_{13} \rightarrow C_4H_9 + C_2H_4$$

$$C_5H_{11} \rightarrow C_3H_7 + C_2H_4$$

$$C_4H_9 \rightarrow C_2H_5 + C_2H_4$$

$$C_3H_7 \rightarrow CH_3 + C_2H_4$$

$$C_2H_5 \rightarrow H + C_2H_4$$
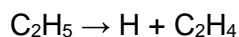
However, this mechanism cannot account for the experimental observation of higher 1-alkenes, especially propene and 1-butene, which are found among major pyrolysis products at 1100 K and are still significant up to 1400 K. One possibility to form 1-alkenes from 1-alkyl radicals is C−H bond β-scission, but the calculations show that C−H β-scission barriers are 20−26 kJ mol^{-1} higher than the corresponding C−C β-scission barriers in 1-alkyls from C_3H_7 to C_8H_{17}. The computed branching ratios for the C−H β-scission channels in C_4H_9 - C_8H_{17} are very small and do not exceed 1−2% until the highest temperatures and pressures (2,500 K and 100 atm), where they reach 5−6%. The relative yield of propene + H is higher from the n-propyl radical (C_3H_7) and constitutes 3−4% at 1100−1600 K and 1 atm increasing to 6%, 9%, and 13% at 2500 K and pressures of 1, 10, and 100 atm, respectively. Thus, C−H bond β-scissions cannot explain the large experimental yields of propene and 1-butene at low temperatures since they are unfavorable compared to the β-scissions involving loss of ethylene (C_2H_4). In summary, C−C bond cleavages leading to 1-alkyl radicals are strongly favored compared to C−H bond rupture processes; the higher 1-alkyl radicals (>C2) do not survive under our experimental conditions and decay via successive C−C β-scissions (C_2H_4 elimination), which dominate over C−H β-scission (alkene formation), to yield eventually the C1 to C2 hydrocarbons methyl (CH_3), ethyl, (C_2H_5), and ethylene (C_2H_4).

Hydrogen Migrations and Consecutive β-Scissions. Can the 1-alkyl radicals isomerize before they decompose by C−C bond β-scission? Isomerization channels involving 1,2- and 1,3-H atom shifts in C_3H_7 and C_4H_9 are not competitive because the corresponding hydrogen migration barriers are 157−162 kJ mol^{-1} , i.e., much higher than the C−C bond β-scission barriers. However, in higher 1-alkyl radicals, beginning from C_5H_{11}, a possibility of 1,4-H, 1,5-H, 1,6-H, and 1,7-H shifts eventually opens up (Figure 3.3). For instance, 1- pentyl can isomerize to 2-pentyl via a 1,4-H shift, 1-hexyl can isomerize to 2-hexyl and 3-hexyl via 1,5-H and 1,4-H shifts, respectively, 1-heptyl can rearrange to 2-, 3-, and 4-heptyls via 1,6-H, 1,5-H, and 1,4-H shifts, respectively, and 1-octyl can isomerize to 2-, 3-, and 4-octyls via 1,7-H, 1,6-H, and 1,5-H or 1,4-H shifts, respectively. Typical calculated barrier heights for 1,4-, 1,5-, 1,6-, and 1,7-H shifts are 92−94, 64−66, 71−72, and 80 kJ mol^{-1} and thus they are lower than that for the C−C bond β-scission of about 124 kJ mol^{-1} . These hydrogen shifts are followed by C−C β-scissions forming higher 1-alkenes rather than ethylene. For example, 2-pentyl dissociates to propene + C_2H_5, 3-hexyl decomposes to either 1-butene + C_2H_5 or 1-pentene + CH3. The C−C β-scission barriers in n-alkyls (n > 1) exhibit similar heights to those in 1-alkyls and hence all C−C β-scission channels are competitive. The calculated branching ratios presented in Tables S3−S6 of Supporting Information show large dependence on temperature and pressure. Qualitatively, at low pressures up to 1 atm, the products formed following a 1,5-H shift are preferable, but at high pressures of 10 and 100 atm the direct C−C β-scission from 1-alkyls producing ethylene (C_2H_4) dominates. Earlier, similar isomerization channels involving H shifts followed by C−C β-scissions producing higher 1-alkenes were proposed by Tsang and co-workers for 1-hexyl and 1-octyl radicals.[27] They derived high-pressure limit rate constants for decomposition and isomerization of hexyl and octyl radicals from shock tube

measurements in the ~850−1000 K temperature range and then deduced the pressure

dependence from a semiempirical RKKM-ME analysis. A comparison of the present

high-pressure limit rate constants with those proposed by Tsang et al. shows general

agreement within a factor or 2 or better in the experimental temperature range for

various β-scission processes. However, deviations are found to be higher for the H shift

reactions, for which the present calculations can overestimate the results reported by

Tsang et al. by up to a factor of 5. A direct comparison of the branching ratios of various

alkenes measured by Tsang et al. in the shock tube experiments from 1-hexyl and 1-

octyl is not warranted because of the fast secondary reactions decomposing smaller

alkyl radicals; the branching ratios are computed only for the primary decomposition.

Clearly, detailed kinetic modeling, which can utilize the rate constants derived here,

would be required for better description of the experimental data both in the shock tubes

and in the pyrolitic reactor, but this is beyond the scope of the present work. In summary,

the reaction mechanism involving hydrogen migration in C5 to C8 1-alkyl radicals

preceding C−C β-scission accounts for the observation of C3−C7 alkenes [propene, 1-

butene, 1-pentene, 1-hexene, and 1-heptene] as monitored in the experiments, and

especially, for the large branching ratios of C_3H_6 and C_4H_8 at low temperatures. At

temperatures of 1500 K and above the lifetime of a single C−C bond approaches 1 µs

and hence higher alkenes are likely to decompose on the time scale of the experiment

and their yield becomes insignificant.

Hydrogen Abstraction. The higher alkenes can be also produced by C−C bond β-

scissions in n-decyl radicals (n > 1, see Figure 3.1 and Table 3.2). While n-decyls are

unlikely to be formed by C−H bond cleavages in n-decane, they can be produced by

direct hydrogen abstractions by hydrogen atoms or other radicals in the reactive system

when such radicals become available. The calculated barrier heights and reaction

exoergicities for the hydrogen abstraction reactions by hydrogen from secondary C−H bonds are ~33 (26) and 23−24 (30−31) kJ mol^{-1} , where the values in parentheses include the HLC correction in the G3(CCSD,MP2) calculations. The hydrogen abstractions from the primary C−H bonds are less favorable exhibiting the barrier and the reaction exothermicity of 47 and 12 kJ mol^{-1}, respectively. The most accurate up-to-date calculations of hydrogen abstraction from C_3H_8 and C_2H_6 gave the reaction barriers and exoergicities as 32 and 27 kJ mol^{-1} , respectively, for the secondary hydrogen abstraction, and 43−44 and 15−16 kJ mol^{-1} for the primary hydrogen abstraction.[94] The calculated rate constants for secondary hydrogen abstractions are similar to each other and are much higher than those for the primary hydrogen abstraction indicating that the most likely products are 2-, 3-, 4- and 5-decyl radicals (Figure 3.1). It is noteworthy that the rate constants for secondary hydrogen abstractions evaluated here agree best with the literature data (the most accurate calculations for C_3H_8[39] and experimental data for C_3H_8, C_4H_{10}, and C_5H_{12}[40,41]) if the HLC correction is not taken into account, but for the primary hydrogen abstraction the agreement is better with the HLC correction. Still, the calculated rate constants for $C_{10}H_{22}$ + H secondary hydrogen abstractions overestimate the literature values for C_3H_8 from by factors of 2−2.5 at 500 K to factors 4−5 at 2500 K. For the primary hydrogen abstraction, the deviation is smaller and the $C_{10}H_{22}$ + H rate constants underestimate those for C_3H_8 + H by 20−50%. Apparently, a more rigorous anharmonic treatment of soft normal modes is required to generate more accurate hydrogen abstraction rate constants but this is beyond our goals in the present work. Here, our main conclusion that the secondary H abstractions are feasible and form n-decyl radicals (n > 1) with roughly equal yields. Once the n-decyl radicals are produced, they can rapidly undergo C−C bond β-scission to yield higher alkenes together with 1-alkyl radicals:

$$C_{10}H_{21} \text{ (2 decyl)} \rightarrow C_3H_6 + C_7H_{15}$$

$$C_{10}H_{21} \text{ (3 decyl)} \rightarrow C_9H_{18} + CH_3$$

$$\rightarrow C_6H_{13} + C_4H_8$$

$$C_{10}H_{21} \text{ (4 decyl)} \rightarrow C_8H_{16} + C_2H_5$$

$$\rightarrow C_5H_{10} + C_5H_{11}$$

$$C_{10}H_{21} \text{ (5 decyl)} \rightarrow C_7H_{14} + C_3H_7$$

$$\rightarrow C_6H_{12} + C_4H_9$$
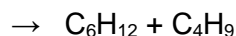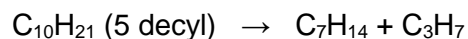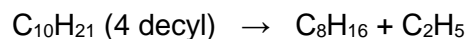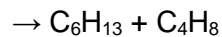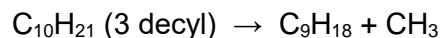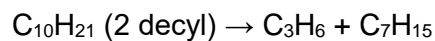
The calculated barriers for these reactions are in the range of 121−126 kJ mol^{-1} and they are endoergic by 89−98 kJ mol^{-1}; the energetic parameters are thus similar as those for C−C β- scissions in smaller alkyl radicals considered above. The rate constants calculated at 1 atm are close for all the reactions considered and indicate that the lifetime of the decyl radicals decreases from 0.1 to 0.2 µs at 1000 K to 3−5 ns at 1600 K. In summary, n-decyl radicals, which may be produced by hydrogen abstraction, can also undergo subsequent C−C bond β-scissions leading to experimentally observed alkenes: 1-butene, 1-pentene, 1-hexene, and 1- heptene. Therefore, the present investigation provides a complete inventory of radicals formed in the initial stage of decomposition, which de facto supply the radical pool for further oxidation of the fuel. This works presents a template of further investigations on the decomposition of JP-8 surrogates and also related to real jet fuel such as JP-10.

References:

1. Bruno, T. J.; Abel, K. R.; Riggs, J. R. Comparison of JP-8 and JP-8 + 100 With the Advanced Distillation Curve Approach. Energy Fuels 2012, 26, 5843−5850.

2. Bezaire, N.; Wadumesthrige, K.; Simon Ng, K. Y.; Salley, S. O. Limitations of the Use of Cetane Index for Alternative Compression Ignition Engine Fuels. Fuel 2010, 89, 3807−3813.

3. Gregg, S. D.; Campbell, J. L.; Fisher, J. W.; Bartlett, M. G. Methods for the Characterization of Jet Propellent-8: Vapor and Aerosol. Biomed. Chromatogr. 2007, 21, 463−472.

4. Gough, R. V.; Bruno, T. J. Composition-Explicit Distillation Curves of Alternative Turbine Fuels. Energy Fuels 2013, 27, 294−302.

5. Meylemans, H. A.; Baldwin, L. C.; Harvey, B. G. LowTemperature Properties of Renewable High-Density Fuel Blends. Energy Fuels 2013, 27, 883−888.

6. Witten, M. L.; Zeiger, E.; Ritchie, G. D. Jet Fuel Toxicology; CRC Press: 2011.

7. Rodgers, R. P.; Blumer, E. N.; Freitas, M. A.; Marshall, A. G. Jet Fuel Chemical Composition, Weathering, and Identification as a Contaminant at a Remediation Site, Determined by Fourier Transform Ion Cyclotron Resonance Mass Spectrometry. Anal. Chem. 1999, 71, 5171−5176.

8. DuBois, T. G.; Nieh, S. In Effects of Hydrocarbon Chemical Class Composition on Autothermal Reforming of JP-8 Fuel; Power Sources Conference: Las Vegas, NV, Jun. 14−17, 2010.

9. Echavarria, C. A.; Jaramillo, I. C.; Sarofim, A. F.; Lighty, J. S. Burnout of Soot Particles in a Two-Stage Burner with a JP-8 Surrogate Fuel. Combust. Flame 2012, 159, 2441−2448.

10. Wang, H.; Oehlschlaeger, M. A. Autoignition Studies of Conventional and Fischer−Tropsch Jet Fuels. Fuel 2012, 98, 249− 258.

11. Merrill, E. A.; Gearhart, J. M.; Sterner, T. R.; Robinson, P. J. Improved Predictive Model for n-Decane Kinetics across Species, as a Component of Hydrocarbon Mixtures. Inhalation Toxicol. 2008, 20, 851−863.

12. Holley, A. T.; Dong, Y.; Andac, M. G.; Egolfopoulos, F. N.; Edwards, T. Ignition and Extinction of Non-Premixed Flames of Single-Component Liquid Hydrocarbons, Jet Fuels, and Their Surrogates. Proc. Combust. Inst. 2007, 31, 1205−1213.

13. Pitz, W. J.; Cernansky, N. P.; Dryer, F. L.; Egolfopoulos, F. N.; Farrell, J. T.; Friend, D. G.; Pitsch, H., Development of an Experimental Database and Chemical Kinetic Models for Surrogate Gasoline Fuels; SAE International: 2007.

14. Allen, C.; Valco, D.; Toulson, E.; Edwards, T.; Lee, T. Ignition Behavior and Surrogate Modeling of JP-8 and of Camelina and Tallow Hydrotreated Renewable Jet Fuels at Low Temperatures. Combust. Flame 2013, 160, 232−239.

15. Natelson, R. H.; Kurman, M. S.; Johnson, R. O.; Cernansky, N. P.; Miller, D. L. Preignition and Autoignition Chemistry of the Xylene Isomers. Combust. Sci. Technol. 2011, 183, 897−914.

16. Joklik, R.; Fuller, C.; Turner, B.; Gokulakrishnan, P. In The Effect of Multi-Component Fuel Evaporation on the Ignition of JP-8. Proceedings of the ASME Turbo Expo: Power for Land, Sea, and Air; ASME: 2010.

17. Honnet, S.; Seshadri, K.; Niemann, U.; Peters, N. A Surrogate Fuel for Kerosene. Proc. Combust. Inst. 2009, 32, 485−492.

18. Tosatto, L.; Mantia, B. L.; Bufferand, H.; Duchaine, P.; Gomez, A. Chemical Structure of a Methane Counterflow Diffusion Flame Perturbed with the Addition of either JP-8 or a Jet Fuel Surrogate. Proc. Combust. Inst. 2009, 32, 1319−1326.

19. Lenhert, D. B.; Miller, D. L.; Cernansky, N. P. The Oxidation of JP-8, Jet-A, and Their Surrogates in the Low and Intermediate Temperature Regime at Elevated Pressures. Combust. Sci. Technol. 2007, 179, 845−861.

20. Kahandawala, M. S. P.; DeWitt, M. J.; Corporan, E.; Sidhu, S. S. Ignition and Emission Characteristics of Surrogate and Practical Jet Fuels. Energy Fuels 2008, 22, 3673−3679.

21. Katta, V. R.; Roquemore, W. M. In Performance of JP-8 Surrogates and Parent Species in a Swirl Combustor. Proceedings of the ASME Turbo Expo: Power for Land, Sea, and Air; ASME: 2010.

22. Ji, C.; Sarathy, S. M.; Veloo, P. S.; Westbrook, C. K.; Egolfopoulos, F. N. Effects of Fuel Branching on the Propagation of Cctane Isomers Flames. Combust. Flame 2012, 159, 1426−1436.

23. Natelson, R. H.; Johnson, R. O.; Kurman, M. S.; Cernansky, N. P.; Miller, D. L. Comparison of Reactivity in a Flow Reactor and a Single Cylinder Engine. Exp. Therm. Fluid Sci. 2010, 34, 928−932.

24. Mensch, A.; Santoro, R. J.; Litzinger, T. A.; Lee, S. Y. Sooting Characteristics of Surrogates for Jet Fuels. Combust. Flame 2010, 157, 1097−1105.

25. Tremblay, R. T.; Martin, S. A.; Fisher, J. W. Novel Characterization of the Aerosol and Gas-Phase Composition of Aerosolized Jet Fuel. Inhalation Toxicol. 2010, 22, 394−401.

26. Mawid, M. A.; Park, T. W.; Sekar, B.; Arana, C. In Development and Validation of a Detailed JP-8 Fuel Chemistry Model. Presented at the 2nd JANNAF Modeling and Simulation Subcommittee Meeting, Destin, FL.

27. Baulch, D. L.; Bowman, C. T.; Cobos, C. J.; Cox, R. A.; Just, Th.; Kerr, J. A.; Pilling, M. J.; Stocker, D.; Troe, J.; Tsang, W., et al. Evaluated Kinetic Data for Combustion Modeling: Supplement II. *The Journal of Physical Chemistry Ref. Data* **2005**, *34*, 757-1397.

28. Tosatto, L.; Mella, F.; Long, M. B.; Smooke, M. D. A Study of JP-8 Surrogate Coflow Flame Structure by Combined Use of Laser Diagnostics and Numerical Simulation. Combust. Flame 2012, 159, 3027−3039. (28) Miller, J. A.; Pilling, M. J.; Troe, J. Unravelling Combustion Mechanisms Through a Quantitative Understanding of Elementary Reactions. Proc. Combust. Inst. 2005, 30, 43−88.

29. Violi, A.; Yan, S.; Eddings, E. G.; Sarofim, F.; Granata, S.; Faravelli, T.; Ranzi, E. Experimental Formulation and Kinetic Model for JP-8 Surrogate Mixtures. Combust. Sci. Technol. 2002, 174, 399− 417.

30. Podlesak, T.; Hendrickson, M.; Matthews, S.; Nawrocki, E.; Seibert, M.; Zalewski, M. Army Stirling Engine Research and Development - Past, Present and Future. Power Sources Conference 2010, 44, 462−465.

31. Singh, D.; Nishiie, T.; Qiao, L. Experimental and Kinetic Modeling Study of the Combustion of n-Decane, Jet-A, and S-8 in Laminar Premixed Flames. Combust. Sci. Technol. 2011, 183, 1002− 1026.

32. Liu, N.; Ji, C.; Egolfopoulos, F. N. Ignition of Non-Premixed C3−C12 n-Alkane Flames. Combust. Flame 2012, 159, 465−475.

33. Ji, C.; Dames, E.; Wang, Y. L.; Wang, H.; Egolfopoulos, F. N. Propagation and Extinction of Premixed C5−C12 n-Alkane Flames. Combust. Flame 2010, 157, 277−287.

34. Pilla, G. L.; Davidson, D. F.; Hanson, R. K. Shock Tube/Laser Absorption Measurements of Ethylene Time-Histories during Ethylene and n-Heptane Pyrolysis. Proc. Combust. Inst. 2011, 33, 333−340.

35. Sarathy, S. M.; Westbrook, C. K.; Mehl, M.; Pitz, W. J.; Togbe, C.; Dagaut, P.; Wang, H.; Oehlschlaeger, M. A.; Niemann, U.; Seshadri, K.; et al. Comprehensive Chemical Kinetic Modeling of the Oxidation of 2-Methylalkanes from C7 to C20. Combust. Flame 2011, 158, 2338−2357.

36. Holley, A. T.; You, X. Q.; Dames, E.; Wang, H.; Egolfopoulos, F. N. Sensitivity of Propagation and Extinction of Large Hydrocarbon Flames to Fuel Diffusion. Proc. Combust. Inst. 2009, 32, 1157−1163. (37) You, X.; Egolfopoulos, F. N.; Wang, H. Detailed and Simplified Kinetic Models of n-Dodecane Oxidation: The Role of Fuel Cracking in Aliphatic Hydrocarbon Combustion. Proc. Combust. Inst. 2009, 32, 403−410.

37. Photoionization Cross Section Database (Version 1.0). National Synchrotron Radiation Laboratory: Hefei, China. http://flame.nsrl. ustc.edu.cn/database/; 2011.

38. Curtiss, L. A.; Raghavachari, K.; Redfern, P. C.; Rassolov, V.; Pople, J. A. Gaussian-3 (G3) Theory for Molecules Containing First and Second-Row Atoms. J. Chem. Phys. 1998, 109, 7764−7776.

39. Baboul, A. G.; Curtiss, L. A.; Redfern, P. C.; Raghavachari, K. Gaussian-3 Theory Using Density Functional Geometries and ZeroPoint Energies. J. Chem. Phys. 1999, 110, 7650−7657.

40. Jasper, A. W.; Miller, J. A. Lennard−Jones Parameters for Combustion and Chemical Kinetics Modeling from Full-Dimensional Intermolecular Potentials. Combust. Flame 2014, 161, 101−110.

41. Klippenstein, S. J.; Georgievskii, Y.; Harding, L. B. Predictive Theory for the Combination Kinetics of Two Alkyl Radicals. Phys. Chem. Chem. Phys. 2006, 8, 1133−1147.

42. Harding, L. B.; Georgievskii, Y.; Klippenstein, S. J. Predictive Theory for Hydrogen Atom - Hydrocarbon Radical Association Kinetics. *The Journal of Physical Chemistry* A 2005, 109, 4646−4656.

Table 3.1 Compilation of Products Observed in the Present Studies on the

Decomposition of n-Decane

Species	Formula	Mass	Structure
Hydrogen	H_2	2	H—H
Methyl radical	CH_3	15	$CH_3\bullet$
Methane	CH_4	16	CH_4
Acetylene	C_2H_2	26	
Vinyl radical	C_2H_3	27	
Ethylene	C_2H_4	28	
Ethyl radical	C_2H_5	29	
Propargyl radical	C_3H_3	39	
Allene	C_3H_4	40	
Methylacetylene	C_3H_4	40	
Allyl radical	C_3H_5	41	
Propene	C_3H_6	42	
1,3-Butadiene	C_4H_6	54	
1-Butene	C_4H_8	56	
2-Butene	C_4H_8	56	
1-Pentene	C_5H_{10}	70	
1-Hexene	C_6H_{12}	84	
1-Heptene	C_7H_{14}	98	

Figure 3.1 Potential Energy for Primary and Secondary Dissociation Channels of n-Decane.
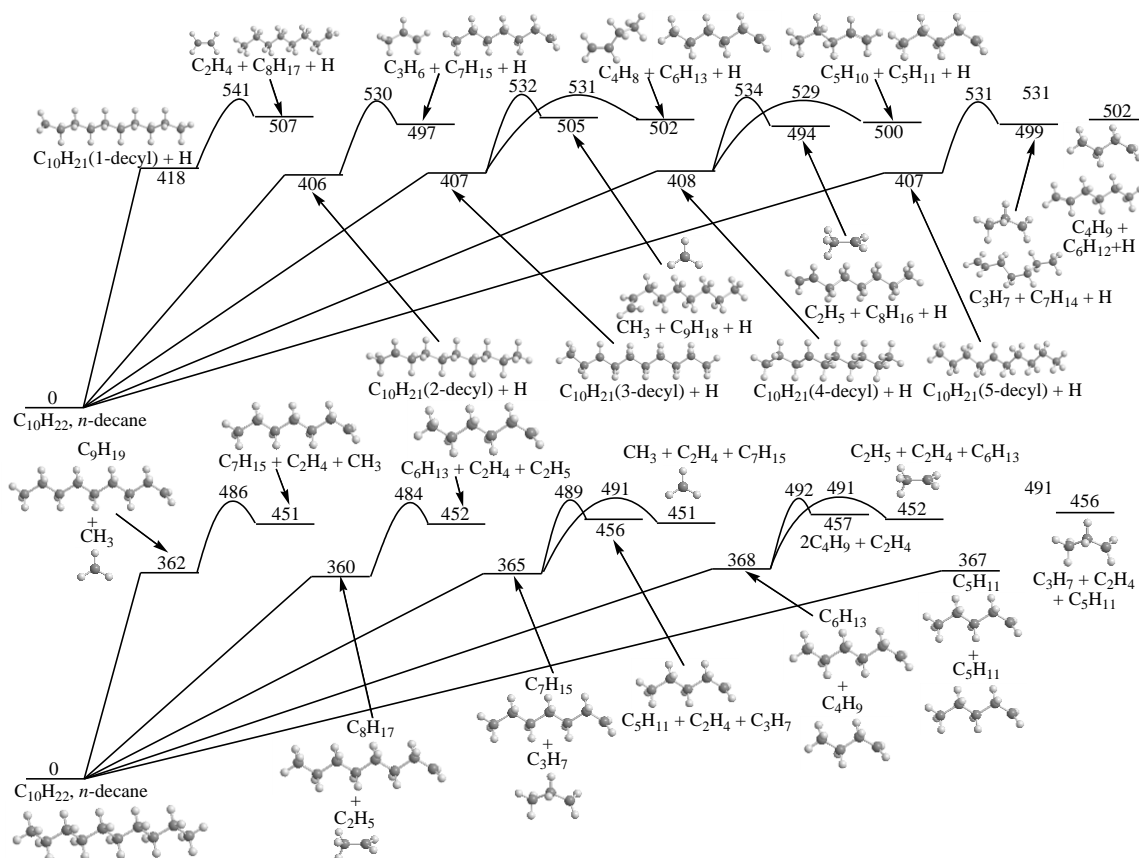
Figure 3.2 Calculated Rate Constants at 1 atm for Unimolecuar Reactions (a) for C-C and C-H Bond Cleavages in $C_{10}H_{22}$; (b) C-C Bond β-scissions in 1-Alkyl Radicals; (c) for $C_{10}H_{22}$ + H Direct H Abstractions; (d) for C-C Bond β-scissions in n-Decyl Radicals $C_{10}H_{21}$ (n=1-5)
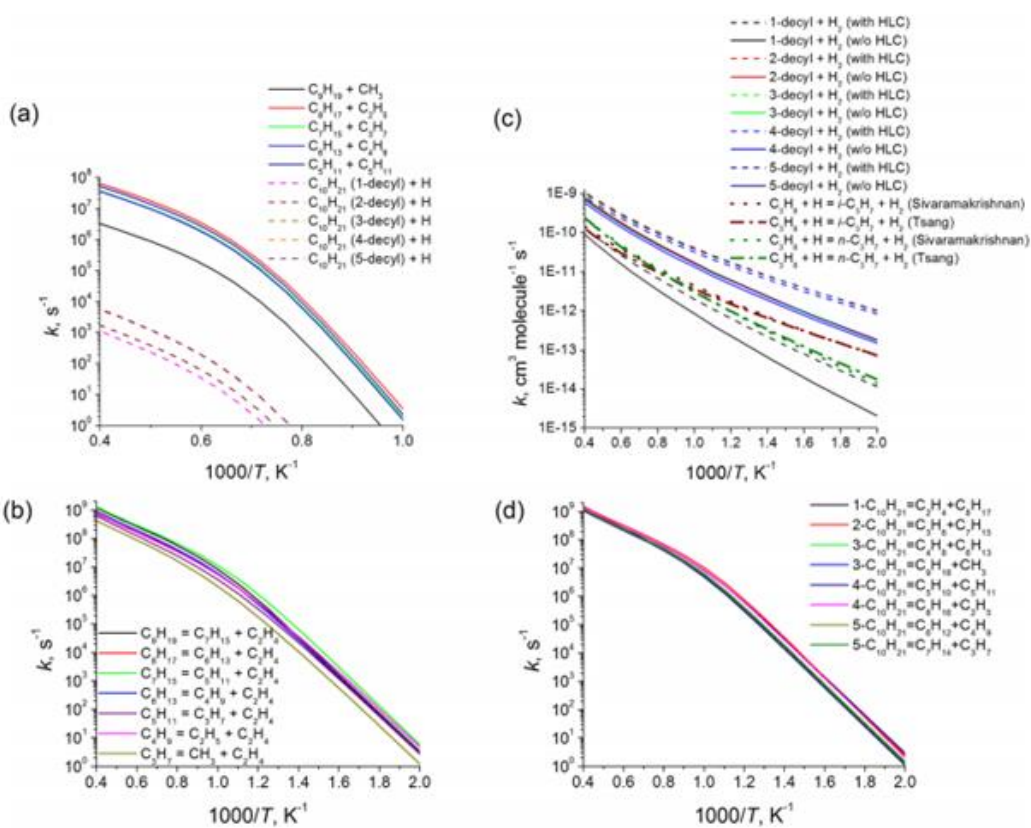
Table 3.2 Calculated Barrier Heights and Reaction Energies for C-C Bond β-Scission

and Direct H Abstraction Reactions of n-Decane

Reaction	Barrier (kJ mol^{-1})	Reaction energy (kJ mol^{-1})
$C_9H_{19} \rightarrow C_7H_{15} + C_2H_4$	124	89
$C_8H_{17} \rightarrow C_6H_{13} + C_2H_4$	124	92
$C_7H_{15} \rightarrow C_5H_{11} + C_2H_4$	124	91
$C_6H_{13} \rightarrow C_4H_9 + C_2H_4$	124	89
$C_5H_{11} \rightarrow C_3H_7 + C_2H_4$	124	89
$C_4H_9 \rightarrow C_2H_5 + C_2H_4$	123	86
$C_3H_7 \rightarrow CH_3 + C_2H_4$	126	86
$C_{10}H_{21}$ (1-decyl) $\rightarrow C_8H_{17} + C_2H_4$	123	89
$C_{10}H_{21}$ (2-decyl) $\rightarrow C_7H_{15} + C_3H_6$	124	91
$C_{10}H_{21}$ (3-decyl) $\rightarrow C_9H_{18} + CH_3$	125	98
$C_{10}H_{21}$ (3-decyl) $\rightarrow C_6H_{13} + C_4H_8$	124	95
$C_{10}H_{21}$ (4-decyl) $\rightarrow C_8H_{16} + C_2H_5$	126	86
$C_{10}H_{21}$ (4-decyl) $\rightarrow C_5H_{10} + C_5H_{11}$	121	92
$C_{10}H_{21}$ (5-decyl) $\rightarrow C_7H_{14} + C_3H_7$	124	95
$C_{10}H_{21}$ (5-decyl) $\rightarrow C_6H_{12} + C_4H_9$	124	92
$C_{10}H_{22} + H \rightarrow C_{10}H_{21}$ (1-decyl) $+ H_2$	47 (40)[a]	-12 (-19)[a]
$C_{10}H_{22} + H \rightarrow C_{10}H_{21}$ (2-decyl) $+ H_2$	34 (26)[a]	-24 (-31)[a]
$C_{10}H_{22} + H \rightarrow C_{10}H_{21}$ (3-decyl) $+ H_2$	33 (26)[a]	-23 (-31)[a]
$C_{10}H_{22} + H \rightarrow C_{10}H_{21}$ (4-decyl) $+ H_2$	33 (26)[a]	-23 (-30)[a]
$C_{10}H_{22} + H \rightarrow C_{10}H_{21}$ (5-decyl) $+ H_2$	33 (26)[a]	-23 (-30)[a]

[a]The values including the higher level correction (HLC) for H abstractions are given in parenthesis.

Figure 3.3 Potential Energy Diagrams for Decomposition Pathways of C_5H_{11}, C_6H_{13}, C_7H_{15}, C_8H_{17} Involving H Shifts and C-C Bond β-Scissions.
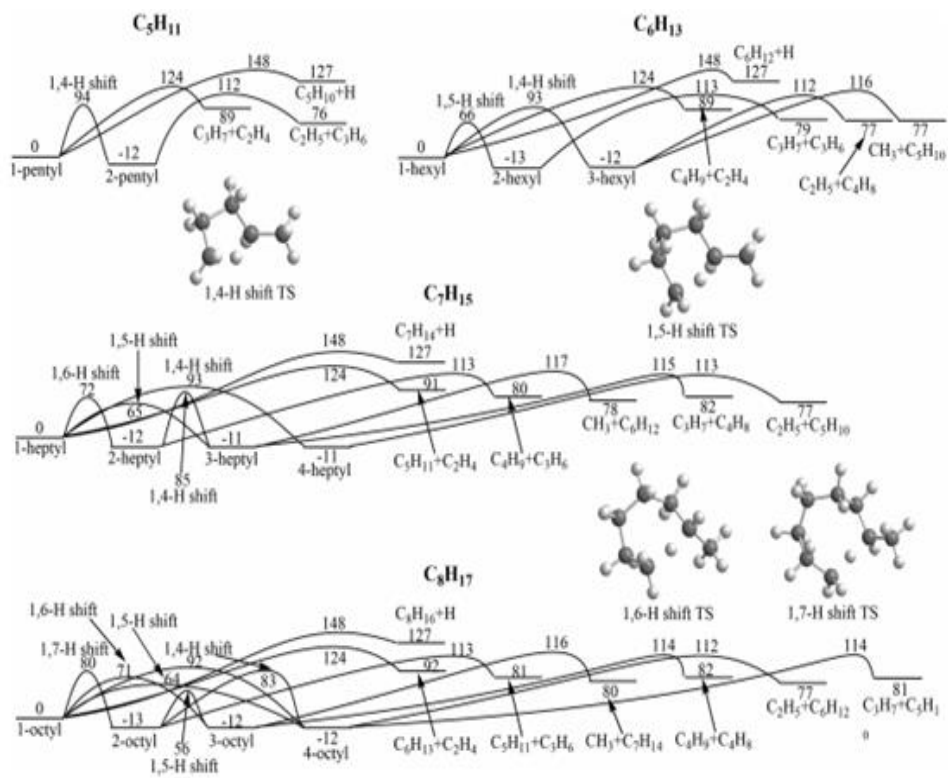
Figure 3.4 Compiled Reaction Mechanism for the Pyrolysis of n-Decane

$C_2H_4 + C_6H_{13}$

C_3H_6 (propene) $+ C_5H_{11}$

C_4H_8 (1-butene) $+ C_4H_9$

C_5H_{10} (1-pentene) $+ C_3H_7$

C_6H_{12} (1-hexene) $+ C_2H_5$

C_7H_{14} (1-heptene) $+ CH_3$

C_8H_{16} (1-octene) $+ H$

$C_8H_{17} + C_2H_5 \longrightarrow H + C_2H_4$

$-H \rightarrow C_2H_3$

$-H$

$-H_2 \rightarrow C_2H_2$

$C_2H_4 + CH_3$

C_3H_6 (propene) $+ H$

$-H$

C_3H_5

$-H$

C_3H_4

$-H$

C_3H_3

$C_5H_{11} + C_5H_{11} \longleftarrow C_{10}H_{22} \longrightarrow C_7H_{15} + C_3H_7$

$C_2H_4 + C_3H_7$

C_3H_6 (propene) $+ C_2H_5$

C_5H_{10} (1-pentene) $+ H$

$C_2H_4 + C_5H_{11}$

C_3H_6 (propene) $+ C_4H_9$

C_4H_8 (1-butene) $+ C_3H_7$

C_5H_{10} (1-pentene) $+ C_2H_5$

C_6H_{12} (1-hexene) $+ CH_3$

C_7H_{14} (1-heptene) $+ H$

$C_2H_4 + C_4H_9$

C_3H_6 (propene) $+ C_3H_7$

C_4H_8 (1-butene) $+ C_2H_5$

C_5H_{10} (1-pentene) $+ CH_3$

C_6H_{12} (1-hexene) $+ H$

$C_6H_{13} + C_4H_9$

$C_2H_5 + C_2H_4$

C_4H_8 (1-butene) $+ H$

isomerization

$-2H$

2-butene $-2H \rightarrow C_4H_6$ (1,3-butadiene)

$C_{10}H_{22} + H$

$C_{10}H_{21}$ (2-decyl) $+ H_2$

$C_{10}H_{21}$ (3-decyl) $+ H_2$

$C_{10}H_{21}$ (4-decyl) $+ H_2$

$C_{10}H_{21}$ (5-decyl) $+ H_2$

C_7H_{14}(1-heptene) $+ C_3H_7$

C_3H_6(propene) $+ C_7H_{15}$

C_9H_{18}(1-nonene) $+ CH_3$

C_4H_8(1-butene) $+ C_6H_{13}$

C_8H_{16}(1-octene) $+ C_2H_5$

C_5H_{10}(1-pentene) $+ C_5H_{11}$

C_6H_{12}(1-hexene) $+ C_4H_9$

Figure 3.5 Summary of Global Reaction Mechanisms Leading to Primary Reaction

Products in the Decomposition of n-Decane

n-decane, $C_{10}H_{22}$

Hydrogen abstraction

C-C bond rupture

n-decyl radicals (n=2 to 5)

1-alkyl radicals (C2-C8)

C-C beta scission

Hydrogen migration

C-C beta scission

C-C beta scission

C3-C9 alkenes ← n-alkyl radicals **CH$_3$, C$_2$H$_5$, C2-C6 alkenes**
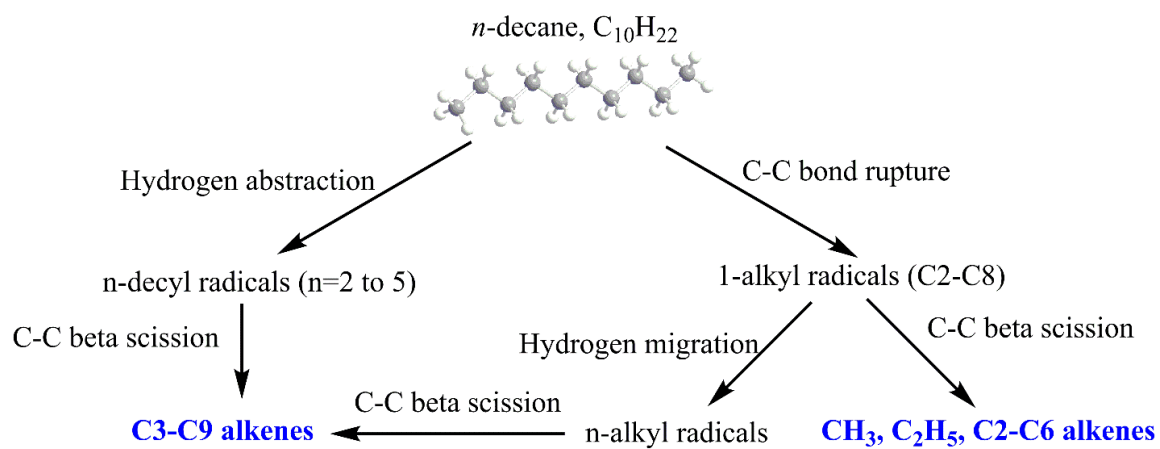
Chapter IV

Combined Experimental and Computational Study on the Unimolecular Decomposition of JP-8 Jet Fuel Surrogates. II: n-Dodecane (n-$C_{12}H_{26}$)

Introduction:

Jet Propellant-8 (JP-8) is a kerosene-based jet fuel which is widely used by the US military. It is comprised of hundreds of hydrocarbons which include aliphatic molecules (33−61% n-alkanes and isoalkanes; 1−5% olefins), monocyclic "paraffins" (10−20%), alkyl-substituted benzenes (12−22%), and polycyclic aromatic hydrocarbons (PAHs) (10−20%).[1] Combustion scientists have been exploiting surrogate fuels in an attempt to convincingly model the performance along with emission characteristics of JP-8 engines.[1−24] While single-component surrogate fuels are suitable to replicate combustion efficiencies, multicomponent surrogates are essential to adequately model the chemistry of soot formation and flames.[25] These kinetic models require precise input parameters and an accurate knowledge of the initial steps, which initiate bond rupture in JP-8 surrogates. These processes essentially supply a pool of highly reactive radicals - often aromatic radicals (AR) and resonantly stabilized free radicals (RSFRs) - ultimately managing the autoignition and successive oxidation processes under combustion relevant conditions of temperatures of up to 1600 K and pressures up to a few atmospheres.[10,26−29] Previous experimental studies on the decomposition of the aliphatic component of JP-8 exploited n-dodecane ($C_{12}H_{26}$) as surrogates. In principle, these experiments revealed that the decomposition and "pyrolysis" of these surrogates lead to smaller C1 to C12 hydrocarbon molecules, but also reveal mass growth processed leading eventually to polycyclic aromatic hydrocarbons (PAHs). The studies of n-dodecane thermal decomposition can be traced back to the 1980s. With high-pressure single pulse shock tube setups, Malewicki and Brezinsky[30] performed an experimental and modeling study on the pyrolysis and oxidation of n-dodecane. The experiment

covered the temperature range from 867 to 1739 K, pressures from 19 to 74 atm, reaction times from 1.15 to 3.47 ms, and equivalence ratios from 0.46 to 2.05 and ∞. They measured the major hydrocarbon intermediates during n-dodecane pyrolysis experiments including ethylene (C_2H_4), methane (CH_4), propylene (C_3H_6), acetylene (C_2H_2), ethane (C_2H_6), 1-butene (C_4H_8), 1,3-butadiene (C_4H_6), 1-hexene (C_6H_{12}), 1-pentene (C_5H_{10}), 1-heptene (C_7H_{14}), 1-octene (C_8H_{16}), vinylacetylene (C_4H_4), 1-nonene (C_9H_{18}), and 1-decene ($C_{10}H_{20}$). Studies found that over the temperature of 1000 K, the process can be divided into two stages, decomposition of the fuel and its intermediates. The second step of intermediate decomposition is always rate limiting. The time history of several hydrocarbon intermediates and final products were measured including methane (CH_4), ethane (C_2H_6), acetylene (C_2H_2), ethylene (C_2H_4), propene (C_3H_6), 1-butene (C_4H_8), 1,3-butadiene (C_4H_6), 1-pentene (C_5H_{10}), 1-hexene (C_6H_{12}) 1,3-hexadiene (C_6H_{10}), and 1-heptene (C_7H_{14}). Observed products included hydrogen (H_2), methane (CH_4), ethane (C_2H_6), 1,3-butadiene (C_4H_6), and 1-alkenes from ethylene (C_2H_4) to 1-undecene ($C_{11}H_{22}$). And at higher temperatures and residence times, mass growth processes to monocyclic and polycyclic aromatic species were observed. The authors found the 1-alkene selectivity strongly depends upon the system pressure in the pyrolysis of straight-chain alkanes as major products; the lower the pressure meaning the higher the selectivity. On the basis of their previous literature data, they revised the kinetic model by Dooley et al.[31] Of particular interest, Westbrook and co-workers carried out a comprehensive detailed chemical kinetic modeling for n-alkanes from n-octane to n-hexadecane. Their mechanism was designed to reproduce n-alkane oxidation at both low and high temperatures, and validated through extensive comparisons between computed and experimental data from a wide variety of different sources, including flow reactor pyrolysis, JSR pyrolysis, JSR oxidation, shock tube, and RCM ignition delay

times. The proposed reaction mechanism can describe the kinetics of n-dodecane, as well as that of n-heptane, iso-octane, and some substituted aromatics (toluene, styrene, ethylbenzene, m-xylene and 1-methylnaphthalene), which are important components of transportation fuel surrogates. These studies reported multiple lower-mass C3−C7 hydrocarbons including alkenes, alkynes, and dienes along with C1 (methane) and C2 (acetylene, ethylene) as final products. Also, five radicals were observed in the n-decane pyrolysis including methyl, vinyl, ethyl, propargyl, and allyl. Further, the study presented branching ratios along with the underlying decomposition mechanisms. Here, we expand our studies to investigate via a combined theoretical and experimental strategy, the decomposition mechanisms of n-dodecane ($C_{12}H_{26}$) within the pyrolytic reactor and compare our findings with those data from previous high pressure shock tubes, flow reactors, and jet stirred reactor studies. It is our goal to provide both qualitative and quantitative identification of all nascent decomposition products (radicals and closed-shell molecules along with their structural isomers), the fundamental decomposition mechanisms, and reveal how their branching ratios depend on the temperature of the reactor. These data are of critical importance to the JP-8 modeling community to eventually optimize combustion efficiency and limit the production of toxic byproducts such as carcinogenic and mutagenic PAHs.

Methods:

Geometries of n-dodecane, its primary and secondary decomposition products, and transition states for secondary decomposition reactions (C−C bond β-scissions) and for direct H atom abstractions by hydrogen atoms have been optimized using the density functional B3LYP/6-311G(d,p) method. Vibrational frequencies of various stationary structures have been computed at the same level of theory. Then, relative energies for

all optimized structures have been reevaluated by single-point calculations at the

G3(CCSD,MP2) level of theory[32-34] with B3LYP/6-311G(d,p) zero-point vibrational energy

corrections (ZPE), including the empirical higher level correction (HLC)[73] and using

B3LYP/6-311G(d,p) optimized geometries. The inclusion of the HLC increases the

calculated strengths of C−H bonds by 7 kJ/mol, decreases relative energies of transition

states and products for the $C_{12}H_{26}$+ H → C$_{12}$H$_{25}$ + H$_2$ hydrogen atom abstraction

reactions also by 7 kJ/mol, is insignificant for C−C bond cleavages, and zero by

definition for C−C bond β-scissions. The G3(CCSD,MP2)//B3LYP theoretical level has

been shown to provide "chemical accuracy" within 3−6 kJ/mol in terms of average

absolute deviations of relative energies of various stationary structures.[33] The ab initio

calculations were performed using the GAUSSIAN 09[35] and MOLPRO 2010[34] program

packages. Rate constants for primary and secondary reactions involved in the pyrolysis

of n-dodecane have been calculated using the RRKM/master equation approach[35] with

the MESS package,[36] generally utilizing the rigid-rotor, harmonic-oscillator (RRHO)

approximation for the evaluation of partition functions for molecular complexes and

transition states. Collisional energy transfer rates in the master equation were expressed

using the "exponential down" model,[37] with the temperature dependence of the range

parameter α for the deactivating wing of the energy transfer function expressed as α(T) =

α_{300}(T/300 K)^n , with n = 0.86 and α_{300} = 228 cm^{-1} obtained earlier from classical

trajectories calculations as "universal" parameters for hydrocarbons in the nitrogen bath

gas.[37] We used the Lennard-Jones parameters (ε/cm^{-1} , σ/Å) = (253, 5.16) for the n-

dodecane/ nitrogen system derived by Jasper et al.[36] using the fit of results using the

"one-dimensional optimization" method.[35] Since our goal in this work is both qualitative

and quantitative evaluation of relative yields of various products at different stages of the

pyrolysis in order to account for the observed experimental results, we used a simplified

approximation to treat C−C and C−H single bond cleavages in the original n-dodecane molecule occurring without barriers. In particular, rate constants for these reactions were calculated using phase space theory with empirical potential energy parameters selected in such a way that the rate constants for the reverse $C_xH_y + C1_{2-x}H_{26-y}$ and $C_{12}H_{25} + H$ radical recombination reactions reproduce the rate constants for the prototype $CH_3 + CH_3$ and $C_2H_5 + H$ reactions in the experimental 1200−1600 K temperature interval studied earlier by Klippenstein and co-workers[38,39] using the most accurate up-to-date theoretical approach, variable reaction coordinated transition state theory (VRC-TST). Another theoretical issue is the appropriate treatment of soft normal modes in $C_{12}H_{26}$ and $C_{12}H_{25}$ radicals, which are represented by convoluted coupled hindered rotations. Identification of such hindered rotors and evaluation of their potential energy profiles in long alkanes is an extremely complex task. However, in our previous work, we showed that in smaller 1-alkyl radicals, from C_3H_7 to C_9H_{19}, the replacement of harmonic oscillators with hindered rotors increased the computed C−C β-scission rate constants by 8−41% at 1000 K and by only 2−25% at 1600 K.[38,39] Here, all calculations have been performed within RRHO keeping in mind the above-mentioned error bars in rate constants. The anticipated errors in ratios of rate constants are expected to be smaller than the errors in their absolute values due to cancelations of similar inaccuracies.

Results and Discussion:

The n-dodecane molecule can decompose by initial cleavage of various C−C (reaction R1) and C−H bonds (reaction R2) producing pairs of 1-alkyl radicals and n-dodecyl radicals plus a hydrogen atom, respectively.

$$C_{12}H_{26} \rightarrow C_xH_y + Cx'H_{y'} \quad (R1)$$

$$C_{12}H_{26} \rightarrow C_{12}H_{25} + H \quad (R2)$$
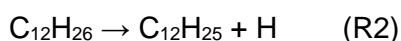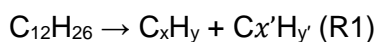
Overall branching ratios of the species obtained in the decomposition of n-dodecane in the temperature range from 1200 to 1600 K.

Homolytic C−C and C−H Bond Cleavages and Consecutive β-Scissions (C−C; C−H).

The energetics of the C−C bond cleavages in $C_{12}H_{26}$ is illustrated in Figure 4.1. The C−C bond strengths are calculated to be in the range of 361− 366 kJ/mol, where the C2−C3 bond was found to be the weakest and the C5−C6 bond to be the strongest. The differences in the C−C bond strengths are so small that one can anticipate that all product pairs, CH_3 + $C_{11}H_{23}$, C_2H_5 + $C_{10}H_{21}$, C_3H_7 + C_9H_{19}, C_4H_9 + C_8H_{17}, C_5H_{11} + C_7H_{15}, and C_6H_{13} + C_6H_{13}, can be in principle formed. On the other hand, the calculated strengths of C−H bonds are significantly higher (Table 4.2). The primary C1−H bonds in terminal CH_3 groups are the strongest, 418 kJ/mol, whereas the secondary C−H bonds in CH_2 groups vary in a very narrow range of 406−407 kJ/mol. These values are close to the corresponding experimental C−C and C−H bond strengths in n-butane, propane, and ethane evaluated based on enthalpies of formation at 0 K from Active Thermochemical Tables and also to the theoretical values for n-decane calculated in our previous work.[42] Because of the large difference in the bond strengths, rate constants for the C−H cleavages appeared to be several orders of magnitude lower than those for the C−C cleavages and therefore the C−C bond cleavage is predicted to dominate the unimolecular decomposition of dodecane. In the temperature range of 1000−1600 K and 1 atm, the rate constants for the C−C cleavages exhibit well-defined Arrhenius behavior and grow from 2.6−3.6 s^{-1} to (1−2) × 10^6 s $^{-1}$. These values agree with the experimental observations that while only a small fraction of n-dodecane is consumed at 1100 K, no parent molecules survive above 1500 K during the residence time in the reactor, about

tens of microseconds. The computed rate constants for the cleavages of the terminal

bonds to produce $CH_3 + C_{11}H_{23}$ are found to be 1-2 orders of magnitude lower than

those for the cleavage of nonterminal C−C bonds. The rate constants calculated at 1

atm, except for the one to produce $CH_3 + C_{11}H_{23}$, grow to $4-6 \times 10^7$ s $^{-1}$ at 2500 K; a

small falloff behavior at higher temperatures is seen in a decrease of the slope of the

rate constant curves. The computed relative product yields are ~1% for $CH_3 + C_{11}H_{23}$,

17−16% for $C_2H_5 + C_{10}H_{21}$, 23−24% for $C_3H_7 + C_9H_{19}$, ~ 19% for $C_4H_9 + C_8H_{17}$, 18−19%

for $C_5H_{11} + C_7H_{15}$, and 21−22% for $C_6H_{13} + C_6H_{13}$ and show very slight temperature

dependence from 1000 to 2500 K. The product yields are also practically independent of

pressure in the range from 30 Torr to 100 atm. Which allows us to conclude that the

pyrolysis of n-dodecane at 1500 K and above should predominantly produce a mixture of

1-alkyl radicals, from ethyl to 1-decyl, on a time scale of 1−2 μs. In our previous work

considering the pyrolysis of n-decane[43] we have shown that the higher 1-alkyl radicals

are unstable in the experimental temperature range and are subject to a rapid C−C bond

β-scission producing ethylene C_2H_4 together with a smaller 1-alkyl. As shown in Figure

4.1 and Table 4.2, the calculated barrier heights and reaction energies for the C−C bond

β-scissions are 123−126 and 86−92 kJ/mol, respectively. The computed rate constants

for C−C bond β-scissions are approximately in the range of 107 −108 s $^{-1}$ at T =

1200−1600 K, and hence, the lifetimes of the primary dissociation products, 1-alkyl

radicals, is shorter than 1 μs under the experimental conditions and they are expected to

rapidly decompose to the ultimate C_2H_4, CH_3, and C_2H_5 products detected

experimentally via the stepwise mechanism shown below. Depending on the residence

time, the ethyl radical may or may not further lose an H atom via a C−H bond β-scission

producing ethylene.

$$C_{10}H_{21} \rightarrow C_8H_{17} + C_2H_4$$

$$C_9H_{19} \rightarrow C_7H_{15} + C_2H_4$$

$$C_8H_{17} \rightarrow C_6H_{13} + C_2H_4$$

$$C_7H_{15} \rightarrow C_5H_{11} + C_2H_4$$

$$C_6H_{13} \rightarrow C_4H_9 + C_2H_4$$

$$C_5H_{11} \rightarrow C_3H_7 + C_2H_4$$

$$C_4H_9 \rightarrow C_2H_5 + C_2H_4$$

$$C_3H_7 \rightarrow CH_3 + C_2H_4$$

$$C_2H_5 \rightarrow H + C_2H_4$$

The mechanism of consecutive direct C−C bond β-scissions unzipping large 1-alkyl radicals down to the mixture of C_2H_4, C_2H_5, and CH_3 cannot explain the experimental observation of higher 1-alkenes, especially propene and 1-butene, which are among major pyrolysis products at 1200 K and are still present up to 1600 K. We discussed several possible formation pathways of 1-alkenes in the previous paper on n-decane.[44] The first one is C−H bond β-scission in 1-alkyls, but according to the calculations C−H β-scission barriers are 20−26 kJ/mol higher than the corresponding C−C β-scission barriers in C_3H_7−C_8H_{17}. Because of this difference, the computed branching ratios for the C−H β-scission channels in C_4H_9−C_8H_{17} are very small and do not exceed 1−2% until the highest temperatures and pressures (2500 K and 100 atm), where they reach 5−6%.[45] The relative yield of propene + H is higher from C_3H_7 and increases from 3 to 4% at 1100−1600 K and 1 atm to 6%, 9%, and 13% at 2500 K and pressures of 1, 10, and 100 atm, respectively. Thus, C−H bond β-scissions cannot explain the large experimental yields of propene and 1-butene since they are largely unfavorable

compared to the β-scissions with the loss of C_2H_4. Summarizing, C−C bond cleavages leading to 1-alkyl radicals are strongly favored compared to C−H bond rupture processes; the higher 1-alkyl radicals (>C2) do not survive under our experimental conditions and decay via successive C−C β-scissions (C_2H_4 elimination), which dominate over C−H β-scission (alkene formation), to yield eventually the C1 to C2 hydrocarbons CH_3, C_2H_5, and C_2H_4.

Hydrogen Migrations and Consecutive β-Scissions.

 The second possible mechanism to form higher alkenes involves H atom shifts in 1-alkyl radicals followed by C−C bond β-scission. We have shown[45] that isomerization channels involving 1,2- and 1,3-H atom shifts in C_3H_7 and C_4H_9 are not competitive because of their high barriers of 157−162 kJ/mol significantly exceeding the C−C bond β-scission barriers of ~124 kJ/mol. On the other hand, a possibility of 1,4-H, 1,5-H, 1,6-H, and 1,7-H shifts eventually opens up in higher 1-alkyl radicals beginning from C_5H_{11} and the corresponding typical barriers for these processes, 92−94, 64−66, 71−72, and 80 kJ/mol, respectively, are lower than those for the C−C bond β-scission. The hydrogen shifts are followed by C−C β-scissions forming higher 1-alkenes rather than ethylene, i.e., propene (C_3H_6), 1-butene (C_4H_8), 1-pentene (C_5H_{10}), and so on, depending on the radical position in the alkyl. We calculated and reported product branching ratios in dissociation of 1-alkyl radicals C_5H_{11}−C_8H_{17} taking into account direct C−C and C−H β-scissions as well as all C−C β-scissions following the H shifts in the previous work (Chapter III)[46!] and demonstrated that at low pressures up to 1 atm, the products formed after a 1,5-H shift are preferable, but at high pressures of 10 and 100 atm, the direct C−C β-scission from 1-alkyls producing ethylene (C_2H_4) dominates. Nevertheless, various alkenes can be formed from the 1-alkyl radicals with non-negligible branching

ratios, e.g., from C_5H_{11}: $C_3H_7 + C_2H_4$ (direct), $C_2H_5 + C_3H_6$ (via 1,4-H shift and 2-pentyl);

from C_6H_{13}: $C_4H_9 + C_2H_4$ (direct), $C_3H_7 + C_3H_6$ (via 1,5-H shift and 2-hexyl), $CH_3 + C_5H_{10}$

and $C_2H_5 + C_4H_8$ (both via 1,4-H shift and 3-hexyl); etc. As compared with n-decane, n-

dodecane has two higher 1-alkyl radicals among its primary products, 1-nonyl (C_9H_{19})

and 1-decyl ($C_{10}H_{21}$). While one can expect that the barriers for 1,4-, 1,5-, 1,6-, and 1,7-

H shifts should retain their typical values in C_9H_{19} and $C_{10}H_{21}$ and hence the

corresponding H shift/C−C β-scission channels would remain competitive, new reaction

channels may additionally open up, 1,8-H shifts both in 1-nonyl and 1-decyl and 1,9-H

shift in 1-decyl. Here, we evaluated the 1,8- and 1,9-H shift barriers in $C_{10}H_{21}$. The

calculation gave the values of 97 and 90 kJ/mol, respectively. While these barriers are

higher than those for 1,5-, 1,6-, and 1,7-H shifts, and are comparable to 1,4-H shifts,

they are still somewhat lower than the barrier for the direct C−C β-scission. Therefore,

the dissociation channels involving the 1,8- and 1,9-H shifts followed by C−C β-scissions

can give minor contributions to the overall product yield. In particular, 1-nonyl can

isomerize to 2-nonyl by 1,8-H shift and then decompose to $C_6H_{13} + C_3H_6$. 1-Decyl can

isomerize to 2-decyl by 1,9-shift and dissociate to $C_7H_5 + C_3H_6$ or isomerize to 3-decyl

and decompose to either $CH_3 + C_9H_{18}$ or $C_6H_{13} + C_4H_8$. Summarizing, the reaction

mechanism involving hydrogen migration in C5 to C10 1-alkyl radicals preceding C−C β-

scission accounts for the observation of C3−C7 alkenes [propene, 1-butene, 1-pentene,

1-hexene, and 1-heptene] observed in our experiments and, in particular, for the large

branching ratios of C_3H_6 and C_4H_8 at low temperatures (and even at 1600 K for

propene). At temperatures of 1500 K and above the lifetime of a single C−C bond

approaches 1 μs and hence higher alkenes are likely to decompose on the time scale of

the experiment and their yield significantly decrease.

Hydrogen Abstraction. The third possible pathway to the higher alkenes involves C−C bond β-scissions in n-dodecyl radicals (n > 1; see Figure 9 and Table 6). While n-dodecyls are not expected to be formed by C−H bond cleavages in n-dodecane, they can be produced by direct hydrogen abstractions by H atoms or other radicals when those radicals appear in the reactive system. The barrier heights and reaction exoergicities for the H abstraction reactions by a hydrogen atom from secondary C−H bonds are computed to be 35−36 (27−28) and 23−24 (30−31) kJ/mol; the numbers in parentheses include HLC in the G3(CCSD,MP2) calculations. The H abstractions from the primary C−H bonds exhibit a higher barrier and a lower reaction exoergicity of 49 (42) and 12 (19) kJ/mol, respectively. These results are close to the corresponding values obtained in the previous work for n-decane.[46] Note that, the most accurate up-to-date calculations of H abstraction from C_3H_8 and C_2H_6 gave the reaction barriers and exoergicities as 32 and 27 kJ/mol, respectively, for the secondary hydrogen abstraction and 43−44 and 15−16 kJ/mol for the primary hydrogen abstraction.[46] The calculated rate constants for secondary H abstractions are generally higher than those for the primary hydrogen abstraction (Figure 10b) and, among secondary H abstractions, the reaction producing 5-dodecyl is preferred and followed by the reactions giving 5-dodecyl, then by 2- and 3-dodecyl (with similar rate constants), and finally by 4-dodecyl. The computed rate constants to form 2- and 3-dodecyl agree best with the literature data (the most accurate calculations for C_3H_8[46] and experimental data for C_3H_8, C_4H_{10}, and C_5H_{12}) for the secondary H abstraction at 500 K but overestimate the literature data at 2500 K by approximately a factor of 3. Alternatively, the rate constants for the production of 4-dodecyl agree closely with the literature values at high temperatures. Our results indicate that the rate constants for secondary H abstraction are sensitive to the attacked hydrogen atom position in the alkane. It should be noted however that a more rigorous

anharmonic treatment of soft normal modes would be required to generate quantitatively accurate H abstraction rate constants. For the primary hydrogen abstraction, the $C_{12}H_{26}$ + H rate constants underestimate those for C_3H_8 + H by 50−60% if HLC is taken into account; the difference is bigger if the correction is not included. Our main conclusion is that the secondary H abstractions are feasible and form n-dodecyl radicals (n > 1). Once the n-dodecyl radicals are produced, they can rapidly undergo C−C bond β-scission to yield higher alkenes together with 1-alkyl radicals:

$$C_{12}H_{25} \text{ (2-dodecyl)} \rightarrow C_3H_6 + C_9H_{19}$$

$$C_{12}H_{25} \text{ (3-dodecyl)} \rightarrow C_{11}H_{22} + CH_3$$

$$\rightarrow C_4H_8 + C_8H_{17}$$

$$C_{12}H_{25} \text{ (4-dodecyl)} \rightarrow C_{10}H_{20} + C_2H_5$$

$$\rightarrow C_5H_{10} + C_7H_{15}$$

$$C_{12}H_{25} \text{ (5-dodecyl)} \rightarrow C_9H_{18} + C_3H_7$$

$$\rightarrow C_6H_{12} + C_6H_{13}$$

$$C_{12}H_{25} \text{ (6-dodecyl)} \rightarrow C_7H_{14} + C_5H_{11}$$

$$\rightarrow C_8H_{16} + C_4H_9$$
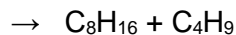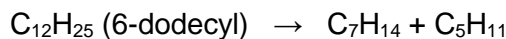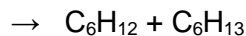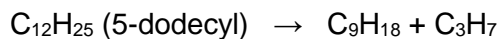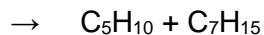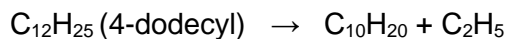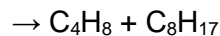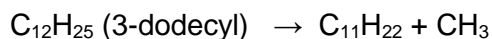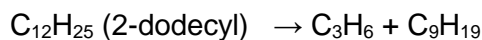
The calculated barriers for these reactions are 123−125 kJ/mol and they are endoergic by 88−93 kJ/mol; these energetic parameters are thus similar to those for C−C β-scissions in smaller alkyl radicals considered above and in the previous work.[46] The rate constants calculated at 1 atm are close for all the reactions considered within a factor of 2 (Figure 4.2). The results indicate that the lifetime of the dodecyl varies in the 5−50 ns range under the experimental conditions. Summarizing, n-dodecyl radicals, which may

be produced by hydrogen abstraction, can also undergo subsequent C−C bond β-

scissions leading to experimentally observed alkenes: 1-butene, 1-pentene, 1-hexene,

and 1-heptene.

References:

1. Bruno, T. J.; Abel, K. R.; Riggs, J. R. Comparison of JP-8 and JP-8 + 100 with the Advanced Distillation Curve Approach. Energy Fuels 2012, 26, 5843−5850.

2. Bezaire, N.; Wadumesthrige, K.; Simon Ng, K. Y.; Salley, S. O. Limitations of the Use of Cetane Index for Alternative Compression Ignition Engine Fuels. Fuel 2010, 89, 3807−3813.

3. Gregg, S. D.; Campbell, J. L.; Fisher, J. W.; Bartlett, M. G. Methods for the Characterization of Jet Propellent-8: Vapor and Aerosol. Biomed. Chromatogr. 2007, 21, 463−472.

4. Gough, R. V.; Bruno, T. J. Composition-Explicit Distillation Curves of Alternative Turbine Fuels. Energy Fuels 2013, 27, 294−302.

5. Meylemans, H. A.; Baldwin, L. C.; Harvey, B. G. Low-Temperature Properties of Renewable High-Density Fuel Blends. Energy Fuels 2013, 27, 883−888.

6. Witten, M. L.; Zeiger, E.; Ritchie, G. D. Jet Fuel Toxicology; CRC Press: 2011.

7. Rodgers, R. P.; Blumer, E. N.; Freitas, M. A.; Marshall, A. G. Jet Fuel Chemical Composition, Weathering, and Identification as a Contaminant at a Remediation Site, Determined by Fourier Transform Ion Cyclotron Resonance Mass Spectrometry. Anal. Chem. 1999, 71, 5171−5176.

8. DuBois, T. G.; Nieh, S. In Effects of Hydrocarbon Chemical Class Composition on Autothermal Reforming of JP-8 Fuel, Presented at the Power Sources Conference, Las Vegas, Nevada, USA, Jun. 14−17.

9. Echavarria, C. A.; Jaramillo, I. C.; Sarofim, A. F.; Lighty, J. S. Burnout of Soot Particles in a Two-Stage Burner With a JP-8 Surrogate Fuel. Combust. Flame 2012, 159, 2441−2448.

10. Wang, H.; Oehlschlaeger, M. A. Autoignition Studies of Conventional and Fischer−Tropsch Jet Fuels. Fuel 2012, 98, 249−258.

11. Merrill, E. A.; Gearhart, J. M.; Sterner, T. R.; Robinson, P. J. Improved Predictive Model for n-Decane Kinetics Across Species, as a Component of Hydrocarbon Mixtures. Inhalation Toxicol. 2008, 20, 851−63.

12. Holley, A. T.; Dong, Y.; Andac, M. G.; Egolfopoulos, F. N.; Edwards, T. Ignition and Extinction of Non-Premixed Flames of SingleComponent Liquid Hydrocarbons, Jet Fuels, and Their Surrogates. Proc. Combust. Inst. 2007, 31, 1205−1213.

13. Pitz, W. J.; Cernansky, N. P.; Dryer, F. L.; Egolfopoulos, F. N.; Farrell, J. T.; Friend, D. G.; Pitsch, H. Development of an Experimental Database and Chemical Kinetic Models for Surrogate Gasoline Fuels; SAE International: 2007.

14. Allen, C.; Valco, D.; Toulson, E.; Edwards, T.; Lee, T. Ignition Behavior and Surrogate Modeling of Jp-8 and of Camelina and Tallow Hydrotreated Renewable Jet Fuels at Low Temperatures. Combust. Flame 2013, 160, 232−239.

15. Natelson, R. H.; Kurman, M. S.; Johnson, R. O.; Cernansky, N. P.; Miller, D. L. Preignition and Autoignition Chemistry of the Xylene Isomers. Combust. Sci. Technol. 2011, 183, 897−914.

16. Joklik, R.; Fuller, C.; Turner, B.; Gokulakrishnan, P. The Effect of Multi-Component Fuel Evaporation on the Ignition of JP-8. In ASME Turbo Expo 2010: Power for Land, Sea, and Air; 2010.

17. Honnet, S.; Seshadri, K.; Niemann, U.; Peters, N. A Surrogate Fuel for Kerosene. Proc. Combust. Inst. 2009, 32, 485−492.

18. Tosatto, L.; Mantia, B. L.; Bufferand, H.; Duchaine, P.; Gomez, A. Chemical Structure of a Methane Counterflow Diffusion Flame Perturbed with the Addition of either JP-8 or a Jet Fuel Surrogate. Proc. Combust. Inst. 2009, 32, 1319−1326.

19. Lenhert, D. B.; Miller, D. L.; Cernansky, N. P. The Oxidation of JP-8, Jet-A, and Their Surrogates in the Low and Intermediate Temperature Regime at Elevated Pressures. Combust. Sci. Technol. 2007, 179, 845−861.

20. Kahandawala, M. S. P.; DeWitt, M. J.; Corporan, E.; Sidhu, S. S. Ignition and Emission Characteristics of Surrogate and Practical Jet Fuels. Energy Fuels 2008, 22, 3673−3679.

21. Katta, V. R.; Roquemore, W. M. In Performance of JP-8 Surrogates and Parent Species in a Swirl Combustor. In ASME Turbo Expo 2010: Power for Land, Sea, and Air; 2010.

22. Ji, C.; Sarathy, S. M.; Veloo, P. S.; Westbrook, C. K.; Egolfopoulos, F. N. Effects of Fuel Branching on the Propagation of Octane Isomers Flames. Combust. Flame 2012, 159, 1426−1436.

23. Natelson, R. H.; Johnson, R. O.; Kurman, M. S.; Cernansky, N. P.; Miller, D. L. Comparison of Reactivity in a Flow Reactor and a Single Cylinder Engine. Exp. Therm. Fluid Sci. 2010, 34, 928−932.

24. Caton, P. A.; Hamilton, L. J.; Cowart, J. S. Understanding Ignition Delay Effects With Pure Component Fuels in a Single-Cylinder Diesel Engine. J. Eng. Gas Turbines Power 2011, 133, 032803.

25. Tosatto, L.; Mella, F.; Long, M. B.; Smooke, M. D. A Study of JP-8 Surrogate Coflow Flame Structure by Combined Use of Laser Diagnostics and Numerical Simulation. Combust. Flame 2012, 159, 3027−3039.

26. Mawid, M. A.; Park, T. W.; Sekar, B.; Arana, C. Development and Validation of A Detailed JP-8 Fuel Chemistry Model. Presented at the 2nd JANNAF Modeling and Simulation Subcommittee Meeting, Destin, FL.

27. Miller, J. A.; Pilling, M. J.; Troe, J. Unravelling Combustion Mechanisms Through a Quantitative Understanding of Elementary Reactions. Proc. Combust. Inst. 2005, 30, 43−88.

28. Violi, A.; Yan, S.; Eddings, E. G.; Sarofim, F.; Granata, S.; Faravelli, T.; Ranzi, E. Experimental Formulation and Kinetic Model for JP-8 Surrogate Mixtures. Combust. Sci. Technol. 2002, 174, 399−417.

29. Podlesak, T.; Hendrickson, M.; Matthews, S.; Nawrocki, E.; Seibert, M.; Zalewski, M. Army Stirling Engine Research and Development - Past, Present and Future. Power Sources Conference 2010, 44, 462−465.

30. Malewicki, T.; Brezinsky, K. Experimental and Modeling Study on the Pyrolysis and Oxidation of n-Decane and n-Dodecane. Proc. Combust. Inst. 2013, 34, 361−368.

31. Dooley, S.; Won, S. H.; Chaos, M.; Heyne, J.; Ju, Y.; Dryer, F. L.; Kumar, K.; Sung, C.-J.; Wang, H.; Oehlschlaeger, M. A.; et al. A Jet Fuel Surrogate Formulated by Real Fuel Properties. Combust. Flame 2010, 157, 2333−2339

32. Curtiss, L. A.; Raghavachari, K.; Redfern, P. C.; Rassolov, V.; Pople, J. A. Gaussian-3 (G3) Theory for Molecules Containing First and Second-Row Atoms. J. Chem. Phys. 1998, 109, 7764−7776.

33. Baboul, A. G.; Curtiss, L. A.; Redfern, P. C.; Raghavachari, K. Gaussian-3 Theory Using Density Functional Geometries and ZeroPoint Energies. J. Chem. Phys. 1999, 110, 7650−7657.

34. Curtiss, L. A.; Raghavachari, K.; Redfern, P. C.; Baboul, A. G.; Pople, J. A. Gaussian-3 Theory Using Coupled Cluster Energies. Chem. Phys. Lett. 1999, 314, 101−107.

35. Georgievskii, Y.; Miller, J. A.; Burke, M. P.; Klippenstein, S. J. Reformulation and Solution of the Master Equation for Multiple-Well Chemical Reactions. *The Journal of Physical Chemistry* A 2013, 117, 12146−12154.

36. Georgievskii, Y.; Klippenstein, S. J. MESS.2016.3.23, http://tcg. cse.anl.gov/papr/codes/mess.html. (78) Troe, J. Theory of Thermal Unimolecular Reactions at Low Pressures. I. Solutions of the Master Equation. J. Chem. Phys. 1977, 66, 4745−4757.

37. Jasper, A. W.; Oana, C. M.; Miller, J. A. Third-Body" Collision Efficiencies for Combustion Modeling: Hydrocarbons in Atomic and Aiatomic Baths. Proc. Combust. Inst. 2015, 35, 197−204.

38. Jasper, A. W.; Miller, J. A. Lennard−Jones Parameters for Combustion and Chemical Kinetics Modeling from Full-Dimensional Intermolecular Potentials. Combust. Flame 2014, 161, 101−110.

39. Harding, L. B.; Georgievskii, Y.; Klippenstein, S. J. Predictive Theory for Hydrogen Atom - Hydrocarbon Radical Association Kinetics. *The Journal of Physical Chemistry* A 2005, 109, 4646−4656. (82) Klippenstein, S. J.; Georgievskii, Y.; Harding, L. B. Predictive Theory for the Combination Kinetics of Two Alkyl Radicals. Phys. Chem. Chem. Phys. 2006, 8, 1133−1147.

40. Cool, T. A.; McIlroy, A.; Qi, F.; Westmoreland, P. R.; Poisson, L.; Peterka, D. S.; Ahmed, M. Photoionization Mass Spectrometer for Studies of Flame Chemistry With a Synchrotron Light Source. Rev. Sci. Instrum. 2005, 76, 094102.

41. Qi, F.; Yang, R.; Yang, B.; Huang, C. Q.; Wei, L. X.; Wang, J.; Sheng, L. S.; Zhang, Y. W. Isomeric Identification of Polycyclic Aromatic Hydrocarbons Formed in Combustion With Tunable Vacuum Ultraviolet Photoionization. Rev. Sci. Instrum. 2006, 77, 084101.

42. Li, Y. Y.; Zhang, L. D.; Tian, Z. Y.; Yuan, T.; Zhang, K. W.; Yang, B.; Qi, F. Investigation of The Rich Premixed Laminar Acetylene/Oxygen/Argon Flame: Comprehensive Flame Structure and Special Concerns of Polyynes. Proc. Combust. Inst. 2009, 32, 1293−1300.

43. Podlesak, T.; Hendrickson, M.; Matthews, S.; Nawrocki, E.; Seibert, M.; Zalewski, M. Army Stirling Engine Research and Development - Past, Present and Future. Power Sources Conference 2010, 44, 462−465.

44. Malewicki, T.; Brezinsky, K. Experimental and Modeling Study on the Pyrolysis and Oxidation of n-Decane and n-Dodecane. Proc. Combust. Inst. 2013, 34, 361−368.

45. MacDonald, M. E.; Ren, W.; Zhu, Y.; Davidson, D. F.; Hanson, R. K. Fuel and Ethylene Measurements During n-Dodecane, Methylcyclohexane, and iso-Cetane Pyrolysis in Shock Tubes. Fuel 2013, 103, 1060−1068.

46. Banerjee, S.; Tangko, R.; Sheen, D. A.; Wang, H.; Bowman, C. T. An Experimental and Kinetic Modeling Study of n-Dodecane Pyrolysis and Oxidation. Combust. Flame 2016, 163, 12−30.

Table 4.1 Compilation of Products Observed in the Experiemental Decomposition of n-

Dodecane

Molecule	Formula	Mass	Structure
Hydrogen	H_2	2	H——H
Methyl radical	CH_3	15	$CH_3\bullet$
Acetylene	C_2H_2	26	
Ethylene	C_2H_4	28	
Ethyl radical	C_2H_5	29	
Allene	C_3H_4	40	
Methylacetylene	C_3H_4	40	
Allyl radical	C_3H_5	41	
Propene	C_3H_6	42	
1,3-Butadiene	C_4H_6	54	
1-Butene	C_4H_8	56	
2-Butene	C_4H_8	56	
1-Pentene	C_5H_{10}	70	
1-Hexene	C_6H_{12}	84	
1-Heptene	C_7H_{14}	98	

Figure 4.1 Potential Energy Diagram for Primary and Secondary Dissociation Channels of n-Decane.

Figure 4.2 Calculated Rate Constants at 1 atm for Unimolecular Reactions: (a) for C-C and C-H Bond Cleavages in $C_{12}H_{26}$ (b) for C_1H_{26} + H Direct H Abstractions and (c) for C-C Bond β-Scissions in n-Dodecyl Radicals $C_{12}H_{25}$ (n=1-6)

(a)

(b)

(c)
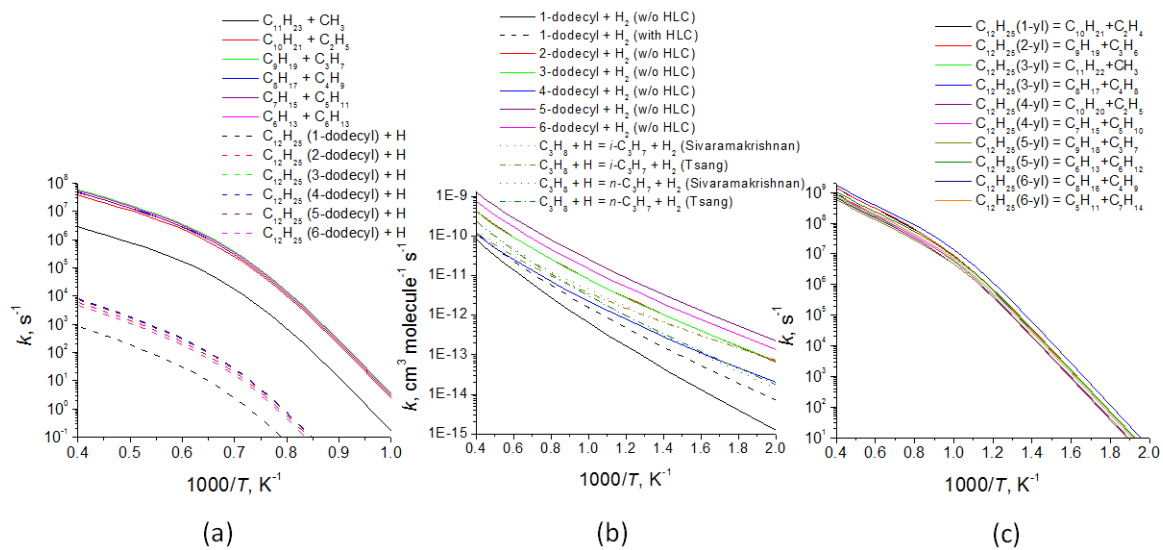
Table 4.2 Calculated Barrier Heights and Reaction Energies for Various C-C Bond β-

Scission and Direct H Abstraction Reactions

Reactions	Barrier (kJ/mol)	Reaction energy (kJ/mol)
$C_{11}H_{23} \rightarrow C_9H_{19} + C_2H_4$	124	90
$C_{10}H_{21} \rightarrow C_8H_{17} + C_2H_4$	123	89
$C_9H_{19} \rightarrow C_7H_{15} + C_2H_4$	124	89
$C_8H_{17} \rightarrow C_6H_{13} + C_2H_4$	124	92
$C_7H_{15} \rightarrow C_5H_{11} + C_2H_4$	124	91
$C_6H_{13} \rightarrow C_4H_9 + C_2H_4$	124	89
$C_5H_{11} \rightarrow C_3H_7 + C_2H_4$	124	89
$C_4H_9 \rightarrow C_2H_5 + C_2H_4$	123	86
$C_3H_7 \rightarrow CH_3 + C_2H_4$	126	86
$C_{12}H_{25}$ (1-dodecyl) $\rightarrow C_{10}H_{21} + C_2H_4$	124	90
$C_{12}H_{25}$ (2-dodecyl) $\rightarrow C_9H_{19} + C_3H_6$	124	92
$C_{12}H_{25}$ (3-dodecyl) $\rightarrow C_{11}H_{22} + CH_3$	125	89
$C_{12}H_{25}$ (3-dodecyl) $\rightarrow C_8H_{17} + C_4H_8$	125	93
$C_{12}H_{25}$ (4-dodecyl) $\rightarrow C_{10}H_{20} + C_2H_5$	123	88
$C_{12}H_{25}$ (4-dodecyl) $\rightarrow C_5H_{10} + C_7H_{15}$	125	93
$C_{12}H_{25}$ (5-dodecyl) $\rightarrow C_9H_{18} + C_3H_7$	125	92
$C_{12}H_{25}$ (5-dodecyl) $\rightarrow C_6H_{12} + C_6H_{13}$	125	93
$C_{12}H_{25}$ (6-dodecyl) $\rightarrow C_7H_{14} + C_5H_{11}$	125	92
$C_{12}H_{25}$ (6-dodecyl) $\rightarrow C_8H_{16} + C_4H_9$	125	92
$C_{12}H_{26} + H \rightarrow C_{12}H_{25}$ (1-dodecyl) $+ H_2$	49 (42)[a]	-12 (-19)[a]
$C_{12}H_{26} + H \rightarrow C_{12}H_{25}$ (2-dodecyl) $+ H_2$	36 (28)[a]	-24 (-31)[a]
$C_{12}H_{26} + H \rightarrow C_{12}H_{25}$ (3-dodecyl) $+ H_2$	36 (28)[a]	-23 (-30)[a]
$C_{12}H_{26} + H \rightarrow C_{12}H_{25}$ (4-dodecyl) $+ H_2$	35 (28)[a]	-23 (-31)[a]
$C_{12}H_{26} + H \rightarrow C_{12}H_{25}$ (5-dodecyl) $+ H_2$	35 (27)[a]	-23 (-31)[a]
$C_{12}H_{26} + H \rightarrow C_{12}H_{25}$ (6-dodecyl) $+ H_2$	35 (27)[a]	-23 (-30)[a]

[a]The values including the higher level correction (HLC) for H abstractions are given in parenthesis.

Figure 4.3 Proposed Reaction Mechanism for the Pyrolysis of n-Dodecane

C_2H_4 (ethylene) + C_6H_{13} ◄

C_3H_6 (propene) + C_5H_{11} ◄

C_4H_8 (1-butene) + C_4H_9 ◄

C_5H_{10} (1-pentene) + C_3H_7 ◄

C_6H_{12} (1-hexene) + C_2H_5 ◄

C_7H_{14} (1-heptene) + CH_3 ◄

C_8H_{16} (1-octene) + H ◄--

−C_8H_{17} + C_4H_9

→ C_2H_5 + C_2H_4 − 2H → C_4H_6 (1,3-butadiene)

→ C_4H_8 (1-butene) + H

isomerization ┊ − 2H

2-butene **C_6H_{13} + C_6H_{13}**

→ C_2H_4 (ethylene) + C_4H_9

→ C_3H_6 (propene) + C_3H_7

→ C_4H_8 (1-butene) + C_2H_5

→ C_5H_{10} (1-pentene) + CH_3

→ C_6H_{12} (1-hexene) + H

C_2H_4 (ethylene) + C_8H_{17} ◄

C_3H_6 (propene) + C_7H_{15} ◄

C_4H_8 (1-butene) + C_6H_{13} ◄

C_5H_{10} (1-pentene) + C_5H_{11} ◄

C_6H_{12} (1-hexene) + C_4H_9 ◄

C_7H_{14} (1-heptene) + C_3H_7 ◄

C_8H_{16} (1-octene) + C_2H_5 ◄

C_9H_{18} (1-nonene) + CH_3 ◄

$C_{10}H_{20}$ (1-decene) + H ◄--

$C_{10}H_{21}$ + C_2H_5 ◄ **$C_{12}H_{26}$** → **C_5H_{11} + C_7H_{15}**

H + C_2H_4
− H_2/−2H ┊
C_2H_2

C_3H_7 + C_2H_4
C_3H_6 (propene) + C_2H_5
C_5H_{10} (1-pentene) + H ◄

→ C_2H_4 (ethylene) + C_5H_{11}

→ C_3H_6 (propene) + C_4H_9

→ C_4H_8 (1-butene) + C_3H_7

→ C_5H_{10} (1-pentene) + C_2H_5

→ C_6H_{12} (1-hexene) + CH_3

--→ C_7H_{14} (1-heptene) + H

C_9H_{19} + C_3H_7

→ C_2H_4 (ethylene) + CH_3

→ C_3H_6 (propene) + H
┊ − H
C_3H_5
┊ − H
C_3H_4

C_2H_4 (ethylene) + C_7H_{15}

C_3H_6 (propene) + C_6H_{13} ◄

C_4H_8 (1-butene) + C_5H_{11} ◄

C_5H_{10} (1-pentene) + C_4H_9 ◄

C_6H_{12} (1-hexene) + C_3H_7 ◄

C_7H_{14} (1-heptene) + C_2H_5 ◄

C_8H_{16} (1-octene) + CH_3 ◄

C_9H_{18} (1-nonene) + H ◄--

$C_{12}H_{26}$ + H

$C_{12}H_{25}$(2-dodecyl)
+ H_2

$C_{12}H_{25}$(3-dodecyl)
+ H_2

$C_{12}H_{25}$(4-dodecyl)
+ H_2

$C_{12}H_{25}$(5-dodecyl)
+ H_2

$C_{12}H_{25}$(6-dodecyl)
+ H_2

$C_{11}H_{22}$(1-undecene)
+ CH_3

$C_{10}H_{20}$(1-decene)
+ C_2H_5

C_9H_{18}(1-nonene)
+ C_3H_7

C_8H_{16}(1-octene)
+ C_4H_9

C_3H_6(propene)
+ C_9H_{19}

C_4H_8(1-butene)
+ C_8H_{17}

C_5H_{10}(1-pentene)
+ C_7H_{15}

C_6H_{12}(1-hexene)
+ C_6H_{13}

C_7H_{14}(1-heptene)
+ C_5H_{11}

69

Figure 4.4 Summary of Reaction Mechanism Leading to Primary Products in the

Decomposition of n-Dodecane

n-dodecane, $C_{12}H_{26}$

Hydrogen abstraction   C-C bond rupture

n-dodecyl radicals (n=2 to 6)   1-alkyl radicals (C2-C10)

C-C beta scission   Hydrogen migration   C-C beta scission

C-C beta scission

C3-C11 alkenes ← n-alkyl radicals   **CH$_3$, C$_2$H$_5$, C2-C8 alkenes**
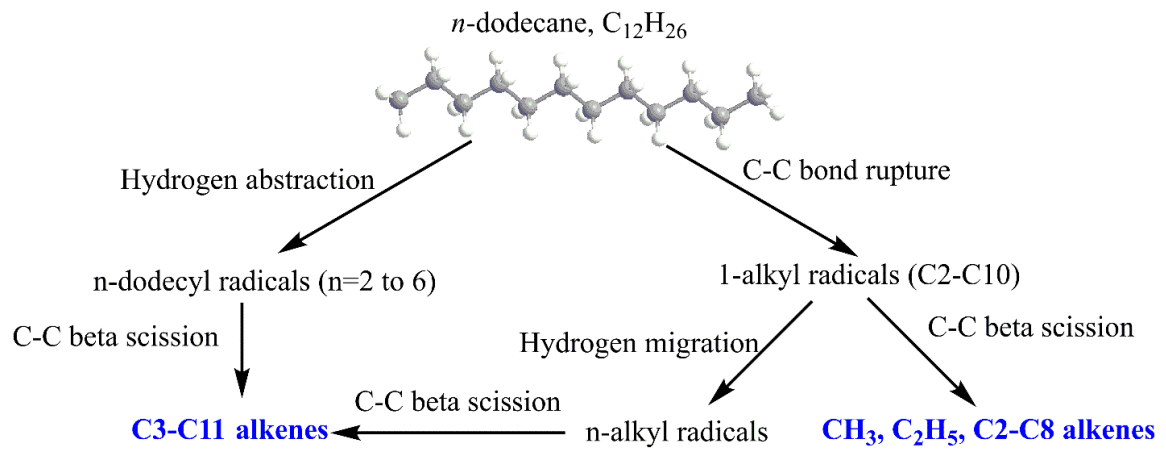
Chapter V

A Theoretical Study on Pyrolysis of Jet Propellant 8 Components: The Behavior of Aliphatic and Non-Aliphatic Alkyl Rings

Introduction:

Kerosene-based jet fuel JP-8 commonly used in airplanes consists of four main groups of hydrocarbons, such as aliphatic 'paraffins' (33-61% *n*-alkanes and isoalkanes; 1-5% olefins), monocyclic 'paraffins' (10–20%), alkyl-substituted benzenes (12-22%) including butylbenzenes, and polycyclic aromatic hydrocarbons (PAHs) (10–20%), as well as of some additives at the sub percent level: fuel system icing inhibitors, corrosion inhibitors, and static dissipaters.[1-11] The underlying elementary chemical steps involved in the oxidation of hydrocarbon fuels such as kerosenes are still not completely understood because the current chemical models are unable to account for the complexity of real systems either in form of multifaceted mixtures of chemicals (as in JP-8) or the complexity of the molecular structure of the hydrocarbon itself (as in the synthetic JP-10 fuel). Considering the molecular complexity, Troe[1] and others[2-5] concluded that understanding has to commence with the knowledge of the elementary reaction mechanisms of the decomposition of the fuel component itself along with the oxidation of the fragments formed in these processes both experimentally and computationally on the most elementary, fundamental level. Such understanding can be achieved by using experiments and theory to decouple the pyrolysis of the fuel from the oxidation of relatively small individual hydrocarbon fragments and their radicals formed as a result of the pyrolysis. Following sophisticated chemical models, Wang et al.[1-3] provided compelling evidence that the pyrolysis of hydrocarbon fuels such as JP-8 and JP-10 requires a few 10 μs such as around 20 μs for the decomposition of dodecane. Since the oxidation of the hydrocarbon fragments occurs at time scales of typically a few 100 μs and the ignition engages at normally close to 1000 μs, the pyrolysis stage can be decoupled from the oxidation chemistry of the hydrocarbon fragments and their radicals.

It is therefore critical to determine which particular fragments and in what proportions are formed at the pyrolysis stage from various significant fuel components.

The development of reliable chemical kinetic models requires accurate input parameters and an intimate understanding of the very first processes, which initiate bond rupture processes in JP-8 components, provide a pool of radicals, and control the autoignition, under realistic, combustion relevant physical conditions.[10,16,1-3] The unimolecular decomposition, or pyrolysis, of these components lead to smaller hydrocarbon molecules and reactive transient species, among them aliphatic radicals, resonantly stabilized free radicals, and aromatic radicals, which initiate and drive the complex chemistry in the combustion of JP-8 jet fuel. Thus, the initial decomposition chemistry delivers the building blocks for the oxidation of JP-8 jet fuel. In our recent works, we began systematic experimental and theoretical studies of the initial (nascent) products of the pyrolysis of the JP-8 fuel components and probed the pyrolysis of prototype JP-8 aliphatic ingredients: n-decane $C_{10}H_{22}$1 and n-dodecane $C_{12}H_{26}$.[2] The pyrolysis was explored in a high temperature chemical reactor allowing us to probe the decomposition of a hydrocarbon molecule under combustion-like temperatures up to 1600 K. The nascent product distribution was probed on line and *in situ* in a supersonic molecular beam utilizing soft photoionization with single photon vacuum ultraviolet (VUV) photons followed by a mass spectroscopic analysis of the ions in a reflectron time-of-flight mass spectrometer (Re-TOF), which allowed us to detect not only stable fragments but also radicals and thermally labile closed shell species,[25,2-10] which usually remain undetected if other experimental techniques are employed. The residence time in the reactor was limited to a few tens microseconds and hence we probed the *nascent reaction products* excluding successive higher-order reactions of the initially formed fragments, which may lead to molecular mass growth processes. The molecular beam

experiments were combined with electronic structure and theoretical kinetics calculations and this synergistic approach elucidated the nature of the products, their branching ratios, and reaction mechanisms involved in the decomposition of *n*-decane and *n*-dodecane over a broad range of combustion relevant temperatures and pressures. The theoretical calculations allowed us to account for all pyrolysis products observed experimentally and showed that, under the conditions in the chemical reactor, the primary and fast secondary decomposition reactions (mostly involving C-C and C-H bond β-scissions in the primary radical fragments) need to be considered to explain the nascent product distribution.

The present theoretical work continues this systematic investigation and addresses the prototype representatives of the second largest group of JP-8 components – alkyl-substituted benzenes, in particular, three different isomers of butylbenzene, $C_{10}H_{14}$, normal (*n*-butylbenzene), 1-*sec* (*s*-butylbenzene), and *tert* (*t*-butylbenzene). Among available experimental studies of the decomposition mechanism of these molecules, Yahagi explored the pyrolysis of *t*-butylbenzene in the presence of hydrogen gas at temperatures up to 923 K. He was able to detect only closed shell reaction products including benzene, toluene, methane, propene, propane, ethylene, and ethane and inferred a free-radical chain mechanism. Early pyrolysis experiments on *n*-butylbenzene followed by chromatographic detection of aromatic hydrocarbons also proposed radical-initiated chain reactions. The involvement of radical transient species likewise gained support from Leigh et al.'s study in which the authors explored the pyrolysis of *n*-butylbenzene and detected ethylene proposing a radical chain mechanism initiated by the dissociation of *n*-butylbenzene into benzyl and propyl radicals, $C_6H_5CH_2CH_2CH_2CH_3$ → $C_6H_5CH_2 + CH_2CH_2CH_3$, followed by decomposition of propyl radicals to ethane and the methyl radical, $CH_3CH_2CH_2$ → $CH_3 + C_2H_4$. Further, Tsang[27] studied the pyrolysis of

t-butylbenzene suggesting the existence of C_4H_9 and C_6H_5 transient radicals. Troe and co-workers exploited flash photolysis followed by UV-VIS spectroscopy to elucidate the formation of the methyl radical plus the 2-phenyl-prop-2-yl radical in the thermally activated decomposition of *t*-butylbenzene at temperature ranging from 885 K to 1700 K. The effect of the molecular structure of the butyl chain (*n*- versus *t*-) in the pyrolysis of butylbenzenes was also investigated by Ma et al.[40] and Peng et al.[41] proposing the initial formation of phenyl (C_6H_5) plus *t*-butyl (*t*-C_4H_9) and benzyl ($C_6H_5CH_2$) and propyl radicals (C_3H_7), respectively. Peng et al. also probed off line and *ex situ* the formation of higher molecular weight products such as naphthalene, biphenyl, methylbiphenyl, fluorene, and phenylnaphthalene. While all these studies provided important data for the development of kinetic models for butylbenzene pyrolysis, the observed products included not only the nascent but also higher-order products. Most recently, Zhang et al. investigated the pyrolysis of *n*-butylbenzene in a flow reactor, with comprehensive detection of both reactive and stable products using synchrotron vacuum UV photoionization mass spectrometry. They evaluated mole fractions for a variety of the observed products vs. temperature at different pressures of 30- 760 Torr and developed a kinetic model of *n*-butylbenzene pyrolysis using their new data to validate the model. The authors concluded that the benzylic C-C bond dissociation producing benzyl + propyl is the key decomposition reaction.

While kinetic models for the pyrolysis of butylbenzenes have been developed, most of the rate constants utilized in these models, especially those for the initial decomposition steps, are not physics-based, i.e., they are not taken either from experimental kinetics measurements for elementary chemical reactions or from theoretical kinetics calculations based on *ab initio* potential energy surfaces (PES). These rate constants are either approximately evaluated from analogous reactions,

estimated from empirical rate rules, or simply guessed and adjusted to achieve the best fit of the measured concentration profiles for various species produced in the pyrolysis. Theoretically, to our best knowledge, the reaction mechanism, rate constants, and product branching ratios for unimolecular decomposition of butylbenzene isomers have never been studied. In fact, high-level reliable theoretical data on the structure and energetics of these molecules computed by *ab initio* or density functional methods are sparse owing to a relatively large molecular size. Most of theoretical works found in the literature address relative stability of different conformers. Several combined theoretical/experimental studies devoted to the conformational stability and the molecular shape, rotational constants, and ionization energies of *n*- and *t*-butylbenzenes have been reported.[44-48] In terms of thermochemical properties, density functional calculations have been performed to evaluate the enthalpy of formation and C-C bond dissociation energies for *t*-butylbenzene along with *n*-decane and *n*-dodecane.[49] Theoretical studies of the reaction mechanism and kinetics have been limited to a study of cyclization pathways for the butylbenzene radical[50] employing rather low-level DFT calculations. The goal of the present work is to bridge the existing knowledge gap: to unravel the pyrolysis mechanism of butylbenzenes using accurate and reliable calculated PESs, to generate physics-based rate constants for the critical reaction steps, which can be utilized in improved kinetic models, to predict the most important nascent pyrolysis products, and to compare them with the available experimental data.

Methods:

Geometries of the *n*-, *s*-, and *t*- isomers of butylbenzene $C_{10}H_{14}$, their primary and secondary decomposition products, and transition states for secondary decomposition reactions on the $C_{10}H_{13}$ PES via C-C and C-H bond β-scissions have been optimized

76

using the density functional B3LYP method[51,52] with the 6-311G(d,p) basis set. Vibrational frequencies of all stationary structures were computed at the same B3LYP/6-311G(d,p) level of theory. Relative energies were refined by single-point calculations using B3LYP/6-311G(d,p) optimized geometries at the G3(CCSD,MP2) level of theory,[53-55] which included B3LYP/6-311G(d,p) zero-point vibrational energy corrections (ZPE) and the empirical higher level corrections (HLC).[54] According to the equations for HLC, which differ for molecules and atoms, the inclusion of the HLC increases the calculated strengths of C-H bonds by 7 kJ mol^{-1}, but is insignificant for C-C bond cleavages, and zero by definition for C-C bond β-scissions in radicals. The G3(CCSD,MP2)//B3LYP theoretical scheme normally provides the energetic parameters with 'chemical accuracy' within 3-6 kJ mol^{-1} for hydrocarbons in terms of average absolute deviations.[54] For secondary reactions on the C_9H_{11} PES we used the molecular parameters and energies calculated at a similar G3(CCSD,MP2)//B3LYP level of theory in relation to the C_6H_5 + C_3H_6 reaction.3 One additional pathway was calculated and included here, the decomposition of 1-phenyl-prop-3-yl radical to benzyl + C_2H_4, which was not considered in the previous work. For decomposition of various primary C_8H_9 products, we employed the doubly-hybrid density functional B2PLYPD3 method[57-59] with Dunning's cc-pVDZ basis set[60] where geometries of various species were optimized and vibrational frequencies were calculated and single-point energies were refined utilizing the explicitly correlated coupled clusters CCSD(T)-F12 approach[61,62] with the cc-pVTZ-f12 basis set. All the ab initio calculations were performed using the GAUSSIAN 09[63] and MOLPRO 2010[63] program packages.

Rate constants for various primary and secondary reactions involved in the pyrolysis of the butylbenzene isomers have been computed using the Rice-Ramsperger-Kassel-Marcus Master Equation (RRKM-ME) approach by solving the one-dimensional

master equation[65] with the MESS package.[66] Rate constants $k(T)$ for individual reaction

steps were calculated within RRKM (unimolecular reactions) or transition state theory

(TST, bimolecular reactions) generally utilizing the Rigid-Rotor, Harmonic-Oscillator

(RRHO) model for the calculations of partition functions for molecular complexes and

transition states. Hindered rotor treatment for low-frequency torsional modes was

applied only to smaller C_9H_{11} and C_8H_9 systems, for which such 'soft' normal modes

were visually examined and those representing internal rotations were considered as

hindered rotors in partition function calculations. One-, two-, and even three- (for some

C_9H_{11} structures[67]) dimensional torsional potentials were calculated by scanning the PES

at the B3LYP/6-311G(d,p) level of theory. However, for butylbenzenes themselves and

$C_{10}H_{13}$ radicals, hindered rotor treatment is rather complicated because they possess up

to four hindered rotors corresponding to four different single bonds and these rotors

could be strongly coupled. For simplicity, all these convoluted rotations were treated as

harmonic oscillators. In our previous work,[23] we compared the results of the RRHO

treatment with and without inclusion of hindered rotors for smaller C_3H_7 and C_4H_9

radicals and found maximal deviations in rate constants of 41% at 1000 K and 25% at

1600 K. Therefore, the initial C-C and C-H bond cleavages in butylbenzenes were

treated within RRHO keeping in mind the above mentioned error bars in rate constants.

It should be noted that absolute errors in the partition function caused by the treatment

of torsional modes as harmonic oscillators in a molecule with multiple coupled torsional

modes could be 1-2 orders of magnitude in error according to Truhlar and coworkers,[68]

but the errors in the rate constants observed in our calculations likely resulted from the

cancellation of errors in the partition functions of transition states (in the numerator) and

reactants (in the denominator) because in the transition states and reactants most of

torsional modes (besides one or two) are similar. For a system with a small number of

torsional modes (ethanol), Truhlar and coworkers found the effect of more accurate internal-coordinate multi-structural treatment to be within a factor of 1.8-3.4 as compared to the use of harmonic oscillators; these values should be considered as an upper limit for error bars of our pure RRHO calculations. The errors in ratios of rate constants are expected to be smaller than the errors in their absolute values as the result of cancelations of similar inaccuracies and hence we anticipate that relative product yields are predicted well by our calculations.

Collisional energy transfer rates in the master equation were expressed using the "exponential down" model,[69] with the temperature dependence of the range parameter α for the deactivating wing of the energy transfer function expressed as $\alpha(T) = \alpha_{300}(T/300 K)^n$, with $n = 0.86$ and $\alpha_{300} = 228$ cm^{-1} obtained earlier from classical trajectories calculations as 'universal' parameters for hydrocarbons in the nitrogen bath gas.[4] For RRKM-ME calculations on the $C_{10}H_{14}$ and $C_{10}H_{13}$ PESs, we used the Lennard-Jones parameters $(\varepsilon/cm^{-1}, \sigma/Å) = (237, 5.02)$ for the n-decane/nitrogen system derived by Jasper et al.[70] using the fit of results using the "one-dimensional optimization" method.[71] For the calculations on the C_9H_{11} surface, we used the collision parameters employed earlier in the study of the $C_6H_5 + C_3H_6$ system; in fact, we used the MESS input file for this system and augmented it with the transition state and bimolecular reactants on the additional pathways leading from benzyl + C_2H_4. Finally, RRKM-ME calculations on the C_8H_9 surface utilized the collision parameters $n = 0.61$ and $\alpha_{300} = 375$ cm^{-1} and $(\varepsilon/cm^{-1}, \sigma/Å) = (317, 4.46)$ derived earlier for the $C_6H_5 + C_2H_2$ system.[72]

The MESS package uses the eigenvalue approach for solving a Master Equation and for a well-defined description of a phenomenological rate constant to exist, chemical time scales (CSEs) must be well separated from vibrational–rotational time scales (IEREs).[73] When CSEs and IEREs overlap, the determination of the phenomenological

rate constants is compromised and no predictions can be made for isomers that rapidly equilibrate (merge) with other, more stable isomers or decomposition products. Merging with decomposition products often occurs in the systems considered here at high temperatures for closed-shell molecules and even at moderate temperatures for radicals. In such cases we used the language throughout the paper stating that a certain species does not survive above a certain temperature at a given pressure meaning that the species rapidly equilibrates with its decomposition products under these conditions but the phenomenological rate constant for the decomposition process is not well-defined.

For barrierless reactions, such as the C-C and C-H single bond cleavages in the original butylbenzene molecules, we used phase space theory.[74] The reverse rate constants for recombination of two hydrocarbon radicals or of a radical and H were fitted using potential parameters (pre-factor and power exponent) to reproduce the most accurate available rate constants for the prototype $CH_3 + C_2H_5$, $C_2H_5 + C_2H_5$, $CH_3 + i\text{-}C_3H_7$, $C_2H_5 + i\text{-}C_3H_7$, $CH_3 + t\text{-}C_4H_9$, $C_2H_5 + t\text{-}C_4H_9$, benzyl $C_7H_7 + H$, $C_2H_5 + H$, and $t\text{-}C_4H_9 + H$ calculated earlier by Klippenstein and co-workers[75-77] using variable reaction coordinated transition state theory (VRC-TST). For each particular case of a C-C or C-H bond cleavage in butylbenzenes, a most appropriate prototype reaction was selected on the basis of chemical similarity and the fits to the VRC-TST rate constants were attained with the accuracy within 1-2% in the entire 500-2500 K temperature range. Then, the fitted parameters were used in phase space theory calculations of rate constants for the decomposition reactions with the MESS package, which also gave results on pressure dependence. The accuracy of the rate constants of the barrierless single bond cleavages also relies upon the accuracy of equilibrium constants, which in turn is determined by the accuracy of the calculated reaction energy (3-6 kJ mol^{-1} for the

G3(CCSD,MP2)//B3LYP method) and the accuracy of the molecular parameters including rotational constants and vibrational frequencies, which is generally considered to be adequate for the B3LYP method.

Results and Discussion:

We first consider primary decomposition pathways of n-butylbenzene illustrated in Figure 1. There are three different C-C bond cleavages, which are favorable energetically. Those lead to the benzyl C_7H_7 + propyl C_3H_7 products with endothermicity of 341 kJ mol^{-1}, 1-phenyl-prop-3-yl C_9H_{11} + methyl CH_3 (369 kJ mol^{-1}), and $C_6H_5C_2H_4$ + ethyl C_2H_5 (375 kJ mol^{-1}). The cleavage of the C-C bond adjacent to the benzene ring and forming phenyl C_6H_5 + 1-butyl C_4H_9 is much less favorable (448 kJ mol^{-1}). Among C-H bond cleavages, the most favorable one occurs from the α carbon in the side chain producing 1-phenyl-but-1-yl with the energy loss of 369 kJ mol^{-1}. The other H losses from sp^3 carbon atoms require higher energies of 411, 408, and 420 kJ mol^{-1} and forming the corresponding 2-yl, 3-yl, and 4-yl 1-phenyl-butyl radicals, respectively. We do not consider here ruptures of C-H bonds on the sp^2 carbons of the aromatic ring, which are unlikely to compete because their bond energies are typically much higher such as 466 kJ mol^{-1} for benzene.[78] Figure 2a illustrates the total rate constant for the unimolecular decomposition of n-butylbenzene calculated at the high-pressure limit (HP) and finite pressure of 30 Torr, 1, 10, and 100 atm. The calculated rate constants were fitted by modified Arrhenius expressions, which are assembled in Table 2. One can observe a fall-off behavior of the rate constants and that at finite pressures, n-butylbenzene can survive dissociation only up to a certain temperature, 1650, 1800, 2000, and 2250 K at 30 Torr, 1, 10, and 100 atm, respectively. At higher temperatures, the lifetime of n-$C_{10}H_{14}$ becomes shorter than the time interval between collision and the RRKM-ME rate constant is no longer well defined. In practice this means that beyond

these temperature thresholds, *n*-butylbenzene would instantly equilibrate with its bimolecular decomposition products. The fall-off behavior is manifested, for example, by the fact that at 1500 K the rate constants calculated at 30 Torr, 1, 10, and 100 atm are factors of 9.2, 2.3, 1.3, and 1.1 lower than the HP values and the deviation from the HP limit further increases with temperature. According to the calculated branching ratios for the dissociation of *n*-butylbenzene (see Fig. 2b and Table 3), the $C_7H_7 + C_3H_7$ products are preferable at lower temperatures but, as temperature increases, the relative yield of $C_6H_5C_2H_4 + C_2H_5$ grows faster and becomes nearly equal or higher than that of $C_7H_7 + C_3H_7$. The formation of the $C_6H_5C_2H_4 + C_2H_5$ is also favored by pressure; at 2500 K and 100 atm the calculated $C_6H_5C_2H_4 + C_2H_5/C_7H_7 + C_3H_7$ branching ratio reaches 1.5. The $C_9H_{11} + CH_3$ products are predicted to be minor, with the maximal branching ratio of ~6% at the highest temperature and pressure considered. The calculated branching ratios of all other products do not exceed 0.3%. Summarizing, primary decomposition of *n*-butylbenzene is predicted to predominantly produce benzyl radical + C_3H_7 and C_8H_9 ($C_6H_5C_2H_4$) + C_2H_5. At the typical combustion conditions of 1500 K and 1 atm, the lifetime of *n*-butylbenzene is computed to be as short as 2.9 μs. We discussed in the previous works that C_3H_7 is likely to further decompose to $C_2H_4 + CH_3$, whereas C_2H_5 dissociates to $C_2H_4 + H$.[23,24] Secondary decomposition of the C_8H_9 and C_9H_{11} isomers will be considered in subsequent sections.

3.2. *s*-Butylbenzene

Unimolecular decomposition pathways of *s*-butylbenzene include C-C and C-H bond cleavages illustrated in Figure 3. The most favorable energetically channels of C-C bond cleavages lead to 1-phenyl-prop-1-yl $C_9H_{11} + CH_3$ (326 kJ mol^{-1}) and $C_6H_5CHCH_3 + C_2H_5$ (328 kJ mol^{-1}) followed by 2-phenyl-prop-3-yl $C_9H_{11} + CH_3$ endothermic by 371 kJ

mol^{-1}. The pathway leading to C_6H_5 + 2-butyl C_4H_9 is by far the least preferable, with the reaction energy of 424 kJ mol^{-1}. Among C-H bond cleavages, the channel in which an H atom is eliminated from the carbon atom linked to the phenyl group has the lowest endothermicity of 366 kJ mol^{-1} and forms a 2-phenyl-but-2-yl radical. The other sp^3 C-H bonds are stronger and their cleavages produce corresponding 1-yl, 3-yl, and 4-yl 2-phenyl-butyl radicals with the reaction energies of 419, 408, and 419 kJ mol^{-1}, respectively. As seen in Figure 4a, the total rate constant for unimolecular decomposition of *s*-butylbenzene behaves in a similar way as that for *n*-butylbenzene. The calculations indicate that *s*-$C_{10}H_{14}$ can survive up to 1500, 1800, 1800, and 2000 K at the pressures of 30 Torr, 1, 10, and 100 atm, respectively, and rapidly equilibrates with its bimolecular products at higher temperatures. The fall-off behavior is somewhat more pronounced than for *n*-$C_{10}H_{14}$; at 1500 K, the finite pressure decomposition rate constants at 30 Torr, 1, 10, and 100 atm are factors 18.8, 3.4, 1.6, and 1.1 lower the HP limit value, respectively. *s*-Butylbenzene is anticipated to be less stable than *n*-butylbenzene with respect to pyrolysis, as the lifetime computed at 1500 K and 1 atm is only 0.8 μs. In terms of the calculated branching ratios (Fig. 4b and Table 3), $C_6H_5CHCH_3$ + C_2H_5 is predicted to be the main decomposition product (83-86%) of *s*-$C_{10}H_{14}$ followed by 1-phenyl-prop-1-yl + CH_3 (14-15%), whereas 2-phenyl-prop-3-yl + CH_3 is a minor product with the relative yield normally below 1% but increasing to 1.6% at 100 atm and 2000 K. The relative yields of all other products of C-C and C-H bond cleavages do not exceed 0.1%. The product branching ratios appeared to be nearly insensitive to pressure (Table 3).

3.3. *t*-Butylbenzene

Taking into account a nearly free rotation of the phenyl group around the C-C bond it is linked to the central C atom, one can consider *t*-butylbenzene as a C_3-symmetric. In addition, each methyl group possesses local C_3 symmetry. As a consequence of such a symmetric structure, only three distinct C-C and C-H bond cleavage channels exist if we exclude unfavorable H eliminations from the aromatic ring (Figure 5). A methyl group loss producing 2-phenyl-prop-2-yl is the least endothermic process (318 kJ mol^{-1}), whereas the other two channels producing C_6H_5 + *t*-butyl C_4H_9 and *t*-phenyl-isobutyl $C_{10}H_{13}$ + H require much higher energies to occur, 412 and 421 kJ mol^{-1}, respectively. The difference in bond strengths is reflected in the fact that 2-phenyl-prop-2-yl + CH_3 is predicted as a nearly exclusive product of the pyrolysis of *t*-butylbenzene with its calculated branching ratio exceeding 99% at all considered temperatures and pressures. Figure 6 illustrates the overall rate constant for the unimolecular decomposition of *t*-$C_{10}H_{14}$, which is nearly identical to the rate constant of the channel producing 2-phenyl-prop-2-yl + CH_3. Clearly, this rate constant behaves in a similar way to those for *n*- and *s*-butylbenzenes considered above. Because of tertiary/benzylic C-C bond in *t*-butylbenzene, the rate constant is faster than the corresponding value for *n*-butylbenzene but comparable with that for *s*-butylbenzene. For instance, at 1500 K and 1 atm, the rate constant for the unimolecular decomposition of *t*-$C_{10}H_{14}$ is 1.29×10^6 s^{-1} (corresponding to the lifetime of 0.78 μs) compared to 3.39×10^5 s^{-1} (2.9 μs) and 1.23×10^6 s^{-1} (0.81 μs) for *n*- and *s*-$C_{10}H_{14}$, respectively. Similar to *s*-$C_{10}H_{14}$, at the pressures of 30 Torr, 1, 10, and 100 atm, *t*-butylbenzene can survive up to 1500, 1800, 1800, and 2000 K, respectively, and at higher temperatures should be considered as equilibrated with the 2-phenyl-prop-2-yl + CH_3 product. The fall-off behavior of the *t*-butylbenzene decomposition rate constant is also similar to that for *s*-

$C_{10}H_{14}$, as the finite pressure values at 1500 K, at 30 Torr, 1, 10, and 100 atm are factors 17.4, 3.2, 1.5, and 1.1 lower the HP limit rate constant, respectively.

Having established the predominant primary pyrolytic products of the three different butylbenzene isomers (C_7H_7 + C_3H_7 and $C_6H_5C_2H_4$ + C_2H_5 for n-$C_{10}H_{14}$, $C_6H_5CHCH_3$ + C_2H_5 and 1-phenyl-prop-1-yl C_9H_{11} + CH_3 for s-$C_{10}H_{14}$, and 2-phenyl-prop-2-yl C_9H_{11} + CH_3 for t-$C_{10}H_{14}$), we now move to consider secondary decomposition channels not studied earlier in detail in the literature and, in particular, discuss unimolecular decomposition of C_8H_9 and C_9H_{11} isomers and related reactions on the corresponding PESs. In addition, we consider decomposition of the most favorable $C_{10}H_{13}$ products, which, though unlikely to be formed directly via unimolecular dissociation of butylbenzenes, could be produced by H abstraction reactions by other radicals, such as by H atoms.

3.4. Reactions on the C_8H_9 PES

The most favorable decomposition pathways of $C_6H_5C_2H_4$ (W1) and $C_6H_5CHCH_3$ (W2) which are also related to the reaction of the phenyl radical C_6H_5 with ethylene C_2H_4 are illustrated in Figure 7. The $C_6H_5C_2H_4$ isomer can dissociate through a C-H β-scission reaction forming styrene via a barrier of 146 kJ mol^{-1} and a C-C β-scission process via a barrier of 162 kJ mol^{-1}, with endothermicities of 126 and 152 kJ mol^{-1}, respectively. Alternatively, W1 can isomerize to W2 or W3 via 1,2-H or 1,4-H shifts overcoming lower barriers of 138 and 123 kJ mol^{-1}, respectively. Four-member ring closure in W1 leading to a bicyclic structure W4 is also possible via a 133 kJ mol^{-1} barrier. Since W3 cannot directly decompose to any energetically favorable product, it is most likely to isomerize back to W1. On the other hand, W4 can dissociate to 1,2-dihydrobenzocyclobutene (1,2-DHB) + H which lies 24 and 50 kJ mol^{-1} above the C_6H_5 + C_2H_4 and styrene + H

bimolecular products, respectively. The most stable $C_6H_5CHCH_3$ isomer W2 dissociates to styrene + H overcoming a 187 kJ mol^{-1} barrier or rearranges to W1 via a 191 kJ mol^{-1} barrier but the isomerization of W2 to W3 via a 1,3-H shift is not competitive because of a much higher barrier of 269 kJ mol^{-1}.

It should be noted that the relative energies of various species calculated here at the CCSD(T)-F12/cc-pVTZ-f12//B2PLYPD3/cc-pVDZ level of theory agree within 5 kJ mol^{-1} with the results obtained by Tokmakov and Lin at the G2M level,[79] with the average absolute deviation between the two methods being 1.8 kJ mol^{-1}. The G2M approach is similar to G3(CCSD,MP2) employed for the $C_{10}H_{14}$ systems in the present study and the two methods normally provide comparable accuracies. Also, our recent calculations on the C_9H_{10} PES in relation to the $C_6H_5 + C_3H_5$ reaction (to be published elsewhere) gave the average absolute deviation between the CCSD(T)-F12/cc-pVTZ-f12 and G3(CCSD,MP2) energies as 2.3 kJ mol^{-1} and the maximal deviation was about 6 kJ mol^{-1}. Therefore, one can expect that the CCSD(T)-F12/cc-pVTZ-f12 method should improve the accuracy of the energetics as compared to G3(CCSD,MP2) by about 2 kJ mol^{-1} on average.

Rate constants for unimolecular decomposition of $C_6H_5C_2H_4$ and $C_6H_5CHCH_3$ are illustrated in Figures 8a and 8b. At low temperatures, W1 would mostly isomerize to W2 and W3, which gets collisionally stabilized, but the reaction is too slow. As temperature increases, the relative yield of the bimolecular products, styrene + H and $C_6H_5 + C_2H_4$, grows, while that of the stabilized intermediates decreases. As seen in Table 4, the branching ratio of styrene + H exceeds that of W1 at the temperatures of 1125, 1375, 1650, and 1800 K if the pressure is 30 Torr, 1, 10, and 100 atm, respectively. At these pressures, $C_6H_5C_2H_4$ is predicted to survive up to 1250, 1500, 1650, and 2250 K, respectively, and at the higher temperatures it would rapidly equilibrate with the

bimolecular products, predominantly styrene + H. The relative yield of C_6H_5 + C_2H_4 is generally smaller but grows with temperature up to 20-24%. Similarly, W2 isomerizes to W1 at low temperatures and predominantly dissociates to styrene + H as the temperature increases. Here, the decomposition channel takes over at the much lower temperature than for W1, 600 K at all considered pressures. It is predicted for W2 to be more stable than W1 and to survive up to 1375, 1650, 1800, and 2000 K at 30 Torr, 1, 10, and 100 atm, respectively. The predominant dissociation channel of W2 is styrene + H, with C_6H_5 + C_2H_4 contributing less than 10% even at high temperatures. At the typical combustion conditions of 1500 K and 1 atm, the rate constants for the $C_6H_5C_2H_4 \rightarrow$ styrene + H / C_6H_5 + C_2H_4 routes are 1.30×10^7 and 3.96×10^6 s^{-1}, respectively, corresponding to the overall lifetime of this radical with respect to the decomposition channels of only 58 ns. At the same conditions, the rate constants for the decomposition of $C_6H_5CHCH_3$ to styrene + H and C_6H_5 + C_2H_4 respectively are 7.34×10^6 and 3.03×10^5 s^{-1} and hence the lifetime of the more stable C_8H_9 isomer W2 is longer, 131 ns. Clearly, both $C_6H_5C_2H_4$ and $C_6H_5CHCH_3$ if formed as primary pyrolysis products of butylbenzenes, would undergo fast secondary dissociation to styrene + H and a minor amount of C_6H_5 + C_2H_4 on a nanosecond scale under typical combustion conditions.

It is also informative to compare the present results for the C_6H_5 + C_2H_4 reaction with the previous experimental and theoretical data. Figure 8c compares the overall rate constant computed here with the theoretical prediction of Tokmakov and Lin[79] based on their G2M PES and experimental values of Yu and Lin[80] in the low-temperature 300-500 K range and of Fahr et al.[81,82] at higher temperatures of 1000-1400 K. There is a very close match between the two sets of theoretical rate constants, which agree within 32%. In the low-temperature range, the present calculated rate values overestimate the experimental results by Yu and Lin by factors 1.36-2.36 but the agreement with the high-

temperature measurements by Fahr et al. is within 10%. Figure 5.8 also shows that the total rate constants for the $C_6H_5 + C_2H_4$ reaction are nearly indistinguishable at the four finite pressures considered here and the their fall off from the HP limit values maximal at 2500 K is only a factor of 1.4. Alternatively, relative product yields in the $C_6H_5 + C_2H_4$ reaction are sensitive to both temperature and pressure (Figure 5.8 and Table 5.4). At low temperatures, the stabilized $C_6H_4C_2H_4$ intermediate W1 is the main product but at higher temperatures the reaction predominantly forms styrene + H. The switch in the preference of these two products occurs around 1000, 1375, 1650, and 2050 K at the pressures of 30 Torr, 1, 10, and 100 atm, respectively, and in the highest temperatures intervals considered where W1 is no longer stable, styrene + H becomes practically the exclusive reaction product.

3.5. Reactions on the C_9H_{11} PES

For a detailed description of the C_9H_{11} surface in relation to the $C_6H_5 + C_3H_6$ reaction we address the reader to our previous work.[56] Kinetic calculations on this PES were also described earlier[67] but they mostly addressed bimolecular product formation in the reaction of phenyl with propene. Here, our interest is unimolecular decomposition of various C_9H_{11} isomers produced as primary products of pyrolysis of butylbenzenes. We employ the same surface and molecular parameters published earlier while considering these decomposition reactions. However, since the 1-phenyl-prop-3-yl ($C_6H_5CH_2CH_2CH_2$) $\rightarrow$ benzyl + C_2H_4 dissociation channel was not considered in the previous studies, it is included here. The present G3(CCSD,MP2)//B3LYP/6-311G(d,p) calculations gave the barrier and endothermicity for this C-C β-scission reaction as 95 and 58 kJ mol^{-1}, respectively. The benzyl + C_2H_4 bimolecular product resides 85 kJ mol^{-1} below $C_6H_5 + C_3H_6$ and is also more thermodynamically favorable than styrene + CH_3, 3-

phenylpropene + H, *trans*- and *cis*-1-phenylpropenes + H, and 2-phenylpropene by 15,

71, 52, 60, and 53 kJ mol^{-1}, respectively.

Calculations of the rate constants for unimolecular dissociation of 1-phenyl-prop-

3-yl (Figure 5.9), which can be formed in primary decomposition of *n*-butylbenzene,

show that this C_9H_{11} radical predominantly decomposes to benzyl + C_2H_4, with the yield

of the alternative products, indane + H and 3-phenylpropene + H, not exceeding 5 and

14%, respectively. The species 1-Phenyl-prop-3-yl can survive only up to 1000, 1250,

1500, and 1800 K at 30 Torr, 1, 10, and 100 atm, respectively, and its lifetime at 1250 K

and 1 atm is evaluated to be 21 ns. Therefore, it can be safely assumed that under

typical combustion conditions 1-phenyl-prop-3-yl rapidly dissociates mostly to benzyl and

ethylene on a nanosecond scale or faster. The primary pyrolysis of *s*-butylbenzene can

produce two C_9H_{11} isomers, 1-phenyl-prop-1-yl and 2-phenyl-prop-3-yl and their

unimolecular decomposition rate constants are shown in Figure 5.9. 1-Phenyl-prop-1-yl

appears to be slightly more stable than 1-phenyl-prop-3-yl as it can be collisionally

stabilized up to 1125, 1250, 1500, and 1650 K at the four pressures considered here and

its lifetime at 1250 K and 1 atm is computed as 43 ns. The predominant decomposition

product of 1-phenyl-prop-1-yl is styrene + CH_3 formed by C-C β-scission, whereas the

yield of *trans*-1-phenylpropene + H while increasing with temperature and pressure,

does not exceed 8%. 2-Phenyl-prop-3-yl (denoted as W2 in our previous work on the

kinetics of the $C_6H_5 + C_3H_6$ reaction[67]) can easily rearrange to 1-phenyl-prop-2-yl W1 by

migration of the phenyl group over the double C=C bond. The calculations show that

such isomerization with collisional stabilization of W1 is the major fate of W2, except at

high pressures and high temperatures when the styrene + CH_3 and 3-phenylpropene + H

products are also formed with significant relative yields (Table 5.3). Hence, in order to

reveal the ultimate decomposition products of W2, we need to additionally consider

unimolecular dissociation of W1 (Figure 5.9). Again, we can see that fast isomerization of W1 to the collisionally stabilized intermediate W2 prevails at low temperatures. Above 1000 K, the preferable dissociation pathways of W1 produce styrene + CH_3 and 3-phenylpropene + H with comparable branching ratios, but the latter product is favored by higher temperatures and pressures. At high temperatures, the branching ratio of the C_6H_5 + C_3H_6 bimolecular product of W1 also becomes significant and can reach 14% (Table 5.3). The calculated lifetime of 1-phenyl-prop-2-yl W1 with respect to its dissociation to the bimolecular products at 1250 K and 1 atm is 43 ns, nearly the same as that for 1-phenyl-prop-3-yl. Finally, we consider the decomposition of 2-phenyl-prop-2-yl, which is the main primary product of the pyrolysis of t-butylbenzene. This C_9H_{11} isomer nearly exclusively dissociates to 2-phenylpropene by an H atom loss from one of the methyl groups (Fig. 5). The rate constant calculations (Fig. 5.9) show that 2-phenyl-prop-2-yl can survive up to higher temperatures as compared to the other C_9H_{11} radicals considered above, 1250, 1500, 1800, and 2000 K at 30 Torr, 1 10, and 100 atm, respectively, and its lifetimes at 1250 K and 1500 K at the pressure of 1 atm are 97 and 43 ns, respectively.

Our RRKM-ME calculations also allow us to address the rate constant and product branching ratios of the reaction of benzyl with ethylene (Figure 5.10). The total rate constant shows a typical fall-off behavior (Figure 5.10) in the intermediate temperatures ranges of 700-1125, 800-1375, 1000-1650, and 1250-2000 K at 30 Torr, 1, 10, and 100 atm, respectively. Behavior attributed to the favorable dissociation of the initial C_9H_{11} intermediate 1-phenyl-prop-3-yl back to the benzyl + C_2H_4 reactants. As a result of the re-dissociation of the intermediate, the maximal deviations from the HP rate constants reach factors of 20 (1125 K, 30 Torr), 11.7 (1375 K, 1 atm), 6.7 (1650 K, 10 atm), and 4.1 (2000 K, 1000 atm). Above 2000 K, all finite-pressure rate constants

merge and their deviation from the HP values decreases. Such shape of finite-pressure

rate constants is characteristic for a reaction leading to an endothermic bimolecular

product via an exothermic intermediate and it reflects a competition between collisional

stabilization of the intermediate prevailing at low temperatures, its re-dissociation back to

the reactants, and dissociation to the products, which takes over at high temperatures. It

is also noteworthy that owing to the higher stability of the benzyl radical as compared to

phenyl, the C_7H_7 + C_2H_4 reaction proceeds via a 37 kJ mol^{-1} entrance barrier (Figure 5.1)

and is anticipated to be much slower than the C_6H_5 + C_2H_4 reaction. The ratio of the rate

constant of the latter and former reactions calculated at 1 atm is as high as 616 at 500 K,

but decreases to 58.5 and 5.3 at 1500 and 2500 K, respectively. As seen in Fig. 10b, at

lower temperatures the C_7H_7 + C_2H_4 reaction would mostly produce the collisionally

stabilized 1-phenyl-prop-3-yl intermediate, but at higher temperatures, 1000, 1250, 1500,

and 1800 K at 30 Torr, 1, 10, and 100 atm, respectively, when this intermediate is no

longer stable, 3-phenylpropene + H is predicted to become the predominant product,

with a minor contribution of indane + H.

3.6. Unimolecular decomposition of $C_{10}H_{13}$ radicals

Although $C_{10}H_{13}$ radicals are not anticipated to be efficiently produced via

unimolecular dissociation of butylbenzene isomers, they can be formed by direct H

abstraction such as by H atoms which become available through secondary

decomposition of the primary pyrolysis products or by other radicals present in flames.

Since the weakest C-H bond in $C_{10}H_{14}$ is most likely to be attacked in an H abstraction

reaction, here we consider secondary decomposition only for the most

thermodynamically favorable $C_{10}H_{13}$ products, 1-phenyl-but-1-yl from *n*-butylbenzene, 2-

phenyl-but-2-yl from *s*-butylbenzene, and *t*-phenyl-isobutyl from *t*-butylbenzene. The

calculated rate constants are illustrated in Figure 5.11. 1-Phenyl-but-1-yl dissociates by

a C-C bond β-scission to form styrene + C_2H_5. It should be noted that H migrations

leading to other 1-phenyl-butyl radicals were not considered here because they are not

anticipated to compete with β-scission. Only 1,2-, 1,3-, and 1,4-H shifts are feasible in 1-

phenyl-but-1-yl, whereas our previous studies of PESs for decyl and dodecyl radicals

have shown that only 1,5-, 1,6-, and 1,7-H shifts can be competitive with a C-C bond β-

scission process.[1] The RRKM-ME calculations indicate that 1-phenyl-but-1-yl can exist

up to temperatures of 1000, 1250, 1375, and 1650 K at the pressure of 30 Torr, 1, 10,

and 100 atm, respectively, and rapidly equilibrates with the styrene + C_2H_5 product at

higher temperatures (Figure 5.11). At 1 atm, the calculated lifetime of 1-phenyl-but-1-yl

at 1250 K is about 36 ns; thus, under typical combustion conditions this metastable

radical would eliminate the ethyl radical and form a stable styrene molecule on a

nanosecond scale or faster. The 2-phenyl-but-2-yl radical also rapidly decomposes by a

C-C bond β-scission producing 2-phenylpropene + CH_3. The stability of 2-phenyl-but-2-yl

is comparable to that of 1-phenyl-but-1-yl, as it is predicted to exist up to the same

temperatures at the same pressures and the lifetime at 1 atm and 1250 K with respect to

the decomposition via β-scission is 42 ns (Figure 5.11). Finally, t-phenyl-isobutyl has two

possible distinct C-C bond β-scission pathways leading to 2-phenylpropene + CH_3 and

phenyl + isobutyl C_4H_8 (Figure 5.5). The rate constant calculation show that the former

product channel is dominant (from 99.7-97.2% at 30 Torr to 99.7-80.7% at 100 atm),

with the latter channel being minor (Figure 5.11). The contribution of the phenyl +

isobutyl channel grows with temperature, especially at high pressures. t-Phenyl-isobutyl

appears to be slightly less stable than 1-phenyl-but-1-yl and 2-phenyl-but-2-yl and is

predicted to exist up to 900, 1125, 1250, and 1500 K at the four considered pressures,

respectively, and its calculated lifetime at the highest temperature it still exists at 1 atm,

is only 39 ns. Hence, the fate of *t*-phenyl-isobutyl is to rapidly undergo secondary decomposition predominantly to 2-phenylpropene + CH_3.

4. Discussion and Conclusions

We are now in position to summarize nascent pyrolytic products of butylbenzene isomers produced by primary dissociation followed by very fast secondary decomposition. Primary dissociation of *n*-butylbenzene produces mostly benzyl radical $C_7H_7 + C_3H_7$ and C_8H_9 ($C_6H_5C_2H_4$) + C_2H_5 with relative yields varying with temperature and pressure and a minor amount of 1-phenyl-prop-3-yl + CH_3. Fast secondary decomposition reactions break C_3H_7 to $C_2H_4 + CH_3$, C_2H_5 to $C_2H_4 + H$, $C_6H_5C_2H_4$ mostly to styrene + H and to a less extent to $C_6H_5 + C_2H_4$, and 1-phenyl-prop-3-yl mostly to benzyl + C_2H_4. Under the conditions where H atoms or other reactive radicals are available, the 1-phenyl-but-1-yl radical can be also formed as a primary product, which then rapidly dissociates to styrene + C_2H_5 and further to styrene + C_2H_4 + H. The main fragments of the pyrolysis of *n*-butylbenzene should include (in the order of a decreasing mass) styrene C_8H_8, benzyl C_7H_7, ethylene C_2H_4, methyl CH_3, and H atoms. Agreement is found with the results of the recent experimental study of the *n*-butylbenzene pyrolysis in a flow reactor using synchrotron vacuum ultraviolet photoionization mass spectrometry for the product detection,[43] which showed styrene, benzyl, and ethylene to be formed with highest mole fractions, along with ethylbenzene, toluene, methane, and ethane, whereas the yield of CH_3 was relatively low. According to our calculations, ethylbenzene, toluene, methane, and ethane are not nascent products. These stable molecules are probably produced via the recombination of benzyl with CH_3, benzyl with H, CH_3 with H, and of CH_3 with CH_3 or C_2H_5 with H, respectively. Such recombination processes would also clearly reduce the observed yield of methyl radicals. Another

noticeable observed product, benzene, can be formed via the C_6H_5 + H reaction. On the basis of their modeling results, the authors of this experimental work deduced that the benzylic C−C bond dissociation leading to C_7H_7 + C_3H_7 was the key decomposition reaction of *n*-butylbenzene under all considered conditions and H abstraction gave increasing contributions with rising pressure. Indeed, the observed mole fraction of styrene grows with temperature and pressure, which can be due to two factors, an increasing primary yield of the $C_6H_5C_2H_4$ radical further decomposing to styrene + H and the contribution of the H abstraction reaction forming 1-phenyl-but-1-yl rapidly dissociating to styrene + C_2H_5. The kinetic modeling results showed a reasonable qualitative agreement with the experimental mole fractions, but we expect that the use of the rate constants generated here from high-level quantum chemical and RRKM-ME calculations can improve the accuracy and reliability of the models and lend them a predictive power.

Li, Dagaut and coworkers have recently published a series of works describing experimental and kinetic modeling studies for a series of alkylbenzenes including toluene,[83.84] ethylbenzene,[85] and *n*-propylbenzene.[86] A direct comparison is not warranted because the experiments in a jet stirred reactor occur on a longer timescale and the kinetic modeling takes into account thousands of secondary reactions following the primary pyrolysis process, whereas our calculations consider the nascent pyrolytic products formed in the unimolecular primary and fast secondary decompositions. Nevertheless, our present results are in accord with the conclusions of Li, Dagaut and coworkers that the benzyl radical and styrene are the critical intermediates in the pyrolysis and oxidation of alkylbenzenes (with exception that for toluene styrene is not important) and that the benzylic C–C bond dissociation reaction is the dominant decomposition channel (benzylic C–H bond for toluene) and, as the alkyl side chain

elongates, the additional alkylic C–C bond cleavages also contribute, as do H abstraction pathways at certain conditions. Li, Dagaut and coworkers have shown that benzyl and styrene participate in a consequent growth of PAHs, such as naphthalene and indene, and hence, similar PAH growth processes can be significant at later stages of the butylbenzene pyrolysis.

Primary decomposition of *s*-butylbenzene is expected to form C_8H_9 ($C_6H_5CHCH_3$) + C_2H_5 and a minor amount of C_9H_{11} (1-phenyl-prop-1-yl) + CH_3. $C_6H_5CHCH_3$ undergoes secondary decomposition predominantly to styrene + H, whereas 1-phenyl-prop-1-yl rapidly dissociates to styrene + CH_3. If the 2-phenyl-but-2-yl radical can be formed by direct H abstraction, its dominant secondary dissociation channel produces 2-phenylpropene C_9H_{10} + CH_3. Thus, we anticipate that the main nascent pyrolysis product of *s*-butylbenzene should include styrene, ethylene (from C_2H_5), CH_3, H, and 2-phenylpropene, where the relative yield of the latter would correlate with the feasibility of direct H abstraction from the parent molecule. The largest difference of the pyrolysis of *s*-butylbenzene from that of *n*-butylbenzene is the absence of the nascent benzyl radical product, which can be traced to the molecular structure; *s*-butylbenzene does not have a $C_6H_5CH_2$ fragment. As in *n*-butylbenzene, the two benzylic C-C bonds in *s*-butylbenzene are weakest and their cleavage dominates the primary decomposition process.

Finally, *t*-butylbenzene gives 2-phenyl-prop-2-yl + CH_3 as a nearly exclusive primary product through a cleavage of one of the three equivalent C-C benzylic bonds. Which is in agreement with the experimental results by Troe et al. who observed the formation of 2-phenyl-prop-2-yl and methyl radicals using flash photolysis followed by UV-VIS spectroscopy.[39] However, our results do not support the suggestion by Ma et al.[40] concerning the initial formation of phenyl C_6H_5 + *t*-C_4H_9. Further, 2-phenyl-prop-2-yl rapidly and also nearly exclusively forms 2-phenylpropene + H. Considering a possibility

of a direct H abstraction from a methyl group, t-phenyl-isobutyl $C_{10}H_{13}$ can be formed and then undergo fast secondary decomposition mostly to 2-phenylpropene + CH_3 and a minor amount of phenyl + isobutene increasing with temperature and pressure. Thus, 2-phenylpropene, CH_3, and H are anticipated to be the dominant nascent products of the pyrolysis of t-butylbenzene, whereas phenyl and isobutene could be minor products serving as tracers of the contribution of H abstraction from the parent molecule. Clearly, the product menagerie from t-butylbenzene pyrolysis is expected to be much narrower than for the other butylbenzene isomers. The most striking difference is the absence of ethylene, which is the main pyrolysis product of alkanes and also gives a large contribution in the decomposition of n- and s-butylbenzenes. Again, this difference can be attributed to the molecular structure of t-butylbenzene, which does not feature any CH_2 groups.

Summarizing, the three butylbenzene isomers considered produce rather different nascent pyrolysis fragments, although there is a significant overlap between n- and s-butylbenzene. The presence of different fragments in distinguishable amounts can therefore influence the oxidation mechanism of these fuel components and hence affect the kinetics of their combustion. Pressure- and temperature-dependent rate constants generated here for the initial stages of pyrolysis of butylbenzenes assembled in Table 5.2 are recommended for kinetic modeling.

References:

1. Bruno, T. J.; Abel, K. R.; Riggs, J. R. Comparison of JP-8 and JP-8 +100 with the Advanced Distillation Curve Approach. *Energy Fuels* **2012,** *26*, 5843-5850.

2. Bezaire, N.; Wadumesthrige, K.; Simon Ng, K. Y.; Salley, S. O. Limitations of the Use of Cetane Index for Alternative Compression Ignition Engine Fuels. *Fuel* **2010,** *89*, 3807-3813.

3. Gregg, S. D.; Campbell, J. L.; Fisher, J. W.; Bartlett, M. G. Methods for the Characterization of Jet Propellent-8: Vapor and Aerosol. *Biomed. Chromatogr.* **2007**, *21*, 463-472.

4. Gough, R. V.; Bruno, T. J. Composition-Explicit Distillation Curves of Alternative Turbine Fuels. *Energy Fuels* **2013**, *27*, 294-302.

5. Meylemans, H. A.; Baldwin, L. C.; Harvey, B. G. LowTemperature Properties of Renewable High-Density Fuel Blends. *Energy Fuels* **2013**, *27*, 883-888.

6. Witten, M., L; Zeiger, E.; Ritchie, G. D. *Jet Fuel Toxicology*. CRC Press: Boca Raton, Florida, USA, 2011.

7. Rodgers, R. P.; Blumer, E. N.; Freitas, M. A.; Marshall, A. G. Jet Fuel Chemical Composition, Weathering, and Identification as a Contaminant at a Remediation Site, Determined by Fourier Transform Ion Cyclotron Resonance Mass Spectrometry. *Anal. Chem.* **1999**, *71*, 5171-5176.

8. DuBois, T. G.; Nieh, S. In *Effects of Hydrocarbon Chemical Class Composition on Autothermal Reforming of JP-8 Fuel*, Power Sources Conference, Las Vegas, Nevada, USA, Jun. 14-17; Curran Associates, Inc.: Las Vegas, Nevada, USA, 2010.

9. Echavarria, C. A.; Jaramillo, I. C.; Sarofim, A. F.; Lighty, J. S. Burnout of Soot Particles in a Two-Stage Burner with a JP-8 Surrogate Fuel. *Combust. Flame* **2012**, *159*, 2441-2448.

10. Wang, H.; Oehlschlaeger, M. A. Autoignition Studies of Conventional and Fischer−Tropsch Jet Fuels. *Fuel* **2012**, *98*, 249-258.

11. Merrill, E. A.; Gearhart, J. M.; Sterner, T. R.; Robinson, P. J. Improved Predictive Model for n-Decane Kinetics across Species, as a Component of Hydrocarbon Mixtures. *Inhalation Toxicol.* **2008**, *20*, 851-863.

12. Troe, J. Toward a Quantitative Understanding of Elementary Combustion Reactions. *Proc. Combust. Inst.* **1989**, *22*, 843-862.

13. Cox, R. A. *Kinetics and Mechanisms of Elementary Chemical Processes of Importance in Combustion. CEC Contract Final Report, EUR 12772.* Harwell Lab.: Harwell, UK, 1990.

14. Baulch, D. L.; Cobos, C. J.; Cox, R. A.; Esser, C.; Frank, P.; Just, Th.; Kerr, J. A.; Pilling, M. J.; Troe, J.; Walker, R. W., et al. Evaluated Kinetic Data for Combustion Modeling. *The Journal of Physical Chemistry Ref. Data* **1992**, *21*, 411-734.

15. Baulch, D. L.; Bowman, C. T.; Cobos, C. J.; Cox, R. A.; Just, Th.; Kerr, J. A.; Pilling, M. J.; Stocker, D.; Troe, J.; Tsang, W., et al. Evaluated Kinetic Data for

Combustion Modeling: Supplement II. *The Journal of Physical Chemistry Ref. Data* **2005**, *34*, 757-1397.

16. Miller, J. A.; Pilling, M. J.; Troe, J. Unravelling Combustion Mechanisms through a Quantitative Understanding of Elementary Reactions. *Proc. Combust. Inst.* **2005**, *30,* 43-88.

17. Sun, C., Sung, C. J.; Wang, H.; Law, C. K. On the Structure of Nonsooting Counterflow Ethylene and Acetylene Diffusion Flames. *Combust. Flame* **1996**, *107*, 321-335.

18. Banerjee, S; Tangko, R.; Sheen, D. A.; Wang, H.; Bowman, C. T. An Experimental and Kinetic Modeling Study of n-Dodecane Pyrolysis and Oxidation. *Combust. Flames* **2016**, *163*, 12–30.

19. Smolke, J.; Carbone, F.; Egolfopoulos, F. N.; Wang, H. Effect of n-Dodecane Decomposition on its Fundamental Flame Properties. *Combust. Flame* **2018**, *190*, 65-73.

20. Violi, A.; Yan, S.; Eddings, E. G.; Sarofim, F.; Granata, S.; Faravelli, T.; Ranzi, E. Experimental Formulation and Kinetic Model for JP-8 Surrogate Mixtures. *Combust. Sci. Technol.* **2002,** *174*, 399-417.

21. Mawid, M. A.; Park, T. W.; Sekar, B.; Arana, C. In *Development and Validation of A Detailed JP-8 Fuel Chemistry Model*, 2nd JANNAF Modeling and Simulation Subcommittee Meeting, Destin, Florida, Destin, Florida, 2002.

22. Podlesak, T.; Hendrickson, M.; Matthews, S.; Nawrocki, E.; Seibert, M.; Zalewski, M. Army Stirling Engine Research and Development - Past, Present and Future. *Proc. Power Sources Conference* **2010,** *44*, 462-465.

23. Zhao, L.; Yang, T.; Kaiser, R. I.; Troy, T. P.; Ahmed, M.; Belisario-Lara, D.; Ribeiro, J. M.; Mebel, A. M. Combined Experimental and Computational Study on the Unimolecular Decomposition of JP-8 Jet Fuel Surrogates. I. n-Decane (n-$C_{10}H_{22}$). *The Journal of Physical Chemistry A* **2017**, *121,* 1261–1280.

24. Zhao, L.; Yang, T.; Kaiser, R. I.; Troy, T. P.; Ahmed, M.; Ribeiro, J. M.; Belisario-Lara, D.; Mebel, A. M. Combined Experimental and Computational Study on the Unimolecular Decomposition of JP-8 Jet Fuel Surrogates. II: n-Dodecane (n-$C_{12}H_{26}$). *The Journal of Physical Chemistry A* **2017**, *121,* 1281–1297.

25. Zhang, F.; Kaiser, R. I.; Kislov, V. V.; Mebel, A. M.; Golan, A.; Ahmed, M. A VUV Photoionization Study of the Formation of the Indene Molecule and Its Isomers. *The Journal of Physical Chemistry Lett.* **2011,** *2*, 1731-1735.

26. Zhang, F.; Kaiser, R. I.; Golan, A.; Ahmed, M.; Hansen, N. A VUV Photoionization Study of the Combustion-Relevant Reaction of the Phenyl Radical (C_6H_5) with Propylene (C_3H_6) in a High Temperature Chemical Reactors. *The Journal of Physical Chemistry A* **2012,** *116*, 3541-3546.

27. Kaiser, R. I.; Belau, L.; Leone, S. R.; Ahmed, M.; Wang, Y. M.; Braams, B. J.; Bowman, J. M. A Combined Experimental and Computational Study on the Ionization Energies of the Cyclic and Linear C_3H Isomers. *Chemphyschem* **2007,** *8*, 1236-1239.

28. Kaiser, R. I.; Mebel, A.; Kostko, O.; Ahmed, M. On the Ionization Potentials of C_4H_3 Isomers. *Chem. Phys. Lett.* **2010,** *485*, 281-285.

29. Kaiser, R. I.; Sun, B. J.; Lin, H. M.; Chang, A. H. H.; Mebel, A. M.; Kostko, O.; Ahmed, M. An Experimental and Theoretical Study on the Ionization Energies of Polyynes $(H(CC)_nH; n = 1-9)$. *Astronom. J.* **2010,** *719*, 1884-1889.

30. Kaiser, R. I.; Maksyutenko, P.; Ennis, C.; Zhang, F. T.; Gu, X. B.; Krishtal, S. P.; Mebel, A. M.; Kostko, O.; Ahmed, M. Untangling the Chemical Evolution of Titan's Atmosphere and Surface - From Homogeneous to Heterogeneous Chemistry. *Faraday Discuss.* **2010,** *147*, 429-478.

31. Kaiser, R. I.; Krishtal, S. P.; Mebel, A. M.; Kostko, O.; Ahmed, M. An Experimental and Theoretical Study of the Ionization Energies of SiC_2H_x (x = 0, 1, 2) Isomers. *Astronom. J.* **2012,** *761*, 178(1)-178(7).

32. Golan, A.; Ahmed, M.; Mebel, A. M.; Kaiser, R. I. A VUV Photoionization Study on the Multichannel Reaction of Phenyl Radicals with 1,3-butadiene Under Combustion Relevant Conditions. *Phys. Chem. Chem. Phys.* **2013,** *15*, 341-347.

33. Kostko, O.; Zhou, J.; Sun, B. J.; Shiuan Lie, J.; Chang, A. H. H.; Kaiser, R. I.; Ahmed, M. Determination of Ionization Energies of C_nN (n = 4 - 12): Vacuum Ultraviolet Photoionization Experiments and Theoretical Calculations. *Astrophys. J.* **2010,** *717*, 674-682.

34. Parker, D. S.; Kaiser, R. I.; Troy, T. P.; Ahmed, M. Hydrogen Abstraction/Acetylene Addition Revealed. *Angew. Chem,. Int. Ed.* **2014,** *53*, 7740-7744.

35. Yahagi, N. Pyrolysis of tert-Butylbenzene in the Presence of Hydrogen. *Sekiyu Gakkaishi* **1981**, *24*, 1-8.

36. Badger, G. M.; Spotswood, T. M. Formation of Aromatic Hydrocarbons at High Temperatures. IX. Pyrolysis of Toluene, Ethylbenzene, Propylbenzene, and Butylbenzene. *J. Chem. Soc.* **1960**, 4420-4427.

37. Leigh, C. H.; Szwarc, M. The Pyrolysis of Butylbenzene and the Heat of Formation of Propyl Radical. *J. Chem. Phys.* **1952**, *20*, 407-411.

38. Tsang, W. Hydrocarbon Decomposition. 6. Thermal Decomposition of 3,4-Dimethylhexane, 2,2,3-Trimethylpentane, tert-Butylcyclohexane, and Related Hydrocarbons. *The Journal of Physical Chemistry* **1972**, *76*, 143-156.

39. Brand, U.; Hippler, H.; Lindemann, L.; Troe, J. C-C and C-H Bond Splits of Laser-Excited Aromatic-Molecules. 1. Specific and Thermally Averaged Rate Constants. *The Journal of Physical Chemistry* **1990**. *94*, 6305-6316.

40. Ma, X.; Peng, Y.; Schobert, H. H. Effects of Structure of the Butyl Chain on the Pyrolysis of Butylbenzenes: Molecular Simulation and Mechanism. *Prepr. - Am. Chem. Soc., Div. Pet. Chem.* **2000**, *45*, 488-492.

41. Peng, Y.; Schobert, H. H.; Song, C.; Hatcher, P. G. Thermal Decomposition Studies of Jet Fuel Components: n-Butylbenzene and t-Butylbenzene. *Prepr. - Am. Chem. Soc., Div. Pet. Chem.* **1992**, *37*, 505-513.

42. Freund, H.; Olmstead, W. N. Detailed Chemical Kinetic Modeling of Butylbenzene Pyrolysis. *Int. J. Chem. Kinet.* **1989**, *21*, 561-574.

43. Zhang, Y.; Cao, C.; Li, Y.; Yuan, W.; Yang, X.; Yang, J.; Qi, F.; Huang, T.-P.; Lee, Y.-Y. Pyrolysis of n-Butylbenzene at Various Pressures: Influence of Long Side-Chain Structure on Alkylbenzene Pyrolysis. *Energ. Fuels* **2017**, *31*, 14270-14279.

44. Tong, X.; Ford, M. S.; Dessent, C. E. H.; Muller-Dethlefs, K. The Effect of Conformation on the Ionization Energetics of n-Butylbenzene. I. A Threshold Ionization Study. *J. Chem. Phys.* **2003**, *119*, 12908-12913.

45. Tong, X.; Cerny, J.; Muller-Dethlefs, K.; Dessent, C. E. H. Effect of Noncovalent Interactions on Conformers of The n-Butylbenzene Monomer Studied by Mass Analyzed Threshold Ionization Spectroscopy and Basis-Set Convergent Ab Initio Computations. *The Journal of Physical Chemistry A* **2008**, *112*, 5866-5871.

46. Mate, B.; Suenram, R. D.; Lugez, C. Microwave Studies of Three Alkylbenzenes: Ethyl, n-propyl, and n-Butylbenzene. *J. Chem. Phys.* **2000**, *113*, 192-199.

47. Campanelli, A. R.; Ramondo, F.; Domenicano, A.; Hargittai, I. Molecular-Structure and Conformation of Tert-Butylbenzene - a Concerted Study by Gas-Phase Electron-Diffraction and Theoretical Calculations. *The Journal of Physical Chemistry* **1994**, *98*, 11046-11052.

48. Halbert, S.; Clavaguera, C.; Bouchoux, G. The Shape of Gaseous n-Butylbenzene: Assessment of Computational Methods and Comparison with Experiments. *J. Comput. Chem.* **2011**, *32*, 1550-1560.

49. Mo, O.; Yanez, M.; Elguero, J.; Roux, M. V.; Jimenez, P.; Davalos, J. Z.; da Silva, M. A. V.; da Silva, M. D. D. M. C.; Cabildo, P.; Claramunt, R. Substituent Effects on Enthalpies of Formation: Benzene Derivatives. *The Journal of Physical Chemistry A* **2003**, *107*, 366-371.

50. Van Speybroeck, V.; Borremans, Y.; Van Neck, D.; Waroquier, M.; Wauters, S.; Saeys, M.; Marin, G. B. Ab Initio Study of Radical Reactions: Cyclization

Pathways for the Butylbenzene Radical (II). *The Journal of Physical Chemistry A* **2001**, *105*, 7713-7723.

51. Becke, A. D. Density-Functional Thermochemistry. III. The Role of Exact Exchange. *J. Chem. Phys.* **1993**, *98*, 5648-5652.

52. Lee, C.; Yang, W.; Parr, R. G. Development of the Colle-Salvetti Correlation-Energy Formula into a Functional of the Electron Density. *Phys. Rev. B* **1988**, *37*, 785-789.

53. Curtiss, L. A.; Raghavachari, K.; Redfern, P. C.; Rassolov, V.; Pople, J. A. Gaussian-3 (G3) Theory for Molecules Containing First and Second-Row Atoms. *J. Chem. Phys.* **1998**, *109*, 7764−7776.

54. Curtiss, L. A.; Raghavachari, K.; Redfern, P. C.; Baboul, A. G.; Pople, J. A. Gaussian-3 Theory Using Coupled Cluster Energies. *Chem. Phys. Lett.* **1999**, *314*, 101−107.

55. Baboul, A. G.; Curtiss, L. A.; Redfern, P. C.; Raghavachari, K. Gaussian-3 Theory Using Density Functional Geometries and ZeroPoint Energies. *J. Chem. Phys.* **1999**, *110*, 7650−7657.

56. Kislov, V. V.; Mebel, A. M.; Aguilera-Iparraguirre, J.; Green, W. H. The Reaction of Phenyl Radical with Propylene as a Possible Source of Indene and Other Polycyclic Aromatic Hydrocarbons: An Ab Initio/RRKM-ME Study. *The Journal of Physical Chemistry A* **2012**, *116*, 4176-4191.

57. Grimme, S. Semiempirical Hybrid Density Functional with Perturbative Second-Order Correlation. *J. Chem. Phys.* **2006**, *124*, 034108.

58. Goerigk, L.; Grimme, S. Efficient and Accurate Double-Hybrid-Meta-GGA Density Functionals—Evaluation with the Extended GMTKN30 Database for General Main Group Thermochemistry, Kinetics, and Noncovalent Interactions. *J. Chem. Theory Comput.* **2011**, *7*, 291-309.

59. Grimme, S.; Ehrlich, S.; Goerigk, L. Effect of the Damping Function in Dispersion Corrected Density Functional Theory. *J. Comput. Chem.* **2011**, *32*, 1456-1465.

60. Dunning, T. H. Gaussian Basis Sets for Use in Correlated Molecular Calculations. I. The Atoms Boron through Neon and Hydrogen. *J. Chem. Phys.* **1989**, *90*, 1007-1023.

61. Adler, T. B.; Knizia, G.; Werner, H.-J. A Simple and Efficient CCSD(T)-F12 Approximation. *J. Chem. Phys.* **2007**, *127*, 221106.

62. Knizia, G.; Adler, T. B.; Werner, H.-J. Simplified CCSD(T)-F12 Methods: Theory and Benchmarks. *J. Chem. Phys.* **2009**, *130*, 054104.

63. Frisch,M.J.;Trucks,G.W.;Schlegel,H.B.;Scuseria,G.E.;Robb,M.A;Cheeseman,J.R.;Scalmani, G.; Barone,V.; Mennucci,B.; Petersson,G.A.,etal. *GAUSSIAN 09*, Revision A.1 Gaussian, Inc., Wallingford, CT, 2009.

64. Werner, H.-J.; Knowles, P. J.; Knizia, G.; Manby, F. R.; Schütz, M.; Celani, P.; Györffy, W.; Kats, D.; Korona, T.; Lindh, R., et al. *MOLPRO*, version 2010.1, a package of ab initio programs, see http://www.molpro.net.

65. Georgievskii, Y.; Miller, J. A.; Burke, M. P.; Klippenstein, S. J. Reformulation and Solution of the Master Equation for Multiple-Well Chemical Reactions. *The Journal of Physical Chemistry A* **2013**, *117* 12146-12154.

66. Georgievskii, Y.; Klippenstein, S. J. 2015, available online at http://tcg.cse.anl.gov/papr.

67. Mebel, A. M.; Georgievskii, Y.; Jasper, A. W.; Klippenstein, S. J. Pressure-Dependent Rate Constants for PAH Growth: Formation of Indene and its Conversion to Naphthalene. *Faraday Discuss.* **2016**, *195*, 637-670.

68. Zheng, J.; Yu, T.; Papajak, E.; Alecu, I. M.; Mielke, S. L.; Truhlar, D. G. Practical Methods for Including Torsional Anharmonicity in Thermochemical Calculations on Complex Molecules: The Internal-Coordinate Multi-Structural Approximation. *Phys. Chem. Chem. Phys.* **2011**, *13*, 10885-10907.

69. Troe, J. Theory of Thermal Unimolecular Reactions at Low-Pressures. 1. Solutions of Master Equation. *J. Chem. Phys.* **1977**, *66*, 4745-4757.

70. Jasper, A. W.; Oana, C. M.; Miller, J. A. Third-Body Collision Efficiencies from Combustion Modeling: Hydrocarbons in Atomic and Diatomic Baths. *Proc. Combust. Inst.* **2015**, *35*, 197-204.

71. Jasper, A. W.; Miller, J. A. Lennard-Jones Parameters for Combustion and Chemical Kinetics Modeling from Full-Dimensional Intermolecular Potentials. *Combust. Flame* **2014**, *161*, 101-110.

72. Mebel, A. M.; Georgievskii, Y.; Jasper, A. W.; Klippenstein, S. J. Temperature- and Pressure-Dependent Rate Coefficients for the HACA Pathways from Benzene to Naphthalene. *Proc. Combust. Inst.* **2017**, *36*, 919-926.

73. Miller, J. A.; Klippenstein, S. J. Determining Phenomenological Rate Coefficients from a Time-Dependent, Multiple-Well Master Equation: ''Species Reduction'' at High Temperatures. *Phys. Chem. Chem. Phys.* **2013**, *15*, 4744-4753.

74. Klippenstein, S. J.; Cline, J. I. Classical Phase Space Theory for Product State Distributions with Application to the V-J Vector Correlation. *J. Chem. Phys.* **1995**, *103*, 5451-5460.

75. Klippenstein, S. J.; Georgievskii, Y.; Harding, L. B. Predictive Theory for the Combination Kinetics of Two Alkyl Radicals. *Phys. Chem. Chem. Phys.* **2006**, *8*, 1133-1147.

76. Harding, L. B.; Georgievskii, Y.; Klippenstein, S. J. Predictive Theory for Hydrogen Atom-Hydrocarbon Radical Association Kinetics. *The Journal of Physical Chemistry A* **2005**, *109*, 4646-4656.

77. Harding, L. B.; Klippenstein, S. J.; Georgievskii, Y. On the Combination Reactions of Hydrogen Atoms with Resonance-Stabilized Hydrocarbon Radicals. *The Journal of Physical Chemistry A* **2007**, *111*, 3789-3801.

Table 5.1. Prototype Reactions of Recombination of Two Hydrocarbon Radicals or of a Radical and H Used for the Fitting of Potential Parameters in Phase Space Calculations of rate Constants of Barrierless Reactions.

Reactant	Products	Prototype Reaction	Reference
n-butylbenzene	C_9H_{11} (1-phenyl-prop-3-yl) + CH_3	$C_2H_5 + CH_3$	75
n-butylbenzene	$C_8H_9 + C_2H_5$	$C_2H_5 + C_2H_5$	75
n-butylbenzene	$C_7H_7 + C_3H_7$	$C_2H_5 + C_2H_5$	75
n-butylbenzene	$C_6H_5 + C_4H_9$ (1-yl)	$C_2H_5 + C_2H_5$	75
n-butylbenzene	$C_{10}H_{13}$ (1-yl) + H	$C_7H_7 + H$	77
n-butylbenzene	$C_{10}H_{13}$ (2-yl) + H	$C_2H_5 + H$	76
n-butylbenzene	$C_{10}H_{13}$ (3-yl) + H	$C_2H_5 + H$	76
n-butylbenzene	$C_{10}H_{13}$ (4-yl) + H	$C_2H_5 + H$	76
s-butylbenzene	C_9H_{11} (2-phenyl-prop-1-yl) + CH_3	$C_2H_5 + CH_3$	75
s-butylbenzene	$C_8H_9 + C_2H_5$	$i\text{-}C_3H_7 + C_2H_5$	75
s-butylbenzene	C_9H_{11} (1-phenyl-prop-1-yl) + CH_3	$i\text{-}C_3H_7 + CH_3$	75
s-butylbenzene	$C_6H_5 + C_4H_9$ (2-yl)	$i\text{-}C_3H_7 + C_2H_5$	75
s-butylbenzene	$C_{10}H_{13}$ (1-yl) + H	$C_2H_5 + H$	76
s-butylbenzene	$C_{10}H_{13}$ (2-yl) + H	$i\text{-}C_3H_7 + H$	75
s-butylbenzene	$C_{10}H_{13}$ (3-yl) + H	$i\text{-}C_3H_7 + H$	75
s-butylbenzene	$C_{10}H_{13}$ (4-yl) + H	$C_2H_5 + H$	76
t-butylbenzene	C_9H_{11} (2-phenyl-prop-2-yl) + CH_3	$t\text{-}C_4H_9 + CH_3$	75
t-butylbenzene	$C_6H_5 + t\text{-}C_4H_9$	$t\text{-}C_4H_9 + C_2H_5$	75
t-butylbenzene	$C_{10}H_{13} + H$	$C_2H_5 + H$	76

Table 5.2. Rate Constants Calculated in the Present Work in the Form $AT^{\alpha}\exp(-E_a/RT)$ and the Temperature Range Where They are Applicable. Units are s^{-1} (Unimolecular Reactions), cm^3 mol^{-1} s^{-1} (Bimolecular Reactions), and cal/mol for E_a.

Reaction	A	α	E_a	T range, K
n-butylbenzene $\rightarrow$ products				
$k_{30\ \text{Torr}}$	0.2819E+137	-34.472	0.15131E+06	1000-1650
$k_{1\ \text{atm}}$	0.1514E+105	-24.839	0.13586E+06	1000-1800
$k_{10\ \text{atm}}$	0.15814E+83	-18.397	0.12380E+06	1000-2000
$k_{100\ \text{atm}}$	0.55489E+64	-13.048	0.11285E+06	1000-2250
n-butylbenzene $\rightarrow$ C$_8$H$_9$[a] +				
C$_2$H$_5$	0.4541E+120	-29.747	0.14297E+06	800-1650
$k_{30\ \text{Torr}}$	0.56452E+89	-20.480	0.12839E+06	800-1800
$k_{1\ \text{atm}}$	0.71658E+95	-21.854	0.13808E+06	1000-2000
$k_{10\ \text{atm}}$	0.32344E+75	-15.953	0.12606E+06	1000-2250
$k_{100\ \text{atm}}$				
n-butylbenzene $\rightarrow$ C$_7$H$_7$ + C$_3$H$_7$				
$k_{30\ \text{Torr}}$	0.2936E+136	-34.289	0.14966E+06	1000-1650
$k_{1\ \text{atm}}$	0.5569E+104	-24.857	0.13397E+06	1000-1800
$k_{10\ \text{atm}}$	0.81242E+83	-18.768	0.12229E+06	1000-2000
$k_{100\ \text{atm}}$	0.55318E+66	-13.803	0.11194E+06	1000-2250
t-butylbenzene $\rightarrow$ C$_9$H$_{11}$[b] + CH$_3$				
$k_{30\ \text{Torr}}$	0.3349E+130	-32.822	0.13649E+06	900-1500
$k_{1\ \text{atm}}$	0.2732E+103	-24.610	0.12490E+06	900-1800
$k_{10\ \text{atm}}$	0.12936E+74	-16.037	0.10842E+06	900-1800
$k_{100\ \text{atm}}$	0.40728E+63	-12.875	0.10409E+06	1000-2000
s-butylbenzene $\rightarrow$ products				
$k_{30\ \text{Torr}}$	0.1022E+133	-33.478	0.13945E+06	900-1500
$k_{1\ \text{atm}}$	0.4768E+106	-25.477	0.12841E+06	900-1800
$k_{10\ \text{atm}}$	0.22139E+77	-16.894	0.11201E+06	900-1800
$k_{100\ \text{atm}}$	0.16494E+67	-13.826	0.10813E+06	1000-2000
s-butylbenzene $\rightarrow$ C$_8$H$_9$[c] +				
C$_2$H$_5$	0.7368E+132	-33.459	0.13935E+06	900-1500
$k_{30\ \text{Torr}}$	0.2680E+106	-25.429	0.12821E+06	900-1800
$k_{1\ \text{atm}}$	0.20675E+77	-16.911	0.11195E+06	900-1800
$k_{10\ \text{atm}}$	0.22675E+67	-13.891	0.10817E+06	1000-2000
$k_{100\ \text{atm}}$				
s-butylbenzene $\rightarrow$ C$_9$H$_{11}$[d] +				
CH$_3$	0.5915E+132	-33.641	0.14007E+06	900-1500
$k_{30\ \text{Torr}}$	0.2386E+106	-25.614	0.12907E+06	900-1800
$k_{1\ \text{atm}}$	0.85572E+76	-16.996	0.11265E+06	900-1800
$k_{10\ \text{atm}}$	0.71654E+66	-13.939	0.10886E+06	1000-2000
$k_{100\ \text{atm}}$				

$C_6H_5 + C_2H_4 \rightarrow$ products				
$k_{30\ Torr}$	9.4464E+05	1.8693	2239.3	300-2500
$k_{1\ atm}$	2.0100E+06	1.778	2397.9	300-2500
$k_{10\ atm}$	2.3850E+06	1.7637	2465.7	300-2500
$k_{100\ atm}$	1.2054E+06	1.8615	2394.3	300-2500
$C_6H_5 + C_2H_4 \rightarrow C_6H_5C_2H_4$ [e]				
$k_{30\ Torr}$	8.2987E+66	-16.65	29108	300-1250
	6.0680E+27	-5.4215	7398.1	
$k_{1\ atm}$	1.1171E+54	-12.347	27727	300-1500
	1.0473E+19	-2.448	5490.5	
$k_{10\ atm}$	1.1757E+45	-9.4512	26260	300-1800
	2.3841E+15	-1.2167	4684.2	
$k_{100\ atm}$	1.3233E+39	-7.5071	26252	300-2250
	1.1015E+13	-0.42344	4186.9	
$C_6H_5 + C_2H_4 \rightarrow C_6H_5CHCH_3$				
$k_{30\ Torr}$ [e]	3.4678E+98	-25.624	52593	700-1375
	1.3945E+93	-12.561	278220	
$k_{1\ atm}$	0.13775E+72	-16.892	48548	800-1650
$k_{10\ atm}$	0.14061E+82	-19.331	63732	900-1800
$k_{100\ atm}$	0.32995E+73	-16.446	69092	1125-2000
$C_6H_5 + C_2H_4 \rightarrow$ styrene + H				
$k_{30\ Torr}$	9881.3	-4.0434	22708	700-2500
$k_{1\ atm}$	0.24473E+13	-6.1864	34763	700-2500
$k_{10\ atm}$	14153.	-3.7364	34237	700-2500
$k_{100\ atm}$	0.77121E-15	1.7171	25424	700-2500
$C_6H_5C_2H_4 \rightarrow C_6H_5CHCH_3$				
$k_{30\ Torr}$	0.13729E+78	-19.670	61528	700-1250
$k_{1\ atm}$	0.42526E+54	-12.317	53277.	700-1500
$k_{10\ atm}$	0.23604E+41	-8.2442	48021.	700-1800
$k_{100\ atm}$	0.57326E+26	-3.8783	40985.	700-2000
$C_6H_5C_2H_4 \rightarrow C_6H_5 + C_2H_4$				
$k_{30\ Torr}$	0.13570E+69	-16.765	63658	700-1250
$k_{1\ atm}$	0.62212E+47	-10.064	56335.	700-1500
$k_{10\ atm}$	0.12289E+35	-6.1854	51030.	700-1800
$k_{100\ atm}$ [e]	0.64577E+97	-23.062	0.11331E+06	800-2250
	0.57481E+47	-9.9048	58034.	
$C_6H_5C_2H_4 \rightarrow$ styrene + H				
$k_{30\ Torr}$	0.28862E+57	-13.172	56563.	700-1250
$k_{1\ atm}$	0.21594E+35	-6.3698	47730	700-1500
$k_{10\ atm}$	0.16083E+25	-3.3029	43274	700-1800
$k_{100\ atm}$	0.29775E+18	-1.2907	40057	700-2250
$C_6H_5CHCH_3 \rightarrow C_6H_5C_2H_4$				
$k_{30\ Torr}$	0.87116E+79	-19.756	74462	700-1250

$k_{1\ atm}$	0.37632E+56	-12.448	66269.	700-1500
$k_{10\ atm}$	0.81224E+51	-10.800	67018.	800-1800
$k_{100\ atm}$	0.45661E+34	-5.6827	58279.	800-2000
$C_6H_5CHCH_3 \rightarrow C_6H_5 + C_2H_4$				
$k_{30\ Torr}$	0.71658E+81	-19.817	88471	800-1375
$k_{1\ atm}$	0.64321E+74	-17.086	95109	800-1650
$k_{10\ atm}$	0.62466E+98	-23.549	0.11889E+06	900-1800
$k_{100\ atm}$	0.90966E+78	-17.558	0.11501E+06	1000-2000
$C_6H_5CHCH_3 \rightarrow$ styrene + H				
$k_{30\ Torr}$	0.39723E+67	-15.788	70609.	700-1350
$k_{1\ atm}$	0.54825E+47	-9.6498	62984.	700-1650
$k_{10\ atm}$	0.17259E+38	-6.7433	59099	700-1800
$k_{100\ atm}$	0.10842E+27	-3.4126	53546	700-2000
1-phenyl-prop-3-yl $\rightarrow C_7H_7 + C_2H_4$	0.15181E+42	-9.1509	33677.	500-1000
$k_{30\ Torr}$	0.11961E+25	-3.6943	28267.	500-1250
$k_{1\ atm}$	0.28783E+17	-1.3103	25564.	500-1500
$k_{10\ atm}$	0.62196E+12	0.12868	23764.	500-1800
$k_{100\ atm}$				
1-phenyl-prop-1-yl $\rightarrow$ styrene + CH_3	0.75140E+74	-18.351	60229.	600-1125
$k_{30\ Torr}$	0.43845E+49	-10.417	51483.	600-1250
$k_{1\ atm}$	0.16947E+38	-6.8643	47292.	600-1500
$k_{10\ atm}$	0.14615E+26	-3.2006	42095.	600-1650
$k_{100\ atm}$				
2-phenyl-prop-3-yl $\rightarrow$ 1-phenyl-prop-2-yl				
$k_{30\ Torr}$	0.12762E+44	-10.176	26387	500-800
$k_{1\ atm}$	0.38095E+22	-3.3033	19250.	500-1000
$k_{10\ atm}$	0.21159E+19	-2.2313	18455.	500-1375
$k_{100\ atm}$	0.29014E+15	-1.0251	17071.	500-1650
2-phenyl-prop-3-yl $\rightarrow$ styrene + CH_3	0.31994E+15	-	28179.	500-800
$k_{30\ Torr}$	0.25419E+26	0.81166	33731.	500-1000
$k_{1\ atm}$	0.12159E+23	-3.9024	33242.	500-1375
$k_{10\ atm}$	0.11140E+17	-2.7569	31080.	500-1650
$k_{100\ atm}$		-0.87002		
2-phenyl-prop-3-yl $\rightarrow$ 3-phenylpropene + H				
$k_{30\ Torr}$	0.13864E+36	-6.6219	43792.	500-800
$k_{1\ atm}$	0.14349E+32	-5.0212	46967.	500-1000
$k_{10\ atm}$	0.33583E+60	-13.223	65893.	700-1375
$k_{100\ atm}$	0.29057E+52	-10.680	67198.	800-1650

107

1-phenyl-prop-2-yl → 2-phenyl-prop-3-yl				
$k_{30\ Torr}$	0.16346E+36	-7.7720	25155.	500-800
$k_{1\ atm}$	0.23712E+20	-2.6140	20735.	500-1000
$k_{10\ atm}$	0.34657E+17	-1.6706	20110.	500-1375
$k_{100\ atm}$	0.67814E+13	-0.51112	18791.	500-1650
1-phenyl-prop-2-yl → C_6H_5 + C_3H_6				
$k_{30\ Torr}$	0.23039E+85	-21.670	67957.	700-1125
$k_{1\ atm}$	0.64665E+60	-13.875	59910.	700-1250
$k_{10\ atm}$	0.31641E+49	-10.287	56360.	700-1500
$k_{100\ atm}$	0.88533E+51	-10.680	61805	900-1800
1-phenyl-prop-2-yl → styrene + CH_3				
$k_{30\ Torr}$	0.52521E+80	-20.237	61759.	700-1125
$k_{1\ atm}$	0.15314E+53	-11.447	55588.	700-1250
$k_{10\ atm}$[e]	0.15110E+59	-13.055	63048.	700-1500
	0.13760E+46	4.7394	0.35964E+06	
$k_{100\ atm}$[e]	0.31534E+51	-10.663	64204.	800-1800
	0.36860E+16	14.560	0.44487E+06	
1-phenyl-prop-2-yl → 3-phenylpropene + H				
$k_{30\ Torr}$	0.17142E+81	-20.308	64300.	700-1125
$k_{1\ atm}$	0.84166E+58	-13.226	56888.	700-1250
$k_{10\ atm}$	0.35020E+49	-10.188	54496.	700-1500
$k_{100\ atm}$[e]	0.44975E+127	-31.498	0.12347E+06	800-1800
	0.10754E+67	-15.311	64197.	
2-phenyl-prop-2-yl → 3-phenylpropene + H				
$k_{30\ Torr}$	0.82275E+73	-17.737	68952	700-1250
$k_{1\ atm}$	0.44801E+49	-10.263	59400	700-1500
$k_{10\ atm}$	0.78328E+37	-6.6856	54392	700-1800
$k_{100\ atm}$	0.15315E+26	-3.2056	48571	700-2000
C_7H_7 + C_2H_4 → products				
$k_{30\ Torr}$	0.42341E-40	14.665	-24338.	800-2500
$k_{1\ atm}$[e]	0.11413E+99	-25.294	57307.	800-2500
	0.15521E+48	-8.8630	64946.	
$k_{10\ atm}$[e]	0.35603E+48	-10.228	32510.	800-2500
	0.11245E+156	-37.117	0.20054E+06	
$k_{100\ atm}$	0.32724E+17	-1.1416	15300.	800-2500
C_7H_7 + C_2H_4 → 1-phenyl-prop-3-yl				
$k_{30\ Torr}$	0.23483E+68	-16.985	33840.	800-1000
$k_{1\ atm}$	0.16908E+46	-9.8538	27855.	800-1250
	0.60656E+27	-4.2276	20084.	800-1500

$k_{10\ \text{atm}}$	0.52053E+14	-	13689.	800-1800
$k_{100\ \text{atm}}$		0.32926		
$C_7H_7 + C_2H_4 \rightarrow$ 3-phenylpropene + H				
$k_{30\ \text{Torr}}$	0.13513E+11	1.0092	24577.	1000-2500
$k_{1\ \text{atm}}$	0.68819E+20	-1.6066	34206.	1000-2500
$k_{10\ \text{atm}}$	0.36348E+34	-5.2361	50066.	1000-2500
$k_{100\ \text{atm}}$	0.32342E+36	-5.5410	59858.	1250-2500
$C_7H_7 + C_2H_4 \rightarrow$ indane + H				
$k_{30\ \text{Torr}}$	1.07908E+07	0.97799	8157.	1125-2500
$k_{1\ \text{atm}}$	6.50858E+28	-4.8767	30219.	1125-2500
$k_{10\ \text{atm}}$	1.85809E+44	-8.9065	50055.	1125-2500
$k_{100\ \text{atm}}$	9.83814E+29	-4.7424	47447.	1125-2500
1-phenyl-but-1-yl $\rightarrow$ styrene + C_2H_5	0.11163E+81	-20.325	60678.	600-1000
$k_{30\ \text{Torr}}$	0.13319E+57	-12.713	53067.	600-1250
$k_{1\ \text{atm}}$	0.81005E+39	-7.3967	46363.	600-1375
$k_{10\ \text{atm}}$	0.44185E+29	-4.2512	42200.	800-1650
$k_{100\ \text{atm}}$				
2-phenyl-but-2-yl $\rightarrow$ 2-phenylpropene + CH_3				
$k_{30\ \text{Torr}}$	0.11181E+82	-20.500	63498.	600-1000
$k_{1\ \text{atm}}$	0.15319E+59	-13.217	56310.	600-1250
$k_{10\ \text{atm}}$	0.52362E+41	-7.8218	49528.	600-1375
$k_{100\ \text{atm}}$	0.37016E+37	-6.4139	49329.	700-1650
t-phenyl-isobutyl $\rightarrow$ 2-phenylpropene + CH_3				
$k_{30\ \text{Torr}}$	0.10652E+77	-19.449	52578.	600-900
$k_{1\ \text{atm}}$	0.15257E+53	-11.783	45522.	600-1125
$k_{10\ \text{atm}}$	0.10899E+36	-6.4538	39110.	600-1250
$k_{100\ \text{atm}}$	0.97064E+25	-3.3583	35144.	600-1500
t-phenyl-isobutyl $\rightarrow$ phenyl + isobutene				
$k_{0.03\ \text{atm}}$	0.57120E+90	-23.742	63227.	600-900
$k_{1\ \text{atm}}$	0.27287E+74	-18.087	61565.	700-1125
$k_{10\ \text{atm}}$	0.14084E+54	-11.708	54635.	700-1250
$k_{100\ \text{atm}}$	0.22147E+36	-6.2632	47250.	700-1500

[a]$C_6H_5C_2H_4$. [b]2-phenyl-prop-2-yl. [c]$C_6H_5CHCH_3$. [d]1-phenyl-prop-1-yl. [e]If two lines of the parameters are given for a particular pressure, then an accurate fit (within 10%) of the calculated rate constants can be achieved only by a sum of two modified Arrhenius expressions.

Table 5.3. Calculated Product Branching Ratios in the Primary Decomposition of n- and s-Butylbenzenes.

T, K	p											
	30 Torr			1 atm			10 atm			100 atm		
	***n*-butylbenzene**											
	$C_9H_{11}{}^a$ + CH_3	$C_8H_9{}^b$ + C_2H_5	C_7H_7 + C_3H_7	$C_9H_{11}{}^a$ + CH_3	$C_8H_9{}^b$ + C_2H_5	C_7H_7 + C_3H_7	$C_9H_{11}{}^a$ + CH_3	$C_8H_9{}^b$ + C_2H_5	C_7H_7 + C_3H_7	$C_9H_{11}{}^a$ + CH_3	$C_8H_9{}^b$ + C_2H_5	C_7H_7 + C_3H_7
1000	1.70%	13.59%	84.70%	1.79%	14.40%	83.79%	1.79%	14.49%	83.70%	1.80%	14.50%	83.69%
1125	2.27%	18.64%	79.07%	2.54%	21.15%	76.27%	2.59%	21.61%	75.76%	2.60%	21.69%	75.67%
1250	2.70%	22.52%	74.75%	3.20%	27.20%	69.54%	3.35%	28.60%	67.98%	3.39%	28.97%	67.57%
1375	3.01%	25.36%	71.58%	3.70%	31.90%	64.31%	3.99%	34.61%	61.28%	4.09%	35.64%	60.13%
1500	3.24%	27.50%	69.21%	4.07%	35.33%	60.49%	4.47%	39.28%	56.08%	4.68%	41.28%	53.82%
1650	3.45%	29.49%	66.99%	4.37%	38.29%	57.19%	4.89%	43.30%	51.58%	5.21%	46.50%	47.96%
1800				4.60%	40.47%	54.76%	5.17%	46.11%	48.43%	5.59%	50.21%	43.76%
2000							5.44%	48.75%	45.45%	5.92%	53.55%	39.94%
2250										6.19%	56.26%	36.80%
	***s*-butylbenzene**											
	$C_9H_{11}{}^c$ + CH_3	$C_8H_9{}^d$ + C_2H_5	$C_9H_{11}{}^e$ + CH_3	$C_9H_{11}{}^c$ + CH_3	$C_8H_9{}^d$ + C_2H_5	$C_9H_{11}{}^e$ + CH_3	$C_9H_{11}{}^c$ + CH_3	$C_8H_9{}^d$ + C_2H_5	$C_9H_{11}{}^e$ + CH_3	$C_9H_{11}{}^c$ + CH_3	$C_8H_9{}^d$ + C_2H_5	$C_9H_{11}{}^e$ + CH_3
1000	0.09%	86.13%	13.77%	0.12%	86.03%	13.85%	0.12%	86.01%	13.86%	0.12%	86.01%	13.87%
1125	0.14%	85.87%	13.99%	0.21%	85.63%	14.16%	0.23%	85.56%	14.20%	0.24%	85.55%	14.21%
1250	0.18%	85.67%	14.14%	0.31%	85.30%	14.39%	0.38%	85.14%	14.48%	0.40%	85.08%	14.50%
1375	0.22%	85.53%	14.24%	0.40%	85.04%	14.55%	0.53%	84.77%	14.69%	0.61%	84.62%	14.75%
1500	0.25%	85.42%	14.32%	0.48%	84.84%	14.66%	0.68%	84.46%	14.84%	0.83%	84.19%	14.95%
1650				0.57%	84.66%	14.76%	0.83%	84.16%	14.97%	1.10%	83.73%	15.12%
1800				0.64%	84.50%	14.84%	0.97%	83.92%	15.07%	1.34%	83.34%	15.24%
2000										1.62%	82.92%	15.36%

[a]1-phenyl-prop-3-yl. [b]$C_6H_5C_2H_4$. [c]2-phenyl-prop-3-yl. [d]$C_6H_5CHCH_3$. [e]1-phenyl-prop-1-yl.

Table 5.4. Calculated Product Branching Ratios of Various Reactions on the C_8H_9 PES.

T, K	p							
$C_6H_5C_2H_4$ (W1) $\rightarrow$ products								
	30 Torr				1 atm			
	W2	W3	$C_6H_5 + C_2H_4$	styrene + H	W2	W3	$C_6H_5 + C_2H_4$	styrene + H
600	33.63%	61.46%	0.51%	4.41%	25.39%	70.39%	0.39%	3.31%
700	51.37%	34.94%	1.98%	11.72%	35.96%	54.66%	1.44%	7.94%
800	58.32%		4.22%	20.62%	44.64%	37.65%	3.46%	14.25%
900	60.74%		7.01%	32.24%	49.11%	23.68%	6.13%	21.08%
1000	50.95%		8.73%	40.32%	48.79%	14.69%	8.82%	27.70%
1125	38.94%		10.58%	50.48%	47.85%		12.84%	39.32%
1250	28.62%		12.12%	59.26%	38.38%		14.92%	46.70%
1375					29.84%		16.63%	53.53%
1500					22.95%		18.01%	59.04%
	10 atm				100 atm			
	W2	W3	$C_6H_5 + C_2H_4$	styrene + H	W2	W3	$C_6H_5 + C_2H_4$	styrene + H
600	24.44%	70.62%	0.37%	3.19%	24.15%	70.10%	0.37%	3.15%
700	32.85%	57.41%	1.32%	7.24%	32.06%	57.17%	1.29%	7.06%
800	39.43%	45.04%	3.07%	12.45%	37.53%	45.58%	2.93%	11.84%
900	43.24%	33.48%	5.43%	17.84%	40.57%	35.98%	5.10%	16.65%
1000	44.83%	24.07%	8.08%	23.01%	42.36%	28.72%	7.62%	21.29%
1125	43.93%	15.76%	11.28%	29.04%	42.15%	21.27%	10.63%	25.95%
1250	40.26%	10.75%	14.02%	34.96%	40.76%	15.90%	13.36%	29.99%
1375	37.72%		17.68%	44.60%	38.30%	12.12%	15.71%	33.86%

1500	30.70%		19.31%	49.98%	34.83%	9.55%	17.69%	37.92%
1650	23.61%		20.88%	55.50%	29.85%		19.64%	42.93%
1800					26.26%		22.66%	51.04%
2000					19.94%		24.09%	55.94%
2250							18.86%	81.10%

C₆H₅CHCH₃ (W2) → products

$C_6H_5CHCH_3$ (W2) → products

	30 Torr			1 atm			10 atm			100 atm		
	W1	$C_6H_5 +$ C_2H_4	styrene + H	W1	$C_6H_5 +$ C_2H_4	styrene + H	W1	$C_6H_5 +$ C_2H_4	styrene + H	W1	$C_6H_5 +$ C_2H_4	styrene + H
700	41.20%	0.07%	58.70%	41.79%	0.00%	58.19%	41.84%	0.00%	58.16%	41.84%	0.00%	58.16%
800	36.92%	0.30%	62.73%	39.03%	0.03%	60.90%	39.24%	0.00%	60.75%	39.27%	0.00%	60.73%
900	32.38%	0.76%	66.86%	37.05%	0.14%	62.76%	37.78%	0.02%	62.18%	37.89%	0.00%	62.10%
1000	27.55%	1.40%	71.05%	34.86%	0.40%	64.65%	36.75%	0.07%	63.12%	37.13%	0.01%	62.85%
1125	22.52%	2.20%	75.28%	31.46%	1.02%	67.53%	35.37%	0.27%	64.26%	36.58%	0.04%	63.35%
1250	19.30%	2.81%	77.90%	27.68%	1.80%	70.52%	33.38%	0.70%	65.78%	36.09%	0.13%	63.71%
1375		6.54%	93.46%	24.56%	2.52%	72.91%	31.05%	1.31%	67.64%	35.35%	0.34%	64.20%
1500				22.42%	3.07%	74.50%	28.61%	1.96%	69.42%	34.18%	0.68%	64.97%
1650					10.12%	89.88%	26.30%	2.63%	71.07%	32.39%	1.23%	66.16%
1800							24.79%	3.11%	72.10%	30.86%	1.79%	67.35%
2000										29.06%	2.39%	68.55%

C₆H₅ + C₂H₄ → products

$C_6H_5 + C_2H_4$ → products

	30 Torr			1 atm			10 atm			100 atm		
	W1	W2	styrene + H	W1	W2	styrene + H	W1	W2	styrene + H	W1	W2	styrene + H
300	99.99%	0.00%	0.00%	100.00%	0.00%	0.00%	100.00%	0.00%	0.00%	100.00%	0.00%	0.00%
400	99.93%	0.03%	0.01%	100.00%	0.00%	0.00%	100.00%	0.00%	0.00%	100.00%	0.00%	0.00%
500	99.64%	0.24%	0.07%	99.98%	0.01%	0.00%	100.00%	0.00%	0.00%	100.00%	0.00%	0.00%
600	98.12%	1.24%	0.57%	99.89%	0.06%	0.02%	99.99%	0.01%	0.00%	100.00%	0.00%	0.00%

700	92.69%	4.17%	3.05%	99.51%	0.28%	0.14%	99.94%	0.03%	0.01%	99.99%	0.00%	0.00%
800	80.21%	8.86%	10.78%	98.18%	1.02%	0.68%	99.76%	0.12%	0.07%	99.97%	0.01%	0.01%
900	61.35%	12.49%	26.16%	94.49%	2.77%	2.55%	99.22%	0.40%	0.28%	99.91%	0.04%	0.03%
1000	40.94%	12.32%	46.74%	86.76%	5.52%	7.41%	97.77%	1.09%	0.95%	99.73%	0.13%	0.10%
1125	21.14%	8.18%	70.67%	71.43%	8.68%	19.88%	93.43%	2.82%	3.41%	99.09%	0.42%	0.38%
1250	9.71%	4.15%	86.13%	52.41%	9.20%	38.39%	84.98%	5.14%	9.31%	97.50%	1.09%	1.19%
1375		3.07%	96.62%	34.80%	7.37%	57.82%	73.40%	6.84%	19.75%	94.26%	2.22%	3.13%
1500			99.97%	21.28%	4.98%	73.72%	59.13%	7.13%	33.73%	88.84%	3.58%	6.97%
1650			99.96%		5.99%	92.66%	42.16%	6.05%	51.76%	79.42%	4.89%	14.70%
1800			99.94%			99.94%	27.82%	4.42%	67.71%	68.94%	5.43%	25.61%
2000			99.91%			99.91%			99.91%	52.26%	5.03%	42.66%
2250			99.87%			99.87%			99.87%	30.92%		68.97%
2500			99.82%			99.82%			99.82%			99.82%

Table 5.5 Calculated product branching ratios of various reactions on the C_9H_{11} PES.

T, K	p											
1-phenyl-prop-3-yl (W4) → products												
	30 Torr			1 atm			10 atm			100 atm		
	3-phenyl propene	indane	$C_7H_7 + C_2H_4$	3-phenyl propene	indane	$C_7H_7 + C_2H_4$	3-phenyl propene	indane	$C_7H_7 + C_2H_4$	3-phenyl propene	indane	$C_7H_7 + C_2H_4$
800	0.09%	4.69%	88.76%	0.17%	2.27%	80.69%	0.18%	0.69%	74.41%	0.18%	0.10%	72.23%
900	0.16%	4.80%	95.04%	0.42%	2.61%	88.77%	0.49%	1.17%	83.45%	0.48%	0.25%	80.12%
1000	0.24%	4.28%	95.47%	0.79%	3.34%	95.85%	1.02%	1.50%	88.75%	1.06%	0.45%	85.17%
1125				1.31%	2.87%	95.80%	2.01%	1.66%	91.68%	2.23%	0.71%	88.64%
1250				1.87%	2.56%	95.53%	3.30%	2.22%	94.40%	3.93%	0.89%	89.78%
1375							4.62%	1.97%	93.30%	6.04%	0.97%	89.36%
1500							5.96%	1.80%	92.11%	8.52%	1.59%	89.63%
1650										11.34%	1.41%	86.94%
1800										14.11%	1.27%	84.34%
1-phenyl-prop-1-yl (W7) → products												
	30 Torr		1 atm		10 atm		100 atm					
	styrene + CH_3	trans-1-phenyl propene	styrene + CH_3	trans-1-phenyl propene	styrene + CH_3	trans-1-phenyl propene	styrene + CH_3	trans-1-phenyl propene				
800	98.47%	1.53%	98.12%	1.88%	98.05%	1.94%	98.04%	1.95%				
900	98.15%	1.85%	97.51%	2.48%	97.31%	2.68%	97.26%	2.73%				
1000	97.89%	2.11%	96.97%	3.01%	96.56%	3.42%	96.42%	3.56%				
1125	97.62%	2.37%	96.44%	3.54%	95.72%	4.25%	95.36%	4.60%				
1375			96.01%	3.97%	95.03%	4.93%	94.36%	5.58%				
1500					94.46%	5.49%	93.49%	6.44%				
1650					93.99%	5.95%	92.75%	7.16%				

1800						92.01%	7.89%				

2-phenyl-prop-3-yl (W2) → products

	30 Torr			1 atm			10 atm			100 atm		
	W1	styrene + CH$_3$	3-phenyl propene	W1	styrene + CH$_3$	3-phenyl propene	W1	styrene + CH$_3$	3-phenyl propene	W1	styrene + CH$_3$	3-phenyl propene
500	99.99%	0.01%	0.00%	99.99%	0.01%	0.00%	99.99%	0.01%	0.00%	99.99%	0.01%	0.00%
600	99.94%	0.05%	0.00%	99.92%	0.08%	0.00%	99.92%	0.08%	0.00%	99.92%	0.08%	0.00%
700	99.66%	0.27%	0.05%	99.57%	0.40%	0.01%	99.54%	0.43%	0.00%	99.54%	0.44%	0.00%
800	98.36%	1.14%	0.36%	98.47%	1.32%	0.11%	98.35%	1.53%	0.02%	98.33%	1.57%	0.00%
900				95.73%	3.29%	0.59%	95.53%	3.99%	0.14%	95.46%	4.18%	0.02%
1000				90.37%	6.59%	1.98%	90.23%	8.18%	0.63%	90.15%	8.84%	0.10%
1125							79.74%	15.48%	2.30%	79.68%	17.44%	0.48%
1250							66.77%	23.49%	5.03%	66.27%	27.49%	1.44%
1375							54.31%	30.68%	7.90%	52.54%	36.76%	2.94%
1500										40.70%	44.05%	4.51%
1650										29.99%	50.19%	5.96%

1-phenyl-prop-2-yl (W1) → products

	30 Torr				1 atm			
	W2	C$_6$H$_5$ + C$_3$H$_6$	styrene + CH$_3$	3-phenyl propene	W2	C$_6$H$_5$ + C$_3$H$_6$	styrene + CH$_3$	3-phenyl propene
500	100.00%	0.00%	0.00%	0.00%	100.00%	0.00%	0.00%	0.00%
600	99.94%	0.00%	0.05%	0.01%	99.98%	0.00%	0.00%	0.01%
700	99.40%	0.02%	0.42%	0.14%	99.79%	0.02%	0.06%	0.12%
800	97.10%	0.12%	1.85%	0.78%	98.71%	0.10%	0.43%	0.67%
900		4.77%	60.57%	28.94%	95.18%	0.42%	1.64%	2.44%

1000		5.52%	56.83%	31.68%	87.97%	1.14%	3.97%	6.10%
1125		6.25%	53.42%	34.15%		8.71%	43.21%	41.29%
1250						9.55%	39.97%	43.55%

	10 atm				100 atm			
	W2	C_6H_5 + C_3H_6	styrene + CH_3	3-phenyl propene	W2	C_6H_5 + C_3H_6	styrene + CH_3	3-phenyl propene
500	100.00%	0.00%	0.00%	0.00%	100.00%	0.00%	0.00%	0.00%
600	99.98%	0.00%	0.00%	0.01%	99.98%	0.00%	0.00%	0.01%
700	99.84%	0.02%	0.01%	0.13%	99.84%	0.02%	0.00%	0.13%
800	99.05%	0.10%	0.07%	0.71%	99.10%	0.10%	0.01%	0.72%
900	96.33%	0.44%	0.33%	2.64%	96.54%	0.45%	0.04%	2.72%
1000	89.80%	1.29%	1.10%	7.09%	90.25%	1.35%	0.15%	7.56%
1125	75.81%	3.22%	2.85%	16.43%	75.58%	3.60%	0.52%	18.63%
1250	59.96%	5.56%	4.65%	27.07%	57.02%	6.59%	1.11%	32.41%
1375	47.00%	7.63%	5.70%	36.06%	40.92%	9.30%	1.67%	44.22%
1500		12.25%	31.04%	49.31%	29.70%	11.28%	1.99%	52.47%
1650					21.38%	12.84%	2.06%	58.72%
1800					13.96%	31.52%	47.40%	

C_7H_7 + $C_2H_4 \rightarrow$ products

	30 Torr			1 atm			10 atm			100 atm		
	W4	3-phenyl propene	indane	W4	3-phenyl propene	indane	W4	3-phenyl propene	indane	W4	3-phenyl propene	indane
500	99.80%	0.00%	0.03%	99.98%	0.00%	0.00%	100.00%	0.00%	0.00%	100.00%	0.00%	0.00%
600	99.49%	0.00%	0.22%	99.94%	0.00%	0.00%	99.99%	0.00%	0.00%	100.00%	0.00%	0.00%
700	98.79%	0.05%	0.87%	99.84%	0.00%	0.03%	99.97%	0.00%	0.00%	100.00%	0.00%	0.00%
800	97.14%	0.29%	2.33%	99.65%	0.04%	0.14%	99.93%	0.01%	0.01%	99.99%	0.00%	0.00%

900	93.68%	1.34%	4.96%	99.20%	0.22%	0.40%	99.84%	0.03%	0.03%	99.97%	0.00%	0.00%
1000	85.66%	4.96%	9.29%	98.29%	0.86%	0.83%	99.62%	0.16%	0.10%	99.94%	0.02%	0.00%
1125		49.81%	49.37%	94.85%	3.30%	1.78%	98.87%	0.74%	0.26%	99.81%	0.10%	0.02%
1250		67.17%	31.78%	86.79%	9.84%	3.19%	97.00%	2.44%	0.50%	99.46%	0.39%	0.05%
1375		78.48%	20.33%		78.52%	20.28%	92.70%	6.29%	0.89%	98.59%	1.19%	0.11%
1500		85.32%	13.39%		85.34%	13.37%	84.79%	13.59%	1.38%	96.86%	2.89%	0.17%
1650		90.07%	8.57%		90.08%	8.56%		90.13%	8.50%	92.68%	6.85%	0.32%
1800		92.77%	5.81%		92.77%	5.81%		92.80%	5.78%	85.63%	13.59%	0.49%
2000		94.78%	3.74%		94.78%	3.74%		94.79%	3.73%		94.83%	3.68%
2250		96.07%	2.38%		96.07%	2.38%		96.07%	2.37%		96.09%	2.35%
2500		96.75%	1.64%		96.75%	1.64%		96.75%	1.64%		96.75%	1.63%

Figure 5.1 Potential Energy Diagram for the Primary and Most Favorable Secondary Decomposition Channels of *n*-Butylbenzene.

$C_7H_7 + C_2H_4 + CH_3$

$C_6H_5 + C_2H_5 + C_2H_4$

benzyl

1-phenyl-prop-3-yl

571

537

521

527

501

467

534

464

427

448

$C_6H_5 + C_4H_9$

369

$C_9H_{11} + CH_3$

375

$C_8H_9 + C_2H_5$

341

427

styrene

$C_7H_7 + C_3H_7$

benzyl

$C_8H_8 + C_2H_5 + H$

0

3-phenylpropene

569

566

$C_6H_5 + C_4H_8 + H$

538

507

503

546

531

styrene

513

504

$C_8H_8 + C_2H_5 + H$

$C_9H_{10} + CH_3 + H$

benzyl

473

$C_7H_7 + C_3H_6 + H$

411

$C_{10}H_{13}$ (2-yl) + H

408

420

$C_{10}H_{13}$ (4-yl) + H

369

$C_{10}H_{13}$ (1-yl) + H

$C_{10}H_{13}$ (3-yl) + H

0

$C_8H_9 + C_2H_4 + H$

118
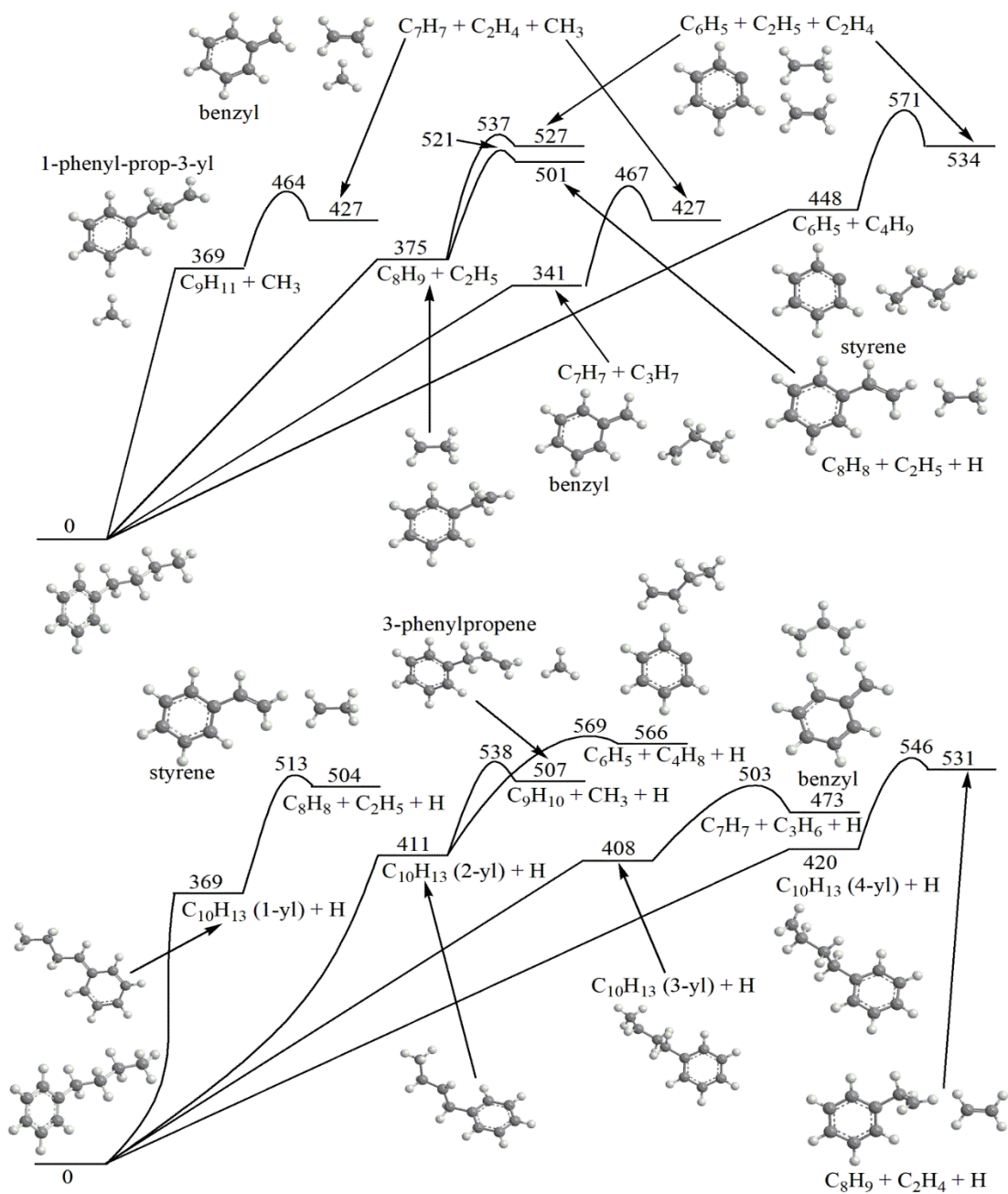
Figure 5.2 Total (a) and Individual Channel (b) Rate Constants for Primary Decomposition of *n*-Butylbenzene. Dotted, Solid, Dashed, and Dot-Dashed Curves Show Values Calculated at the Pressures of 30 Torr, 1, 10, and 100 atm, Respectively. The Bold Curve on Panel (a) Shows the HP Limit Total Rate Constant.
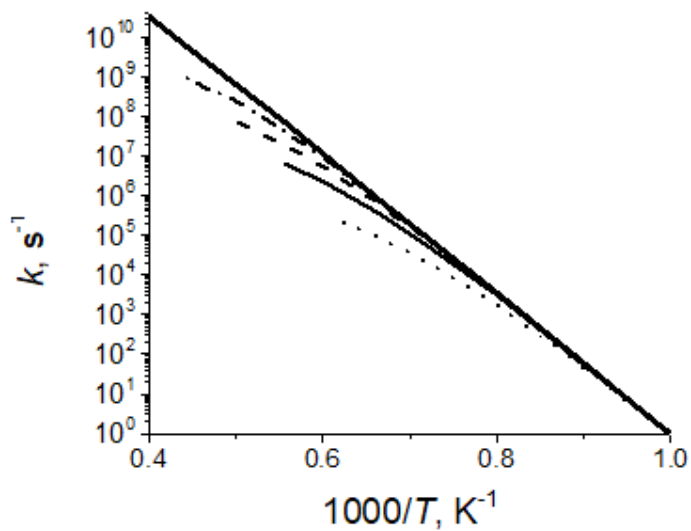
(a)
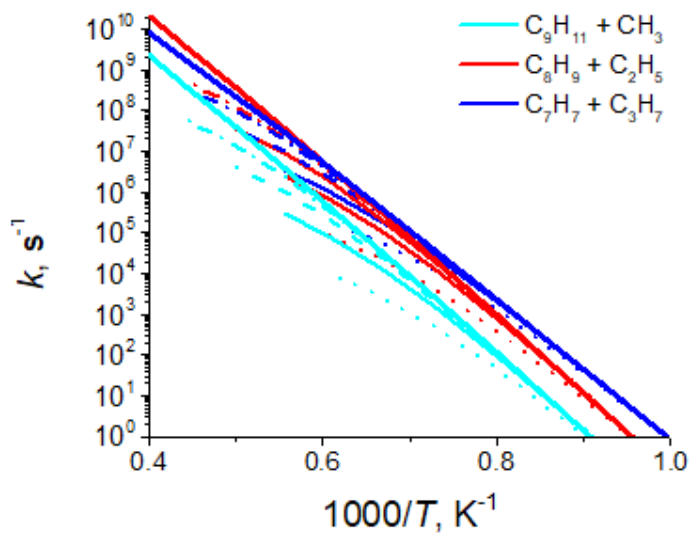
(b)

Figure 5.3 Potential Energy Diagram for the Primary and Most Favorable Secondary Decomposition Channels of *s*-Butylbenzene.
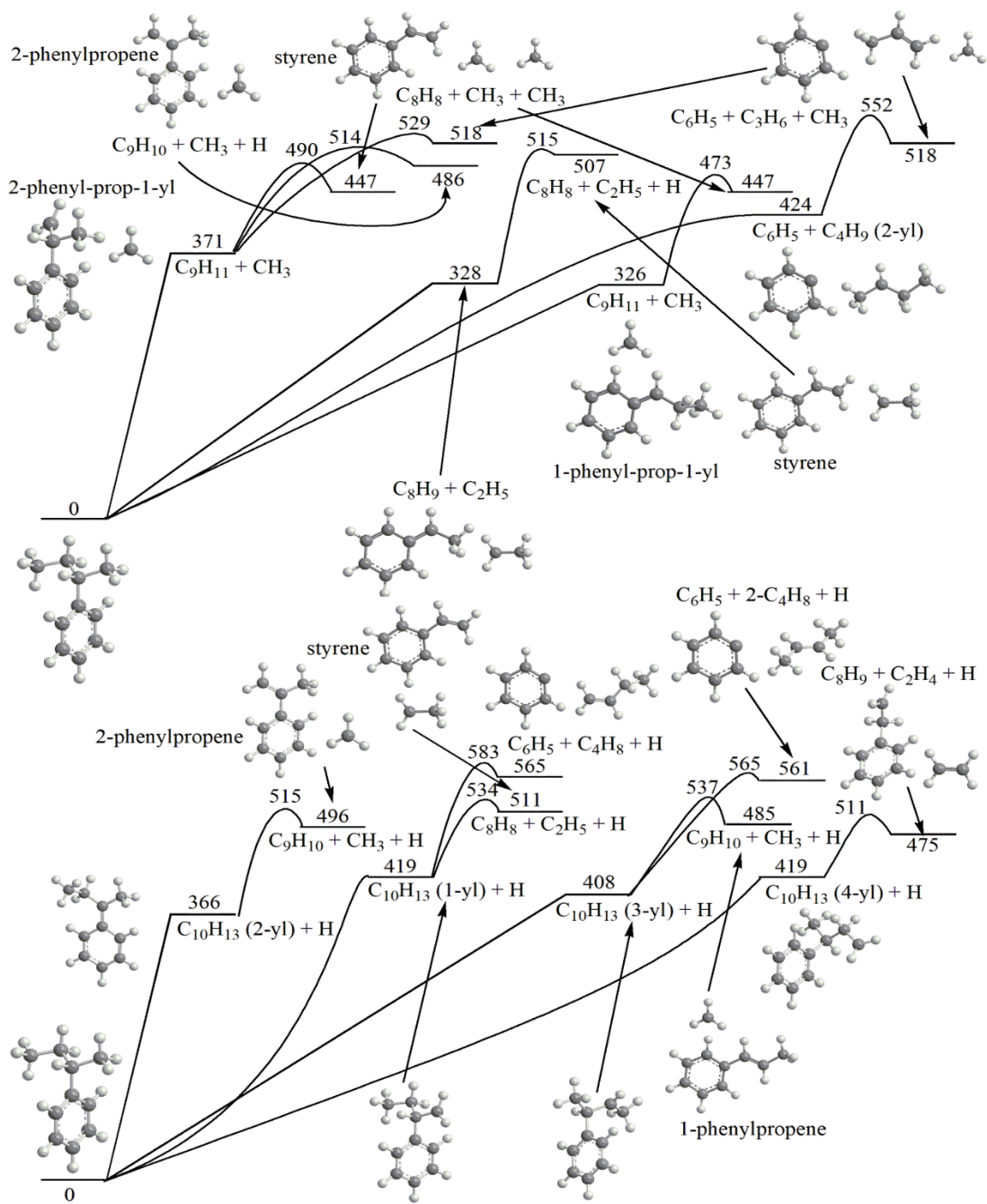
Figure 5.4 Total (a) and Individual Channel (b) Rate Constants for Primary Decomposition of *s*-Butylbenzene. Dotted, Solid, Dashed, and Dot-Dashed Curves Show Values Calculated at the Pressures of 30 Torr, 1, 10, and 100 atm, Respectively. The Bold Curve on Panel (a) Shows the HP Limit Total Rate Constant.
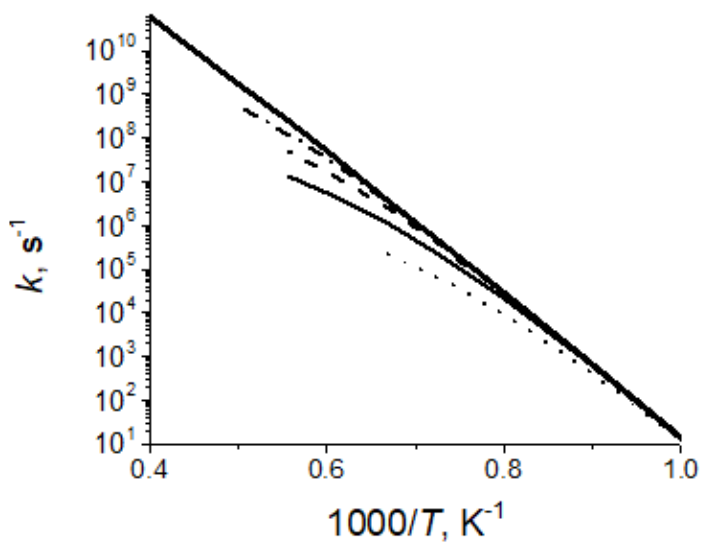
(a)
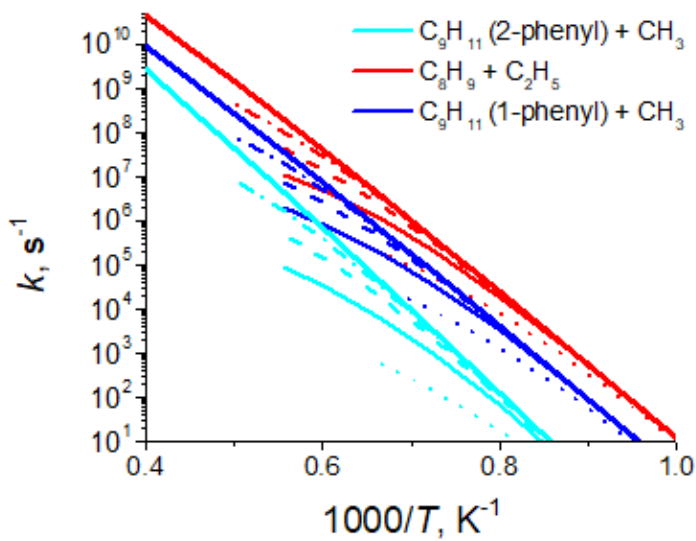
(b)

Figure 5.5 Potential Energy Diagram for the Primary and Most Favorable Secondary Decomposition Channels of *t*-Butylbenzene. All Relative Energies With Respect to the Parent Molecule are Given in kJ mol^{-1}.

2-phenylpropene

2-phenyl-prop-2-yl

576 559

$C_6H_5 + C_4H_8 + H$

572 559

$C_6H_5 + C_4H_8 + H$

$C_9H_{10} + CH_3 + H$

487

541

487

$C_9H_{10} + CH_3 + H$

412

$C_6H_5 + C_4H_9$

421

$C_{10}H_{13} + H$

318

$C_9H_{11} + CH_3$

0
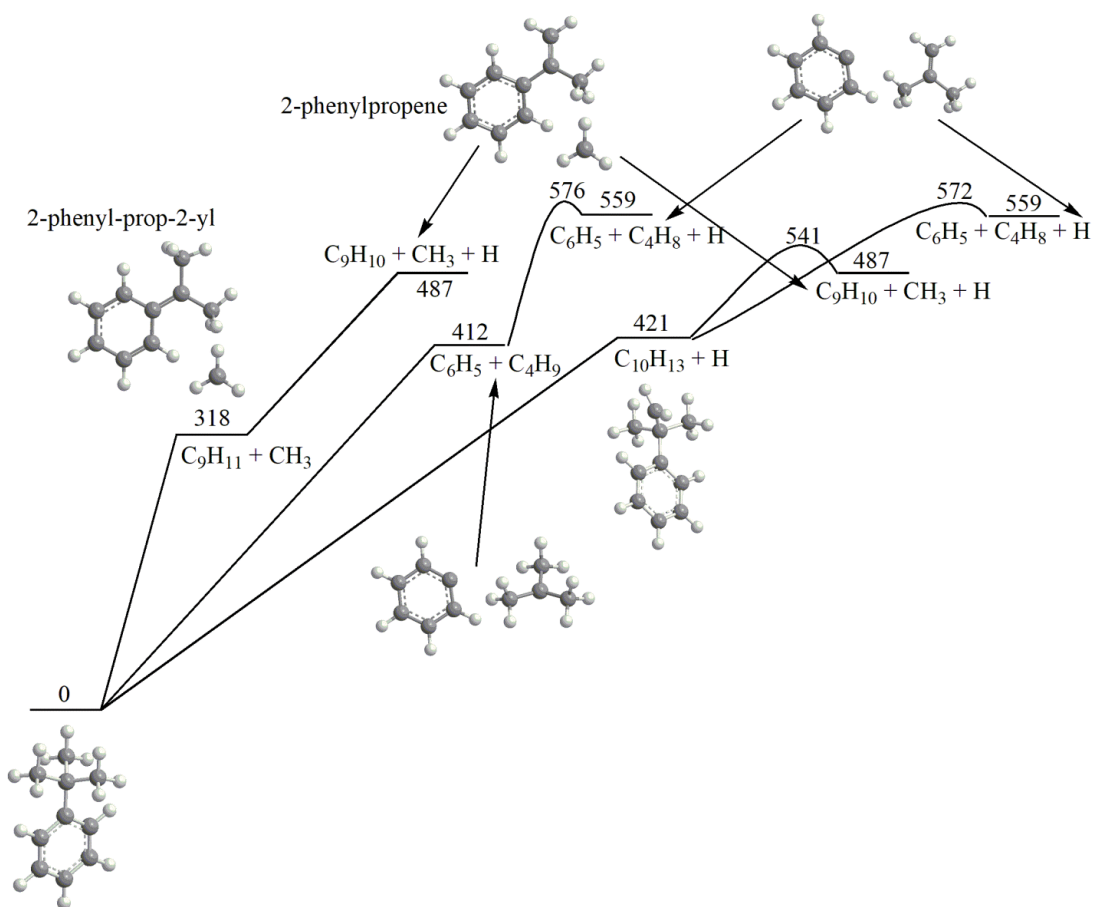
Figure 5.6 Total Rate Constant for Primary Decomposition of *t*-Butylbenzene, Which Nearly Exclusively Produces 2-Phenyl-Prop-2-yl + CH_3. Dotted, Solid, Dashed, and Dot-Dashed Curves Show Values Calculated at the Pressures of 30 Torr, 1, 10, and 100 atm, Respectively. The Bold Curve Shows the HP Limit Total Rate Constant.
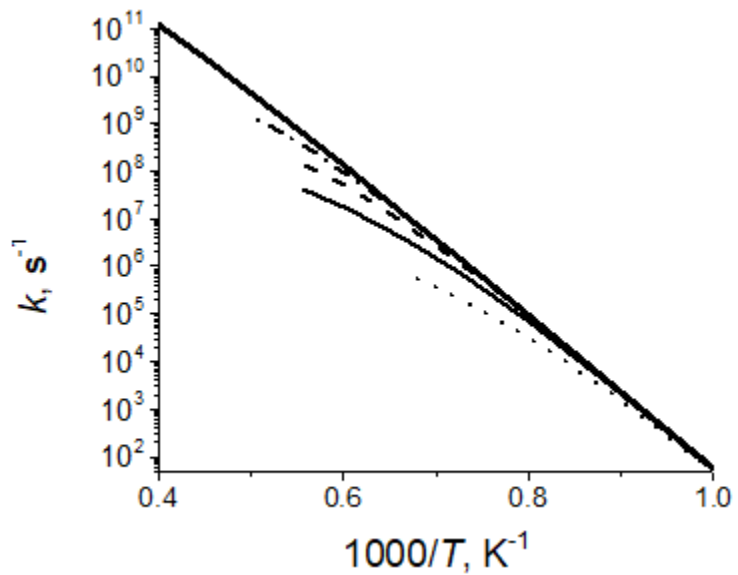
Figure 5.7 Potential Energy Diagram for Unimolecular Decomposition of the $C_6H_5C_2H_4$ (W1) and $C_6H_5CHCH_3$ (W2) Isomers of C_8H_9 and the $C_6H_5 + C_2H_4$ Reaction. All Relative Energies with Respect to $C_6H_5CHCH_3$ are Given in kJ mol^{-1}.
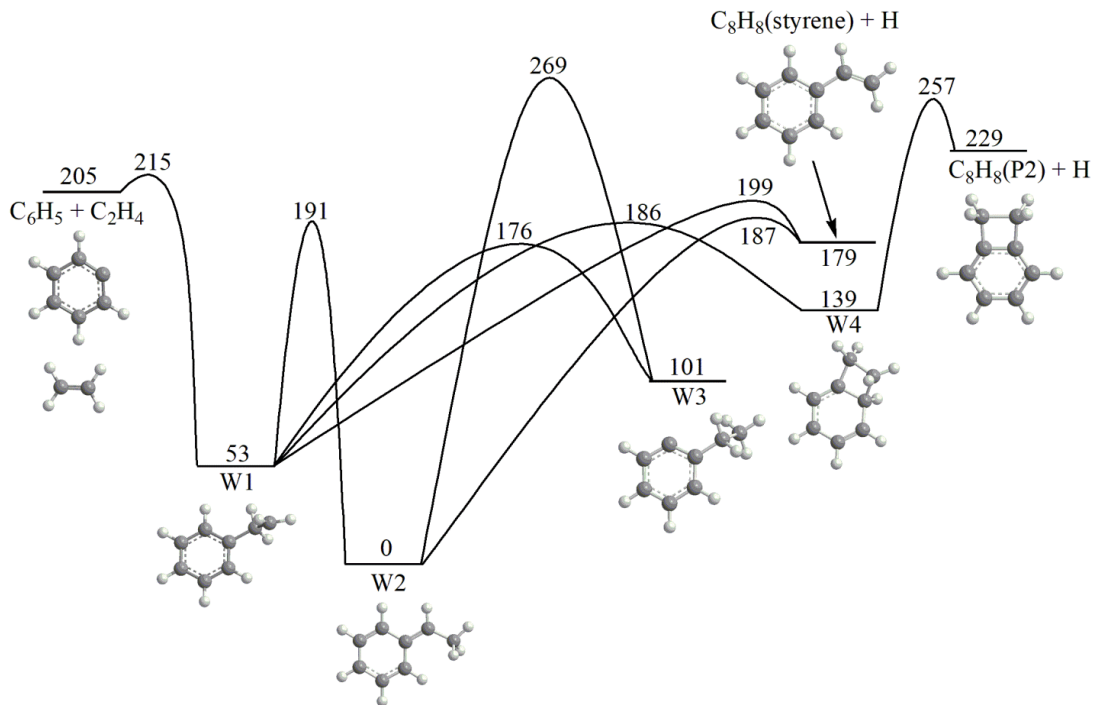
Figure 5.8 Rate Constants for Various Reactions Involving the C_8H_9 PES: (a) Isomerization and Unimolecular Decomposition of $C_6H_5C_2H_4$; (b) Isomerization and Unimolecular Decomposition of $C_6H_5CHCH_3$; (c) Total Rate Constant for the $C_6H_5 + C_2H_4$ Reaction in Comparison with the Literature Values from Tokmakov and Lin, Yu and Lin, and Fahr et al. (d) Individual Rate Constants for the Stabilization of $C_6H_5C_2H_4$ (W1) and the Formation of Styrene + H in the $C_6H_5 + C_2H_4$ Reaction. Dotted, Solid, Dashed, and Dot-Dashed Curves Show Values Calculated at the Pressures of 30 Torr, 1, 10, and 100 atm, Respectively. The Bold Curve on Panel (c) Shows the HP Limit Total Rate Constant.
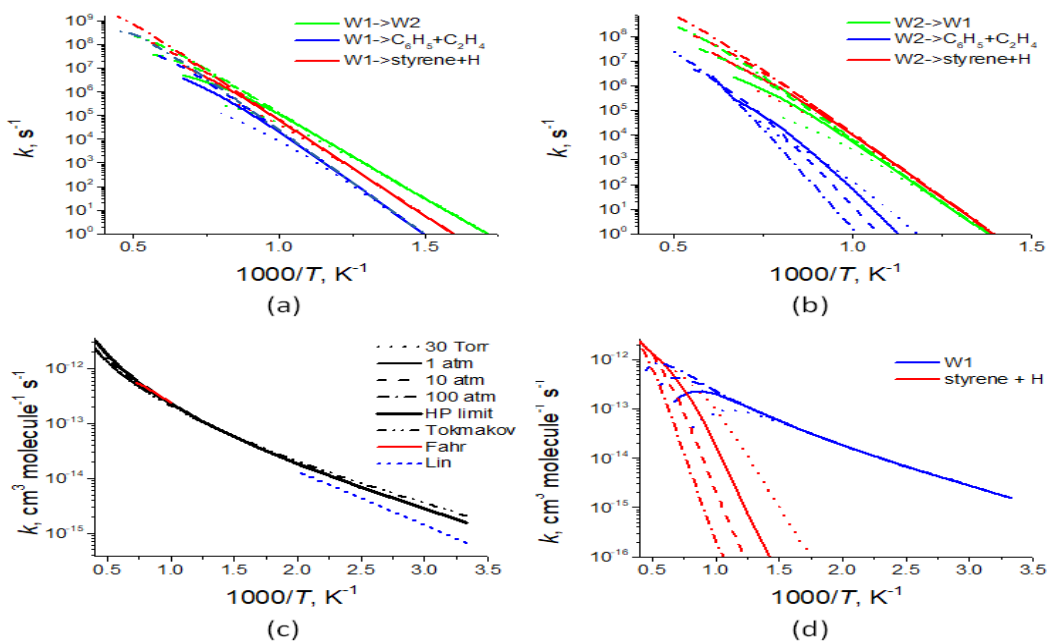
Figure 5.9 Rate Constants for Isomerization and Decomposition of Various C_9H_{11} Isomers: (a) 1-Phenyl-Prop-3-yl $\rightarrow$ Benzyl C_7H_7 + C_2H_4; (b) 1-Phenyl-Prop-1-yl $\rightarrow$ Styrene C_8H_8 + CH_3; (c) Isomerization of 2-Phenyl-Prop-3-yl (W2) to 1-Phenyl-Prop-2-yl (W1) and Dissociation of W2 to Styrene + CH_3; (d) Isomerization of 1-Phenyl-Prop-2-yl (W1) to 2-Phenyl-Prop-3-yl (W2) and Dissociation of W1 to Styrene + CH_3 and 3-Phenylpropene + H; (e) 2-Phenyl-Prop-2-yl $\rightarrow$ 2-Phenylpropene + H. Dotted, Solid, Dashed, and Dot-Dashed Curves Show Values Calculated at the Pressures of 30 Torr, 1, 10, and 100 atm, Respectively.
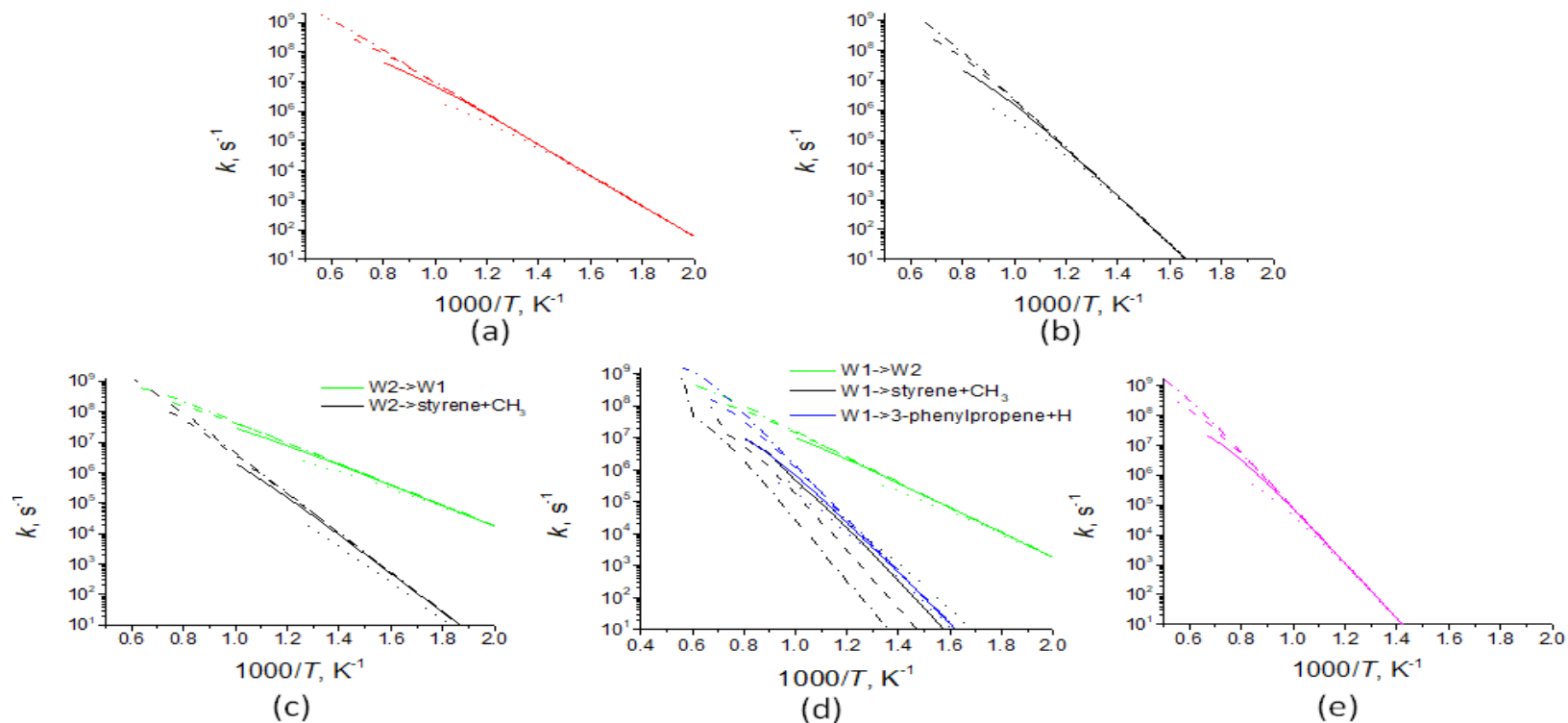
Figure 5.10 Total (a) and Individual Channel (b) Rate Constants for the Benzyl C_7H_7 + C_2H_4 Reaction. Dotted, Solid, Dashed, and Dot-Dashed Curves Show Values Calculated at the Pressures of 30 Torr, 1, 10, and 100 atm, Respectively. The Bold Curve on Panel (a) Shows the HP Limit Total Rate Constant.
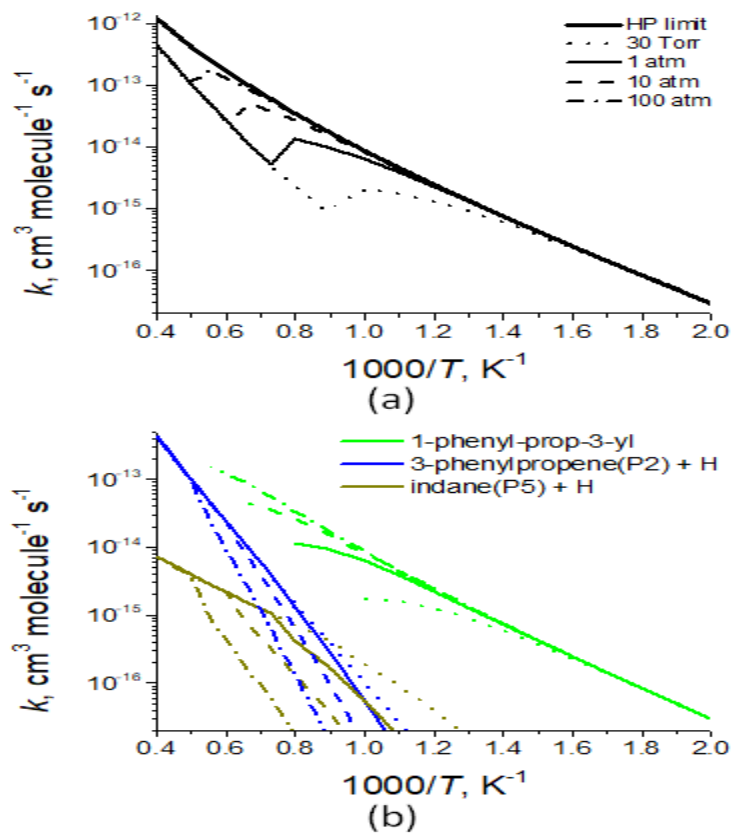
Figure 5.11 Rate Constants for Unimolecular Decomposition of Various $C_{10}H_{13}$ Radicals: (a) 1-Phenyl-But-1-yl; (b); 2-Phenyl-But-2-yl; (c) *t*-Phenyl-Isobutyl. Dotted, Solid, Dashed, and Dot-Dashed Curves Show Values Calculated at the Pressures of 30 Torr, 1, 10, and 100 atm, Respectively.
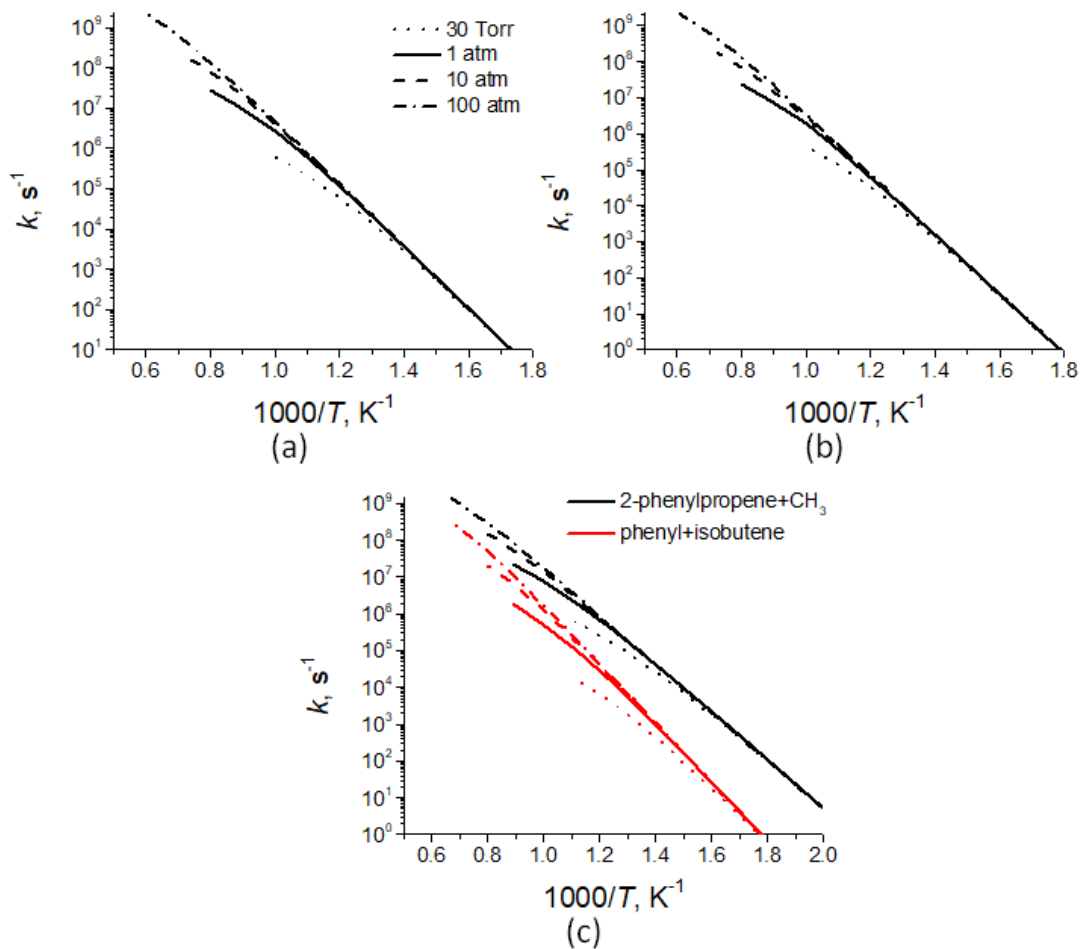
Chapter VI

A Combined Experimental Vacuum Ultraviolet Photoionization and Theoretical Study on

High-Temperature Decomposition of JP-10 (*exo*-Tetrahydrodicyclopentadiene)

Introduction:

Tricyclo[5.2.1.02,6]decane (exo-tetrahydrodicyclopentadiene; exoTCD; Fig. 7.1 represents a single component hydrocarbon fuel and is the principal constituent of Jet Propellant-10 (JP-10; $C_{10}H_{16}$) as exploited in detonation engines, missiles, and supersonic combustion ramjets. With attractive properties such as high thermal stability, high-energy density, low freezing point, and high energy storage, JP-10 attracts extensive attention[1–39] triggering extensive experimental, theoretical, and modeling investigations to examine the features of oxidative and thermal decomposition mechanisms (Table 7.1). Green et al. presented shock tube experiments combined with kinetic modeling efforts on the pyrolysis and combustion of JP-10.[5] The experiments were performed at 6–8 atm using 2000 ppm of JP-10 over a temperature range of 1000–1600 K for pyrolysis and oxidation equivalence ratios from 0.14 to 1.0. Gas chromatography-mass spectrometry coupled with electron impact ionization (GC-MS-EI) was utilized to identify and quantify the products. They observed that JP-10 decomposed primarily to ethylene (C_2H_4), propene (C_3H_6), cyclopentadiene (C_5H_6), and aromatics such as benzene (C_6H_6) and toluene (C_7H_8), along with trace components like 1,2-divinylcyclohexane ($C_{10}H_{16}$) butadiene (C_4H_6), and 1,3-cyclohexadiene (C_6H_8). Anderson et al. utilized a small flow tube reactor to investigate the decomposition of JP-10 over the temperature range up to 1700 K on the millisecond time scale.[6] Chemical ionization and electron impact ionization mass spectrometry were utilized to identify the products. They observed that cyclopentadiene (C_5H_6), benzene (C_6H_6), methylacetylene (C_3H_4), and C_4H_x were the principal products in the initial decomposition. At higher temperatures, major products were identified as benzene (C_6H_6), acetylene (C_2H_2), and ethylene (C_2H_4). Reyniers et al. performed JP-10 pyrolysis in a continuous flow tubular reactor near atmospheric pressure in the temperature range of 930–1080 K at 1.7 bar, with

residence times to be 2.1–9.35 ms.[7] They concluded that polycyclic aromatic hydrocarbon (PAH) formation started from cyclopentadiene (C_5H_6); successive reactions resulted in the formation of naphthalene ($C_{10}H_8$), indene (C_9H_8), and substituted derivatives of bicyclic aromatic compounds. Marquaire et al. performed atmospheric thermal decomposition of JP-10 in a jet-stirred reactor at temperatures from 848 to 933 K with residence times between 500 and 6000 ms.[8] They observed eleven products. Major products were hydrogen (H_2), ethylene (C_2H_4), propene (C_3H_6), cyclopentadiene (C_5H_6), benzene (C_6H_6), and toluene (C_7H_8). Rao and Kunzru investigated the product distribution and kinetics of thermal cracking of JP-10 in an annular tubular reactor at atmospheric pressure, in the temperature range of 903–968 K with residence times of 680–6400 ms.[9] The major products were methane (CH_4), ethylene (C_2H_4), propene (C_3H_6), cyclopentene (C_5H_8), cyclopentadiene (C_5H_6), benzene (C_6H_6), and toluene (C_7H_8); rate constants for thermal cracking of JP-10 were determined by non-linear regression analysis to follow 2.4 $10^{13}T^{1.1}$ exp(30815.5/T), respectively. Striebich and Lawrence explored JP-10 pyrolysis with a high-temperature and pressure flow reactor.[10] The experiment was carried out in the temperature range from 373 K to 873 K at a pressure over 25 atm and residence times between 1 and 5 seconds. This study suggested that the JP-10 pyrolysis products included alkanes, alkenes, cycloalkenes, cyclopentadiene (C_5H_6), and alkylbenzenes. Wohlwend et al. experimentally examined the thermal decomposition behavior of high-energy density hydrocarbons under condensed-phase high-temperature conditions from 473 K to 923 K.[11] The pressure was kept at 34 atm with the residence time of 1800 ms at 473 K. They tested several fuels and concluded that JP-10 degradation led to the formation of small amounts of benzene (C_6H_6) and toluene (C_7H_8). Fang et al. studied the thermal cracking of JP-10 in a batch reactor under various pressures.[12] The temperature ranged from 823 K to 903 K and the

131

pressure range comprised 1–30 bar. They quantitatively determined the products with GC and GC/MS revealing that with an increase of the pressure, the relative content of ethylene (C_2H_4) or propene (C_3H_6) decreased while those of methane (CH_4), ethane (C_2H_6), and propane (C_3H_8) increased simultaneously. They also found that liquid products including cyclopentane (C_5H_{10}), cyclopentene (C_5H_8), cyclopentadiene (C_5H_6), and cis-bicyclo[3.3.0]oct-2-ene (C_8H_{12}) were the major components. Substituted cyclopentene, benzene (C_6H_6), toluene (C_7H_8), and naphthalene ($C_{10}H_8$) were observed at high pressures and temperatures. Later, this group also performed an experimental and kinetic modeling study on the atmospheric pyrolysis of JP-10, iso-octane and JP-10/iso-octane in a stainless-steel tubular reactor at temperatures from 883 K to 963 K.[13] They concluded that the reaction pathway analyses show that the hydrogen abstraction reactions account for more than 80% of the decomposition of JP-10. Bruno et al. studied high-pressure JP-10 thermal decomposition in the temperature range from 623 to 698 K.[14] Fifteen products were observed and the decomposition reaction rate constants were determined. Kim et al. performed an experimental and molecular modeling investigation on the thermal stability and the primary initiation mechanism of JP-10 in a batch-type reactor.15 JP-10 was initially decomposed at a temperature of 623 K in their study. 1-Cyclopentylcyclopentene ($C_{10}H_{16}$) and 4-methyl-2,3,4,5,6,7-hexahydro1H-indene ($C_{10}H_{16}$) were the primary decomposition products of JP-10, and C10 hydrocarbons were determined to be the major products. Recently, Liu et al. presented an experimental and kinetic modeling study on JP-10 pyrolysis at low pressure (40 mbar) in the temperature range from 900 K to 1600 K in a flow tube reactor, with synchrotron vacuum ultraviolet photoionization mass spectrometry (SVUV-PIMS) as the diagnostic method.[16] Under their experimental conditions, JP-10 was initially and completely decomposed at 970 K and 1600 K, respectively. Approximately 28 species were identified and quantified in

their study, including some major closed-shell molecules and radicals such as molecular hydrogen (H_2), methyl (CH_3), methane (CH_4), acetylene (C_2H_2), ethylene (C_2H_4), ethyl (C_2H_5), propargyl (C_3H_3), allene (C_3H_4), methylacetylene (C_3H_4), allyl (C_3H_5), propene (C_3H_6), vinylacetylene (C_4H_4), 1,3-butadiene (C_4H_6), 1-butene (C_4H_8), cyclopentadienyl (C_5H_5) and cyclopentadiene (C_5H_6). Besides these experimental investigations, computational chemistry was also exploited to unravel the decomposition mechanism of JP-10. Herbinet et al. carried out a kinetic modeling study on JP-10 pyrolysis.[8] They constructed a comprehensive kinetic mechanism with the EXGAS program (used for performing an automatic generation of mechanisms) and the Thergas program (used to calculate thermodynamic data). The kinetic parameters were taken from literature data and estimated from density function theory (DFT) calculations in the case of reactions involving cyclic compounds and diradicals. Reyniers et al.[17] developed a detailed kinetic model of JP-10 pyrolysis and refined these data based on rate constant calculations using ab initio calculations. Their model predictions agreed well with five independent experimental data sets for JP-10 pyrolysis that cover a wide range of operating conditions without any adjustment of the model parameters eventually updating rate coefficients of the tricyclodecyl radical decomposition reactions via a CBS-QB3 calculation. This study revealed further that the decomposition pathways of JP-10 are mainly initiated via hydrogen abstraction, and only to a minor amount via biradicals generated through carbon–carbon bond rupture processes. Yue et al.[18] exploited DFT calculations to compute barrier heights of plausible decomposition pathways of multiple diradicals formed by carbon–carbon bond scission processes of JP-10. Based on the calculations, they proposed possible pathways for diradicals obtained via homolytic C–C bond cleavages of JP-10; this project concluded that those diradicals resemble the intermediates of the final products. To elucidate the initial decomposition mechanism,

Chenoweth et al.[19] carried out molecular dynamic simulations using a reactive force field. This work reported that the decomposition is initiated by carbon–carbon bond scission leading to ethylene (C_2H_2) plus C8 hydrocarbons or to two C5 hydrocarbons such as 1,4-pentadiene (C_5H_8) and cyclopentene (C_5H_8). Subsequently, Magoon et al.[20] investigated the barrier heights of ring opening processes and intramolecular disproportionation reactions to understand the pyrolysis mechanism of JP-10. Their results provided evidence that the barriers to the disproportionation reactions may be much lower (by up to 32 kJ mol) than previously thought in the case of intramolecular disproportionation in a key JP-10 decomposition pathway. Bozzelli et al. used density functional theory and the G3MP2B3 (a modified version of the G3MP2 method where the geometries and zero-point vibration energies are taken from B3LYP/6-31G(d) calculations) and CBS-QB3 composite computational methods to evaluate the standard enthalpy of formation of the parent JP-10 molecule and the different tricyclodecyl ($C_{10}H_{15}$) radicals corresponding to loss of a hydrogen atom from the carbon sites.[21] They calculated the enthalpy of formation for JP-10 to be 82 kJ mol^{-1}. Later, they also determined the carbon–carbon bond dissociation energies in JP-10 corresponding to diradical and carbene formation using density functional theory (DFT), and composite methods in conjunction with a series of isodesmic reactions are employed to increase the accuracy in their work.[22] They calculated that the C–C bond dissociation energies (BDEs) range from 324 to 354 kJ mol^{-1} for JP-10 singlet diradical intermediates; C–H BDEs for the parent carbon sites were found to range from 389 to 422 kJ mol^{-1}; and a wider range for C–C BDEs of carbenes from about 322 to 418 kJ mol^{-1} was revealed. Zehe et al.[23] studied the thermochemistry of JP-10 employing a variety of quantum chemistry methods, including the Gaussian Gx and Gx(MPx) (including G2, G2(MP2), G3, G3(MP2), G3(MP2)//B3LYP) composite methods, as well as the CBS-QB3 method,

and a variety of isodesmic and homodesmotic reaction schemes, suggesting a heat of formation of 126.4 kJ mol^{-1} at 298.15 K. However, the summary of the previous studies suggests that an understanding of the unimolecular decomposition of JP-10 (Table 7.1) is incomplete both from the experimental and theoretical viewpoints. Whereas these investigations yielded valuable information on the formation of closed-shell hydrocarbon intermediates and products, these species were mainly analyzed off-line and ex situ (GC-MS); however, GC-MS cannot sample radical transient species or thermally labile closed-shell molecules. Recently, Liu et al. presented an experimental and kinetic modeling study on JP-10 pyrolysis with SVUVPIMS as the diagnostic method and detected some unstable intermediates.[16] But with a relatively long residence time, some information for unstable products was still missing. Therefore, the 'molecular inventory' might have been altered since its formation, crucial reaction intermediates cannot be sampled, and detailed information on the reaction mechanisms – the role of radicals and intermediates – cannot always be obtained, but are at best inferred indirectly and qualitatively. Further, excessive pressures facilitate consecutive reactions of the initial decomposition products as evident from the formation of bicyclic PAHs such as naphthalene ($C_{10}H_8$) effectively excluding the elucidation of the initial decomposition products of JP-10. A novel approach requires probing the open- and closed-shell products online and in situ without changing the initial 'molecular inventory' from the decomposition and exploiting versatile, non-spectroscopic detection systems so that the complete product spectrum can be sampled quantitatively. These studies will be combined with electronic structure calculations to yield a unified picture on the temperature and pressure dependent decomposition mechanisms of JP-10. The present investigation represents the combined experimental and theoretical studies to probe the pyrolysis and initial decomposition products of JP-10 ($C_{10}H_{16}$). In this work, the pyrolysis

experiments were explored in two complementary high temperature reactors, in which the decomposition of JP-10 can be probed systematically at combustion-like temperatures. The nascent product distribution – including radicals and thermally labile closed-shell species – are probed on-line and in situ in a supersonic molecular beam exploiting soft photoionization with single photon VUV light followed by a mass spectroscopic analysis of the ions in a Re-TOF. Two sets of experiments with different residence times of a few 10 ms and of 100 ms were carried out. By limiting the residence time in the reactor to a few tens of microseconds in the first experiment, we aim to probe the initial reaction products excluding successive (higher order) reactions of the initially formed species, which may lead to molecular mass growth processes. By performing a second set of experiments with a much longer residence time at the level of at least 100 ms, we aim to explore interesting phenomena and conclusions on molecular growth and of the stability/decomposition of the initial radical fragments formed in the decomposition of JP-10. Finally, by carrying out molecular beam experiments and combining these studies with electronic structure calculations, we elucidate data on the products, their branching ratios, and reaction mechanisms involved in the decomposition of JP-10 over a broad range of combustion relevant temperatures and pressures.

Methods:

A detailed computational study of the complete mechanism of JP-10 pyrolysis is very tricky considering the existence of a great variety of decomposition pathways, extreme complexity of the $C_{10}H_{16}$ potential energy surface (PES) with a large number of possible isomers and transition states, and the presence of multiple primary products, which in turn can undergo secondary decomposition reactions. Therefore, our strategy here is first to identify favorable reaction channels, which may lead to the formation of the most

abundant dissociation products observed experimentally. Once such channels are identified, the corresponding regions of the PES are studied in more detail in order to characterize them quantitatively and to generate the energetic and molecular parameters to be used in calculations of rate constants and product branching ratios. Here, the decomposition of a JP-10 molecule can be initiated by a C–C bond cleavage leading to biradical intermediates or by a hydrogen atom loss or abstraction of atomic hydrogen by radicals leading to radical $C_{10}H_{15}$ isomers. A recent theoretical analysis of the reaction pathways by Vandewiele et al. has provided evidence that biradical pathways are not expected to play a major role as their overall contribution to the total product yield does not exceed 19%.[7] This result can be attributed to the fact that although C–C bonds in JP-10 are weaker than C–H bonds, additional processes, such as a β-scission-type rupture of another C–C bond or a hydrogen shift followed by a C–C bond cleavage, are required for the initial fragmentation to complete; this results in a higher overall barrier than for a C–H bond cleavage producing a radical fragment in one step. Hence, here we focus on the decomposition pathways of the $C_{10}H_{15}$ radicals R1 to R6 formed by cleavages of various C–H bonds in JP-10. As demonstrated in the present work, these channels occur predominantly via β-scission leading to ring opening and/or dissociation but may also involve hydrogen migrations and 'reverse β-scissions', i.e. ring closures for which a reverse process is a β-scission. Geometries of various local minima structures and transition states on the $C_{10}H_{15}$ PES and on the PESs corresponding to decomposition fragments were optimized using the hybrid DFT B3LYP[75,76] method with the 6-311G** basis set and the same method was applied to calculate vibrational frequencies and zero-point energy (ZPE) corrections. All transition states were tested by animating the motions corresponding to imaginary modes, and in cases where the connectivity of a transition state was not obvious, intrinsic reaction coordinate (IRC)

calculations were performed. To refine single-point energies of the optimized structures we applied a modified G3(MP2,CC)//B3LYP composite scheme where the energies were computed as $E_0[G3(MP2,CC)] = E[RCCSD(T)/6-311G^{**}] + \Delta E_{MP2} + E(ZPE)$, where $\Delta E_{MP2} = E[MP2/G3large] - E[MP2/6-311G^{**}]$ is a basis set correction and $E(ZPE)$ is the zero-point energy. T1 diagnostics were checked during coupled cluster calculations to ensure that wave functions do not possess any multireference character. The described calculation scheme represents a modification of the original G3 method; hereafter, we denote this approach as G3 for brevity. Relative energies computed within this scheme are expected to be accurate within 10 kJ mol^{-1}. All calculations were performed using Gaussian 09 and MOLPRO 2010 program packages.

Results and Discussion:

Initial C–H bond cleavages

Fig. 6.2 illustrates the energetics of various C–H bond cleavages in JP-10 to form the $C_{10}H_{15}$ radicals R1–R6. Based on these energetics, the C–H bond cleavages leading to R1, R4, R5, and R6 are clearly preferable, as they are computed to be endoergic by 397–406 kJ mol^{-1} as compared to 423 and 437 kJ mol^{-1}for the cleavages leading to R3 and R2, respectively. Therefore, hereafter we only consider decomposition processes of the R1 and R4–R6 radicals. All possible initial C–C bond b-scission processes in these radicals are compiled in Fig. 6.3 These radicals undergo ring opening in the initial tricyclic carbon skeleton of JP-10, but do not lead to a one-step fragmentation. For instance, R1 can isomerize to the radical intermediates R1-1, R1-2, and R1-3 via barriers of 150, 106, and 122 kJ mol1 , respectively; R1-1, R1-2, and R1-3 lie 40–52 kJ mol1 higher in energy than R1. R4 exhibits five possible C–C β-scission channels with barriers ranging from 108 to 146 kJ mol^{-1}, and the resulting R4-1–R4-5 intermediates

reside 34–73 kJ mol^{-1}above R4. R5 can undergo three possible b-scissions via barriers of 97–140 kJ mol^{-1}forming R5-1, R5-2, and R5-3 lying 56–131 kJ mol^{-1}higher in energy than R5. Finally, R6 features only one distinct b-scission pathway producing R6-1 (72 kJ mol^{-1}above R6) over a 141 kJ mol^{-1}barrier. The intermediates accessed after the first β-scission can further isomerize or dissociate giving a variety of JP-10 pyrolysis products. Potential energy diagrams of the dissociation channels including secondary and consequent dissociations of primary products are presented in figures below.

The R1 radical

Let us begin with pathways initiated from R1-1. A C–C bond β-scission in a five-membered ring of R1-1 leads to the intermediate R1-1_i1 over a 118 kJ mol^{-1}barrier (169 kJ mol^{-1}relative to R1). Yet another β-scission breaks the remaining five membered ring and produces an open-chain $C_{10}H_{15}$ intermediate R1-1_i2 via a barrier of a similar height. Next, R1-1_i2 features a third b-scission step and dissociates to C_4H_6 (1,3-butadiene) + C_6H_9 (R1-1_p1). The last step is rate-determining for the entire pathway from R1 and the corresponding transition state (TS) lies 274 kJ mol^{-1}above the initial reactant. The R1-1_p1 product can in principle further dissociate by b-scission to ethylene (C_2H_4) plus C_4H_5 but the barrier for ethylene loss by b-scission is as high as 157 kJ mol^{-1}and therefore, a reverse b-scission, i.e., a sixmembered ring closure to R1-1_p2 (a cyclohexenyl radical; C_6H_9) featuring a barrier of only 45 kJ mol^{-1}should be more favorable. Next, cyclohexenyl can lose a hydrogen atom and produce 1,3-cyclohexadiene (C_6H_8), but this requires overcoming of a significant barrier of 193 kJ mol^{-1}. Alternatively, if the R1-1_p2 product is thermalized in the reactor, it may attach a hydrogen atom via a barrierless and highly exothermic reaction to form cyclohexene (C_6H_{10}). The R1-1_p1 product can also be formed Fig. 7.11 –check the figure number!

JP-10 via an alternative pathway involving b-scission of the bond common for the two five-membered rings in R1-1 leading to an eight-membered ring intermediate R1-1_i3. The latter ring opens to the chain structure R1-1_i4, another conformer of R1-1_i2, and then a β-scission process splits C_4H_6 and forms R1-1_p1. However, the critical transition state for C_4H_6 loss on this pathway is higher in energy and resides 331 kJ mol^{-1} above R1. There are other two β-scission reactions in R1-1_i3, vinyl radical (C_2H_3) elimination to R1-1_p4 and ring opening to a branched intermediate R1-1_i5, but both exhibit higher barriers. R1-1_p4 is 1,4-cyclooctadiene (C_8H_{12}) and it may serve as a precursor for 1,3,5-cyclooctatriene (C_8H_{10}) observed experimentally in minor amounts. R1-1_i5 can eliminate the terminal ethylene moiety by β-scission forming a branched C_8H_{11} product R1-1_p5, the fate of which can be threefold. In the most favorable path, R1-1_p5 ring closes to a six-membered ring structure R1-1_p6 overcoming a barrier of only 36 kJ mol^{-1} and the latter can decompose to either 1,4-cyclohexadiene plus vinyl or to 2,5-dihydrostyrene, a precursor of the experimentally observed trace styrene product. Higher-energy and hence much less likely decomposition pathways of R1-1_p5 include terminal acetylene (C_2H_2) elimination forming a branched C_6H_9 structure R1-1_p10, which in turn can fragment to vinyl plus 1,3-butadiene. The most favorable fragmentation pathway of R1-2 is straightforward (Fig. 7.5): the bond linking two five-membered rings is cleaved by β-scission leading directly to the cyclopentyl (C_5H_7) plus cyclopentene (C_5H_8) products (R1-2_p1) via a barrier of only 168 kJ mol^{-1}. Alternative reaction channels are less competitive. For instance, two different β-scissions in one of the five-membered rings lead to intermediates R1-2_i1 and R1-2_i2 F via similar barriers of 195–197 kJ mol^{-1} (relative to R1). Next, both intermediates lose ethylene to form the same C_8H_{11} product R1-2_p2, cyclopentene-allyl via identical barriers of 217 kJ mol^{-1}. R1-2_p2 can lose an H atom to form C_8H_{10} products R1-2_p4 and R1-2_p5 via barriers of 172 and 243 kJ mol^{-1}

[1]or, more favorably, undergo a five-membered ring opening followed by a six-membered ring closure leading to the R1-1_p6 product discussed above, a precursor of 1,4-cyclohexadiene and 2,5- dihydrostyrene. The critical transition states for the formation of these products from R1-2_p2 are the vinyl radical and atomic hydrogen loss transition states on the final step residing 184 and 171 kJ mol^{-1}above R1-1_p2. Thus, if some amount of cyclopentene-allyl is produced from R1-2, it is likely to further decompose to the C_8H_{10} isomers R1-2_p4 and R1-1_p7 or to 1,4-cyclohexadiene plus vinyl. The dissociation mechanism of R1-3 is illustrated in Fig. 6.6. Here it appears that favorable reaction channels involve not only β-scissions but also hydrogen atom migrations. For instance, a 1,2-H shift in R1-3 creating an out-of-ring CH_3 group in the R1-3_i1 intermediate proceeds with a barrier of 199 kJ mol^{-1}relative to R1. Next, R1-3_i1 rearranges to R1-3_i2 by another 1,2-H shift along the six-membered ring via a transition state residing 193 kJ mol^{-1}above R1. The primary fragmentation is then completed by b-scission leading to elimination of the methyl group producing a dihydroindane molecule C_9H_{12} (R1-3_p1). In secondary fragmentation channels, dehydrogenation of dihydroindane may lead to indane (C_9H_{10}) and eventually to indene (C_9H_8), both of which were observed in experiments as trace products at high temperatures. Alternatively, following a first hydrogen atom loss from dihydroindane, the reaction may proceed by various β-scissions in C_9H_{11} radicals ultimately resulting in a number of six- and five-membered ring and chain products. Alternatively, to the hydrogen atom migration/CH_3 loss pathway, R1-3 can feature two different β-scission processes, both breaking the six-membered ring. The first process leads to the intermediate R1-3_i3 via a barrier located 164 kJ mol^{-1}above R1 and then the remaining five-membered ring opens producing a chain R1-3_i4 structure, a conformer of R1-1_i2 and R1-1_i4. Next R1-3_i4 eliminates trans-1,3-butadiene producing an open chain C_6H_7 structure R1-3_p2, which is a

different conformation of R1-1_p1. Similar to R1-1_p1, R1-3_p2 can ring close and then either eliminate an H atom to form 1,3-cyclohexadiene or add a hydrogen to Fig. 1 produce cyclohexene. The highest in energy TS on the pathway to C_6H_7 occurs at the last C_4H_6 loss step and resides 274 kJ mol^{-1} above R1. The second β-scission pathway from R3-1 is slightly less favorable. It begins from the formation of R1-3_i5, which next features additional β-scissions making either an open R1-3_i6 or a branched R1-3_i7 intermediate. Both of them eliminate ethylene giving rise to the same C_8H_{11} product R1-3_p3, which can further dissociate to hexatriene plus vinyl or, more favorably, undergo a five-membered ring closure to R1-3_p7 and only then decompose to cyclopentadiene plus an allyl radical. In another channel, R1-3_i5 can dissociate to cyclopentene plus 1,4-pentadien-5-yl, C_5H_7, and the latter can further fragment to allyl (C_3H_5) plus acetylene (C_2H_2), or to serve as a precursor of 1,3-pentadiene observed experimentally. Summarizing various decomposition channels of R1, R1 - R1-2 - cyclopentene plus cyclopentyl is clearly favored as it features the highest in energy transition at 168 kJ mol^{-1} above R1. This is followed by R1 - R1-3 - R1-3_i1 - R1-3_i2 - R1-3_p1 (dihydroindane plus methyl) (199 kJ mol^{-1}), and then by R1 - R1-1 - R1-1_i1 - R1-1_i2 - R1-1_p1 (C_6H_7 + C_4H_6) (274 kJ mol^{-1}), R1 - R1-3 - R1-3_i3 - R1-3_i4 - R1-3_p2 (C_6H_7 + C_4H_6) (274 kJ mol^{-1}), and R1 - R1-3 - R1-3_i5 - R1-3_p8 (cyclopentene + 1,4-pentadien-5-yl) (274 kJ mol^{-1}). Therefore, dissociation of R1 can largely contribute to the yield of the major five-membered ring products (cyclopentene, cyclopentadiene, cyclopentadienyl) and also provides six-membered rings (cyclohexadienes, cyclohexene, styrene), bicyclic products (indane, indene), as well as smaller molecules and radicals (1,3-butadiene, allyl, ethylene, vinyl radical, acetylene, methyl radical).

The R4 radical

Next, we consider dissociation of R4 via R4-1 and R4-2 (Fig. 6.7). Two β-scissions in R4 breaking a five-membered ring give similar isomers R4-1 and R4-2, both of which have a common bicyclo core. R4-1 has two side chains, CH_2 and CH_2CH_2, attached to this core, whereas R4-2 has only one CH2CH2CH2 side chain. R4-1 and R4-2 fragment by β-scission eliminating ethylene and forming the same C_8H_{11} product R4-1_p1 in which the bicyclo core is maintained. The decomposition channel R4 - R4-1 (R4-2) - C_8H_{11} plus C_2H_4 has a critical barrier of 157 (167) kJ mol^{-1}relative to R4. The primary R4-1_p1 product can further undergo secondary decomposition. The preferable step in the beginning is β-scission breaking the bicyclo core and producing a six-membered ring with two out-of-ring CH_2 groups (R4-1_p2) occurring via a barrier of 148 kJ mol^{-1}. Then it appears that a multi-step Fig. 6.1 process involving a series of 1,2-H shifts is more energetically favorable than another β-scission in R4-1_p2 followed by fragmentation. The hydrogen migration sequence, R4-1_p2 - R4-1_p3 - R4-1_p4 - R4-1_p5 - R4-1_p6, has the highest barrier of 212 kJ mol^{-1}relative to the initial C_8H_{11} radical R4-1_p1. The alternative β-scission sequence R4-1_p2 - R4-1_p11 - C6H7 (R4-1_p12) plus C_2H_4 features a much higher barrier of 301 kJ mol^{-1}relative to R4-1_p1. The C_8H_{11} intermediate R4-1_p6 can lose a hydrogen forming o-xylene or be subjected to two additional 1,2-H shifts, R4-1_p6 - R4-1_p7 - R4-1_p8, and then eliminate a methyl group and form toluene. Here, the R4-1_p7 and R4-1_p8 intermediates can also dissociate to o-xylene plus hydrogen. If some amount of the R4-1_p12 (C_6H_7) product is formed, it can either dissociate to a C_4H_5 radical and acetylene via a barrier of 163 kJ mol^{-1}or more likely feature a five-membered ring closure to R4-1_p13 via a barrier of only 48 kJ mol^{-1}. The C_6H_7 radical R4-1_p13 is a well-known precursor of fulvene and benzene. Whereas the dissociation of R4-1_p13 predominantly produces fulvene, hydrogen atom-assisted isomerization of fulvene to benzene is fast under combustion conditions. Among other

products, the C_4H_5 radical formed here can serve as a precursor of both vinylacetylene and 1,2,3-butatriene observed in the present experiments at high temperature. Decomposition of the R4-3 intermediate can account for the prompt formation of the ethyl (C_2H_5) radical, which shows the highest branching ratio of all products at the lowest ALS experimental temperature of 1200 K. As seen in Fig. 6.8, a 1,4-H shift to the terminal CH_2 group of the side chain in R4-3 requires a relatively low barrier of 70 kJ mol^{-1} (144 kJ mol^{-1} with respect to R4) and leads to the R4-3_i1 intermediate. A β-scission in the latter forms the C_8H_{10} (R4-3_p1) plus ethyl radical products after overcoming a barrier lying 154 kJ mol^{-1} higher in energy than R4. Alternatively, ethylene elimination from R4-3 proceeds via a barrier of 103 kJ mol^{-1} (177 kJ mol^{-1} with respect to R4) and forms a C_8H_{11} product R4-3_p2. Secondary decomposition of R4-3_p2 should be rather facile as it proceeds by two consecutive β-scissions (five-membered ring opening followed by ethylene elimination) via the highest barrier of 130 kJ mol^{-1} relative to the C_8H_{11} reactant R4-3_p2. This decomposition produces C_6H_7, R4-1_p13, a precursor of fulvene and benzene. Secondary decomposition of the closed-shell C_8H_{10} product R4-3_p1 requires further investigation, but it is probable that after activation of R4-3_p1 by a C–H bond cleavage, a C_8H_9 radical would decompose to fulvene plus vinyl also contributing to the yield of C_6H_6 species. The most favorable pathway of R4-4 decomposition, R4-4 - R4-4_i1 - R4-4_i2 - R4-4_p1 plus methyl, Fig. 6.5 consists of two 1,2-H shifts followed by elimination of the methyl group (Fig. 6.8). The highest barrier along this reaction channel is 188 kJ mol^{-1} with respect to R4. The bicyclic C6–C5 core is conserved and the R4-4_p1 product is dihydroindane, a precursor of indane, indene, or other fragments containing either a six- or a five-membered ring, similarly to its R1-3_p1 isomer considered above. In contrast to R4-4, R4-5 prefers to fragment via two consecutive b-scissions, R4-5 - R4-5_i1 - R4-5_p1 plus allyl. The critical barrier on this

pathway, 195 kJ mol^{-1}, is slightly higher than that for the decomposition of R4-4. The R4-5_p1 product C_7H_{10} is 1-vinyl-1-cyclopentene. It may serve as a precursor of the observed trace products fulvenallene, C_7H_6, and fulvenallenyl, C_7H_5; however, a large number of dehydrogenation steps are required to form those species. If R4-5_p1 is activated by hydrogen atom abstraction or a C–H bond cleavage, the C_7H_9 radicals produced are likely to decompose through β-scissions, but a detailed mechanism requires further investigations. In summary, the fragmentation pathways of R4 can be ranked in terms of their kinetic favorability based on the height of the highest barrier (given in parentheses relative to R4) as follows: (1) R4 - R4-3 - R4-3_i1 - C_8H_{10} (R4-3_p1) + C_2H_5 (154 kJ mol^{-1}), (2) R4 - R4-1 - C_8H_{11} (R4-1_p1) + C_2H_4 (157 kJ mol^{-1}), (3) R4 - R4-3 - C_8H_{11} (R4-3_p2) + C_2H_4 (177 kJ mol^{-1}), (4) R4 - R4-4 - R4-4_i1 - R4-4_i2 - C_9H_{12} (R4-4_p1) + CH_3 (188 kJ mol^{-1}), and (5) R4 - R4-5 - R4-5_i1 - C_7H_{10} (1-vinyl-1-cyclopentene, R4-5_p1) + C_3H_5 (195 kJ mol^{-1}). Therefore, decomposition of R4 represents a source of the methyl, ethyl, and allyl radicals, ethylene, fulvene and benzene (via secondary decomposition of R4-3_p1 and R4-3_p2), and also provides feasible pathways to the minor products o-xylene and toluene (via secondary dissociation of R4-1_p1), indane and indene (from R4-4_p1), as well as fulvenallene and fulvenallenyl (R4-5_p1).

The R5 radical

Decomposition of R5 appeared to favorably proceed via R5-1 rather than R5-2 or R5-3 and hence Fig. 6.9 shows only pathways involving R5-1. Here, R5-1 can be subjected to two different β-scissions breaking a five-membered ring via similar barriers of 193 and 200 kJ mol^{-1} and forming the R5-1_i1 and R5-1_i2 intermediates. Both intermediates can decompose by eliminating allyl and forming the C_7H_{10} product 3-vinyl-1-cyclopentene

R5-1_p1. Alternatively, R5-1_i2 can also dissociate to cyclopentyl (C5H7) plus 1,4-pentadiene (R5-1_p2). The critical barriers for the product formation from R5 are found to be in a narrow range of 217–222 kJ mol^{-1}. An alternative pathway from R5-1_i1 to an open-chain structure R5-1_i3 followed by ethylene elimination is unlikely to be competitive because of a much higher critical barrier of 344 kJ mol^{-1}with respect to R5. Thus, decomposition of R5 is a source of the cyclic and open chain C5 (Fig. 17 check figure number) fragments and may also contribute to the formation of the trace fulvenallene and fulvenallenyl products through dehydrogenation of 3-vinyl-1-cyclopentene R5-1_p1. Due to the higher barriers, the primary decomposition of R5 is expected to be somewhat slower than that of R1 and R4.

The R6 radical

Two channels may compete in dissociation of R6 proceeding via R6-1 (Fig. 6.10). In the first one, R6-1 decomposes to the bicyclic C_7H_{10} structure R6-1_p1 plus allyl via a barrier of 177 kJ mol^{-1}relative to R6. In the second channel, a first β-scission in R6-1 breaks a five-membered ring and forms the R6-1_i1 intermediate and a second β-scission eliminates ethylene leading to the C_8H_{11} product R6-1_p2, with the highest in energy transition state lying 231 kJ mol^{-1}above R6. The R6-1_p2 product can then easily dissociate to cyclopentadiene (C_5H_6) plus allyl (C_3H_5) overcoming a barrier of only 87 kJ mol^{-1}. Since the C_7H_{10} product R6-1_p1 was not observed in the experiments, it is likely to undergo further fragmentation in the reactor. While a more detailed study is needed to consider all possible decomposition pathways of R6-1_p1, here we consider only one of them, initiated by the cleavage of one of the C–H bonds leading to the C_7H_9 radical R6-1_p4. The strength of this C–H bond (endoergicity of R6-1_p1 - R6-1_p4 + H) is computed to be 401 kJ mol^{-1}, very similar to the analogous C–H bond strength in JP-10,

JP-10 → R1 + H. R6-1_p4 can decompose via two competitive mechanisms involving β-scissions. The R6-1_p4 - R6-1_p5 - 5-methylene-1,3-cyclohexadiene (R6-1_p6) plus atomic hydrogen sequence involves reformation of the bicyclic structure into a six-membered ring with an out-of-ring CH_2 followed by H elimination. The highest barrier on this reaction pathway is 136 kJ mol^{-1} relative to the initial C_7H_9 radical R6-1_p4. This channel can account for the observation of a minor 5-methylene1,3-cyclohexadiene product. Alternatively, the R6-1_p4-R6-1_p7- C_5H_6 + C_2H_3 sequence first produces a five-membered ring intermediate with an outer vinyl group and the intermediate then decomposes to cyclopentadiene plus vinyl via a barrier of 155 kJ mol^{-1}. In summary, decomposition of R6 contributes to the production of an allyl radical, ethylene, cyclopentadiene (both directly and via dissociation of the primary C_7H_{10} R6-1_p1 product), as well as a vinyl radical and 5-methylene-1,3-cyclohexadiene both of which can be formed via R6-1_p1.

References:

1. A. Osmont, I. Gokalp and L. Catoire, Propellants, Explos., Pyrotech., 2006, 31, 343–354.

2. H. Chung, C. Chen, R. Kremer, J. Boulton and G. Burdette, Energy Fuels, 1999, 13, 641–649.

3. L. Q. Maurice, H. Lander, T. Edwards and W. Harrison, Fuel, 2001, 80, 747–756.

4. B. Van Devener and S. L. Anderson, Energy Fuels, 2006, 20, 1886–1894.

5. C. W. Gao, A. G. Vandeputte, N. W. Yee, W. H. Green, R. E. Bonomi, G. R. Magoon, H.-W. Wong, O. O. Oluwole, D. K. Lewis and N. M. Vandewiele, Combust. Flame, 2015, 162, 3115–3129.

6. S. Nakra, R. J. Green and S. L. Anderson, Combust. Flame, 2006, 144, 662–674.

7. N. M. Vandewiele, G. R. Magoon, K. M. Van Geem, M.-F. Reyniers, W. H. Green and G. B. Marin, Energy Fuels, 2014, 28, 4976–4985.

8. O. Herbinet, B. Sirjean, R. Bounaceur, R. Fournet, F. BattinLeclerc, G. Scacchi and P.-M. Marquaire, *The Journal of Physical Chemistry* A, 2006, 110, 11298–11314.

9. P. N. Rao and D. Kunzru, J. Anal. Appl. Pyrolysis, 2006, 76, 154–160.

10. R. Striebich and J. Lawrence, J. Anal. Appl. Pyrolysis, 2003, 70, 339–352.

11. K. Wohlwend, L. Maurice, T. Edwards, R. Striebich, M. Vangsness and A. Hill, J. Propul. Power, 2001, 17, 1258–1262.

12. Y. Xing, W. Fang, W. Xie, Y. Guo and R. Lin, Ind. Eng. Chem. Res., 2008, 47, 10034–10040.

13. G. Li, C. Zhang, H. Wei, H. Xie, Y. Guo and W. Fang, Fuel, 2016, 163, 148–156.

14. T. J. Bruno, M. L. Huber, A. Laesecke, E. W. Lemmon and R. A. Perkins, Tech. Rep. NISTIR, 2006, 6640, 325.

15. S. H. Park, C. H. Kwon, J. Kim, B. H. Chun, J. W. Kang, J. S. Han, B. H. Jeong and S. H. Kim, Ind. Eng. Chem. Res., 2010, 49, 8319–8324.

16. H. Li, G. Liu, R. Jiang, L. Wang and X. Zhang, Combust. Flame, 2015, 162, 2177–2190.

17. N. M. Vandewiele, G. R. Magoon, K. M. Van Geem, M.-F. Reyniers, W. H. Green and G. B. Marin, Energy Fuels, 2014, 29, 413–427.

18. L. Yue, H.-J. Xie, X.-M. Qin, X.-X. Lu and W.-J. Fang, J. Mol. Model., 2013, 19, 5355–5365.

19. K. Chenoweth, A. C. T. van Duin, S. Dasgupta and W. A. Goddard Iii, *The Journal of Physical Chemistry* A, 2009, 113, 1740–1746.

20. G. R. Magoon, J. Aguilera-Iparraguirre, W. H. Green, J. J. Lutz, P. Piecuch, H. W. Wong and O. O. Oluwole, Int. J. Chem. Kinet., 2012, 44, 179–193.

21. J. M. Hudzik, R. Asatryan and J. W. Bozzelli, *The Journal of Physical Chemistry* A, 2010, 114, 9545–9553.

22. J. M. Hudzik, A. Castillo and J. W. Bozzelli, *The Journal of Physical Chemistry* A, 2015, 119, 9857–9878.

23. M. J. Zehe and R. L. Jaffe, J. Org. Chem., 2010, 75, 4387–4391.

24. S. S. Cheng, K. F. Liou and Y. T. Lin, J. Chin. Chem. Soc., 1986, 33, 335–340.

25. O. Prakash, R. K. Tiwari, S. L. Kalra and P. S. Venkataramani, Indian J. Chem. Technol., 1995, 2, 295–297.

26. D. F. Davidson, D. C. Horning, J. T. Herbon and R. K. Hanson, Proc. Combust. Inst., 2000, 28, 1687–1692.

27. S. C. Li, B. Varatharajan and F. A. Williams, AIAA J., 2001, 39, 2351–2356.

28. D. W. Mikolaitis, C. Segal and A. Chandy, J. Propul. Power, 2003, 19, 601–606.

29. F. Parsinejad, C. Arcari and H. Metghalchi, Combust. Sci. Technol., 2006, 178, 975–1000.

30. C. Q. Jiao, C. A. DeJoseph and A. Garscadden, Int. J. Mass Spectrom., 2007, 266, 92–96.

31. S. Wang, H.-J. Gou, B.-C. Fan, Y.-Z. He, S.-T. Zhang and J.-P. Cui, Chin. J. Chem. Phys., 2007, 20, 48–52.

32. Y. Xing, Y. S. Guo, D. Li, W. J. Fang and R. S. Lin, Energy Fuels, 2007, 21, 1048–1051.

33. F. J. Yang, Y. S. Guo, Y. Xing, D. Li, W. J. Fang and R. S. Lin, J. Chem. Eng. Data, 2008, 53, 2237–2240.

34. X. H. Su, H. M. Hou, G. Li, R. S. Lin and S. L. Cai, Acta Chim. Sin., 2009, 67, 587–592.

35. R. Seiser, U. Niemann and K. Seshadri, Proc. Combust. Inst., 2011, 33, 1045–1052.

36. F. Guo, X. L. Cheng and H. Zhang, Combust. Sci. Technol., 2012, 184, 1233–1243.

37. K. H. H. Goh, P. Geipel, F. Hampp and R. P. Lindstedt, Proc. Combust. Inst., 2013, 34, 3311–3318.

38. L. Tu¨rker, S. Varis- and Ç. Çelik Bayar, Fuel, 2013, 104, 128–132.

39. X. M. Qin, H. J. Xie, L. Yue, X. X. Lu and W. J. Fang, J. Mol. Model., 2014, 20, 8.

Figure 6.1 The Molecular Structure of JP-10
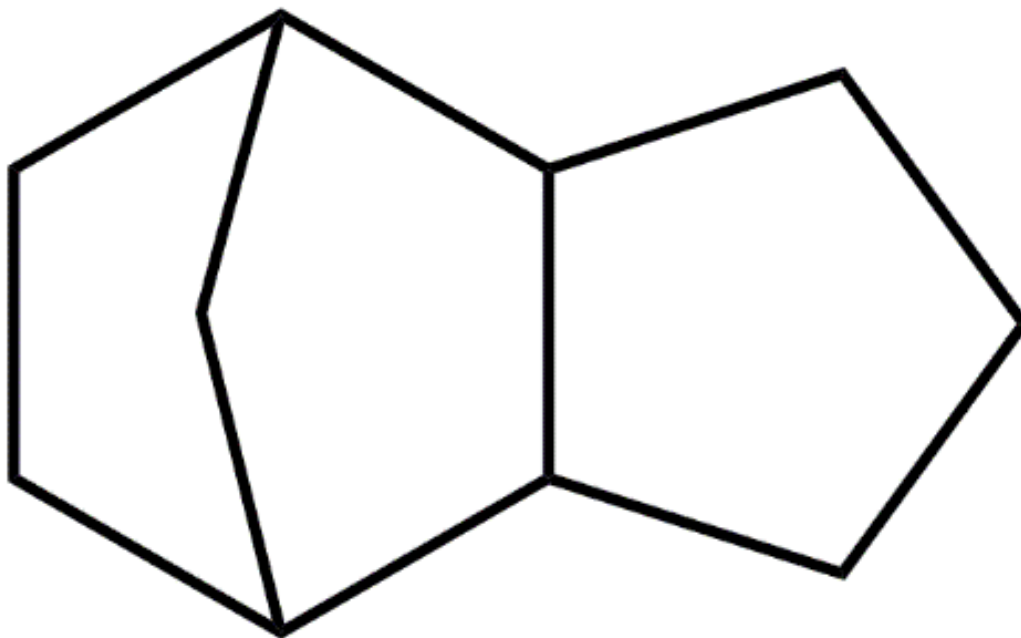
Figure 6.2 Radicals Formed by C-H Bond Cleavages in JP-10.

B3LYP
G3

R2 **422**
437

R1 **394**
400

R6 **390**
399

H
0
H

R3 **415**
423

R4 **395**
406

R5 **388**
397

151
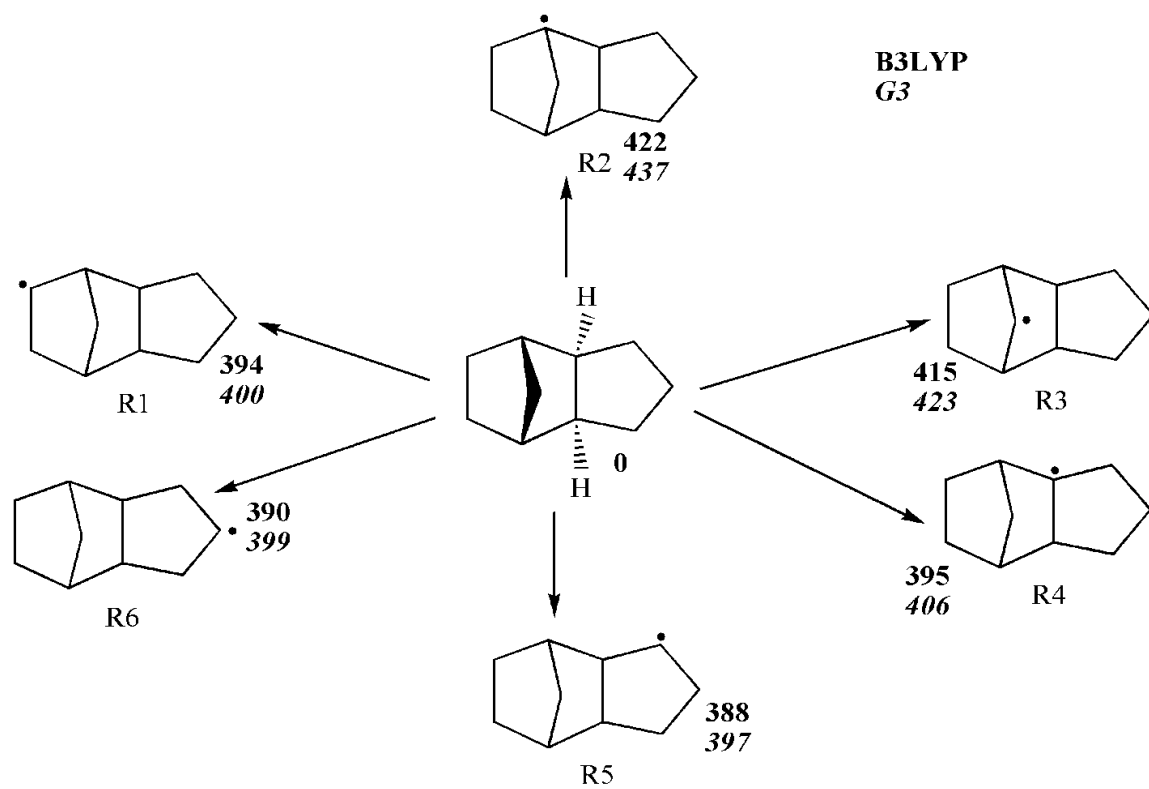
Figure 6.3 Energetics of Various Initial β-Scission Processes in the R1, R4, R5, and R6 Radicals.
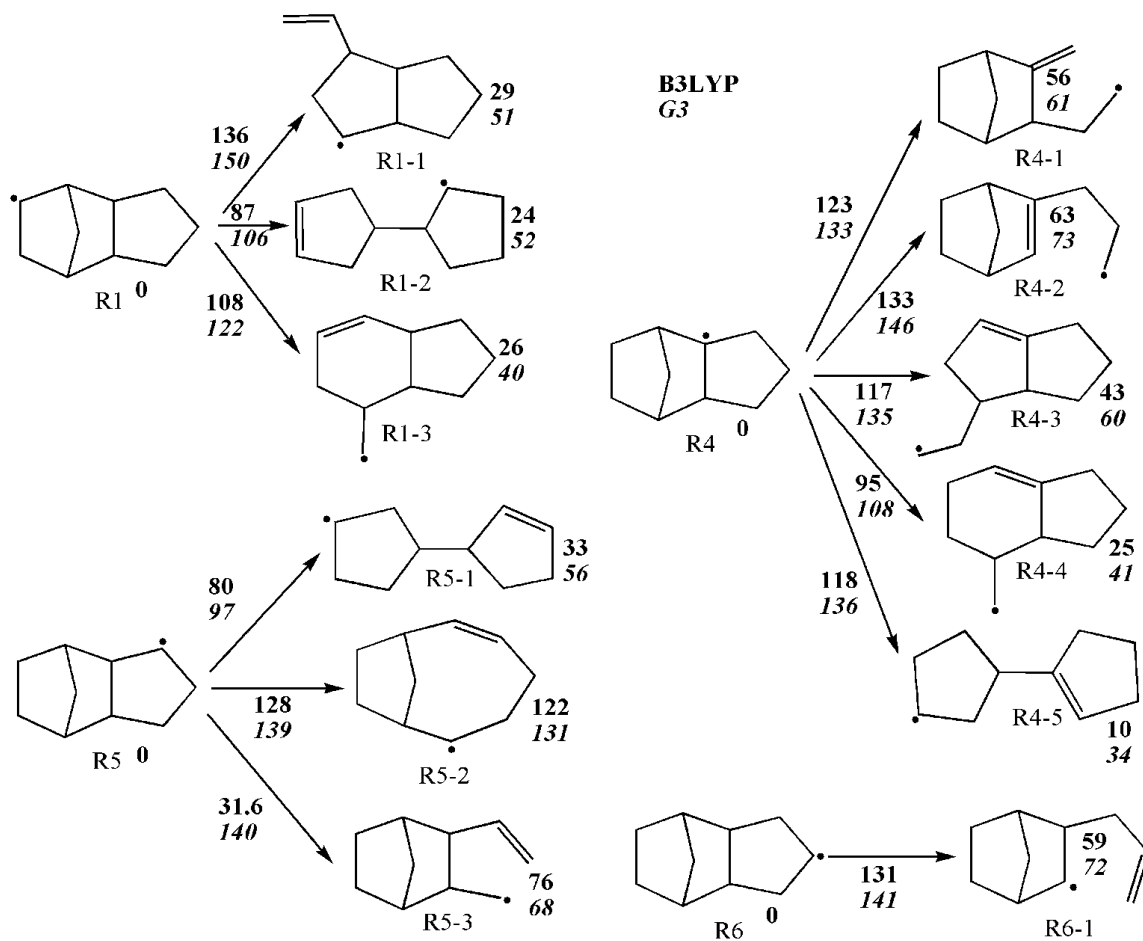
Figure 6.4 Potential Energy Diagram for Decomposition of R1-1. All Relative Energies are Computed at the G3 level and are Given in kJ mol^{-1}
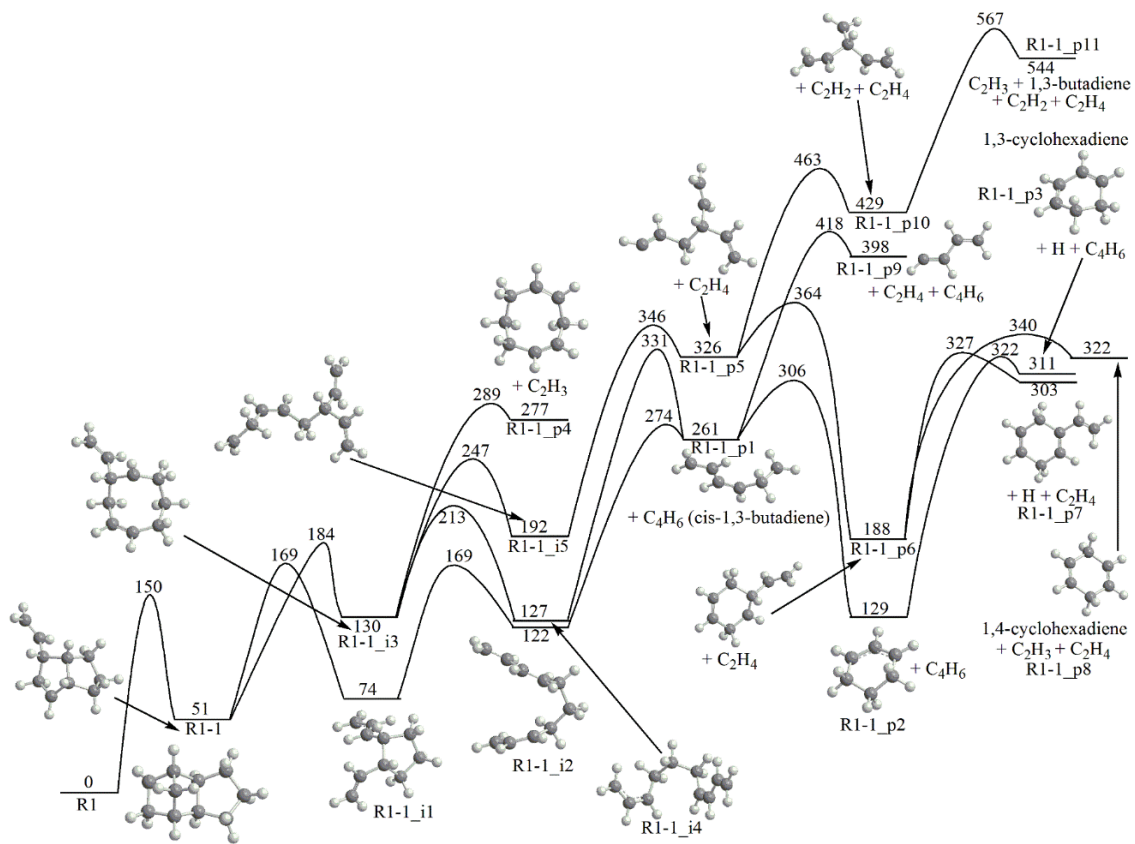
Figure 6.5 Potential Energy Diagram for Decomposition of R1-2. All Relative Energies are Computed at the G3 Level and are Given in kJ mol^{-1}
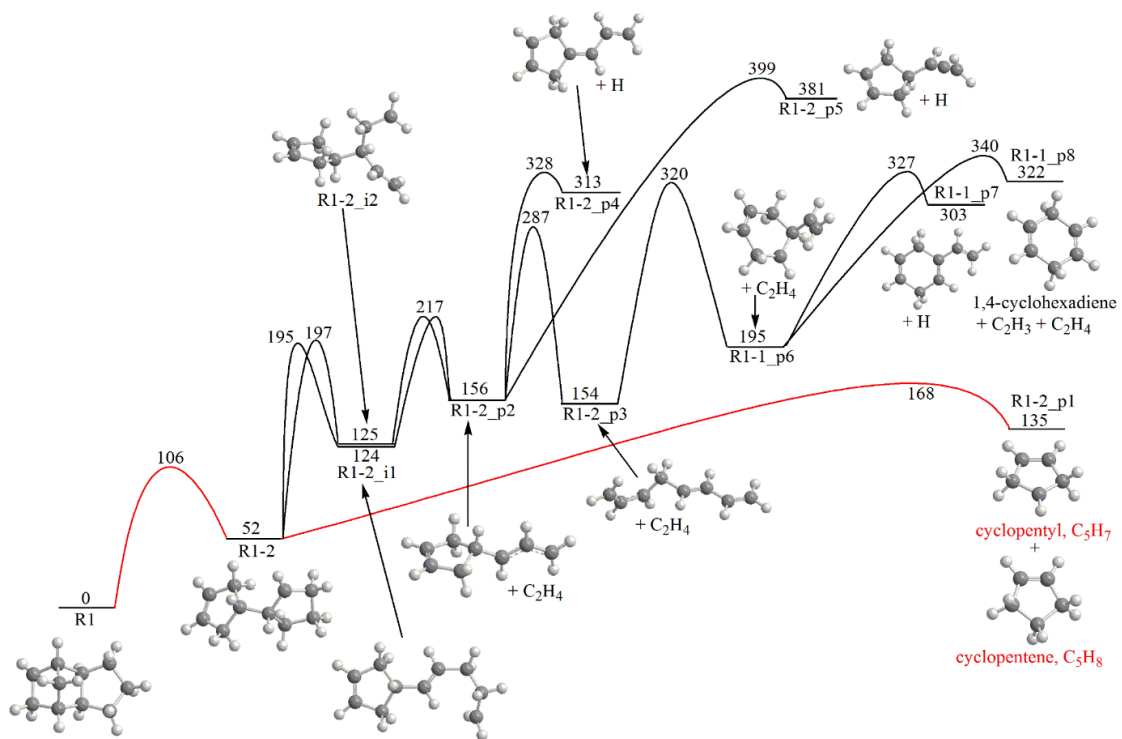
Figure 6.6 Potential Energy Diagram for Decomposition of R1-3. All Relative Energies are Computed at the G3 Level and are Given in kJ mol⁻¹
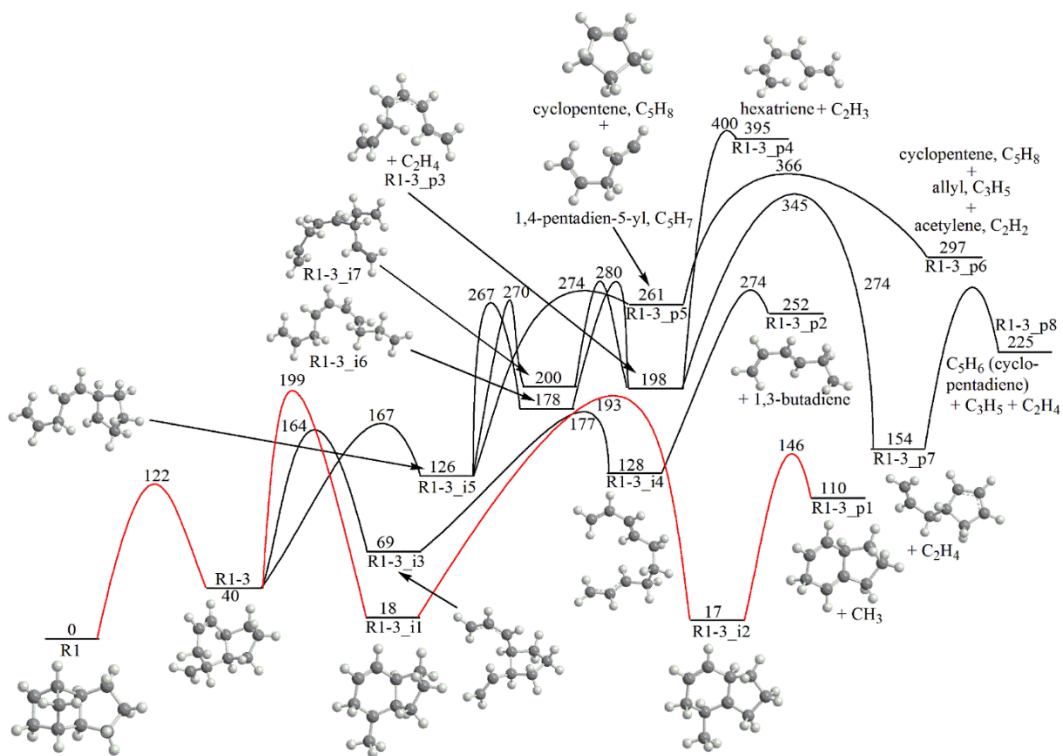
Figure 6.7 Potential Energy Diagram for Decomposition of R4-2. All Relative Energies are Computed at the G3 Level and are Given in kJ mol^{-1}
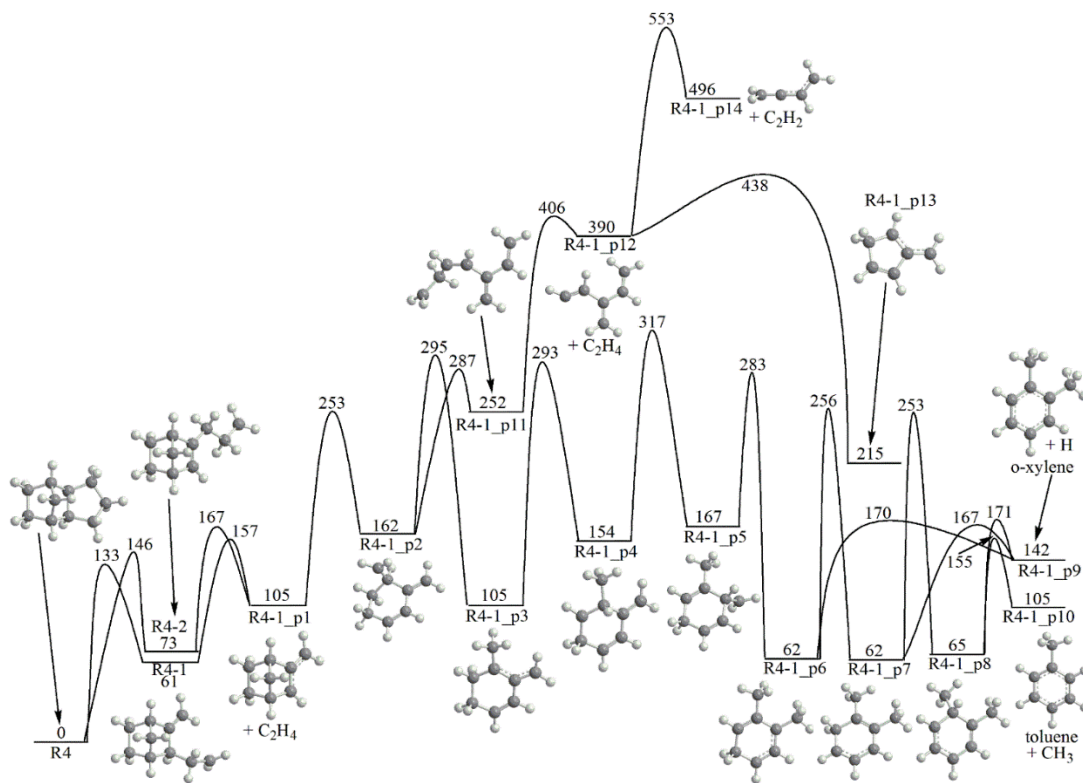
Figure 6.8 Potential Energy Diagram for Decomposition of R4-3(Top) and R4-4 and R4-5 (Bottom). All Relative Energies are Computed at the G3 Level and are Given in kJ mol^{-1}
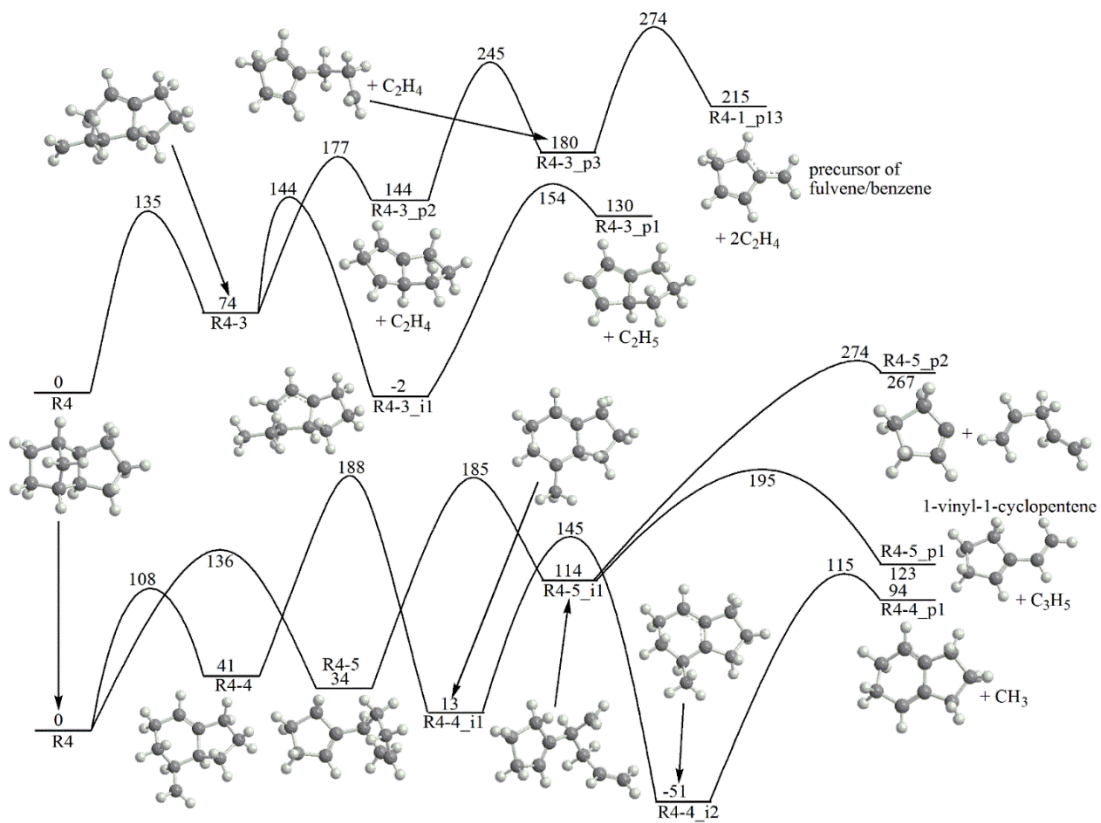
Figure 6.9 Potential Energy Diagram for Decomposition of R5-1. All Relative Energies are Computed at the G3 Level and are Given in kJ mol^{-1}
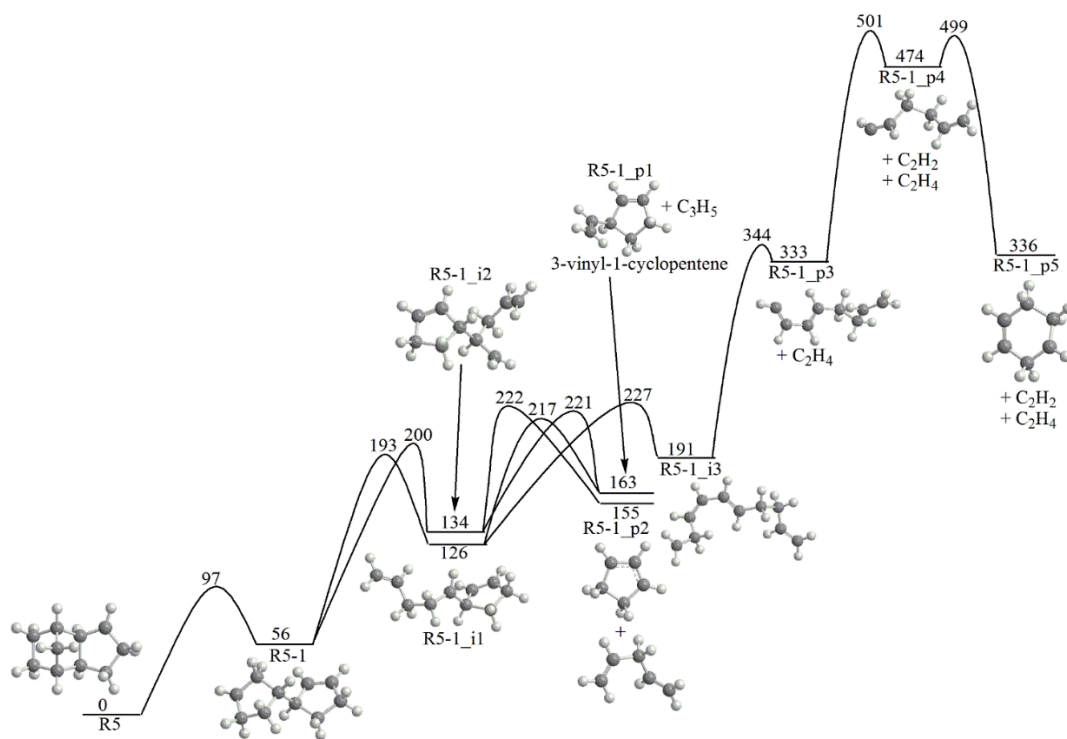
Figure 6.10 Potential Energy Diagram for Decomposition of R6 (Top) and its C_7H_{10}

Product (R6-1_p1) Activated by H Loss/Abstraction (Bottom). Energies Given in kJ mol^{-1}
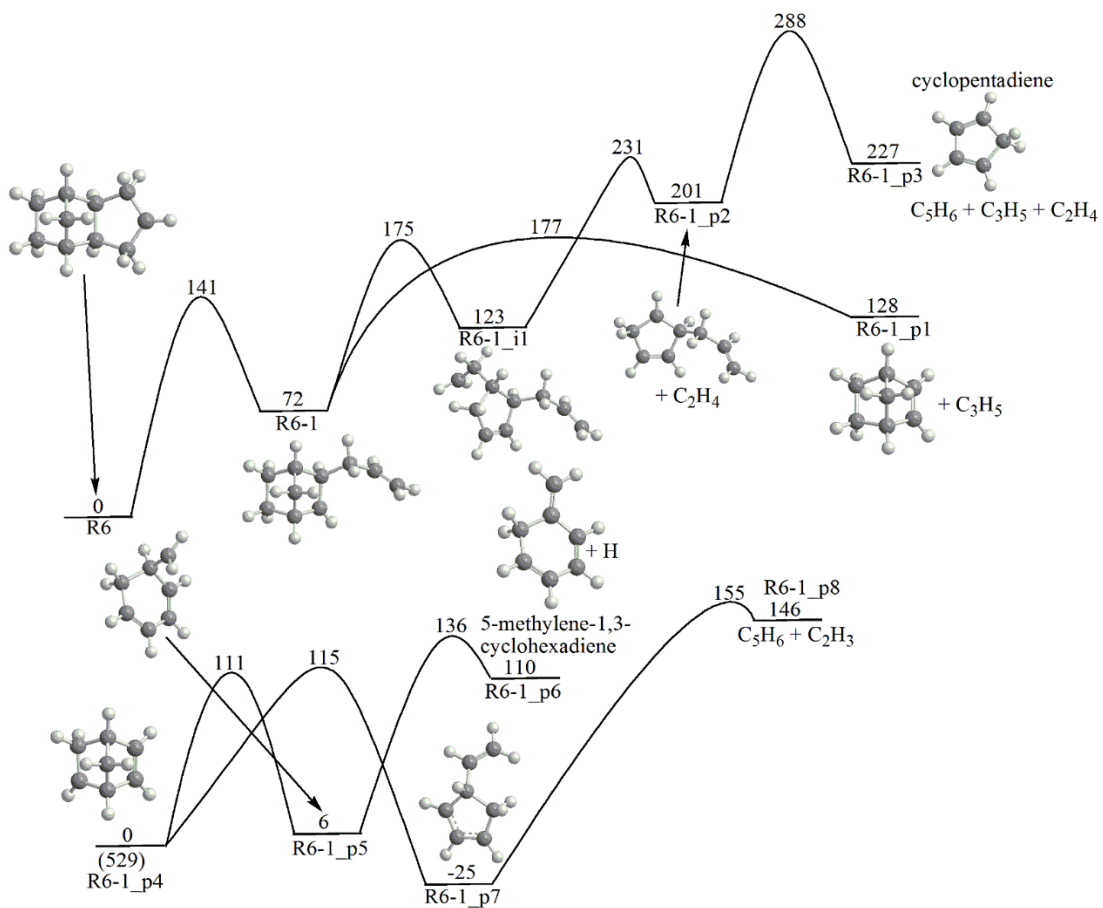
CHAPTER VII

Reaction Mechanism of Acenaphthyl Radicals with Molecular Oxygen

Introduction

Polycyclic aromatic hydrocarbons(PAHs) are expected to be associated with roughly 20% of all the carbon in the universe.[1] This class of compounds also contributes highly to the formation of combustion generated particles known as soot. In industrialized locations these PAH particles can aggregate and contribute to polluted air quality causing diseases in the populations that live there. By investigating the mechanisms of formation of these compounds systems for removal or prevention can be designed leading to improvements in urban quality of life. Acenapthylene is of special interest as a precursor to soot growth being a naphthalene molecule with an added acetylene (C_2H_2) unit. This tricyclic molecule is a natural staring point to further elucidate the mechanism of overall PAH growth and would advance previous work done by Mebel et al. which investigated the growth of both the initial ring and second ring in soot formation.[2] An important process that competes with this growth is of oxidation reactions, the interplay between the two effectively determines the quantity of soot that will be produced. In order to compare the two, the information required is the mechanism, product yields at various combustion conditions, and rate constants. The oxidation of both the phenyl radical (C_6H_5) and napthyl radical ($C_{10}H_7$) are expected to be prototypical for the acenapthyl radical which contains both 5- and 6- member aromatic rings.

On the analogous cyclopentadienyl oxidation surface investigated by Robinson et al indicates the formation of a cyclopentadienyl-peroxy adduct which can dissociate into product species C_5H_5O + O or undergo a hydrogen shift followed by expulsion of a hydroxyl group leading to C_5H_4O + OH.[3] It is expected the stability of these structures prevents ring opening and the acenaphthyl surface while behaving similarly for the entrance channels will diverge at the final products.

The initial adduct that forms on the potential energy surface of the napthyl radical is a napthylperoxy radical ($C_{10}H_7O_2$) which can rearrange to a bicyclic dioxiranyl species.[4] This dioxiranyl species can then lead to a seven member ring becoming a 2-oxepinyloxy radical or lose a terminal oxygen atom and yield a napthoxy radical plus the oxygen atom. The decomposition of this radical is through a multistep pathway ending in carbon dioxide elimination and the formation of indenyl. The dioxyranyl species can also directly eliminate an oxygen atom which form van der Waal complexes based around an O-O bond and eventually forming $C_{10}H_7O$. Decomposition of this radical eventually leads to carbon monoxide loss and the formation of indenyl. In both cases of oxidation, cyclopentadienyl and napthyl, kinetics work has shown that the major pathway involves the direct elimination of the oxygen atom. The major focus of this work will be on this reaction pathway in regards to the six member ring oxidation. This work seeks to describe the most relevant reaction channels for acenapthyl oxidation and develop a chemically accurate potential energy surface and provide insight in the most abundant products that will form.

Methods

The hybrid density functional and level of theory used for all initial geometry optimizations was B3LYP/6-311G**. This method was used to model all reactants, intermediates, products, and transition states present in the reaction of molecular oxygen with various acenaphthyl radicals of the form $1\text{-}C_{12}H_7+O_2$, $2\text{-}C_{12}H_7+O_2$, $3\text{-}C_{12}H_7+O_2$, and $4\text{-}C_{12}H_7+O_2$.(R1) Once all optimized geometries were collected, potential energy surfaces were generated and most favorable channels chosen for rate constant calculations. The aforementioned level of theory was also used to calculate molecular

structure parameters, zero-point energy corrections, and vibrational frequencies. Unscaled B3LYP frequencies were used to calculate zero point energy corrections as well as rate constants since the scaling of B3LYP frequencies does not greatly alter relative energies of transitions states and isomers. Structures were checked for number of imaginary frequencies in order to identify these stationary points as either transition states or local minima. The connections between these identified transition states and minima were then verified by further intrinsic reaction coordinate calculations. The coordinates of these structures is available in supporting information. Energetics of each structure were then refined using the G3 composite method.[20-23] This allowed for high-level single-point energy calculations involving the use of Moller-Plesset second level perturbation theory (MP2) and coupled cluster with single double and estimated triple excitations calculations. Doing so incorporated a basis set correction as the MP2 calculations were done at basis set levels of 6-311g** and with an extended G3 large basis set. This was done using restricted RHF-RCCSD(T) energies to specify partially spin-adapted open-shell calculations obtained from molecular orbitals using restricted open shell Hartree-Fock calculations were used. Diagnostic values for all coupled cluster calculations were checked and fell into acceptable ranges. B3LYP calculations were done using the GAUSSIAN 09 program package while RHF-RCCSD(T) and MP2 calculations were done using MOLPRO 2010.[24-25] Rate constants were calculated with the use of Rice-Ramsperger Kassel Marcus (RRKM) theory at temperatures ranging from 500 K t o 2000 K and pressures ranging 0.01 atm to 100 atm. These rate constants were calculated using the MESS program and also incorporated variable reaction coordinate-transition state theory (VRC-TST) and phase space theory.[26]

Results and Discussion

Initially for the reaction to the 1-acenaphthyl radical site there is barrierless addition of O_2 which forms a 1-acenaphthyl peroxy radical as shown in Figure 6.1. The depth of this well differs only by 0.54 kcal/mol when compared at levels of theory G3(MP2,CC)//B3LYP and B3LYP/6-311g**. The formation of 1-acenaphthyl as compared to the other three unique radical sites comprises 10.27% of the products, a discussion of the oxidation of this position follows. Upon formation of the peroxy radical in the 1-acenaphthyl position there were two energertically favorable pathways. A shift of the terminal oxygen atom to the adjacent hydrogen bearing carbon or adding on to said carbon. The shift to the adjacent hydrogen bearing carbon contains a higher barrier at 34.2 kcal/mol versus 20.6 kcal/mol however it results in a metastable ring opening. This ring opening leads to very deep wells, 105.7 kcal/mol, from the formation of CO and HCO groups that can be eliminated. The elimination of the carbon monoxide group is possible after surmounting a barrier of 22.4 kcal/mol eventually leading to the formation of 1-naphthylmethanone after a hydrogen shift. This hydrogen shift exhibits a barrier of 13.5 kcal/mol. Another path to 1-napthylmethanone is closing of the ring followed by a hydrogen shift in the HCO unit onto the nearest oxygen. The barrier for this reaction is 23 kcal/mol towards closing and 56.5 kcal/mol on reopening. What follows next is the elimination of two carbon monoxide units producing 1-napthyl. The formation rate of 1-napthyl will primarily be determined by the formation of i_06 due to the nature of the barriers on the potential energy surface. Rates for both CO eliminations were investigated. For the first CO elimination pathways $C_{12}H_7+O_2 \rightarrow$ i_10/i_09, 1-acenaphthyl peroxy radical $\rightarrow$ i_10/i_09 were disregarded as their contributions are so low as to be negligible. In both pairs of reactions, bimolecular $C_{12}H_7+O_2 \rightarrow$ i_01 and

$C_{12}H_7+O_2 \rightarrow$ i_06 or monomolecular i_01 $\rightarrow C_{12}H_7+O_2$ and i_01 $\rightarrow$ i_06, the rate constants are comparable at least in some temperature range. Thus, one must take into consideration both paths to i_06: either through stabilization in i_01 well $(C_{12}H_7+O_2 \rightarrow$ i_01 $\rightarrow$ i_06) or the direct one $(C_{12}H_7+O_2 \rightarrow$ i_06) with well skipping. Overall the mechanism for oxidation of the 1-acenapthyl position leads to two consecutive CO eliminations and the formation of 1-napthyl.

The formation of radicals 2-acenapththyl, 3-acenapththyl, and 4-acenapththyl constitute 89.73 % of the products formed from hydrogen abstraction. With the individual contributions being 29.82 % for 2-acenapththyl, 33.91 % for 3-acenapththyl, and 25.99 % for 4-acenapththyl. This implies that the dominant reaction pathways will involve oxidation of the 6-member ring and behave similarly to systems such as phenyl and naphthyl radicals. After initial radical formation at the unique positions all surfaces there are two possible reaction pathways. As discussed with the napthyl radical a peroxy species or dioxyranyl species can be formed. For the purposes of this work the dioxyranyl pathway will be ignored as it is entropically unfavored. While initially there is a large energetic favorability due to a deep well, -95.1 kcal/mol, the pathway requires seven individual steps which are too demanding in terms of entropy decrease. These steps require multiple cyclizations with the formation of a 7-member ring and 4-member ring before eventual carbon dioxide loss. The kinetically favored pathway is the formation of a acenaphthyl peroxy species which undergoes oxygen atom elimination. After this elimination ring shrinkage occurs reducing the 6-member ring to a 5-member ring fused to a 3-member ring. This 3-member ring can then proceed to carbon monoxide loss through two unique carbon-carbon bond scissions leading to $C_{11}H_7$.

References

1. Hoover, R. (2014). Need to Track Organic Nano-Particles Across the Universe? NASA's Got an App for That. *NASA. Retrieved February*, *22*, 2014.

2. Kislov, V. V., Singh, R. I., Edwards, D. E., Mebel, A. M., & Frenklach, M. (2015). Rate coefficients and product branching ratios for the oxidation of phenyl and naphthyl radicals: A theoretical RRKM-ME study. *Proceedings of the Combustion Institute*, *35*(2), 1861-1869.

3. Robinson, R. K., & Lindstedt, R. P. (2011). On the chemical kinetics of cyclopentadiene oxidation. *Combustion and Flame*, *158*(4), 666-686.

4. Harris, S. J.; Weiner, A. M.; Blint, R. J.Combust. Flame 1988,77,91.

5. Richter, H.; Howard, J. B.Prog. Energy Combust. Sci.2000,26,565.

6. Bittner, J. D.; Howard, J. B. Symp. Proc. Combust. Inst.1981,18,1105.

7. Frenklach, M.; Clary, D. W.; Gardiner, W. C.; Stein, S. E.Proc.Combust. Inst.1984,20, 887.

8. Frenklach, M.; Clary, D. W.; Gardiner, W. C.; Stein, S. E.Proc.Combust. Inst.1986,21, 1067.

9. Wang, H.; Frenklach, M.*The Journal of Physical Chemistry*1994,98, 11465.

10. Miller, J. A.Proc. Combust. Inst.1996,26, 461.

11. Castaldi, M. J.; Marinov, N. M.; Melius, C. F.; Hwang, J.; Senkan,S. M.; Pitz, W. J.; Westbrook, C. K.Proc. Combust. Inst.1996,26, 693.

12. Marinov, N. M.; Pitz, W. J.; Westbrook, C. K.; Castaldi, M. J.;Senkan, S. M.Combust. Sci.Technol.1996,116/117, 211.

13. Wang, H.; Frenklach, M.Combust. Flame1997,110, 173.

14. Appel, J.; Bockhorn, H.; Frenklach, M.Combust. Flame2000,121, 122.

15. Lindstedt, P.; Maurice, L.; Meyer, M.Faraday Discuss.2001,119, 409.

16. Richter, H.; Mazyar, O. A.; Sumathi, R.; Green, W. H.; Howard,J. B.; Bozzelli, J. W.J. Phys.Chem. A2001,105, 1561.

17. Frenklach, M.Phys. Chem. Chem. Phys.2002,4, 2028.

18. Marsh, N. D.; Ledesma, E. B.; Sandrowitz, A. K.; Wornat, M. J.Energy Fuels2004,18, 209.

19. Ciajolo, A.; Tregrossi, A.; Mallardo, M.; Faravelli, T.; Ranzi, E.Proc. Combust. Inst.2009,32, 585.

20. (a) Becke, A. D.J. Chem. Phys.1992,96, 2155. (b) Becke, A. D.J. Chem. Phys.1992,97,9173. (c) Becke, A. D.J. Chem. Phys.1993,98,5648. (d) Lee, C.; Yang, W.; Parr, R. G.Phys. Rev.1988,B37, 785.

21. Gonzalez, C.; Schlegel, H. B.J. Chem. Phys.1989,90, 2154.

22. (a) Baboul, A. G.; Curtiss, L. A.; Redfern, P. C.; Raghavachari,K.J. Chem. Phys.1999,110, 7650. (b) Curtiss, L. A.; Raghavachari, K.;Redfern, P. C.; Baboul, A. G.; Pople, J. A.Chem.Phys.Lett.1999,314,101.

23. Curtiss, L. A.; Raghavachari, K.; Redfern, P. C.; Rassolov, V.;Pople, J. A.J. Chem. Phys.1998,109, 7764.

24. Frisch, M. J.; Trucks, G. W.; Schlegel, H. B.; Scuseria, G. E.;Robb, M. A.; Cheeseman, J. R.; Zakrzewski, V. G.; Montgomery, J. A.,Jr.; Stratmann, R. E.; Burant, J. C.; Dapprich, S.; Millam, J. M.; Daniels,R. E.; Kudin, K. N.; Strain, M. C.; Farkas, O.; Tomasi, J.; Barone, V.;Cossi, M.; Cammi, R.; Mennucci, B.; Pomelli, C.; Adamo, C.; Clifford,S.; Ochterski, J.; Petersson, G. A.; Ayala, P. Y.; Cui, Q.; Morokuma, K.Salvador, P.; Dannenberg, J. J.; Malick, D. K.; Rabuck, A. D.;Raghavachari, K.; Foresman, J. B.; Cioslowski, J.; Ortiz, J. V.; Baboul,A. G.; Stefanov, B. B.; Liu, G.; Liashenko, A.; Piskorz, P.; Komaromi,I.; Gomperts, R.; Martin, R. L.; Fox, D. J.; Keith, T.; Al-Laham, M. A.;Peng, C. Y.; Nanayakkara, A.; Challacombe, M.; Gill, P. M. W.;Johnson, B.; Chen, W.; Wong, M. W.; Andres, J. L.; Gonzalez, C.;Head-Gordon, M.; Replogle, E. S.; Pople, J. A.Gaussian 98, RevisionA.11; Gaussian: Pittsburgh, PA, USA, 2001.

25. Amos, R. D.; Bernhardsson, A.; Berning, A.; Celani, P.; Cooper,D. L.; Deegan, M. J. O.; Dobbyn, A. J.; Eckert, F.; Hampel, C.; Hetzer,G.; Knowles, P. J.; Korona, T.; Lindh, R.; Lloyd, A. W.; McNicholas, S.J.; Manby, F. R.; Meyer, W.; Mura, M. E.; Nicklaß, A.; Palmieri, P.;Pitzer, R.; Rauhut, G.; Schutz, M.; Schumann, U.; Stoll, H.; Stone, A.J.; Tarroni, R.; Thorsteinsson, T.; Werner, H.-J.MOLPRO, Version 2002.6; University of Birmingham: Birmingham, U.K., 2003.

26. Pechukas, P.; Annual Review of Physical Chemistry 32.1 (1981): 159-177.

Figure 7.1 Potential Energy Surface for 1-Acenapthyl Oxidation

$C_{12}H_7+O_2$

ts_03
-14,4

ts_add_03
-27.28g

add_03
-42.08g

ts_add_04b
16.40g

i_01
-48,6

ts_10
-75,5

ts_06a
-83,3

i_06
-88,0

ts_12
-67,1

ts_14
-56,9

+CO

ts_07
-74,5

+CO

ts_08
-86,4

i_08
-87,5

+2CO

i_03
-98,5

i_04
-105,7

+CO

i_12
-67,5

ts_09b
-103,1

i_14
-107,5

i_09
-110,7

+CO

ts_04
-99,2

ts_11
-122,5

i_11
-126,1

i_10
-132,0
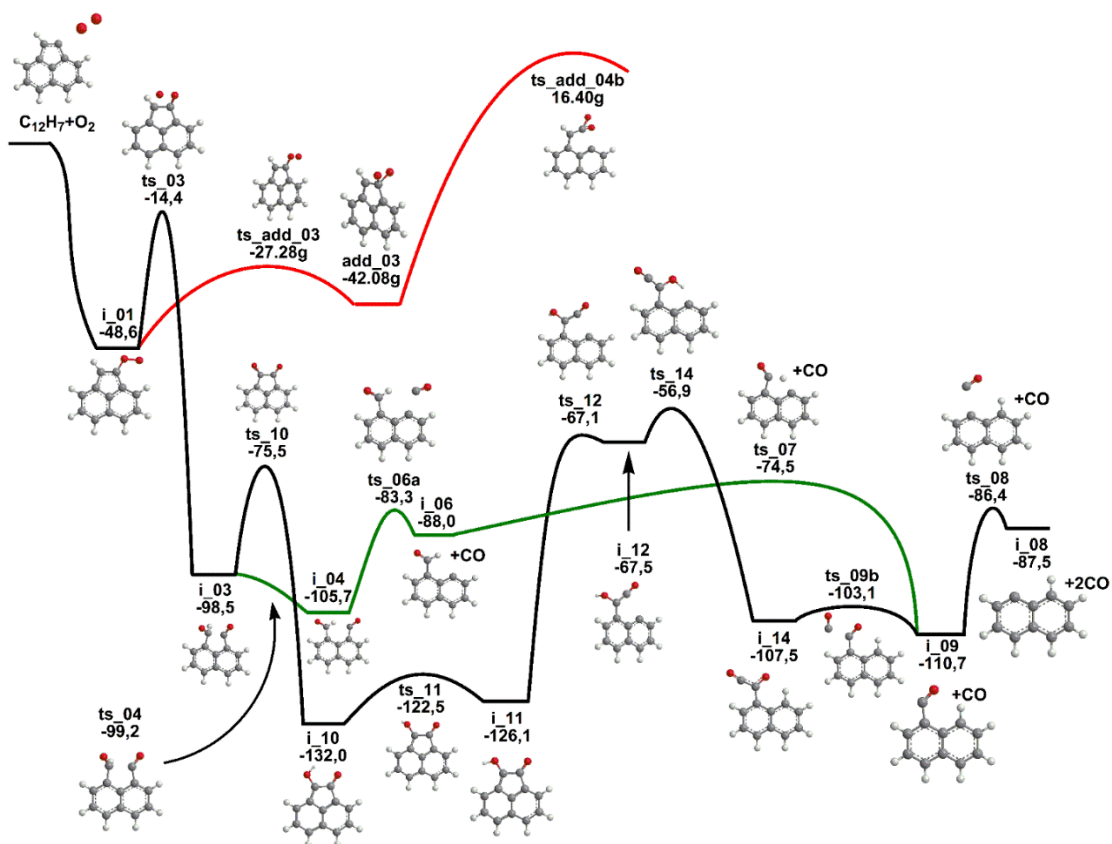
Figure 7.2 Schematic Profile of the Potential Energy Surface for 1-Acenaphthyl
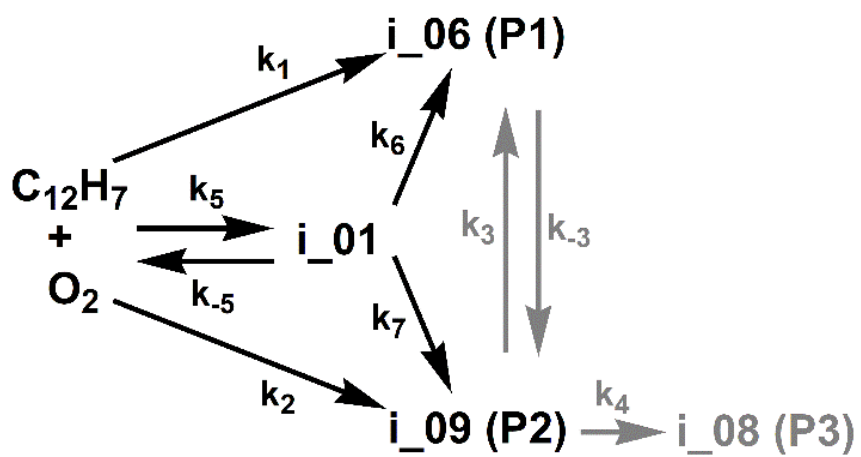
Figure 7.3 Potential Energy Surface for 2-Acenapthyl Oxidation

AZO1C5
57.6

AZ2
0.0

AZO2C2
-9.09

AZO2C4

AZO2C
44.0

AZO1O7
+CO
+O

23.0

AZO2
-43.1

AZO2O1

AZO2O3
-103.7

AZO2O2

-104.7

AZO1O7
+CO$_2$

-106.2
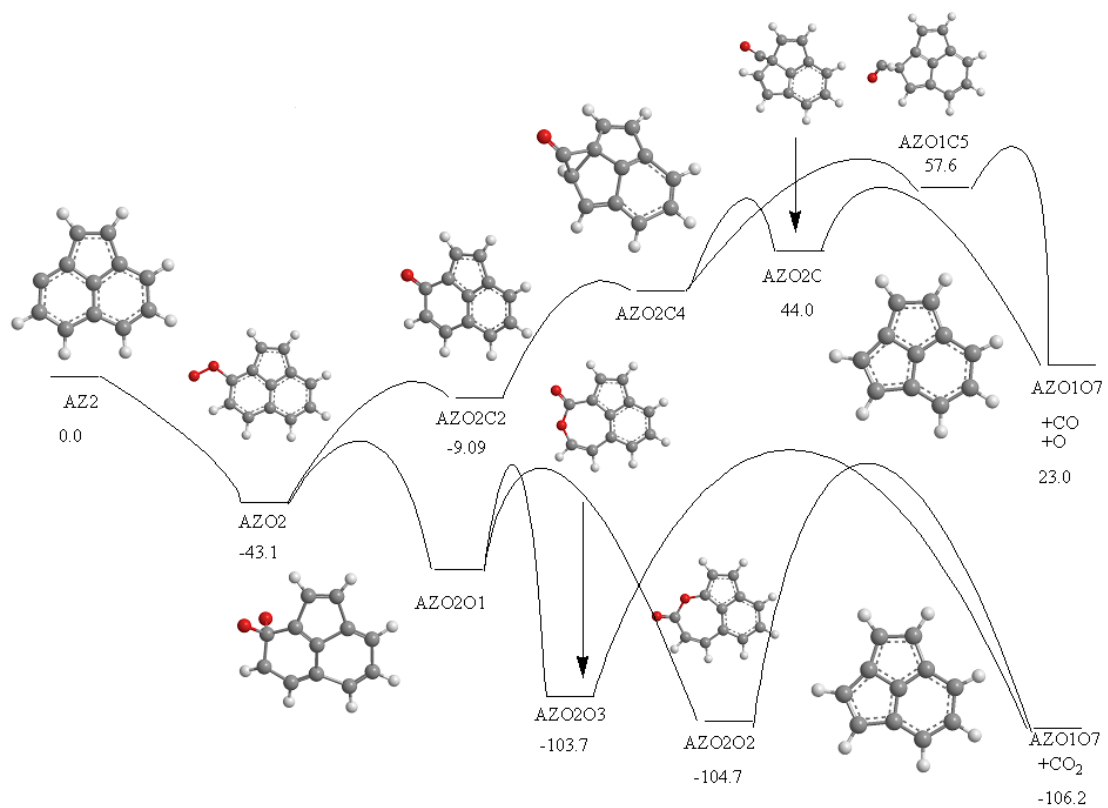
Figure 7.4 Potential Energy Surface for 3-Acenapthyl.

AZO1C4
42.3

AZO1C5
57.6

AZO1C2
-7.48

AZO1C6
35.9

23.0
+CO
+O

AZ1
0.0

AZO1
-43.0

AZO1O1

AZO1O2
-95.1

AZO1O3
-100.1

AZO1O7
-106.2

+CO$_2$
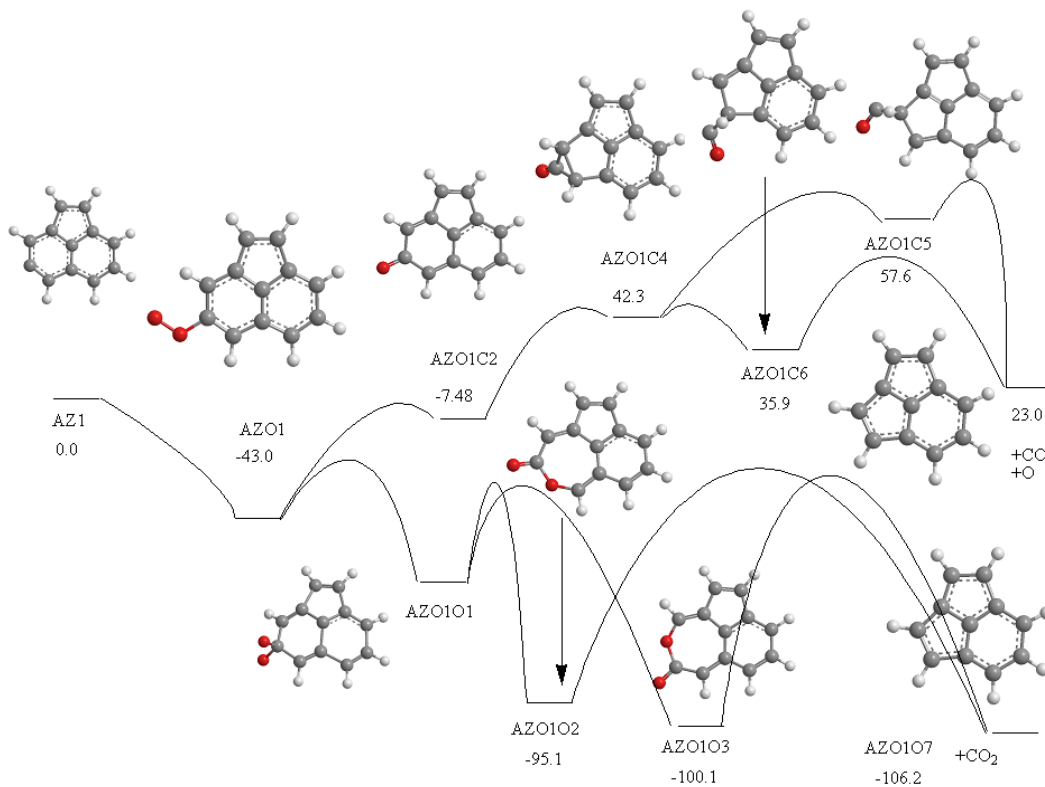
Figure 7.5 Potential Energy Surface for 4-Acenaphthyl Oxidation

AZ4
0.0

AZO4
-43.6

AZO4C2
-15.1

AZO4C4

AZO4C5
20.1

AZO1C6
35.9

AZO1C7
+CO
+O
22.3

AZO4O1

AZO4O2
-108.2

AZO4O3
-108.6

AZO1C7
+CO$_2$
106.8
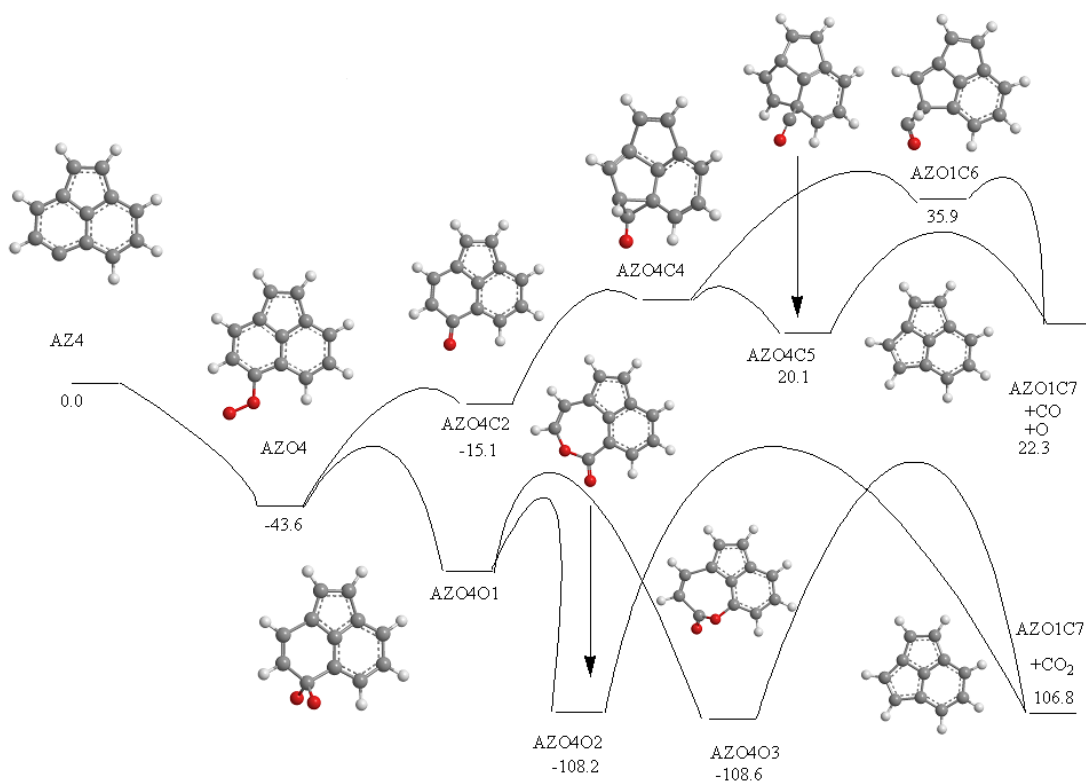
Table 7.1 Acenaphthylene Hydrogen Abstraction Branching Product Ratios

Reaction	Barrier (kcal/mol)	Rate Constant (1000 K)	Branching Product Ratio
$C_{12}H_8$ -> (1-acenaphthyl) $C_{12}H_7$ + H	113.57	1.57E-14	10.27 %
$C_{12}H_8$ -> (2-acenaphthyl) $C_{12}H_7$ + H	109.61	4.54E-14	29.82 %
$C_{12}H_8$ -> (3-acenaphthyl) $C_{12}H_7$ + H	109.48	5.16E-14	33.91 %
$C_{12}H_8$ -> (4-acenaphthyl) $C_{12}H_7$ + H	110.23	3.96E-14	25.99 %

Figure 7.6 Rate Constants for Hydrogen Abstraction of Acenapthalene

Hydrogen Abstraction of Acenapthalene

- C12H8 -> C12H7 + H (3-Acenapthyl)
- C12H8-> C12H7 + H (2-acenapthyl)
- C12H8 -> C12H7 + H (1-acenapthyl)
- C12H8 -> C12H7 + H (4-acenapthyl)

Rate constants (cm^3/ sec)

1/T(K)
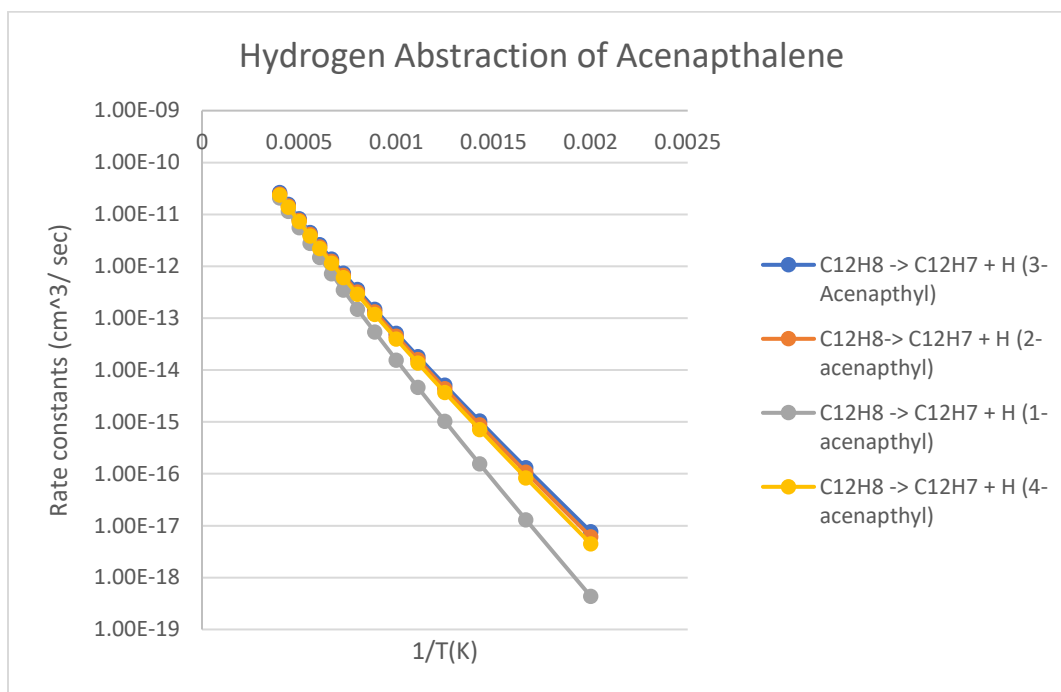
Chapter VIII

An Experimental and Theoretical Investigation of the Formation of C_7H_7 Isomers   in the

Bimolecular Reaction of Dicarbon Molecules with 1,3-Pentadiene

Introduction:

Resonantly stabilized free radicals (RSFRs) and aromatic radicals (ARs) are considered key reaction intermediates in hydrocarbon flames and in extraterrestrial environments classifying them as important reaction intermediates involved in the mass growth processes and in the formations of polycyclic aromatic hydrocarbons (PAHs).[1–4] Due to this importance, the role of various C_7H_7 radicals – benzyl ($C_6H_5CH_2$), o-, m-, p-tolyl (or 2-, 3-, and 4-tolyl) ($C_6H_4CH_3$), and cycloheptatrienyl (C_7H_7) – have been explored computationally and experimentally.[5–7] Due to the potential key role of the benzyl radical, which is both aromatic and resonance-stabilized, reaction pathways to distinct C_7H_7 isomers have been explored theoretically.[6,8,9] The reaction of methylene (CH_2) with the phenyl radical (C_6H_5), of acetylene (C_2H_2) with the cyclopentadienyl radical (c-C_5H_5)[10], of atomic hydrogen with fulvenallene (C_7H_6) and/or 1-ethynyl-cyclopentadiene (C_7H_6)[5], and of the propargyl radical (C_3H_3) with vinylacetylene (C_4H_4) have been proposed to access various points of the C_7H_7 potential energy surfaces (PESs). Alternatively, bimolecular reactions via C_7H_8 complex formation followed by hydrogen atom elimination might involve reactions of methyl (CH_3) with the phenyl radical (C_6H_5)[8] and of methylene (CH_2) with benzene (C_6H_6).[8] Similarly, acetylene (C_2H_2) was predicted to react with cyclopentadiene (C_5H_6) via photochemically [2+2] or thermally induced [4+2] cycloaddition.[11] However, the formation of C_7H_7 isomers – among them the thermodynamically most stable benzyl ($C_6H_5CH_2$) radical – via the bimolecular reaction of ubiquitous dicarbon molecules (C_2) in their electronic ground ($X^1\Sigma_g^+$) and/or first excited ($a^3\Pi_u$) states with C_5H_8 isomers such as 1-methyl1,3-butadiene (1,3-pentadiene, C_5H_8; X^1A') has never been explored. The dicarbon molecule is abundant in hydrocarbon flames and in the interstellar medium[12,13] while the 1-methyl-1,3-butadiene can be

formally derived from 1,3-butadiene (C_4H_6) by replacing the hydrogen atom at the C1 carbon atom by a methyl group. 1,3-Butadiene together with its C_4H_6 isomers 1,2-butadiene, 1-butyne, and 2-butyne is omnipresent in combustion flames such as of ethylene[14] and cyclohexane.[15] Distinct C_5H_8 isomers, including 1,3-pentadiene, have been probed in hydrocarbon flames such as of premixed methane/oxygen/cyclopentene[16] and ethylene/oxygen/argon systems.[17] The C_7H_7 species have been identified explicitly via mass spectrometric detection coupled with photoionization in premixed combustion flames of hydrogen/argon/benzene[18], hydrogen/argon/toluene[18], hydrogen/argon/cyclohexane[18], benzene/oxygen/argon[19] and toluene/oxygen/argon.[20] Photoionization efficiency curves suggest the benzyl radical to be the major C_7H_7 species. The benzyl radical is also suggested to be the major intermediate detected in the decomposition of benzylallene[21] and phenylacetic acid.[22] In combustion processes, the benzyl radicals may also form in the high temperature thermal decomposition of mono-substituted aromatics such as toluene, ethylbenzene, propylbenzene, and butylbenzene, which represent primary aromatic surrogates for gasoline, diesel, and jet fuel.[23] Since the C_7H_7 radicals can reach significant concentrations in combustion flames due to their inherent thermodynamical stability, understanding of their chemistry, in particular their formation and decomposition processes as well as bimolecular reactions, is essential for the development of accurate and predictive combustion engine models. Note that the dicarbon reactions are also relevant for carbon-rich circumstellar environments. For example, Dhanoa and Rawlings implicated dicarbon as a crucial building block in the synthesis of AR and RSFR; therefore, the reaction of dicarbon with 1-methyl-1,3-butadiene may provide a convenient pathway to synthesize C_7H_7 radicals in those environments.[24] However, the formation of these C_7H_7 radicals including the benzyl radical ($C_6H_5CH_2$) via the

bimolecular reaction of dicarbon with 1-methyl-1,3-butadiene has to be verified

experimentally and computationally. The chemical evolution of macroscopic

environments such as combustion flames and the interstellar medium can be best

understood in terms of successive bimolecular reactions.[10,25–27] This understanding must

be achieved on the molecular level exploiting experiments conducted under single

collision conditions, in which the nascent reaction products fly undisturbed toward the

detector.[28,29] Very recently, it has been shown that the benzyl radical can be synthesized

via reaction of dicarbon with 2-methyl-1,3-butadiene (isoprene).[30] Herein, we report on

the results of the crossed molecular beams reaction of dicarbon molecules with the 1-

methyl-1,3-butadiene isomer accessing various collision complexes and chemically

activated reactive intermediates on the singlet and triplet C_7H_8 surfaces, which then

decompose to products including distinct C_7H_7.

Methods:

Stationary points on the singlet and triplet C_7H_8 PES accessed by the reaction of

dicarbon, $C_2(X^1\Sigma_g^+/a^3\Pi_u)$, with 1-methyl-1,3-butadiene, including intermediates, transition

states, and possible products, were optimized at the hybrid density functional B3LYP

level of theory[34] with the 6-311G** basis set. Vibrational frequencies were computed

using the same B3LYP/6-311G** method and were used to obtain zero-point vibrational

energy (ZPE) corrections. Relative energies of various species were refined employing

the coupled cluster CCSD(T) method[35] with Dunning's correlation consistent cc-pVDZ

and cc-pVTZ basis sets.[36] Then the total energies were extrapolated to the complete

basis set (CBS) limit using the equation $E_{total}(CBS) = (E_{total}(VTZ) - E_{total}(VDZ) \times 2.5^3 / 3.5^3)/(1 - 2.5^3/3.5^3)$.[37] For selected reaction products, we additionally carried out

CCSD(T) calculations with the larger cc-pVQZ basis set and extrapolated CCSD(T)/CBS

total energies from the CCSD(T)/cc-pVDZ, CCSD(T)/cc-pVTZ, and CCSD(T)/cc-pVQZ values using the following formula, $E_{tot}(x) = E_{tot}(\infty) + Be^{-Cx}$ where x is the cardinal number of the basis set (2, 3, and 4) and $E_{tot}(\infty)$ is the CCSD(T)/CBS total energy.[38] Relative energies discussed in the paper are thus computed at the CCSD(T)/CBS//B3LYP/ 6-311G** + ZPE(B3LYP/6-311G**) level of theory with two-point (dt) and three-point (dtq) CBS extrapolations and are expected to be accurate within ±15 and ±10 kJ mol^{-1}, respectively. The B3LYP and CCSD(T) quantum chemical calculations were performed using the GAUSSIAN 09 and MOLPRO 2010 program packages. Unimolecular rate constants of reaction steps following initial addition of dicarbon to 1-methyl-1,3-butadiene were computed using Rice–Ramsperger–Kassel–Marcus (RRKM) theory[41], as functions of available internal energy of each intermediate or transition state. The internal energy was taken as a sum of the negative of relative energy of a species (the chemical activation energy) and collision energy and one energy level was considered throughout as for a zero pressure limit. For the reaction channels which do not exhibit exit barriers, such as hydrogen atom and methyl eliminations from various C_7H_8 intermediates, we applied the microcanonical variational transition state theory[42] (VTST) and computed variational transition states, so that the individual microcanonical rate constants were minimized along the reaction paths of the barrier-less single-bond cleavage processes. Sums and densities of states required to compute the rate constants were obtained within the harmonic approximation using B3LYP/6- 311G** computed frequencies. The rate constants were then utilized to calculate product branching ratios by solving first-order kinetic equations within steady-state approximation.

Results and Discussion:

The results from the electronic structure calculations propose that one or more of the cyclic (aromatic) C_7H_7 isomers are formed: benzyl, o-, m-, p-tolyl, and/or cycloheptatrienyl. The formation of solely noncyclic C_7H_7 isomers, which are energetically less stable by at least 120 kJ mol^{-1}, can be ruled out. However, we have to concede that based on the experimental data alone, we cannot discriminate which of these isomers – benzyl, o-, m-, p-tolyl, and/or cycloheptatrienyl – is formed. Therefore, we have a closer look at the electronic structure calculations for guidance. On the triplet PES (Figure 8.1), dicarbon adds to either C1 or C4 atoms of 1-methyl-1,3-butadiene forming initial complexes ti1 and ti2 without barriers. Intermediate ti1 can decompose to products tp1 and tp2, which are 104 and 63 kJ mol^{-1}exoergic relative to the initial reactants as computed at the CCSD(T)/CBS(dt) (CCSD(T)/CBS(dtq)) levels of theory. There is no exit barrier for the hydrogen loss (tp2) whereas that for the methyl loss (tp1) is 22 kJ mol^{-1}. Otherwise, ti1 can isomerize to ti3 by rotation around the C2–C3 bond, to ti5 by a four-member closure, or to ti15 by 1,3- H migration. According to our earlier calculations for the analogous $C_2(a^3\Pi_u)$ + 1,3-butadiene reaction [47], the further fate of ti5 involves an opening of the four-member ring leading to a chain C_7H_8 intermediate and effectively resulting in an insertion of the dicarbon into the $C_1–C_2$ bond of 1-methyl-1,3-butadiene; the chain intermediate can further decompose to various chain C_7H_7 isomers by hydrogen eliminations from different positions or to C_6H_5 by methyl loss. However, since rate constant calculations show that the reaction flux from ti1 to ti5 is insignificant, we do not pursue these reaction channels further. The intermediate ti2 can lose a hydrogen atom from C4 to form tp3, undergo a trans–cis conformational change to ti4 or a four-member ring closure to ti6. Similar to ti5, ti6 can further ring-open to a chain C_7H_8 structure and decompose to different acyclic products, but the reaction flux from ti2 to ti6

is negligible. According to the computed barrier heights and rate constants ti1 would

mostly dissociate to tp1 plus methyl or isomerize to ti3, whereas ti2 would nearly

exclusively rearrange to ti4. The intermediates ti3 and ti4 then can easily cyclize to the

six-member ring structure ti7. The further fate of the ti7 intermediate is threefold, as it

can undergo a 1,2-H shift from the $C(CH_3)H$ group in the ring to the neighboring carbon

atom to form ti9, a 1,2-H shift from the CH_2 group to ti8, or a 1,3-H shift from the methyl

group to give ti17. The ti9 structure preferentially loses a hydrogen atom from the CH_2

group producing m-tolyl radical with the overall reaction exoergicity of 383 kJ mol^{-1}, but

to a lesser extent may also rearrange to the triplet toluene structure ti10. ti8 may

isomerize to ti10 too, but would preferentially dissociate to phenyl plus methyl (exoergic

by 429 (427) kJ mol^{-1}) or o-tolyl plus hydrogen (exoergic by 384 kJ mol^{-1}). A hydrogen

shift from the methyl group in ti8 to the bare ring carbon atom produces ti18. The

intermediate ti17, which can formed from ti7 and also from ti16 via the less kinetically

favorable ti1 -> ti15 -> ti16 -> ti17 and ti1 -> ti3 -> ti16 -> ti17 routes, can feature 1,2-H

migration leading to ti18 or ring opening to ti19. The ti18 intermediate decomposes to the

most thermodynamically favorable product benzyl radical exoergic by 475 (478) kJ mol^{-}

^{1}by H elimination from the $C(CH_2)H$ group over an exit barrier. A small amount of ti10,

which can be formed in the reaction, can dissociate to o-, m-, and p-tolyl radicals, to

phenyl plus methyl, all via exit barriers, or to the benzyl radical without an exit barrier.

There also exists a pathway to the seven-member ring product, cycloheptatrienyl radical.

It begins from a conformational change ti4 -> ti11, then proceeds by 1,7-H migration

from the methyl group to the opposite end of the molecule to ti12, by seven-member ring

closure to ti13, by 1,2-H shift to ti14, and completes by the H elimination from the

remaining CH2 group to produce cycloheptatrienyl without an exit barrier and with

overall exoergicity of 408 (411) kJ mol^{-1}. Here, ti12 can be also formed from ti17 via ti19

by a C–C bond rotation in the latter. Table 8.1 presents product branching ratios calculated using RRKM rate constants at collision energies of 0–50 kJ mol^{-1}. Both initial intermediates ti1 and ti2 are formed without barriers and the branching of the reaction flux between the two is determined by the dynamics in the entrance channel. Therefore, the branching ratios were computed using either ti1 or ti2 as the initial species, or assuming equal probabilities of the dicarbon addition to the C1 and C4 atoms of 1-methyl-1,3-butadiene leading to ti1 and ti2, respectively. If the reaction begins from ti1, a large amount of tp1 is predicted to be produced by a direct CH$_3$ loss from the initial intermediate. The rest of significant products includes m-tolyl formed via the ti1 -> ti3 -> ti7 -> ti9 route, cycloheptatrienyl mostly via ti1 -> ti3 -> ti7 -> ti17 -> ti19 -> ti12 -> ti13 -> ti14, phenyl plus methyl by the ti1 -> ti3 -> ti7 -> ti8 mechanism, and benzyl via ti17 and ti18. Alternatively, if the reaction begins with ti2, the formation of cycloheptatrienyl is favorable due to the kinetic preference of the ti2 -> ti4 -> ti11 -> ti12 -> ti13 -> ti14 pathway, followed by benzyl, m-tolyl, and phenyl, with the paths proceeding via the same pivotal ti7 intermediate. If both ti1 and ti2 are formed with equal probabilities in the entrance channel, the reaction products are predicted to include a mixture of cyclic C$_7$H$_7$ isomers cycloheptatrienyl, m-tolyl, and benzyl (45:14:9) and the methyl loss products phenyl (8%) and the acyclic C6H5 isomer tp1 (24%). An increase in collision energy should result in a higher yield of tp1 and a slight growth of the yield of benzyl, whereas the branching ratios of cycloheptatrienyl and m-tolyl decrease by 8–10% in the considered 0–50 kJ mol^{-1}range.

On the singlet surface, dicarbon can barrierlessly add to either C1–C2 or C3–C4 bonds of 1-methyl-1,3-butadiene forming initial complexes si1 and si2 (Figure 8.2). Both si1 and si2 subsequently undergo a facile insertion of the C2 unit into the C1–C2 and C3–C4 bonds leading to the chain C$_7$H$_8$ molecules (heptatetraenes) si3 and si4. The

intermediate si3 can decompose by hydrogen and methyl eliminations without exit barriers to six different acyclic products sp1–sp6 with overall exoergicities ranging from 88 (81) to 247 (239) kJ mol^{-1} as computed at the CCSD(T)/CBS(dt) (CCSD(T)/CBS(dtq)) levels of theory with sp5 plus atomic hydrogen and sp3 plus the methyl group being most favorable of them. si4 can also give rise to six different acyclic products sp7–sp12 exoergic by 106 (99)–235 (227) kJ mol^{-1}, where sp11 is thermodynamically much more favorable than the others. On the other hand, both si3 and si4 can undergo a 1,3-H shift to form the same intermediate si5. The intermediate si5 can dissociate by cleaving the central C–C bond to the propargyl + 3-methylpropargyl products exoergic by 239 (222) kJ mol^{-1}. Starting from si5, the reaction mechanism is very similar to that studied earlier for the C2($X^1\Sigma_g^+$) plus 1,3-butadiene reaction[47], with the methyl group playing only a spectator role until the toluene molecule si15 is formed. The pathways from si5 to si15 include the trans– cis conformational change si5 -> si6, followed by 1,5-H migrations (si6 -> si7 or si6 -> si8), rotations around single C–C bonds (si7 -> si9 or si8 -> si10), six-member ring closures (si9 -> si11 or si10 -> si12), and two consecutive 1,2-H shifts (si11 -> si13 -> si15 For si12 -> si14 ->si15). Note that once si7 or si8 are produced, the subsequent barriers on the reaction pathways are rather low (and much lower than those in the reverse direction to si6) which indicates the reactions forming these intermediates are irreversible and they ultimately lead the reaction flux to si15. Also, the si13 and si14 intermediates are found to be unstable or metastable; the transition states for their isomerization to si15 can be found at the B3LYP level but their energies refined at the CCSD(T)/CBS level are either very close or even lower than those of the intermediates indicating that the rearrangement of si13 or si14 to si15 would be nearly spontaneous. Finally, the toluene intermediates can decompose without exit barriers to benzyl exoergic by 466 (467) kJ mol^{-1}, o-, m-, or p-tolyl radicals exoergic by 373–375 kJ mol^{-1},

and phenyl plus methyl exoergic by 420 (415) kJ mol^{-1}. Table 2 shows product branching ratios on the singlet surface, which were computed with several simplifying assumptions in order to avoid a large number of time-consuming variational RRKM calculations required for single-bond cleavage channels occurring without exit barriers. For si3 and si4 we considered only the most favorable channels leading to sp3, sp5, and sp11, while the other hydrogen and methyl loss channels were neglected. This means that the other products among sp1–sp12 can be also formed in principle, but based on the unfavorable energetics and the fact that all reaction steps leading to them exhibit no exit barriers and thus proceed via loose variational transition states, we assume that their relative yields should be insignificant as compared to those of sp3, sp5, and sp11. The second assumption that dissociation of toluene si15 would predominantly produce the benzyl radical rather than tolyl radicals or phenyl plus methyl is also justified by the much more favorable energy of benzyl and a loose character of all corresponding variational transition states. With these assumptions, we can now analyze the results in Table 7.2. If the reaction starts from si1, the major products are predicted to be sp5 and sp3, which are formed by the H and CH$_3$ loss from si3. However, if the reaction begins from si2, the dominant products would be sp11 and the yield of the benzyl radical would be also significant. If si1 and si2 are formed in the entrance channel with equal probabilities, the reaction would produce three major products, sp11 (45%), sp5 (30%), and sp3 (19%), and two minor products, benzyl (5%) and CH$_3$CHCCH + C$_3$H$_3$ (under 2%). The dependence of the calculated branching ration on the collision energy is weak. Clearly, the singlet reaction alone cannot explain the observations as it mostly produces acyclic C$_7$H$_7$ isomers exoergic by 230–240 kJ mol1 and only 5% of benzyl exoergic by 467 kJ mol^{-1}, which cannot account for the long tail in the translational energy distribution beyond 283 kJ mol^{-1}. The triplet reaction is computed to form a mixture of

cycloheptatrienyl, m-tolyl, and benzyl radicals exoergic by 411 ± 10, 383 ± 15, and 478 ± 10 kJ mol^{-1}, respectively, which is generally consistent with the experimentally determined reaction exoergicity of 412 ± 52 kJ mol^{-1}. Moreover, the calculations predict cycloheptatrienyl to be the major C_7H_7 product on the triplet PES and its exoergicity shows the best match with the experimental value. [6]

Experimental data were combined with ab initio and statistical calculations to reveal the underlying reaction mechanism and chemical dynamics. On both the singlet and triplet surfaces, the reactions involve indirect scattering dynamics and are initiated by the barrier-less addition of dicarbon to the carbon–carbon double bond of the 1,3-pentadiene molecule. These initial addition complexes rearrange via multiple isomerization steps leading eventually through atomic hydrogen elimination to the formation of distinct C_7H_7 radical species. The experimentally derived reaction exoergicity of 412 ± 52 kJ mol^{-1} is consistent with the formation of several cyclic C_7H_7 isomers, including o-, m-, and p-tolyl radicals, cycloheptatrienyl, and benzyl, but the calculations predict cycloheptatrienyl, m-tolyl, and benzyl to be the major products on the triplet surface with the branching ratios of 45:14:9. On the singlet surface, mostly acyclic C_7H_7 isomers, such as $CH_2CHCHCHCCCH_2$ (sp11) and $CH_2CHCHCCCHCH_2$ (sp5), are anticipated to be formed with much lower reaction exoergicities of 230–240 kJ mol^{-1}. The calculations predict a significant yield of C_6H_5 products via CH3 elimination both in the triplet (acyclic CCCHCHCHCH$_2$ (tp1) and phenyl radicals) and singlet (acyclic $CH_2CHCHCCCH$ (sp3)) reactions, but these products could not be identified in the experiment due to the interference with the products of the C(3 P) + 1,3-pentadiene reaction, as the atomic carbon is also present in the beam.

References:

1. M. Frenklach, Phys. Chem. Chem. Phys. 4 (2002) 2028.

2. J.A. Miller, S.J. Klippenstein, Y. Georgievskii, L.B. Harding, W.D. Allen, A.C. Simmonett, *The Journal of Physical Chemistry* A 114 (2010) 4881.

3. J.A. Miller, M.J. Pilling, E.P. Troe, Combust. Inst. 30 (2005) 43.

4. J.A. Miller, C.F. Melius, Combust. Flame 91 (1992) 21.

5. G. da Silva, J.A. Cole, J.W. Bozzelli, *The Journal of Physical Chemistry* A 114 (2010) 2275.

6. M. Derudi, D. Polino, C. Cavallotti, Phys. Chem. Chem. Phys. 13 (2011) 21308.

7. T.C. Zhang et al., Combust. Flame 156 (2009) 2071.

8. S.J. Klippenstein, L.B. Harding, Y.P. Georgievskii, Combust. Inst. 31 (2007) 221.

9. V.V. Kislov, A.M. Mebel, *The Journal of Physical Chemistry* A 111 (2007) 3922.

10. S. Fascella, C. Cavallotti, R. Rota, S. Carra, *The Journal of Physical Chemistry* A 109 (2005) 7546.

11. R.D.J. Froese, J.M. Coxon, S.C. West, K. Morokuma, J. Org. Chem. 62 (1997) 6991.

12. G.P. Smith, C. Park, J. Schneiderman, J. Luque, Combust. Flame 141 (2005) 66.

13. H.A. Gueniche, P.A. Glaude, R. Fournet, F. Battin-Leclerc, Combust. Flame 151 (2007) 245.

14. Q. Zhang, Y.Y. Li, Z.Y. Tian, T.C. Zhang, J. Wang, F.Chinese. Qi, J. Chem. Phys. 19 (2006) 379.

15. W.J. Li, M.E. Law, P.R. Westmoreland, T. Kasper, N. Hansen, K. KohseHoinghaus, Combust. Flame 158 (2011) 2077.

16. H.A. Gueniche, P.A. Glaude, R. Fournet, F. Battin-Leclerc, Combust. Flame 152 (2008) 245.

17. C. Renard, P.J. Van Tiggelen, J.P. Vandooren, Combust. Inst. 29 (2002) 1277.

18. T. Mcallister, J.D. Scott, Int. J. Mass Spectrom. 33 (1980) 63.

19. B. Yang et al., P. Combust. Inst. 31 (2007) 555.

20. V. Detilleux, J. Vandooren, *The Journal of Physical Chemistry* A 113 (2009) 10913.

21. J.A. Sebree, N.M. Kidwell, T.M. Selby, B.K. Amberger, R.J. McMahon, T.S. Zwier, J. Am. Chem. Soc. 134 (2012) 1153.

22. F.L. Cozens, W. Ortiz, N.P. Schepp, J. Am. Chem. Soc. 120 (1998) 13543.

23. R. Sivaramakrishnan, M.C. Su, J.V.P. Michael, Combust. Inst. 33 (2011) 243.

24. H. Dhanoa, J.M.C. Rawlings, Mon. Not. R. Astron. Soc. 440 (2014) 1786.

25. J.A. Mulholland, M. Lu, D.H.P. Kim, Combust. Inst. 28 (2000) 2593.

26. N.W. Moriarty, M.P. Frenklach, Combust. Inst. 28 (2000) 2563.

27. H. Sabbah, L. Biennier, S.J. Klippenstein, I.R. Sims, B.R. Rowe, *The Journal of Physical Chemistry* Lett. 1 (2010) 2962.

28. R.I. Kaiser et al., Faraday Discuss. 147 (2010) 429.

29. P. Casavecchia, N. Balucani, G.G. Volpi, Annu. Rev. Phys. Chem. 50 (1999) 347.

30. B.B. Dangi, D.S.N. Parker, T. Yang, R.I. Kaiser, A.M. Mebel, Angew. Chem., Int. Ed. 53 (2014) 4608.

31. Y. Guo, X. Gu, E. Kawamura, R.I. Kaiser, Rev. Sci. Instrum. (2006) 77. 034701/1- 034701/9.

32. N.R. Daly, Rev. Sci. Instrum. 31 (1960) 264.

33. Weiss, P. S. University Of California, Berkeley, 1986.

34. C.T. Lee, W.T. Yang, R.G. Parr, Phys. Rev. B 37 (1988) 785.

35. G.D. Purvis III, R.J. Bartlett, J. Chem. Phys. 76 (1982) 1910.

36. T.H. Dunning Jr., J. Chem. Phys. 90 (1989) 1007.

37. S.B. Huh, J.S. Lee, J. Chem. Phys. 118 (2003) 3035.

38. K.A. Peterson, T.H. Dunning, *The Journal of Physical Chemistry* 99 (1995) 3898.

39. Frisch, M. J. et al.: GAUSSIAN 09, Revision A.1. Gaussian Inc: Wallingford CT, 2009.

40. Werner, H.-J.; Knowles, P. J.; Kinizia, G.; Manby, F. R.; Schutz, M.; Celani, P.; Korona, T.; Lindh, R.: MOLPRO, version 2010.1, a package of ab initio programs. 2010.

41. P.J. Robinson, K.A. Holbrook, Unimolecular Reactions (1972).

42. D.G. Truhlar, B.C. Garrett, Acc. Chem. Res. 13 (1980) 440.

43. X.B. Gu, Y. Guo, A.M. Mebel, R.I. Kaiser, Chem. Phys. Lett. 449 (2007) 44.

44. Y.T. Lee, Science 236 (1987) 793.

45. R.D. Levine, Molecular Reaction Dynamics, Cambridge University Press, Cambridge, UK, 2005.

46. R.I. Kaiser, C. Ochsenfeld, M. HeadGordon, Y.T. Lee, A.G. Suits, Science 274 (1996) 1508.

47. F.T. Zhang, B. Jones, P. Maksyutenko, R.I. Kaiser, C. Chin, V.V. Kislov, A.M. Mebel, J. Am. Chem. Soc. 132 (2010) 2672.

Figure 8.1 Potential Energy Surface for the Reaction of Triplet Dicarbon with 1,3-Pentadiene Calculated at the CCSD(T)/CBS(dt)/B3LYP/6-311G** + ZPE(B3LYP/^-311G**) and CCSD(T)/CBS(dtq)/B3LYP/6-311G** + ZPE(B3LYP/6-311G**) Levels of Theory. Energies in kJ mol⁻¹
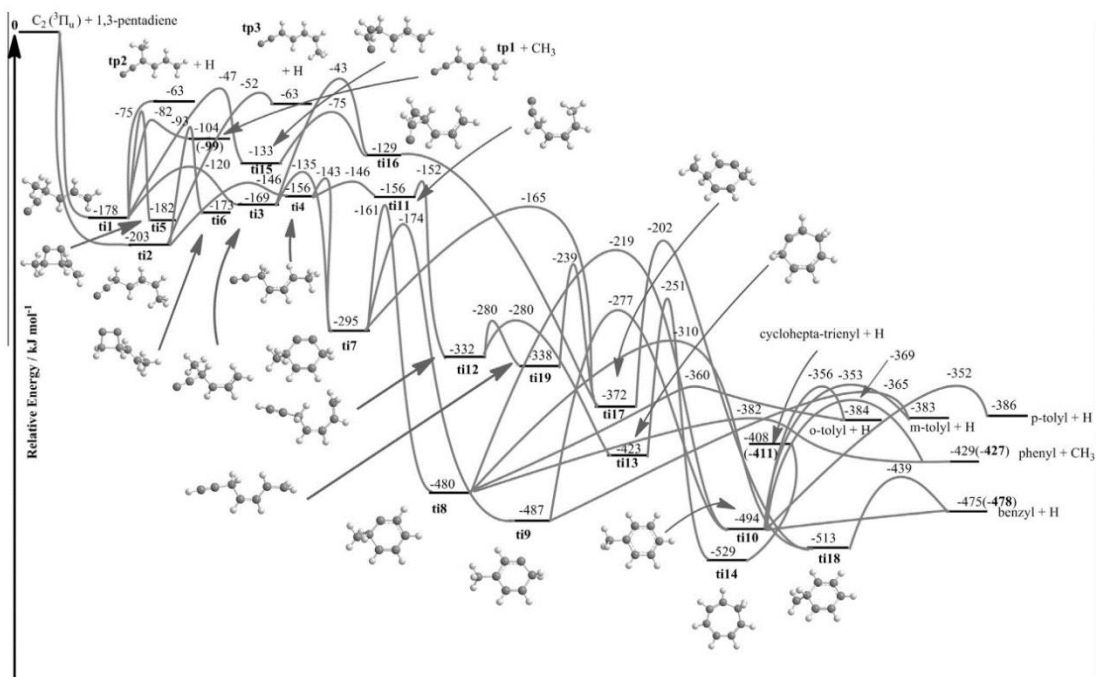
Figure 8.2 Potential Energy Surface for the Reaction of Singlet Dicarbon with 1,3-Pentadiene Calculated at the CCSD(T)/CBS(dt)/B3LYP/6-311G** + ZPE(B3LYP/^-311G**) and CCSD(T)/CBS(dtq)/B3LYP/6-311G** + ZPE(B3LYP/6-311G**) Levels of Theory. Energies in kJ mol^{-1}
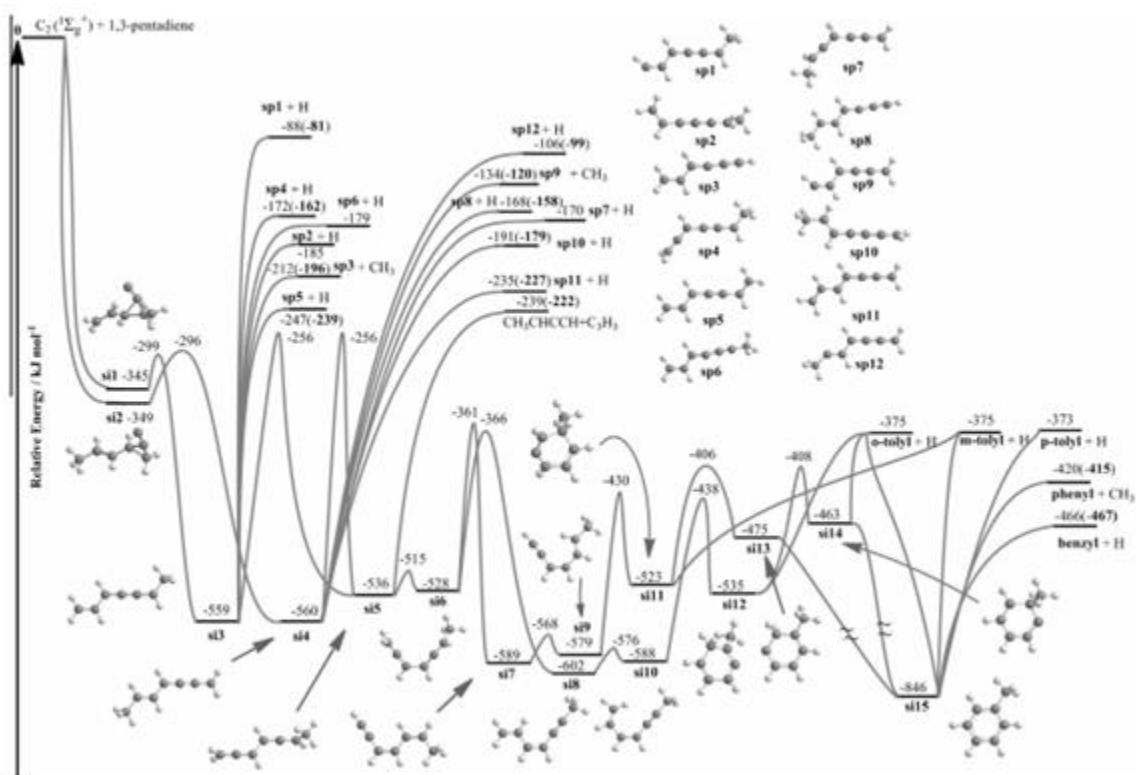
Table 8.1 Branching Ratios on the Triplet Surface

E_{col}, kJ mol^{-1}

Products	0 from ti1	from ti2	av	10 from ti1	from ti2	av	25 from ti1	from ti2	av	43 from ti1	from ti2	av	50 from ti1	from ti2	av
tp1 + CH$_3$	16.28	0.07	8.17	22.73	0.11	11.42	33.90	0.19	17.04	47.09	0.31	23.70	51.72	0.37	26.04
ti5	0.10	0.00	0.05	0.13	0.00	0.07	0.18	0.00	0.09	0.24	0.00	0.12	0.26	0.00	0.13
ti6	0.01	0.07	0.04	0.01	0.09	0.05	0.01	0.13	0.07	0.02	0.19	0.10	0.02	0.21	0.11
tp3	0.00	0.00	0.00	0.00	0.01	0.00	0.00	0.02	0.01	0.00	0.04	0.02	0.01	0.06	0.03
o-tolyl	1.57	0.47	1.02	1.49	0.49	0.99	1.33	0.50	0.92	1.11	0.52	0.81	1.03	0.52	0.77
m-tolyl	33.08	9.97	21.52	29.67	9.65	19.66	24.32	9.15	16.73	18.48	8.61	13.54	16.51	8.38	12.45
cyclohepta-trienyl	27.91	74.38	51.14	26.08	73.81	49.94	22.60	72.66	47.63	18.37	71.26	44.82	16.86	70.72	43.79
benzyl	4.07	9.92	6.99	4.13	10.72	7.42	4.14	12.26	8.20	3.91	14.04	8.97	3.79	14.75	9.27
phenyl + CH$_3$	16.99	5.12	11.05	15.76	5.13	10.44	13.52	5.09	9.31	10.78	5.03	7.91	9.80	4.98	7.39

Table 8.2 Branching Ratios on the Singlet Surface

E_{col}, kJ mol^{-1}	0			10			25			43			50		
Products	from si1	from si2	av	from si1	from si2	av	from si1	from si2	av	from si1	from si2	av	from si1	from si2	av
benzyl	1.91	9.51	5.71	1.85	9.09	5.47	1.75	8.49	5.12	1.64	7.80	4.72	1.60	7.54	4.57
sp5	62.26	0.01	31.13	61.69	0.01	30.85	60.89	0.01	30.45	59.86	0.02	29.94	59.37	0.02	29.69
sp3 + CH$_3$	35.49	0.01	17.75	36.09	0.01	18.05	36.92	0.01	18.46	37.98	0.01	18.99	38.48	0.01	19.24
sp11	0.00	88.80	44.40	0.00	89.03	44.52	0.00	89.35	44.68	0.01	89.69	44.85	0.01	89.82	44.91
CH$_3$CHCCH + C$_3$H$_3$	0.34	1.67	1.00	0.38	1.86	1.12	0.44	2.14	1.29	0.52	2.48	1.50	0.55	2.61	1.58

Chapter IX

A Free-Radical Pathway to Hydrogenated Phenanthrene in Molecular Clouds—Low Temperature Growth of Polycyclic Aromatic Hydrocarbons

Introduction:

The hydrogen-abstraction/acetylene-addition (HACA) mechanism[1] has been
instrumental for rationalizing the synthesis of polycyclic aromatic hydrocarbons (PAHs)—
organic molecules carrying fused benzene rings—in high temperature combustion
systems[2–3] and in circum stellar envelopes of carbon rich asymptotic giant branch (AGB)
stars.[3–4] The ubiquity of PAHs along with their (de)hydrogenated, ionized, and side-
chain-substituted counterparts in the interstellar medium (ISM)[5–6] is surmised from the
unidentified infrared (UIR) emission bands(3 to 20 mm)[7–8] and the UV-bump[9–11]—an
absorption feature super imposed on the interstellar extinction curve near 217.5 nm—
that correlate with laboratory spectra of aromatic hydrocarbons. Although individual
PAHs have not been detected in the ISM yet, the explicit identification of PAHs like
phenanthrene and anthracene ($C_{14}H_{10}$) in carbonaceous chondrites like Murchison and
Orgueil bearing anomalous[13]C/^{12}C and D/H isotopic ratios[12–15] strongly suggests an
interstellar origin with fashionable astrochemical reaction networks mainly loaned from
the combustion chemistry community. Here, under fuel rich conditions, acetylene (C_2H_2)
has been proposed to react with aromatic hydrocarbons undergoing ring formation and
expansion through a series of bimolecular reactions assembled in the HACA
mechanism. Kinetic modeling [16–19] along with electronic structure calculations [20–24]
suggest recurring progressions of hydrogen atom abstractions from the aromatic
hydrocarbon followed by sequential addition of two acetylene molecules to the radical
sites prior to cyclization and aromatization. Recent studies exploiting tunable vacuum
ultraviolet (VUV) light exposed that the naphthalene molecule ($C_{10}H_8$) can be formed via
the reaction of the phenyl radical (C_6H_5C)with two acetylene molecules (C_2H_2)[25] through
key transients in the HACA framework—styrenyl (C_8H_7C)and ortho-vinylphenyl
(C_8H_7C).[26] HACA-type reactions involving naphthyl ($C_{10}H_7$) and of biphenylyl radicals

($C_6H_5C_6H_4$) with acetylene also produced the three-membered ring PAHs

acenaphthylene ($C_{12}H_8$)[27] and phenanthrene ($C_{14}H_{10}$),[28] respectively, under combustion-

relevant conditions. High temperatures along with acetylene enrichment near the

photospheres of carbon-rich AGB stars underscore HACA's applicability to describing

soot production in these outflows. Aromatic species [benzene (C_6H_6) or phenyl (C_6H_5)]

likely form within the envelope and undergo processing into polycyclic compounds via

HACA[4] before exiting to the ISM as "free" PAHs, or condensed as carbonaceous grains

or fullerenes.[4, 29–30] Carbonaceous grains comprising aromatic interiors[31] could contribute

to the interstellar PAH budget through shattering facilitated by turbulence or supernova-

induced shockwaves that release aromatic content to the ISM.[32–33] However, in recent

years, astronomical models combined with observations revealed that the destruction of

interstellar PAHs and carbonaceous grains by, for example, high velocity shockwaves,

limit their lifetime to a few 10^8 years.[34–35] This time span is much shorter than the PAH

injection time from stellar sources, including C-rich AGB stars such as CW Leo (IRC +

10216), of some 10^9 years, and thus the ubiquitous distribution of PAH-like species in

the interstellar medium coupled with the less-than-expected production of PAHs in

circumstellar envelopes suggests that crucial routes for the fast chemical growth of

PAHs are missing. These routes may involve low temperature interstellar environments

such as cold molecular clouds that hold temperatures down to 10 K.

Methods:

Geometries of the reactants, products and various intermediates and transition states on

the $C_{14}H_{13}$ potential energy surface were optimized at the hybrid density functional

B3LYP level of theory[4-5] with the 6-311G** basis set. The same B3LYP/6-311G**

method was employed to calculate vibrational frequencies, which were then used to

compute zero-point energy (ZPE) corrections, to characterize the stationary points as minima or first-order saddle points, and to evaluate rate constants for unimolecular reaction steps. Single-point energies were refined using the G3(MP2,CC)//B3LYP modification[6-7] of the original Gaussian 3 (G3) scheme,[8] which provides accuracy for relative energies within 10 kJ mol^{-1}. The ab initio and DFT calculations were carried out using the GAUSSIAN 09 and MOLPRO 2010 program packages. Relative reaction product yields under single-collision conditions were computed using Rice−Ramsperger−Kassel−Marcus (RRKM) theory.[11-13] The rate constants were calculated as functions of available internal energy, where the internal energy was taken as a sum of the energy of chemical activation in the reaction of 1-naphthyl with 1,3-butadiene and the collision energy, assuming that a dominant fraction of the latter is converted to internal vibrational energy. Only a single total-energy level was considered throughout, as for single-collision conditions (zero pressure limit).[14] The harmonic approximation was employed to compute numbers and densities of state required for evaluating the rate constants. Using the calculated rate constants, product branching ratios were computed by solving first-order kinetic equations within the steady-state approximation for unimolecular isomerization and fragmentation steps of initial reaction intermediates formed as a result of the addition of 1-naphthyl to 1,3-butadiene.

Results and Discussion:

The computational data together with the experimental results in crossed molecular beams allowed us to untangle the underlying reaction mechanism(s) and to evaluate to what extent reaction of 1-naphthyl with 1,3-butadiene can lead to the formation of a tricyclic PAH (Figure 8.1). The computations at the G3(MP2,CC)//B3LYP/6-311G** level of theory reveal five exit channels leading to distinct $C_{14}H_{12}$ isomers, p1 to p5, with overall

exoergicities ranging from 16 to 106 kJ mol^{-1}. A comparison of these data with the experimental reaction energy of -104$\pm$25 kJ mol^{-1} reveals that the formation of the thermodynamically most favorable isomer p3 (1,4-dihydrophenanthrene) can account for the experimentally derived reaction energy; based on the energetics alone, we cannot eliminate contributions of the thermodynamically less favorable isomers. The electronic structure calculations exposed a barrier less pathway to 1,4-di-hydrophenanthrene initiated by the formation of a van-der-Waals complex i0 from the separated reactants. This complex is weakly bound by 8 kJmol^{-1}and isomerizes via a barrier of only 3 kJmol^{-1} through addition of the radical center of the 1-naphthyl radical to the C1-carbon of 1,3-butadiene forming a resonantly stabilized intermediate i1.After a facile cis-trans isomerization from i1 to i2,cyclization leads to intermediate i3 ,which is boundby193 kJ mol^{-1} with respect to 1-naphthyl plus 1,3-butadiene. A hydrogen elimination from the bridging carbon atom leads to aromatization and formation of p3 (1,4-dihydrophenanthrene) through a tight exit transition state that lies 25 kJ mol^{-1} above the separated products. This order of magnitude is in line with the experimental observation of an exit barrier close to 14$\pm$4 kJmol^{-1} with the hydrogen atom eliminated almost perpendicularly to the plane of the decomposing complex. It is important to recall that in the reaction of 1-naphthyl with 1,3-butadiene-d6, only the hydrogen atom loss was observed. In conclusion, our study reveals the first low temperature pathway accounting for the barrier less formation of a tricyclic (polycyclic) aromatic hydrocarbon—1,4-dihydrophenanthrene($C_{14}H_{12}$)—via the elementary bimolecular gas phase reaction of the 1-naphthyl radical($C_{10}H_7$) with 1,3-butadiene (C_4H_6). The reaction proceeds by a de-facto barrier less addition of the naphthyl radical with its radical center to the H_2C moiety of the 1,3-butadiene reactant—facilitated by a weakly bound van der Waals complex—followed by isomerization and atomic hydrogen loss accompanied by aromatization to form 1,4-

dihydrophenanthrene. Statistical (RRKM) calculations confirm that the pathway leading to1,4-dihydrophenanthrene plus atomic hydrogen accounts for 100 % of all products in the limit of zero collision energy as closely present in cold molecular clouds such as TMC-1. This combination of experimental, ab initio, and statistical methodologies reveals a novel reaction mechanism of aryl-type radical additions to conjugated hydrocarbon systems like 1,3-butadiene and vinylacetylene (C_4H_4), and changes how we think about molecular growth processes to PAHs in the cold regions of space.

References:

1. M. Frenklach, D. W. Clary, W. C. Gardiner, S. E. Stein, Int. Symp. Combust.[Proc.] 1985, 20,887 –901.

2. M. Frenklach, Phys. Chem.Chem. Phys. 2002, 4,2028 –2037.

3. M. Frenklach, E. D. Feigelson , Astrophys. J. 1989, 341,372 –384.

4. I. Cherchneff, Astron.Astrophys. 2012, 545,A12.

5. L. d'Hendecourt, P. Ehrenfreund, Adv. Space Res. 1997, 19,1023 –1032.

6. Y. M. Rhee, T. J. Lee, M. S. Gudipati, L. J. Allamandola, M. Head-Gordon,Proc. Natl. Acad. Sci. USA 2007, 104,5274 –5278.

7. L. Allamandola, A. Tielens, J. Barker, Astrophys. J. Suppl. Ser. 1989, 71,733 –775.

8. M. R. Allen, E. D. Gary, A. D. Michael, Astrophys. J. 2009, 702,301 –306.

9. W. W. Duley, Astrophys. J. 2006, 639,L59.

10. M. Steglich, C. J-ger,G.Rouill8,F.Huisken, H. Mutsch ke, H. Th, Astro-phys. J. 2010, 712,6.

11. M. Steglich, J. Bouwman, F. Huisken, H. Th, Astrophys. J. 2011, 742,12.

12. Y. Huang, J. C. Aponte, J. Zhao, R. Tarozo, C. Hallmann, Earth Planet. Sci. Lett. 2015, 426,101 –108.

13. H. Naraoka, A. Shimoyama, K. Harada, Earth Planet. Sci. Lett. 2000, 184,1–7.

14. S. Messenge r, S. Amari, X. Gao, R. M. Walker,S.J.Clemett, X. D. F. Chillier,R. N. Zare, R. S. Lewis, Astrophys. J. 1998, 502,284 –295.

15. S. J. Clemett, C. R. Maechling, R. N. Zare, P. D. Swan, R. M. Walker, Science1993, 262,721 –725.

16. M. Frenklach, H. Wang, Int. Symp. Combust. [Proc.] 1991, 23,1559 –1566.

17. J. D. Bittner, J. B.Howard, Int. Symp. Combust. [Proc.] 1981, 18,1105 –1116.

18. H. Wang, M. Frenklach, *The Journal of Physical Chemistry* 1994, 98,11465 – 11489.

19. H. Wang, M. Frenklach, Combust.Flame 1997, 110,173 –221.

20. V. V. Kislov,N.I.Islamova,A.M.Kolker,S.H.Lin, A. M. Mebel, J. Chem.Theory Comput . 2005, 1,908 –924.

21. H. Richter, J. B. Howard, Prog.Energy Combust. Sci. 2000, 26, 565 –608.

22. N. D. Marsh, M. J. Wornat, Proc. Combust. Inst. 2000, 28, 2585 –2592.

23. I. V. Tokmakov,M.C.Lin, J. Am. Chem. Soc. 2003, 125, 11397–11408.

24. V. V. Kislov,A.I.Sadovnikov,A.M.Mebel, *The Journal of Physical Chemistry* A 2013, 117, 4794 –4816.

25. D. S. N. Parker,R.I.Kaiser,T.P.Troy,M.Ahmed, Angew.Chem. Int. Ed.2014, 53, 7740 –7744; Angew.Chem. 2014, 126, 7874 –7878.

26. T. Yang, T. P. Troy,B.Xu, O. Kostko, M. Ahmed, A. M. Mebel, R. I. Kaiser,Angew.Chem. Int. Ed. 2016, 55,14983 –14987; Angew.Chem. 2016, 128, 15207 –15211.

27. D. S. N. Parker, R. I. Kaiser,B.Bandyopadhyay,O.Kostko, T. P. Troy, M .Ahmed, Angew.Chem. Int. Ed. 2015, 54, 5421 –5424; Angew.Chem.2015, 127, 5511– 5514.

28. T. Yang, R. I. Kaiser,T.P.Troy,B.Xu, O. Kos ko, M. Ahmed, A. M. Mebel, M. V. Zagidullin, V. N. Azyazov, Angew.Chem. Int. Ed. 2017, 56,4515 –4519; Angew.Chem. 2017, 129,4586 –4590.

29. C. J-ger,F.Huisken, H. Mutschke, I. L. Jansa,H.Th, Astrophys. J. 200 9,696,706.

30. O. Bern,A.G.G.M.Tielens, Proc. Natl. Acad. Sci. USA 2012, 109,401 –406.

31. J. E. Chiar,A.G.G.M.Tielens, A. J. Adamson, A. Ricca, Astrophys. J. 2013,770,78.

32. H. Hirashita, Mon. Not. R. Astron. Soc. 2010, 407,L49 –L53.

33. J. Y. Seok, H. Hirashita, R. S. Asano, Mon. Not. R. Astron. Soc. 2014, 439,2186 –2196.

34. E. R. Micelotta, A. P. Jones, A. G. G. M. Tielens, Astron. Astrophys. 2010, 510, A36.

35. A. P. Jones, J. A. Nuth, Astron. Astrophys. 2011, 530, A44.

36. R. I. Kaiser, P. Maksyutenko, C. Ennis, F. Zhang, X. Gu, S. P. Krishtal, A. M. Mebel, O. Kostko, M. Ahmed, Faraday Discuss. 2010, 147, 429 –478.

37. B. M. Jones, F. Zhang, R. I. Kaiser,A.Jamal, A. M. Mebel, M. A. Cordiner,S. B. Charnley, Proc. Natl. Acad. Sci. USA 2011, 108,452 –457.

38. P. S. Weiss, Ph.D. Dissertation thesis, University of California (Berkeley,CA), 1986.

39. M. F. Vernon, Ph.D. Dissertation thesis, University of California (Berkeley,CA), 1983.

40. R. I. Kaiser, A. M. Mebel, Int. Rev.Phys. Chem. 2002 , 21,307 –356.

41. R. I. Kaiser, D. S. N. Parker, F. Zhang, A. Landera, V. V. Kislov, A. M. Mebel, *The Journal of Physical Chemistry* A 2012, 116, 4248 –4258.

42. D. S. N. Parker, F. Zhang, Y. S. Kim, R. I. Kaiser, A. Landera, V. V. Kislov, A. M. Mebel, A. G. G. M. Tielens, Proc. Natl.Acad. Sci. USA 2012, 109, 53–58.

43. A. M. Mebel, A. Landera, R. I. Kaiser, *The Journal of Physical Chemistry* A 2017, 121, 901 –926.

Figure 9.1 Potential Energy Surface for 1-Naphthyl Plus 1,3-Butadiene

Chapter X

Conclusions

The pyrolysis mechanism for various chemical species as well theoretical rate coefficients were calculated and compared to experimental data. It is known that the predominant reaction product in pyrolysis of alkanes is ethylene and our calculations allowed us to rationalize this observation. The dominating temperature-dependent decomposition pathways for *n*-decane are as follows. Initially *n*-decane decomposes via carbon-carbon bond cleavage, excluding the terminal carbon bonds, to form a mixture of primary alkyl radicals ranging from ethyl to octyl. Under these combustion conditions these alkyl radicals rapidly dissociate through beta scissions or by 1,4-, 1,5-, 1,6- or 1,7-H shifts followed by beta scissions. If beta scission is the first reaction to occur an ethylene molecule is formed along with a primary alkyl two carbon units shorter. Through the second process of a H shift followed by a beta scission molecules of carbon length ranging from propene to 1-heptene and smaller primary alkyl radicals are formed. This explains the experimental presence of species that previously models could not explain. A complete inventory of radicals formed in the initial stage of decomposition was compiled here for the first time. For the larger system *n*-dodecane the results are similar but more complex. Initially carbon-carbon bond cleavages form a mixture of primary radicals in size from ethyl to decyl. These rapidly dissociate via beta scissions or by 1,4-, 1,5-, 1,6-,1,7-, 1,8-, or 1,9-H shifts followed by beta scissions. This explains the presence of 1-butene, 1-pentene, 1-hexene, and 1-heptene. Compared to *n*-decane there is a higher yield of ethyl radical here most likely due to the larger amount of primary alkyl radicals formed in the primary decomposition. In both these studies the major chemical mechanism for large *n*-alkane molecule pyrolysis, which are the major fuel components of JP-8, was clearly formulated.

Primary decomposition of *n*-butylbenzene produces mostly benzyl radical C_7H_7 + C_3H_7 and C_8H_9 ($C_6H_5C_2H_4$) + C_2H_5 with relative yields varying with temperature and

pressure and a minor amount of 1-phenyl-prop-3-yl + CH$_3$. Secondary reactions form ethylene and small radicals ranging from methyl to propyl with minor amounts styrene and benzyl radicals formed as well. This is in agreement with experimental results using vacuum UV photoionization mass spectroscopy which indicated the presence of styrene, benzyl, and ethylene to be formed with highest mole fractions, along with ethylbenzene, toluene, methane, and ethane, whereas the yield of CH$_3$ was relatively low. Initial decomposition of *s*-butylbenzene is expected to form C$_8$H$_9$ (C$_6$H$_5$CHCH$_3$) + C$_2$H$_5$ and a minor amount of C$_9$H$_{11}$ (1-phenyl-prop-1-yl) + CH$_3$. The major difference between *n*-butylbenzene and *s*-butylbenzene pyrolysis is the lack of benzyl formation due to the molecular structure of *s*-butylbenzene. In both structures the dominate decomposition pathway involves the benzylic carbon-carbon bonds. *t*-butylbenzene produces 2-phenyl-prop-2-yl + CH$_3$ upon decomposition nearly exclusively as it contains three equivalent benzylic carbon-carbon bonds. Overall the kinetics of combustion in this system is affected by the variation in fragments present. Pressure and temperature-dependent rate coefficients calculated here can be used in further kinetic modeling for pyrolysis of butylbenzenes.

Major, minor and trace decomposition products of JP-10 were also elucidated. Species present at long residence times include molecular hydrogen, ethylene, propene, cyclopentadiene, cyclopentane, fulvene, and benzene. For short residence times many radicals are formed that scavenge ethylene and propene to mainly form ethyl, allyl, and methyl. This points to the time of availability of oxygen drastically affecting the oxidation mechanism. Longer residence times would provide the overall product yields of oxygen-bearing products but to derive the underlying pathways of oxidation individual hydrocarbon radicals formed in the decomposition process need to be investigated.

Low temperature growth mechanisms of PAHs were also investigated. Involving growth of PAHs leading to the formation of a single ring the barrier-less addition of dicarbon to 1,3-pentadiene was shown to occur via multiple isomerization steps eventually leading to the formation of distinct C_7H_7 radical species via atomic hydrogen elimination. The energetics calculated were consistent with the formation of C_7H_7 isomers such as o-, m-, and p-tolyl radicals, cycloheptatrienyl, and benzyl. Calculations predict phenyl products through methyl elimination however this could not be confirmed experimentally due to interference with the molecular beam. The first low temperature pathway to a tricyclic aromatic hydrocarbon was deduced as well. The barrier-less formation of 1,4-dihyrophenanthrene via the elementary bimolecular gas phase reaction of the 1-naphthyl radical with 1,3-butadiene was shown to be energetically feasible. This reaction occurs by addition of the naphthyl radical to 1,3-butadiene which is facilitated by a van der Waals complex. This complex isomerizes and loses atomic hydrogen leading to aromatization form the dihydrophenanthrene. This novel reaction mechanism shows that molecular growth processes of PAHs are not limited to high temperature situations as was previously thought. Thus, the combustion of hydrocarbons has been thoroughly studied and major progress towards understanding of the fundamental mechanism has been achieved.

VITA

DANIEL EDUARDO BELISARIO-LARA

Born, Miami, United States of America

2013   B.S., Chemistry

Florida International University

Miami, Florida

2016   M.S., Chemistry

Florida International University

Miami, Florida

2013-2018   Teaching Assistant

Florida International University

Miami, Florida

PUBLICATIONS AND PRESENTATIONS

1. Dangi, B. B., Parker, D. S., Kaiser, R. I., Belisario-Lara, D., & Mebel, A. M. (2014). An experimental and theoretical investigation of the formation of C 7 H 7 isomers in the bimolecular reaction of dicarbon molecules with 1, 3-pentadiene. *Chemical Physics Letters*, *607*, 92-99.
2. Zhao, L., Yang, T., Kaiser, R. I., Troy, T. P., Ahmed, M., Belisario-Lara, D., & Mebel, A. M. (2017). Combined Experimental and Computational Study on the Unimolecular Decomposition of JP-8 Jet Fuel Surrogates. I. n-Decane (n-C10H22). *The Journal of Physical Chemistry A*, *121*(6), 1261-1280.
3. Zhao, L., Yang, T., Kaiser, R. I., Troy, T. P., Ahmed, M., Ribeiro, J. M., ... & Mebel, A. M. (2017). Combined Experimental and Computational Study on the Unimolecular Decomposition of JP-8 Jet Fuel Surrogates. II: n-Dodecane (n-C12H26). *The Journal of Physical Chemistry A*, *121*(6), 1281-1297.
4. Zhao, L., Yang, T., Kaiser, R. I., Troy, T. P., Xu, B., Ahmed, M., ... & Cao, C. (2017). A Vacuum Ultraviolet Photoionization Study on High-Temperature Decomposition of JP-10 (exo-Tetrahydrodicyclopentadiene). *Physical Chemistry Chemical Physics*.

Physical Chemistry Chemical Physics, 2017, DOI: 10.1039/C7CP01571B 15780-15807

5. Kaiser, R., Thomas, A., Lucas, M., Yang, T., Fuentes, L., Belisario-Lara, D., Mebel, A. (2017) "A Free Radical Pathway to Hydrogenated Phenanthrene in Molecular Clouds- A Low Temperature Growth of Polycyclic Aromatic Hydrocarbons" *ChemPhysChem DOI: 10.1002/cphc.201700515* 1971-1976.

6. Belisario-Lara, D., Mebel, A. M., & Kaiser, R. I. (2018). A Computational Study on the Unimolecular Decomposition of JP-8 Jet Fuel Surrogates III: Butylbenzene Isomers (n-, s-, and t-C14H10). *The Journal of Physical Chemistry A*, in press, DOI: 10.1021/acs.jpca.8b01836.

7. Belisario-Lara, D., Mebel, A.M., Investigation on Pyrolysis of JP-8 *253rd ACS National Meeting and Exposition, San Francisco, Ca.,* April 2-6, 2017 (Poster).

8. Belisario-Lara, D,. Mebel, A.M., Riberio, J.M. Theoretical Study on Pyrolysis of Jet Propellant 8 Components: The Behavior of Aliphatic and Non-Aliphatic Rings *254th ACS National Meeting and Exposition, Washington D.C., Va.,* August 20-24, 2017 (Poster).